Summaries of the Third Annual JPL Airborne Geoscience Workshop

June 1–5, 1992

Volume 1. AVIRIS Workshop

Robert O. Green
Editor

June 1, 1992

NASA

Summaries of the Third Annual JPL Airborne Geoscience Workshop June 1–5, 1992

Volume 1. AVIRIS Workshop

Robert O. Green
Editor

June 1, 1992

NASA
National Aeronautics and
Space Administration

Jet Propulsion Laboratory
California Institute of Technology
Pasadena, California

ABSTRACT

This publication contains the preliminary agenda and summaries for the Third Annual JPL Airborne Geoscience Workshop, held at the Jet Propulsion Laboratory, Pasadena, California, on June 1–5, 1992. This main workshop is divided into three smaller workshops as follows:

- The Airborne Visible/Infrared Imaging Spectrometer (AVIRIS) workshop, on June 1 and 2. The summaries for this workshop appear in Volume 1.

- The Thermal Infrared Multispectral Scanner (TIMS) workshop, on June 3. The summaries for this workshop appear in Volume 2.

- The Airborne Synthetic Aperture Radar (AIRSAR) workshop, on June 4 and 5. The summaries for this workshop appear in Volume 3.

CONTENTS

Volume 1: AVIRIS Workshop

Volume 2: TIMS Workshop

AGENDA

THIRD ANNUAL JPL AIRBORNE GEOSCIENCE WORKSHOP:
AIRBORNE VISIBLE/INFRARED IMAGING SPECTROMETER
(AVIRIS)

June 1 and 2, 1992
Von Karman Auditorium
Jet Propulsion Laboratory
Pasadena, California 91109

MONDAY, JUNE 1, 1992

7:15 a.m.   Shuttle bus departs Pasadena Ritz-Carlton Hotel for JPL.

7:30 a.m.   Registration and continental breakfast at JPL.

8:00 a.m.   Welcome

8:30 a.m.   In-Flight Calibration of the Spectral and Radiometric Characteristics of AVIRIS
in 1991
*Robert O. Green, James E. Conel, Carol J. Bruegge, Jack S. Margolis,
Veronique Carrere, Gregg Vane, and Gordon Hoover*

9:00 a.m.   Using AVIRIS Images To Measure Temporal Trends in Abundance of
Photosynthetic and Nonphotosynthetic Canopy Components
*Susan L. Ustin, Milton O. Smith, Dar Roberts, John A. Gamon, and
Christopher B. Field*

9:30 a.m.   Unmixing AVIRIS Data To Provide a Method for Vegetation Fraction
Subtraction
J.A. Zamudio

10:00 a.m.   Break

10:30 a.m.   Mapping the Mineralogy and Lithology of Canyonlands, Utah With Imaging
Spectrometer Data and the Multiple Spectral Feature Mapping Algorithm
Roger N. Clark, Gregg A. Swayze, and Andrea Gallagher

11:00 a.m.   Spatial Resolution and Cloud Optical Thickness Retrievals
Rand E. Feind, Sundar A. Christopher, and Ronald M. Welch

11:30 a.m.   Evaluation of Spatial Productivity Patterns in an Annual Grassland During an
AVIRIS Overflight
John A. Gamon, Christopher B. Field, and Susan L. Ustin

12:00 noon   Lunch

1:00 p.m.   Hyperspectral Modeling for Extracting Aerosols From Aircraft/Satellite Data
G. Daniel Hickman and Michael J. Duggin

1:30 p.m.   The Spectral Image Processing System (SIPS)—Software for Integrated Analysis
of AVIRIS Data
*F.A. Kruse, A.B. Lefkoff, J.W. Boardman, K.B. Heidebrecht, A.T. Shapiro,
P.J. Barloon, and A.F.H. Goetz*

THIRD ANNUAL JPL AIRBORNE GEOSCIENCE WORKSHOP:
AIRBORNE VISIBLE/INFRARED IMAGING SPECTROMETER
(AVIRIS)

2:00 p.m.	First Results From Analysis of Coordinated AVIRIS, TIMS, and ISM (French) Data for the Ronda (Spain) and Beni Bousera (Morocco) Peridotites *J.F. Mustard, S. Hurtrez, P. Pinet, and C. Sotin*
2:30 p.m.	AVIRIS Study of Death Valley Evaporite Deposits Using Least-Squares Band-Fitting Methods *J.K. Crowley and R.N. Clark*
3:00 p.m.	Break
3:30 p.m.	A Field Measure of the "Shade" Fraction *Alan R. Gillespie, Milton O. Smith, and Donald E. Sabol*
4:00 p.m.	A Linear Spectral Matching Technique for Retrieving Equivalent Water Thickness and Biochemical Constituents of Green Vegetation *Bo-Cai Gao and Alexander F.H. Goetz*
4:30 p.m.	Poster Previews
5:00 p.m.	Poster Previews
5:30 p.m.	End of session.
5:45 p.m.	Shuttle bus departs JPL for the Pasadena Ritz-Carlton Hotel.
6:30 p.m.	Reception and poster sessions at the Pasadena Ritz-Carlton Hotel.
9:00 p.m.	Close of reception and poster sessions.

AGENDA

THIRD ANNUAL JPL AIRBORNE GEOSCIENCE WORKSHOP:
POSTER SESSION

Monday, June 1, 1992
6:30 to 9:00 p.m.
Pasadena Ritz-Carlton Hotel

1. Use of AVIRIS Data to the Definition of Optimised Specifications for Land
    Applications With Future Spaceborne Imaging Spectrometers
    J. Bodechtel

2. Primary Studies of Trace Quantities of Green Vegetation in Mono Lake Area
    Using 1990 AVIRIS Data
    Zhikang Chen, Chris D. Elvidge, and David P. Groeneveld

3. JPL Activities on Development of Acousto-Optic Tunable Filter Imaging
    Spectrometer
    Li-Jen Cheng, Tien-Hsin Chao, and George Reyes

4. Measuring Dry Plant Residues in Grasslands: A Case Study Using AVIRIS
    Michael Fitzgerald and Susan L. Ustin

5. Analysis of AVIRIS San Pedro Channel Data: Methods and Applications
    Richard B. Frost

6. Tracking Photosynthetic Efficiency With Narrow-Band Spectroradiometry
    John A. Gamon and Christopher B. Field

7. Separation of Cirrus Cloud From Clear Surface From AVIRIS Data Using the
    1.38-μm Water Vapor Band
    Bo-Cai Gao and Alexander F.H. Goetz

8. Software for the Derivation of Scaled Surface Reflectances From AVIRIS Data
    Bo-Cai Gao, Kathleen Heidebrecht, and Alexander F.H. Goetz

9. Integrating Remote Sensing Techniques at Cuprite, Nevada: AVIRIS, Thematic
    Mapper, and Field Spectroscopy
    Bradley Hill, Greg Nash, Merrill Ridd, Phoebe Hauff, and Phil Ebel

10. Evaluation of AVIRISwiss-91 Campaign Data
    K.I. Itten, P. Meyer, K. Staenz, T. Kellenberger, and M. Schaepman

11. AVIRIS Investigator's Guide
    Howell Johnson

12. Oregon Transect: Comparison of Leaf-Level Reflectance With Canopy-Level and
    Modelled Reflectance
    Lee F. Johnson, Frederic Baret, and David L. Peterson

13. AVIRIS as a Tool for Carbonatite Exploration: Comparison of SPAM and
    Mbandmap Data Analysis Methods
    Marguerite J. Kingston and James K. Crowley

14. Expert System-Based Mineral Mapping Using AVIRIS
    F.A. Kruse, A.B. Lefkoff, and J.B. Dietz

AGENDA

THIRD ANNUAL JPL AIRBORNE GEOSCIENCE WORKSHOP:
AIRBORNE VISIBLE/INFRARED IMAGING SPECTROMETER
(AVIRIS)

June 1 and 2, 1992
Von Karman Auditorium
Jet Propulsion Laboratory
Pasadena, California 91109

TUESDAY, JUNE 2, 1992

7:15 a.m.   Shuttle bus departs Pasadena Ritz-Carlton Hotel for JPL.

7:30 a.m.   Registration and continental breakfast at JPL.

8:00 a.m.   Mapping the Spectral Variability in Photosynthetic and Non-Photosynthetic
               Vegetation, Soils and Shade Using AVIRIS
               *Dar A. Roberts, Milton O. Smith, Donald E. Sabol, John B. Adams, and
               Susan Ustin*

8:30 a.m.   Volcanic Thermal Features Observed by AVIRIS
               *Clive Oppenheimer, David Pieri, Veronique Carrere, Michael Abrams,
               David Rothery, and Peter Francis*

9:00 a.m.   Retrieval of Biophysical Parameters With AVIRIS and ISM—The Landes Forest,
               South West France
               *F. Zagolski, J.P. Gastellu-Etchegorry, E. Mougin, G. Giordano, G. Marty,
               T. Le Toan, and A. Beaudoin*

9:30 a.m.   Ground-Truthing AVIRIS Mineral Mapping at Cuprite, Nevada
               Gregg Swayze, Roger N. Clark, Fred Kruse, Steve Sutley, and Andrea Gallagher

10:00 a.m.   Break

10:30 a.m.   Exploring the Remote Sensing of Foliar Biochemical Concentrations With
               AVIRIS Data
               Geoffrey M. Smith and Paul J. Curran

11:00 a.m.   Seasonal and Spatial Variations in Phytoplanktonic Chlorophyll in Eutrophic
               Mono Lake, California, Measured With the Airborne Visible and Infrared
               Imaging Spectrometer (AVIRIS)
               John M. Melack and Mary Gastil

11:30 a.m.   AVIRIS Calibration and Application in Coastal Oceanic Environments
               Kendall L. Carder

12:00 noon   Lunch

1:00 p.m.   Mapping Vegetation Types With the Multiple Spectral Feature Mapping
               Algorithm in Both Emission and Absorption
               Roger N. Clark, Gregg A. Swayze, Christopher Koch, and Cathy Ager

THIRD ANNUAL JPL AIRBORNE GEOSCIENCE WORKSHOP:
AIRBORNE VISIBLE/INFRARED IMAGING SPECTROMETER
(AVIRIS)

1:30 p.m.   Multiple Dataset Water-Quality Analyses in the Vicinity of an Ocean Wastewater
              Plume
              Michael Hamilton, Curtiss O. Davis, W. Joseph Rhea, and
              Jeannette van den Bosch

2:00 p.m.   MAC Europe 91: Evaluation of AVIRIS, GER Imaging Spectrometry Data for
              the Land Application Testsite Oberpfaffenhofen
              F. Lehmann, R. Richter, H. Rothfuss, K. Werner, P. Hausknecht, A. Müller, and
              P. Strobl

2:30 p.m.   Using Endmembers in AVIRIS Images To Estimate Changes in Vegetative
              Biomass
              Milton O. Smith, John B. Adams, Susan L. Ustin, and Dar A. Roberts

3:00 p.m.   Break

3:30 p.m.   Atmospheric Correction of AVIRIS Data in Ocean Waters
              Gregory Terrie and Robert Arnone

4:00 p.m.   The 1991 AVIRIS/POLDER Experiment in Camargue, France
              F. Baret, C. Leprieur, S. Jacquemoud, V. Carrère, X.F. Gu, M. Steven,
              V. Vanderbilt, J.F. Hanocq, S. Ustin, G. Rondeaux, C. Daughtry, L. Biehl,
              R. Pettigrew, D. Modro, H. Horoyan, T. Sarto, C. Despontin, and
              H. Razafindraibe

4:30 p.m.   AVIRIS Sensor and Ground Data System: Status and Plans
              Thomas Chrien and Earl Hansen

5:00 p.m.   Wrap up.

5:30 p.m.   End of AVIRIS Workshop.

5:45 p.m.   Shuttle bus departs JPL for the Pasadena Ritz-Carlton Hotel.

AGENDA

THIRD ANNUAL JPL AIRBORNE GEOSCIENCE WORKSHOP:
THERMAL INFRARED MULTISPECTRAL SCANNER
(TIMS)

June 3, 1992
Von Karman Auditorium
Jet Propulsion Laboratory
Pasadena, California 91109

WEDNESDAY, JUNE 3, 1992

7:15 a.m.   Shuttle bus departs Pasadena Ritz-Carlton Hotel for JPL.

7:30 a.m.   Registration and continental breakfast at JPL.

8:00 a.m.   Welcome

8:30 a.m.   TIMS Performance Evaluation Summary
              Bruce Spiering, G. Meeks, J. Anderson, S. Jaggi, and S. Kuo

              A Quantitative Analysis of TIMS Data Obtained on the Learjet 23 at Various
              Altitudes
              S. Jaggi

              Analysis of TIMS Performance Subjected to Simulated Wind Blast
              S. Jaggi and S. Kuo

9:30 a.m.   Sensitivity of Blackbody Reference Panels to Wind Blast
              Gordon Hoover

10:00 a.m.   Break

10:30 a.m.   Preliminary Analysis of TIMS Performance on the ER-2
              S.J. Hook, V.J. Realmuto, and R.E. Alley

11:00 a.m.   Comparison of Preliminary Results From Airborne ASTER Simulator (AAS)
              With TIMS Data
              Yoshiaki Kannari, Franklin Mills, Hiroshi Watanabe, Teruya Ezaka,
              Tatsuhiko Narita, and Sheng-Huei Chang

11:30 a.m.   Simulation of ASTER Data Using AVIRIS Images
              Michael Abrams

12:00 noon   Lunch

1:00 p.m.   Application of Split Window Technique to TIMS Data
              Tsuneo Matsunaga, Shuichi Rokugawa, and Yoshinori Ishii

1:30 p.m.   Atmospheric Corrections for TIMS Estimated Emittance
              T.A. Warner and D.W. Levandowski

2:00 p.m.   An Algorithm for the Estimation of Bounds on the Emissivity and Temperatures
              From Thermal Multispectral Airborne Remotely Sensed Data
              S. Jaggi, D. Quattrochi, and R. Baskin

THIRD ANNUAL JPL AIRBORNE GEOSCIENCE WORKSHOP:
THERMAL INFRARED MULTISPECTRAL SCANNER
(TIMS)

2:30 p.m.   Multi-Resolution Processing for Fractal Analysis of Airborne Remotely Sensed
                Data
                S. Jaggi, D. Quattrochi, and N. Lam

3:00 p.m.   Break

3:30 p.m.   Preliminary Analysis of Thermal-Infrared Multispectral Scanner Data of the Iron
                Hill, Colorado Carbonatite-Alkalic Rock Complex
                Lawrence C. Rowan, Kenneth Watson, and Susanne H. Miller

4:00 p.m.   The Use of TIMS for Mapping Different Pahoehoe Surfaces: Mauna Iki, Kilauea
                Scott K. Rowland

4:30 p.m.   Ejecta Patterns of Meteor Crater, Arizona Derived From the Linear Un-Mixing of
                TIMS Data and Laboratory Thermal Emission Spectra
                Michael S. Ramsey and Philip R. Christensen

5:00 p.m.   The Use of TIMS Data To Estimate the SO_2 Concentrations of Volcanic Plumes:
                A Case Study at Mount Etna, Sicily
                Vincent J. Realmuto

5:30 p.m.   End of TIMS Workshop.

5:45 p.m.   Shuttle bus departs JPL for the Pasadena Ritz-Carlton Hotel.

AGENDA

THIRD ANNUAL JPL AIRBORNE GEOSCIENCE WORKSHOP:
AIRBORNE SYNTHETIC APERTURE RADAR
(AIRSAR)

June 4 and 5, 1992
Von Karman Auditorium
Jet Propulsion Laboratory
Pasadena, California 91109

THURSDAY, JUNE 4, 1992

7:15 a.m. Shuttle bus departs Pasadena Ritz-Carlton Hotel for JPL.

7:30 a.m. Registration and continental breakfast at JPL.

8:00 a.m. Welcome

8:30 a.m. The NASA/JPL Three-Frequency AIRSAR System
J. van Zyl, R. Carande, Y. Low, T. Miller, and K. Wheeler

9:00 a.m. A Snow Wetness Retrieval Algorithm for SAR
Jiancheng Shi and Jeff Dozier

9:30 a.m. Comparison of JPL-AIRSAR and DLR E-SAR Images from the MAC Europe '91
Campaign Over Testsite Oberpfaffenhofen: Frequency and Polarization
Dependent Backscatter Variations From Agricultural Fields
C. Schmullius and J. Nithack

10:00 a.m. Break

10:30 a.m. Monitoring Environmental State of Alaskan Forests With AIRSAR
*Kyle C. McDonald, JoBea Way, Eric Rignot, Cindy Williams, Les Viereck, and
Phylis Adams*

11:00 a.m. Comparison of Modeled Backscatter With SAR Data at P-Band
Yong Wang, Frank W. Davis, and John M. Melack

11:30 a.m. SAR Backscatter From Coniferous Forest Gaps
John L. Day and Frank W. Davis

12:00 noon Lunch

1:00 p.m. Panel Discussion on Future Emphasis of the AIRSAR System
J. van Zyl, Moderator

1:30 p.m. Retrieval of Pine Forest Biomass Using JPL AIRSAR Data
A. Beaudoin, T. Le Toan, F. Zagolski, C.C. Hsu, H.C. Han, and J.A. Kong

2:00 p.m. Characterization of Wetland, Forest, and Agricultural Ecosystems in Belize With
Airborne Radar (AIRSAR)
Kevin O. Pope, Jose Maria Rey-Benayas, and Jack F. Paris

2:30 p.m. Strategies for Detection of Floodplain Inundation With Multi-Frequency
Polarimetric SAR
Laura L. Hess and John M. Melack

THIRD ANNUAL JPL AIRBORNE GEOSCIENCE WORKSHOP:
AIRBORNE SYNTHETIC APERTURE RADAR
(AIRSAR)

3:00 p.m.   Break

3:30 p.m.   Supervised Fully Polarimetric Classification of the Black Forest Test Site: From
                MAESTRO1 to MAC Europe
                G. De Grandi, C. Lavalle, H. De Groof, and A. Sieber

4:00 p.m.   Relating Multifrequency Radar Backscattering to Forest Biomass: Modeling and
                AIRSAR Measurement
                Guoqing Sun and K. Jon Ranson

4:30 p.m.   Poster Previews

5:00 p.m.   Poster Previews

5:30 p.m.   End of session.

5:45 p.m.   Shuttle bus departs JPL for the Pasadena Ritz-Carlton Hotel.

6:30 p.m.   Reception and poster sessions at the Pasadena Ritz-Carlton Hotel.

9:00 p.m.   Close of reception and poster sessions.

AGENDA

THIRD ANNUAL JPL AIRBORNE GEOSCIENCE WORKSHOP:
POSTER SESSION

Thursday, June 4, 1992
6:30 to 9:00 p.m.
Pasadena Ritz-Carlton Hotel

THIRD ANNUAL JPL AIRBORNE GEOSCIENCE WORKSHOP:
THURSDAY POSTER SESSION (CONTINUED)

AGENDA

THIRD ANNUAL JPL AIRBORNE GEOSCIENCE WORKSHOP:
AIRBORNE SYNTHETIC APERTURE RADAR
(AIRSAR)

June 4 and 5, 1992
Von Karman Auditorium
Jet Propulsion Laboratory
Pasadena, California 91109

FRIDAY, JUNE 5, 1992

7:15 a.m.   Shuttle bus departs Pasadena Ritz-Carlton Hotel for JPL.

7:30 a.m.   Registration and continental breakfast at JPL.

8:00 a.m.   Oceanic Features Detected by SAR in the Mediterranean Sea During the MAC
               Europe '91 Campaign
               Werner Alpers

8:30 a.m.   SAR Observations in the Gulf of Mexico
               David Sheres

9:00 a.m.   Investigation of AIRSAR Signatures of the Gulf Stream
               G.R. Valenzuela, J.S. Lee, D.L. Schuler, G.O. Marmorino, F. Askari, K. Hoppel,
               J.A.C. Kaiser, and W.C. Keller

9:30 a.m.   Mapping of Sea Bottom Topography
               C.J. Calkoen, G.J. Wensink, and G.H.F.M. Hesselmans

10:00 a.m.   Break

10:30 a.m.   Sea Bottom Topography Imaging With SAR
               M.W.A. van der Kooij, G.J. Wensink, and J. Vogelzang

11:00 a.m.   AIRSAR Surveys of Upper-Ocean Fronts Off California and Hawaii
               P. Flament

11:30 a.m.   Preliminary Results of Polarization Signatures for Glacial Moraines in the Mono
               Basin, Eastern Sierra Nevada
               Richard R. Forster, Andrew N. Fox, and Bryan Isacks

12:00 noon   Lunch

1:00 p.m.   Detecting Surface Roughness Effects on the Atmospheric Boundary Layer Via
               AIRSAR Data: A Field Experiment in Death Valley, California
               Dan G. Blumberg and Ronald Greeley

1:30 p.m.   Extraction of Quantitative Surface Characteristics From AIRSAR Data for Death
               Valley, California
               K.S. Kierein-Young and F.A. Kruse

2:00 p.m.   The TOPSAR Interferometric Radar Topographic Mapping Instrument
               Howard A. Zebker, Søren N. Madsen, Jan Martin, Giovanni Alberti,
               Sergio Vetrella, and Alessandro Cucci

THIRD ANNUAL JPL AIRBORNE GEOSCIENCE WORKSHOP:
AIRBORNE SYNTHETIC APERTURE RADAR
(AIRSAR)

2:30 p.m.   Evaluation of the TOPSAR Performance by Using Passive and Active Calibrators
G. Alberti, A. Moccia, S. Ponte, and S. Vetrella

3:00 p.m.   Break

3:30 p.m.   Fitting a Three-Component Scattering Model to Polarimetric SAR Data
A. Freeman and S. Durden

4:00 p.m.   Application of Symmetry Properties to Polarimetric Remote Sensing With JPL
AIRSAR Data
S.V. Nghiem, S.H. Yueh, R. Kwok, and F.K. Li

4:30 p.m.   External Calibration of Polarimetric Radar Images Using Distributed Targets
Simon H. Yueh, S.V. Nghiem, and R. Kwok

5:00 p.m.   Wrap up.

5:30 p.m.   End of AIRSAR Workshop.

5:45 p.m.   Shuttle bus departs JPL for the Pasadena Ritz-Carlton Hotel.

IN-FLIGHT CALIBRATION OF THE SPECTRAL AND RADIOMETRIC CHARACTERISTICS OF AVIRIS IN 1991

Robert O. Green, James E. Conel, Carol J. Bruegge, Jack S. Margolis,
Veronique Carrere, Gregg Vane, and Gordon Hoover

Jet Propulsion Laboratory
California Institute of Technology
4800 Oak Grove Drive
Pasadena, California 91109

SUMMARY

On March 7, 1991, an in-flight calibration experiment was held
at the Ivanpah Playa in southeastern California for the AVIRIS imaging
spectrometer. This experiment was modeled on previous work for the
in-flight calibration of imaging spectrometers (Conel et al., 1987,
Green et al., 1988, Conel et al., 1988, Green et al., 1990, and Green et
al., 1992).

Five AVIRIS overflights were acquired of a calibration target
designated on the Ivanpah Playa surface. At the time of the overflights,
the reflectance of the calibration target was measured with a field
spectrometer. In addition, the atmospheric optical depths and water
vapor abundance were measured from a radiometer station adjacent to
the calibration target. These in situ measurements were used to
constrain the MODTRAN radiative transfer code (Berk et al., 1989) to
model the upwelling spectral radiance incident to the sensor aperture
during the overflights. Analyses of this modeled radiance in
conjunction with the laboratory-calibrated radiance were used to
determine the spectral and radiometric calibration of AVIRIS while in
flight. Figure 1 gives the comparison of one of the MODTRAN-
modeled and AVIRIS-laboratory-calibrated radiance for the overflights
of the Ivanpah Playa calibration target.

The modeled and measured spectra used in this experiment are
generated through independent pathways allowing direct validation of
AVIRIS performance in flight. The MODTRAN spectrum is derived
from a measured solar irradiance spectrum imbedded in the computer
code. The AVIRIS-laboratory-calibrated spectrum is derived from to a
National Institute of Standards and Technology (NIST) traceable
standard lamp maintained at JPL.

The in-flight radiometric calibration of AVIRIS is validated by
the agreement between these spectra. This agreement is better than 7%
excluding the opaque regions of the terrestrial atmosphere. To generate
the in-flight calibration directly, radiometric calibration coefficients
were calculated from the MODTRAN-modeled radiance and the AVIRIS
digitized signal for the Ivanpah Playa calibration target.

Spectral calibration was validated by the agreement between the
modeled and the laboratory-calibrated data in spectral regions of strong
atmospheric gas absorption features. For example, the oxygen band at
760 nm is expressed equivalently in these two independently derived
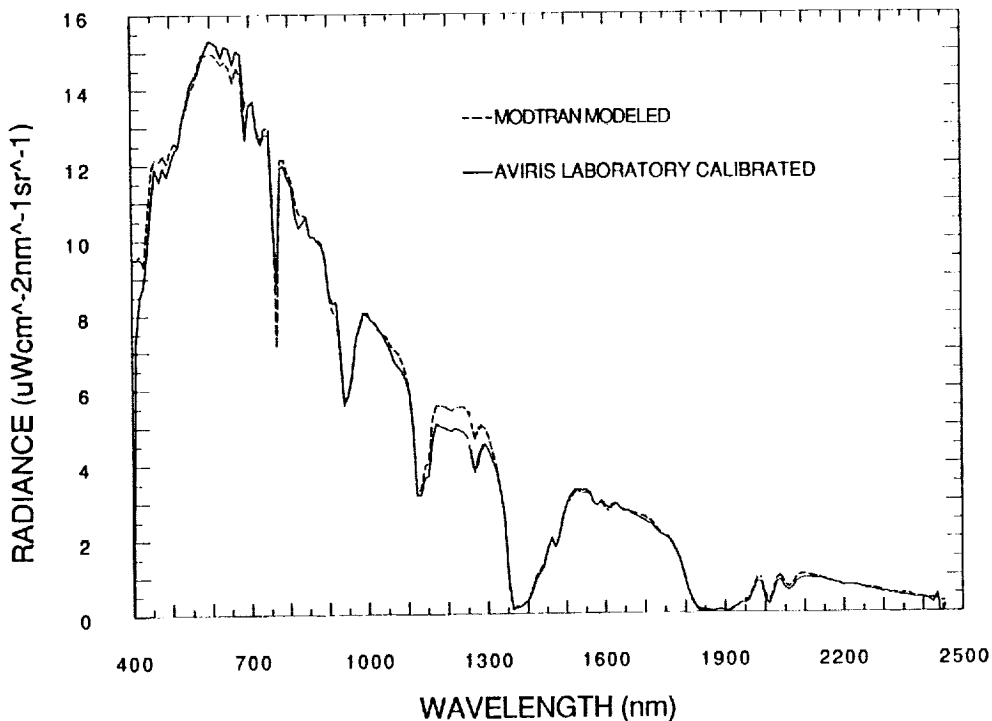
Figure 1. Comparison of the MODTRAN radiative transfer code modeled and AVIRIS laboratory calibrated radiance from the Ivanpah Playa calibration target.

spectra. Quantitative analysis of the 14 strong absorption features present in the AVIRIS spectral range with a nonlinear least squared fitting algorithm was used to validate the calibration across the spectral range. A complete in-flight spectral calibration was generated for all 224 AVIRIS channels through interpolation between the spectral absorption feature analyzed.

Data from this calibration experiment were used to determine the precision or signal-to-noise of AVIRIS in-flight. Sensor noise was determined as the root mean squared deviation (RMSD) of the AVIRIS dark signal spectra measured for the overflight of the calibration target. The AVIRIS measured signal from the calibration target was normalized to the AVIRIS reference radiance to allow comparison with previous signal-to-noise determinations. In-flight signal-to-noise was calculated as the ratio of normalized-signal to the RMSD noise and is shown in Figure 2.

Based on this experiment, AVIRIS was shown to be well calibrated at the beginning of the operational season in 1991. Experiments in May and late June showed the calibration to be maintained with the exception of the 1900- to 2450-nm spectral region. Damage to the sensor caused throughput reduction in this spectral region in early June. Radiometric calibration of this 1900- to 2450-nm region was reestablished using the late June in-flight calibration experiment.
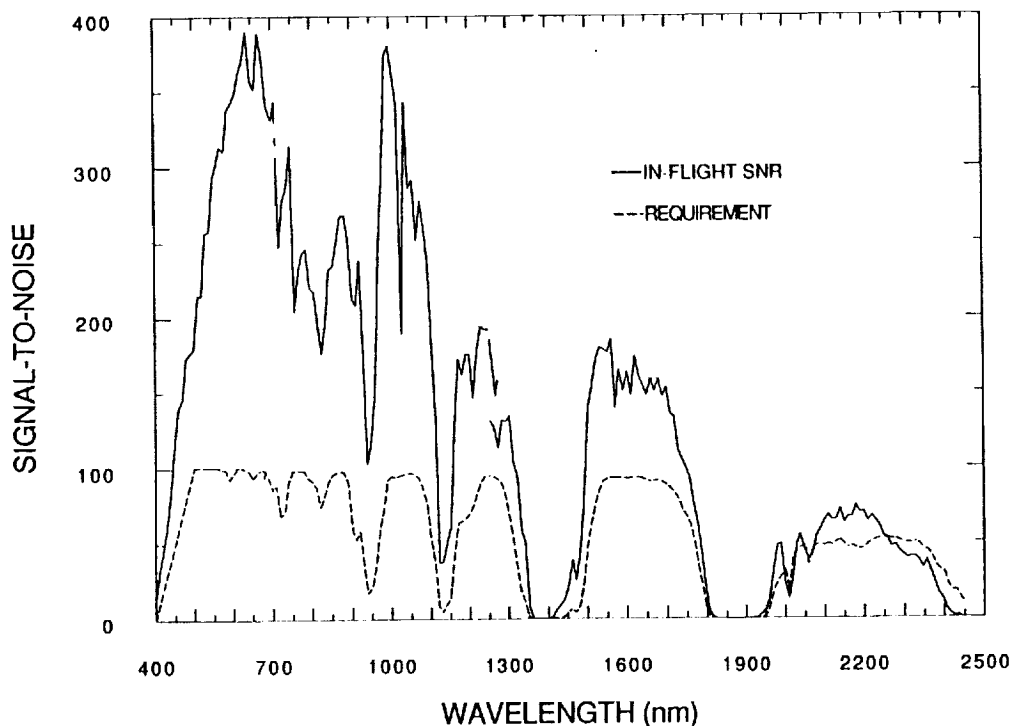
Figure 2. In-flight determined signal-to-noise at the AVIRIS reference radiance for the March 7, 1991, calibration experiment.

ACKNOWLEDGMENTS

REFERENCES

Berk, A., L.S. Bernstein, and D.C. Robertson, MODTRAN: A moderate resolution model for LOWTRAN 7, Final report, GL-TR-0122, Air Force Geophysics Laboratory, Hanscomb AFB, MA, 42 pp., 1989.

Conel, J.E., R.O. Green, R.E. Alley, C.J. Bruegge, V. Carrere, J.S. Margolis, G. Vane, T.G. Chrien, P.N. Slater, S.F. Biggar, P.M. Teillet, R.D. Jackson and M.S. Moran, In-flight radiometric calibration of the Airborne Visible/Infrared Imaging Spectrometer (AVIRIS), SPIE Vol. 924, Recent Advance in Sensors, Radiometry and Data Processing for Remote Sensing, 1988.

Conel, J.E., R.O. Green, G. Vane, C.J. Bruegge, R.E. Alley, and B.J. Curtiss. Airborne Imaging Spectrometer-2: Radiometric and spectral characteristics and comparison of ways to compensate for the atmosphere, in press, SPIE Proceedings, 1987.

Green, R.O., G. Vane, and J.E. Conel, Determination of aspects of the in-flight spectral, radiometric, spatial and signal-to-noise performance of the Airborne Visible/Infrared Imaging Spectrometer over Mountain Pass, Ca., in Proceeding of the Airborne Visible/Infrared Imaging Spectrometer (AVIRIS) Performance Evaluation Workshop, JPL Pub. 88-38, 162–184, 1988.

Green, R.O., and G. Vane, Validation/calibration of the Airborne Visible/Infrared Imaging Spectrometer (AVIRIS) in-flight, Proc. SPIE Conference on Aerospace Sensing, Imaging Spectroscopy of the Terrestrial Environment, Orlando, Florida, 16–20 April, 1990.

Green, R.O., J.E. Conel, C.J. Bruegge, J.S. Margolis, V. Carrere, G. Vane, and G. Hoover, In-flight calibration and validation of the spectral and radiometric characteristics of the Airborne Visible/Infrared Imaging Spectrometer (AVIRIS), submitted to Remote Sensing of Environment, 1992.

USING AVIRIS IMAGES TO MEASURE TEMPORAL TRENDS IN ABUNDANCE OF PHOTOSYNTHETIC AND NONPHOTOSYNTHETIC CANOPY COMPONENTS

SUSAN L. USTIN, DEPARTMENT OF LAND, AIR, AND WATER RESOURCES,
UNIVERSITY OF CALIFORNIA, DAVIS, CALIFORNIA 95616

MILTON O. SMITH, DAR ROBERTS, DEPARTMENT OF GEOLOGICAL SCIENCES, UNIVERSITY OF WASHINGTON, SEATTLE, WASHINGTON 98519

JOHN A. GAMON, DEPARTMENT OF BIOLOGY,
CALIFORNIA STATE UNIVERSITY, LOS ANGELES, CALIFORNIA 90032
AND
CHRISTOPHER B. FIELD, DEPARTMENT OF PLANT BIOLOGY,
CARNEGIE INSTITUTION OF WASHINGTON, STANFORD,
CALIFORNIA 94035

INTRODUCTION

The Jasper Ridge Biological Preserve, Stanford, California is a good example of hardwood rangeland ecosystems in California. Structurally, it is composed of a mosaic of serpentine grasslands, oak savannah, coastal chaparral, and mixed evergreen woodland, representing a broad cross-section of physiognomic classes. The Mediterranean climate produces an extended seasonal drought lasting throughout most of the growing season and has significant impact on the expression of divergent phenological patterns related to contrasting ecological strategies of these taxa. The region is well understood biologically due to the rich history of ecological research at the site. Thus, community characteristics, physiological characteristics, phenology, and temporal dynamics are reasonably well understood for many of the dominant species. Because of its proximity to NASA Ames Research Center, it has been subject to a large number of aircraft data acquisitions over many years. A more complete examination of this database would provide an opportunity to test current remote sensing hypotheses for measurement and detection of ecological attributes, particularly those involving canopy chemistry and physiology. Better definition of ecological rules might permit development of remotely sensed surrogate variables for biological properties that cannot be directly measured or measured with sufficient accuracy.

RESEARCH

An AVIRIS image of Jasper Ridge was acquired May 15, 1991 (910515B, run 10, segment 2) under clear sky conditions. Linear and non-linear spectral mixture analysis was performed and four spectral endmembers were identified. These endmembers corresponded with

those reported for Jasper Ridge in 1989 and 1990 and included a green photosynthetic canopy component, a non-photosynthetic canopy component, greenstone soil, and shade. This cross-calibration among multidate AVIRIS scenes implies that analyses can be examined for temporal trends (changes in endmember proportions and residuals) using a consistent reference base. In 1991, plant characteristics and surface reflectance measurements were made at 20m intersections over a 6 ha. permanently staked grid referenced to known coordinates. Additional points were located using Trimble Navigation Pathfinder Basic and Professional GPS. We examined spatial patterns for the photosynthetic and nonphotosynthetic canopy fractions in the grasslands in relation to field data and from aerial photography and their temporal trends.

RESULTS

Our field studies show that when a high fraction of the canopy is nonphotosynthetic, NDVI from field data underestimates the abundance of the photosynthetic fraction. Interactions among the photosynthetic and nonphotosynthetic vegetation fractions , subpixel shade, and residuals, derived in mixture analysis provide a basis for further evaluation. Foliar chlorophyll and nitrogen concentrations in the grasslands varied within limited ranges and were proportional to the foliar biomass per unit surface area (Gamon et al., this proceeding). Preliminary results indicate that the abundance of the photosynthetic endmember fraction in the grasslands approximates spatial abundance patterns in the green foliar biomass (and other correlated measures, gLAI, chlorophyll, and nitrogen). This relationship results because the enzyme for carbon fixation, RUBP carboxylase, is the largest foliar pool of soluble nitrogen. The summation of photosynthetic and nonphotosynthetic fractions provides a basis for estimating total canopy biomass, which for grasslands represents a measure of the net primary productivity, and over time, the magnitude of change in carbon storage. The ratio of photosynthetic fraction : total canopy fraction provides a basis to measure canopy N:C ratios.

We examined the patterns of endmember abundances and residuals for temporal trends related to site conditions (Fig. 1). One example of the temporal and spatial patterns we observed is shown for the three endmember models for July and October 1989. This figure shows endmember abundances from 10 sites including grasslands, chaparral, oaks, forest and a golf course. During this period photosynthetic endmember abundances did not indicate appreciable changes except in the evergreen oak and forested areas (sites 7,8) where photosynthetic fraction decreased. Grasslands and chaparral had lowest photosynthetic fractions, forest and the golf course had the highest. These results demonstrate that for a given region, the same endmembers can model images from different seasons and produce consistent fractional conditions that follow expected ecological trends. We believe that this approach has promise for providing an internally consistent basis for interpreting environmental gradients and temporal changes.

6
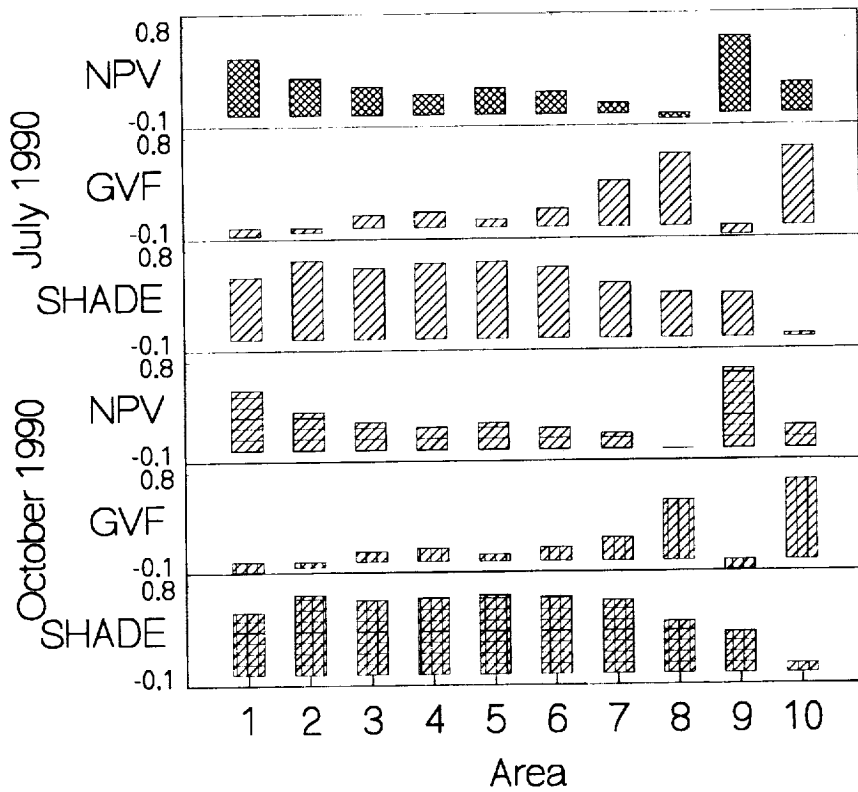
Figure 1. Endmember abundances for two AVIRIS images of Jasper Ridge, California. The endmembers are labeled npv (non-photosynthetic vegetation), GVF (green vegetation fraction), and shade. The 10 sites correspond to 1) non-serpentine grassland, 2) serpentine grassland, 3) serpentine chaparral, 4) non-serpentine chaparral, 5) non-serpentine chaparral of lowest cover, 6) blue oak, 7) evergreen oak, 8) forest wetland, 9) Webb Ranch grassland, and 10) golf course. The endmembers from the two different times indicate similar endmember fractions. The greatest changes are in the evergreen oak and the forest wetland.

UNMIXING AVIRIS DATA TO PROVIDE A METHOD FOR VEGETATION FRACTION SUBTRACTION

J. A. Zamudio

Center for the Study of Earth from Space (CSES)
Cooperative Institute for Research in Environmental Sciences (CIRES)
and
Department of Geological Sciences
University of Colorado, Boulder, Colorado 80309

1. DATA CHARACTERISTICS AND CALIBRATION

Five flight lines of AVIRIS data were acquired over the Dolly Varden Mountains in northeastern Nevada on June 2, 1989 (Zamudio and Atkinson, 1990). Signal-to-noise ratio values are given in figure 1.

The empirical line method (Conel et al., 1987) was used to convert AVIRIS radiance values to reflectance. This method involves calculating gain and offset values for each band. These values are based upon a comparison of the imaging spectrometer data and field reflectance measurements, both taken over the same ground targets. The targets used in this study were a dark andesite flow and a bright playa.

2. STUDY AREA

The study area contains a variety of geologic materials, including sedimentary, volcanic, plutonic and contact metamorphic rocks. Carbonate-dominated formations underlie much of the area.

Other than some high relief areas of 100% outcrop, vegetation cover typically ranges from about 10% to 50%, with some places along drainages and on high, north-facing slopes where vegetation cover approaches 100%. Vegetation is primarily sagebrush at lower elevations, with piñon pine and juniper prevalent from about 2000 meters on up. Little soil is found in the area.

3. ANALYSIS TECHNIQUES

Three-band color composites were made of the AVIRIS segments in order to view different rock types in their spatial context. Also, in order to produce geologic maps derived from spectral data, pixels with spectra characteristic of various rock types were selected from the reflectance data and then, using a binary encoding algorithm (Goetz et al., 1985), other pixels whose spectra matched within a certain tolerance were selected and color coded.

A linear unmixing routine (Boardman, 1991) was also applied to the data to aid in the mapping of rock units. A spectral library of materials found on the ground was compared to each spectrum in a particular scene. The proportions of each library endmember found in each pixel were then calculated. The result is a series of fraction images showing, in gray levels correlating with abundance, the areal distribution of each library endmember. Noisy bands, located in the atmospheric water absorption regions around 1.4 and 1.9 μm, were not used in the unmixing. Using the unmixing results, a routine to subtract out the vegetation fraction on a pixel-by-pixel basis was applied to the AVIRIS data.

4. RESULTS

Three-band color composites were linearly stretched to enhance the contrast between various rock units. Deformation of the rock units is apparent in some of these scenes.

The AVIRIS reflectance spectra were analyzed and various minerals were identified, including goethite, calcite and dolomite. Binary encoding enabled the

delineation of certain limestone-dominated and dolomite-dominated formations. In some areas, faults that did not appear on published maps are evident in the encoded data.

The unmixing routine was applied to an area where the limestone-dominated Gerster Formation, the dolomite-dominated Plympton Formation and Triassic shale and limestone of the Thaynes Formation crop out. The library of materials used in the unmixing includes limestone, dolomite, chert, brown limestone from the Thaynes, intermediate volcanic rocks and a mix of materials from the Thaynes Formation. Because the Thaynes is comprised of limestone and shale commonly interbedded on a finer scale than the AVIRIS pixel size, the Thaynes library spectrum was obtained from a mix of those materials. The Thaynes also includes a sizeable section of distinctive brown limestone which was used as another endmember. The Plympton contains abundant chert as well as dolomite, so chert was included in the library. The library spectra were obtained in the laboratory from samples collected in the field. The resulting six fraction images generally show good differentiation between rock types.

Also calculated in the unmixing is the sum of all endmember fractions for each pixel. If the sum for any pixel is less than one, then it is likely that either that pixel contains some material not represented in the library, or that the remaining fraction is a measure of how much the illumination conditions vary from 100%. Figure 2 shows the distribution of significant amounts of the limestone, dolomite and Thaynes fractions. As can be seen by comparison with figure 3, which shows formational contacts as mapped in the field, the differentiation between the three formations is good. In some places, the contacts in figure 2 reflect the extent of significant amounts of colluvium and alluvium, and therefore do not exactly match the bedrock contacts in figure 3. The distribution of the three formations in figure 2 suggests that they are deformed.

5. VEGETATION SUBTRACTION

Using the unmixing results and a vegetation spectrum obtained in the field, a routine was applied which subtracts the vegetation fraction from each pixel in a scene. This is accomplished by first multiplying the field vegetation spectrum by the fraction that represents the amount of vegetation present in a particular pixel. Then, this resulting fractional vegetation spectrum is subtracted from the pixel in the original scene. For example, if the unmixing routine showed that a certain pixel in the scene contains 50% vegetation, then the vegetation spectrum (100% vegetation) would be multiplied by 0.5, resulting in a fractional vegetation spectrum. Then, this spectrum would be subtracted from the spectrum for that pixel. Figure 4 compares a spectrum from a pixel containing vegetation to the resulting spectrum after the fraction of vegetation present has been subtracted. The vegetation removal can be viewed in a spatial context as well. A color image was made using a band near 0.8 μm displayed as green. Some areas of the scene have a green tint due to the high reflectance of vegetation at that wavelength. After vegetation subtraction, another color image was made using the same band combination. This scene is less green and drainages which contain close to 100% vegetation are almost black.

Color composite images made in this manner consequently show just geologic information. Any worker considering that some part of the data is masking what is important, either in a spatial or a spectral context, could consider using this technique. The ability to subtract out part of the spectrum might enable one to see features that are hidden in the total spectral signature.

REFERENCES
Boardman, J.W., and Goetz, A.F.H., 1991, Sedimentary facies analysis using AVIRIS data: a geophysical inverse problem: Proceedings of the Third Airborne Visible/Infrared Imaging Spectrometer (AVIRIS) Workshop, Jet Propulsion Laboratory: JPL Publ. 91-28, p. 4-13.

Conel, J.E., Green, R.O., Vane, G., Bruegge, C.J., Alley, R.E. and Curtiss, B.J., 1987, Airborne Imaging Spectrometer-2: Radiometric spectral characteristics and comparison of ways to compensate for the atmosphere in Vane, G., ed., Imaging

Spectroscopy II, Proceedings of SPIE-Society of Photo-Optical Instrumentation Engineers, v. 834, p. 140-157.

Goetz, A.F.H., Vane, G., Solomon, J. E., and Rock, B. N., 1985, Imaging spectrometry for Earth remote sensing: Science, v. 228, p. 1147-1153.

Zamudio, J.A., and Atkinson, W.W., Jr., 1990, Analysis of AVIRIS data for spectral discrimination of geologic materials in the Dolly Varden Mountains, Nevada: Proceedings of the Second Airborne Visible/Infrared Imaging Spectrometer (AVIRIS) Workshop, Jet Propulsion Laboratory: JPL Publ. 90-54, p. 162-166.
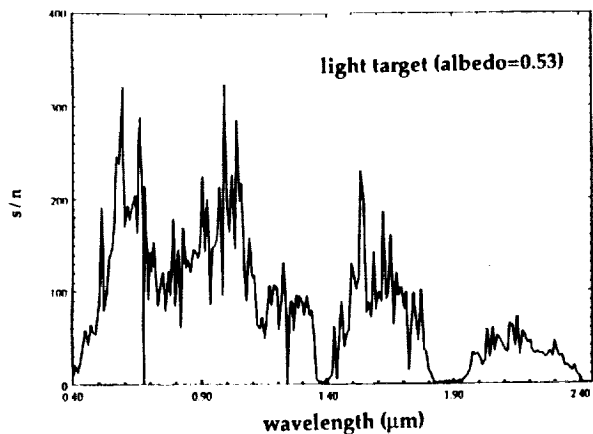
Figure 1. Signal-to noise ratio values for a playa target.
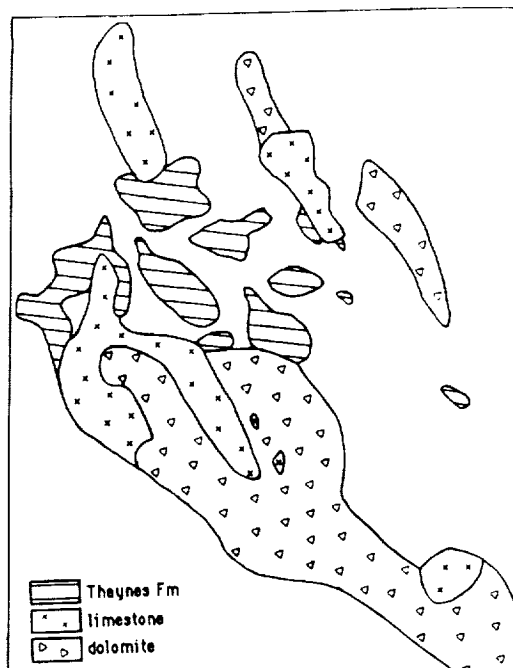
Figure 2. Extent of significant amounts of three fractions: dolomite, limestone, and the Thaynes Formation.
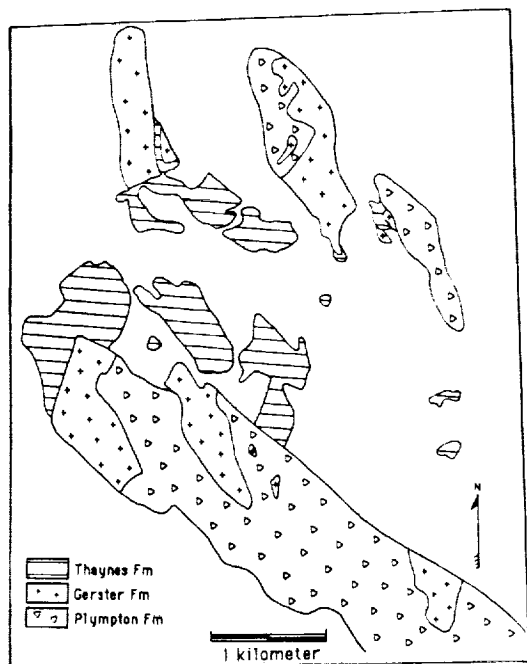
Figure 3. Extent of the dolomite-dominated Plympton, limestone-dominated Gerster, and the Thaynes Formation as mapped in the field.
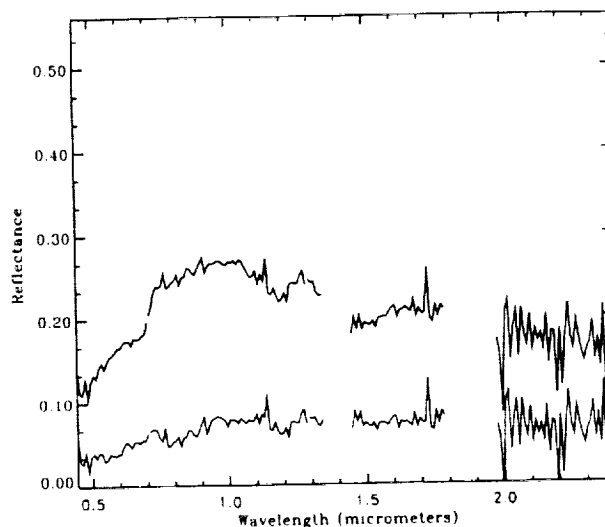
Figure 4. Comparison of AVIRIS reflectance spectra before (top spectrum) and after (bottom spectrum) vegetation subtraction.

Mapping the Mineralogy and Lithology of Canyonlands, Utah with Imaging Spectrometer Data and the Multiple Spectral Feature Mapping Algorithm

Roger N. Clark, Gregg A. Swayze, and Andrea Gallagher

U. S. Geological Survey, MS 964
Box 25046 Federal Center
Denver, Colorado 80225

The sedimentary sections exposed in the Canyonlands and Arches National Parks region of Utah (generally referred to as "Canyonlands") consist of sandstones, shales, limestones and conglomerates. Reflectance spectra of weathered surfaces of rocks from these areas show two components: 1) variations in spectrally detectable mineralogy and 2) variations in the relative ratios of the absorption bands between minerals. Both types of information can be used together to map each major lithology and we are applying the Clark *et al.* (1990, 1991) spectral features mapping algorithm to do the job.

AVIRIS was flown over Upheaval Dome in Canyonlands National Park and over Arches National Park in May 1991. The data were calibrated to ground reflectance using multiple ground calibration sites to derive the offset due to path radiance as well as a set of multipliers to correct to ground reflectance. The resulting data set (about 11 km wide by 30 km in length for each of two flight lines) shows reflectance spectra of well exposed sedimentary units. Several vegetation communities, microbiotic soils, lichens, and desert varnish are also present and add to the difficulty of mapping lithologies.

In the Canyonlands region, several formations of Pennsylvanian through Cretaceous age are exposed (Table 1). Many of the same minerals are present in the different formations, with variable band strengths, usually related to abundance changes. Mapping these different lithologies requires not only the detection of the individual minerals but also their relative proportions. Such analysis can be accomplished by mapping specific minerals (e.g. Clark et al. 1990, 1991) and examining the ratios of the band depths of indicator minerals. Another approach is to use spectra representative of each unit as a reference spectrum. The minerals in these spectra display absorption bands in their different proportions, and the "Multiple Spectral Feature Mapping Algorithm" weights each feature according to the

area between the continuum and the reflectance curve, thus
restricting allowable mineralogy. Examples of the success
of this method in mapping the above units will be presented.

                      Table 1
        Detectable (0.4-2.5 μm) Mineralogy of Geologic
        Formations in Canyonlands, Utah, as Indicated by
                Reflectance Spectroscopy

Mancos Shale:	(S) calcite	(M) kaolinite	
	(W) gypsum	(t) goethite	
Dakota Sandstone:	(M) illite	(M) goethite	
	(W) kaolinite	(t) calcite	
Morrison Formation:	(S) Fe-illite	(M) Chert	
	(M) hematite	(W) calcite	
	(W) V-illite		
Entrada Sandstone:	(M) kaolinite	(M) hematite	
Navajo Sandstone:	(M) hematite	(t) kaolinite	
	(M) illite/smectite		
Kayenta Formation:	(M) hematite	(M) calcite	
	(t) kaolinite		
Wingate Sandstone	(S) hematite	(M) kaolinite	
	(W) muscovite		
Chinle Formation	(S) muscovite	(S) hematite	
	(W) kaolinite	(W) calcite	
Moenkopi Formation	(M) hematite	(M) muscovite	
	(W) kaolinite	(t) calcite	
Cutler Formation	(S) kaolinite	(W) goethite	
	(t) calcite		
Paradox Formation	(S) illite/smectite		
	(M) goethite	(M) Gypsum	

Spectral band intensity:
(S)= strong, (M)= medium, (W)= weak (t)= trace

References

Clark, R.N., A.J. Gallagher, and G.A. Swayze, Material Absorption Band Depth Mapping of Imaging Spectrometer Data Using a Complete Band Shape Least-Squares Fit with Library Reference Spectra, *Proceedings of the Second Airborne Visible/Infrared Imaging Spectrometer (AVIRIS) Workshop*. JPL Publication 90-54, 176-186, 1990.

Clark, R.N., G.A. Swayze, A. Gallagher, N. Gorelick, and F. Kruse, Mapping with Imaging Spectrometer Data Using the Complete Band Shape Least-Squares Algorithm Simultaneously Fit to Multiple Spectral Features from Multiple Materials, *Proceedings of the Third Airborne Visible/Infrared Imaging Spectrometer (AVIRIS) Workshop*, JPL Publication 91-28, 2-3, 1991.

SPATIAL RESOLUTION AND CLOUD OPTICAL THICKNESS RETRIEVALS

Rand E. Feind, Sundar A. Christopher and Ronald M. Welch

Institute of Atmospheric Sciences
South Dakota School of Mines and Technology
501 E. St. Joseph Street
Rapid City, South Dakota 57701-3995

1. INTRODUCTION

In this study, we investigate the impact of sensor spatial resolution and accurate cloud pixel identification on cloud property retrievals. Twelve fair weather cumulus (FWC) scenes of high spectral and spatial resolution Airborne Visible and Infrared Imaging Spectrometer (AVIRIS) data are analyzed. A variation of the 3-band ratio technique of Gao and Goetz is used to discriminate clouds from the background, and then a discrete ordinate radiative transfer model is used to obtain optical thickness of cloudy regions for each scene. To study the effect of spatial resolution upon retrieved optical thickness, the 20 m AVIRIS data was spatially degraded to spatial resolutions ranging from 40 to 960 m. Cloud area, scene average optical thickness, and distribution of retrieved optical thickness are determined at each spatial resolution. Finally, a comparison between the 3-band ratio technique and monospectral reflectance thresholding, using 20 m spatial resolution data, is presented.

2. METHODOLOGY

Gao and Goetz (1991) developed a method that takes advantage of high spectral resolution imagery and greatly facilitates the ability to distinguish between cloud and background pixels. The method for cloud pixel identification employs a 3-band ratio and is computed as the sum of the radiance from the imagery at 0.94 and 1.14 μm divided by twice the radiance at 1.04 μm. In the 3-band ratio imagery, the land background is somewhat homogenized, while the clouds retain their features. Identification of cloud pixels at a non-absorbing wavelength (such as 0.74 μm) is a three-step process: 1) the selection of a threshold for water/shadow background areas; 2) the selection of a 3-band ratio threshold in the 3-band ratio image; and 3) the application of a cloud pixel mask (determined by the first two steps) to the appropriate wavelength imagery.

Each cloud pixel in the masked 0.74 μm radiance image is assigned one of 18 different optical thickness values based on the results of a discrete ordinate radiative transfer model (Stamnes et al., 1988). Lower spatial resolution instrument imagery is emulated through spatial averaging of the 20 m AVIRIS data. Three-band ratio masks are obtained at lower spatial resolutions and are applied to like imagery at 0.74 μm. Estimates of average optical thickness and cloud area are then obtained at all spatial resolutions.

3. RESULTS

Figure 1 shows the percent change in cloud area as a function of spatial resolution for the 12 images used in this investigation. There is a large dependence upon spatial resolution. Of interest is the fact that there is a great deal of scatter in the

results, especially as spatial resolution is degraded, suggesting no precise way to correct for these errors. The effect of spatial resolution upon cloud average optical thickness retrieval is shown in Fig. 2. The results are expressed in terms of the percent change in average cloud optical thickness, relative to 20 m resolution imagery, as a function of spatial resolution. Figure 2 shows that cloud optical thickness decreases monotonically with decreasing spatial resolution. Figure 3 shows the product of optical thickness and cloud area as a function of spatial resolution. One would expect the curves to be relatively flat and they are relatively flat out to spatial resolutions on the order of 300 m; however, the curves still decrease with decreasing spatial resolution.

Histograms of cloud optical thickness for one of the analyzed scenes appear in Fig. 4. It shows that the distribution of cloud optical thickness changes with spatial resolution; however, it does not change in a predictable manner. Perhaps the most notable trend is that the frequency of occurrence of the largest values of optical thickness decreases with decreasing spatial resolution.

We examine the consequences upon cloud optical depth retrieval when applying simple reflectance thresholds. First we compute the monospectral (0.74 μm) reflectance threshold which produces the same cloud area as obtained by the 3-band ratio technique. The results for the 12 scenes, in % above background albedo, are as follows: A - 3.2, B - 5.5, C - 4.1, D - 4.3, E - 3.2, F - 4.5, G - 5.8, H - 3.1, I - 8.4, J - 8.0, K - 3.7, L - 5.0. These results indicate that the required reflectance threshold is scene dependent. Shown in Fig. 4 is the impact of assigning a monospectral reflectance for optical thickness retrievals. The optical thickness histogram is shown for both the 3-band ratio technique and for the aforementioned monospectral reflectance thresholds. Differences in the optical thickness retrievals are found in the optically thinner areas of the cloud, t < 4. These differences are found at all spatial resolutions. In addition, the distribution of gray levels for cloud edges is determined by histogramming the edge maps of the masked 0.74 μm images. Results (not presented herein) show that the distributions are relatively broad (approximately 10% of the available scene reflectance), indicating that a single monospectral reflectance threshold is inadequate for identifying cloud edge pixels.

4.   CONCLUSIONS

The present results demonstrate that both spatial and spectral resolution significantly impact our ability to retrieve cloud optical thickness properties accurately. Decreasing spatial resolution from 20 m to 960 m dramatically affects estimates of cloud area, average optical thickness, and the distribution of retrieved optical thickness. The change in these estimates with change in spatial resolution is scene dependent. It is shown that some of the error in estimates for average optical thickness is due to the error in estimates of cloud area; however, when the effect of increasing cloud area with decreasing spatial resolution is removed, average optical thickness still decreases with decreasing spatial resolution. It is also shown that the use of a single, monospectral reflectance threshold is inadequate for identifying cloud pixels in FWC scenes, pointing to the necessity of using high spectral resolution data, combined with appropriate processing algorithms. In a monospectral image, not only is the optimum threshold (with respect to background albedo) scene dependent, but also the edge around a single cloud cannot be located by using a single threshold. Although cloud edges are, in general, optically thin, they can significantly impact estimates of average optical thickness. These results have potentially important consequences because most commonly used cloud retrieval algorithms apply a single reflectance threshold.

As a caveat, it should be noted that the results reported here are only for FWC over land, perhaps one of the most difficult cloud types to retrieve accurately using satellite imagery. Obviously, stratiform cloud properties are retrieved with far greater certainty. Nevertheless, even a cursory examination of a GOES image demonstrates that a large fraction of cloudiness is inhomogeneous. Problems with correct cloud edge identification and spatial resolution can be expected for all inhomogeneous cloud fields.

REFERENCES

Gao, B. C. and Goetz, A. F. H., "Cloud area determination from AVIRIS data using water vapor channels near 1 mm," *J. Geophys. Res.* vol. **96**, no. D2, pp. 2857-2864, 1991.

Stamnes, K., Tsay, S. C., Wiscombe, W., and Jayaweera, K., "A numerically stable algorithm for discrete-ordinate-method radiative transfer in multiple scattering and emitting layered media," *Appl. Opt.*, vol. **17**, pp. 2502-2509, 1988.
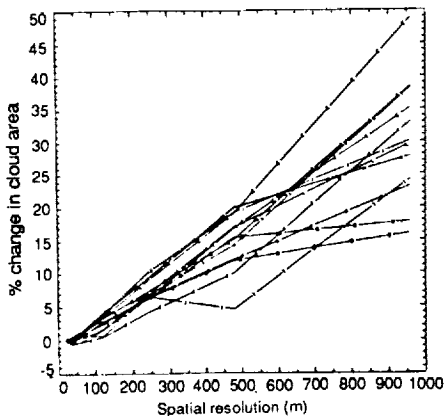
Fig. 1: Percent change in cloud cover, referenced to 20 m resolution, as a function of spatial resolution for the 12 scenes.
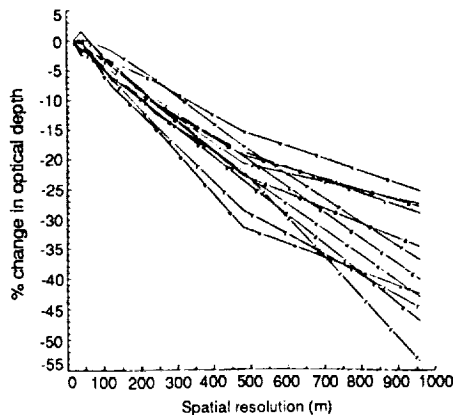
Fig. 2: Percent change in cloud average optical thickness, referenced to 20 m resolution, as a function of spatial resolution.
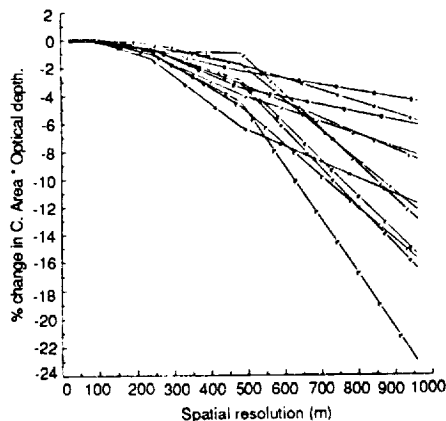
Fig. 3: Percent change in the product of cloud area and cloud optical thickness, referenced to 20 m resolution, as a function of spatial resolution.
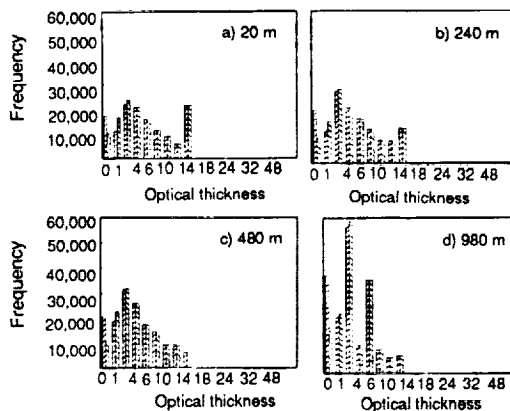
Fig. 4: Frequency distribution of cloud optical thickness for spatial resolutions of A) 20 m; B) 240 m; C) 480 m; and D) 960 m. ▨ denote the 3-band ratio results, and the ▨ denote results for a reflectance threshold of 4.95 above background.

16

EVALUATION OF SPATIAL PRODUCTIVITY PATTERNS IN AN ANNUAL GRASSLAND DURING AN AVIRIS OVERFLIGHT*

John A. Gamon[1], Christopher B. Field[2] and Susan L. Ustin[3]

[1]California State University, Los Angeles
5151 State University Drive
Los Angeles, CA 90032

[2]Carnegie Institution of Washington
Department of Plant Biology
290 Panama Street
Stanford, CA 90035

[3]Department of Land, Air and Water Resources
University of California, Davis
Davis, CA 95616

1. BACKGROUND

In May, 1991, coincident with an AVIRIS overflight, we completed a ground-based study covering 9 hectares of an annual grassland. There were two goals to this ground study:

1) Obtain ecologically and physiologically meaningful data for relating AVIRIS images to canopy structure, biochemistry and physiology.

2) Evaluate the suitability of the 20-m AVIRIS pixel size for depicting detailed spatial patterns of productivity.

2. MATERIALS AND METHODS

A 9-hectare annual grassland at Stanford University's Jasper Ridge Biological Preserve was sampled every 20 m for biomass, leaf area index (LAI), intercepted photosynthetically active radiation (PAR), chlorophyll, nitrogen, surface temperature and spectral reflectance. These measurements coincided with the May 14 and 15, 1991, AVIRIS overflights, providing a basis for biological interpretations of the AVIRIS images. Measurements of photosynthetic fluxes by eddy correlation were also completed during the overflight.

Three 20x20 m pixels were chosen for detailed ground sampling (every 5-m). The goal was to evaluate the 20-m AVIRIS pixel size by examining the semivariance in productivity estimates as a function of between-sample distance.

3. RESULTS

Images derived from ground-based measurements at the 20-m scale depict the influence of topography, soil and vegetation type on productivity in the grassland (Fig. 1). Preliminary geostatistical tests of the ground data also indicate that the 20-m between-sample distance (comparable to the AVIRIS pixel size) is suitable for studying spatial productivity patterns in this relatively uniform grassland. Different results might have been obtained if the study had been conducted on adjacent chaparral and woodland,

---

composed of complex mosaics of individual canopies 1-10 meters in diameter.

Good correlations were obtained between ground-based reflectance indices (SR and NDVI) and several ecologically or physiologically significant indicators of productivity, including biomass, LAI, canopy chlorophyll and nitrogen content (Fig. 2). Ground data will be compared with endmember and residual images derived from mixture models to estimate productivity patterns from AVIRIS images (Ustin et al., this volume).

Results from this study will be compared with AVIRIS images obtained at other dates and at other sites and will be compared to CO_2 flux measurements that were made concurrently with the overflight. These studies should assist in development and validation of ecological and physiological models for AVIRIS image interpretation.

4. ACKNOWLEDGEMENTS
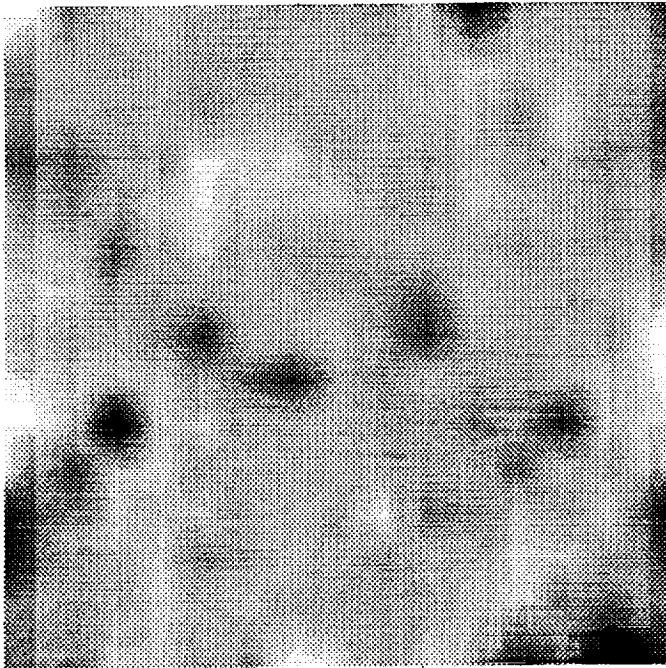
Fig. 1.

Interpolated image derived from ground-based LAI measurements of 9 hectares of the Jasper Ridge grassland at a 20-m sampling distance. LAI values ranged from 0.1 (light) to 3.5 (dark). Low-productivity areas are either hilltops or regions of serpentine-derived soil. High productivity areas are valley bottoms or patches with perennial vegetation.
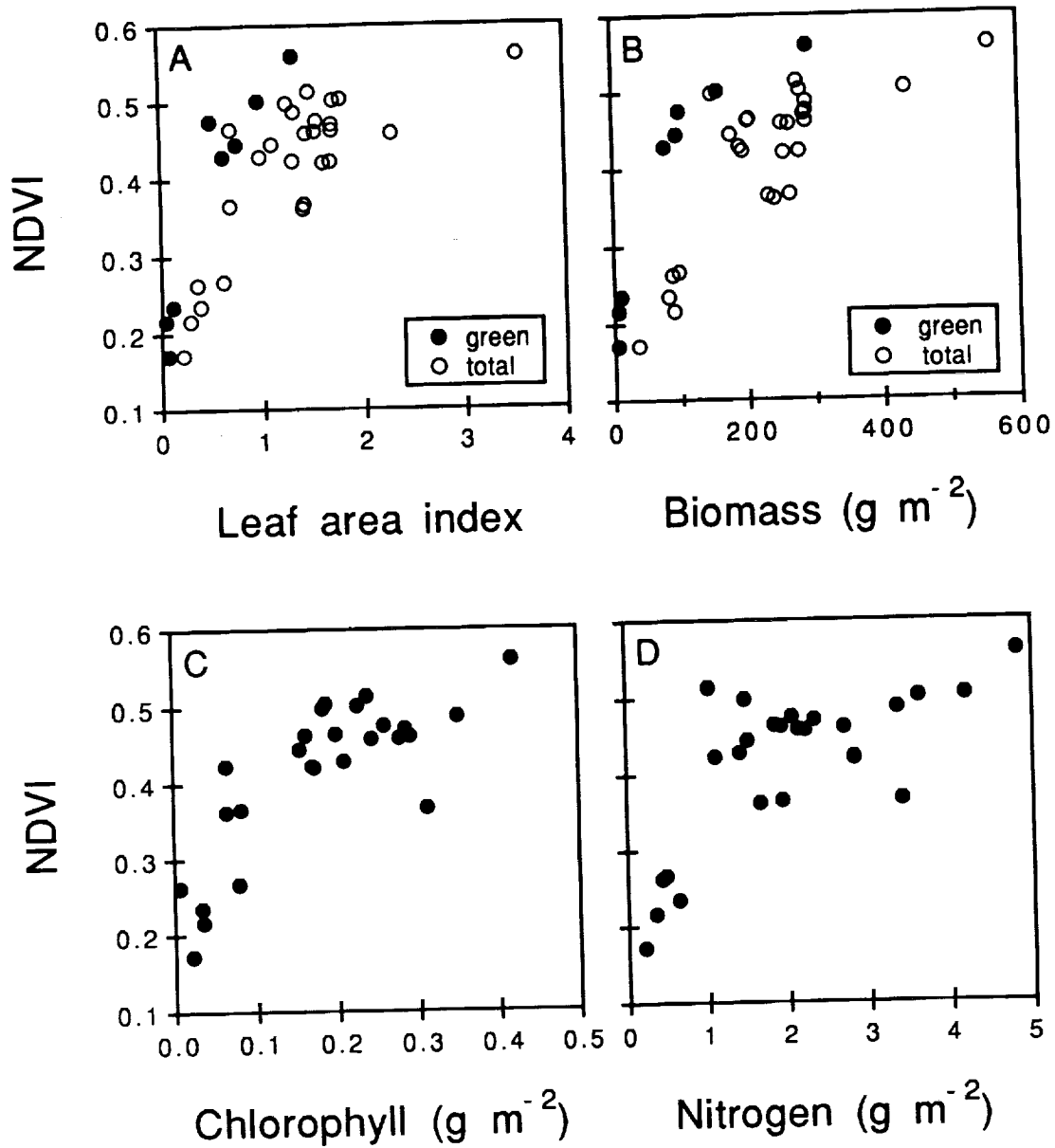
Fig. 2.

Relationships between NDVI and indicators of canopy structure (A and B) or total canopy chlorophyll (C) and nitrogen (D). Correcting for canopy "greenness" improves the correlations (A and B) and indicates the presence of standing dead biomass.

HYPERSPECTRAL MODELING FOR EXTRACTING AEROSOLS FROM AIRCRAFT/SATELLITE DATA

G. DANIEL HICKMAN
NAVAL RESEARCH LABORATORY
CODE 321
STENNIS SPACE CENTER, MS   39529-5004
AND
MICHAEL J. DUGGIN
STATE UNIVERSITY OF NEW YORK
SYRACUSE, NY   13210

1.0   INTRODUCTION:

The upwelling radiance due to aerosols (L_A) detected by satellite sensors is related to the aerosol optical depth (δ_A) through the approximation given by Durkee, 1984, equation (1).

$$L_A = \frac{\omega_o F_o}{4\cos\phi} \, P(\theta) \cdot \delta_A \tag{1}$$

where

ω_o = *SINGLE SCATTERING ALBEDO*

ϕ = *SATELLITE ZENITH ANGLE*

$P(\theta)$ = *SCATTERING PHASE FUNCTION AT ANGLE θ*

F_o = *INCIDENT SOLAR IRRADIANCE*

The above equation is valid for relatively thin optical depths (<0.3). Also, to first approximation L_A is approximately linear with (δ_A). The value of $P(\theta)$ is dependent upon the size and distribution of the aerosol particles (given in part by the ratio S_{12} identified below).

Currently the National Oceanic and Atmospheric Administration (NOAA) uses channel 1 (0.58 – 0.68 μm) of the Advanced Very High Resolution Radiometer (AVHRR) sensor to produce weekly global maps of aerosol optical depths. Durkee (1984) showed that a measure of the type and distribution of aerosols could be determined by the ratio S_{12} given by equation (2).

$$S_{12} = \frac{L_A \; (Channel \; 1) \; AVHRR}{L_A \; (Channel \; 2) \; AVHRR} \tag{2}$$

where

$$Channel\ 1\ = 0.58 - 0.68\ \mu m$$
$$Channel\ 2\ = 0.725 - 1.10\ \mu m$$

It is noted that the calculations for δ_A and S_{12} are performed after subtraction of the Rayleigh optical depth.

For large values of S_{12} the aerosols are identified as continental origin (high concentration of small particles). For smaller values of S_{12} the aerosols are closer to marine origin (higher concentration of large particles).

2.0 PRESENT RESEARCH

Sensitivity studies using the AVIRIS bands are currently under investigation. The objective of this research is to develop improved algorithms for the determination of aerosol type (e.g., presently described by S_{12}).

Preliminary computer calculations have been made using LOWTRAN 7, which is the most advanced atmospheric code of the Air Force Geophysics Laboratory. LOWTRAN 7 permits the calculation of atmospheric transmission and absorption caused by aerosols and molecules along a non-homogenous path for a variety of aerosol models. The calculations used the Navy Aerosol Model (NAM) (Gathman, 1983), which was constructed for the marine environment using a three component size distribution model.

Calculations of the total transmittance (L_T), the path radiance (L_P) and the reflected radiance (L_r) were made as a function of wavelength (λ) from 0.4 to 2.4 μm for each of the 224 10 nm wide AVIRIS bands. These calculations were made for various types of atmospheres for the troposphere (0-2 km).

3.0 RESULTS

Figure 1 is a typical LOWTRAN 7 curve of upwelling total radiance (surface albedo = 0; 23 km horizontal visibility) at an altitude of 2 km. These curves were generated for the AVIRIS bands for the marine boundary layer of the troposphere using two different aerosol models: a) the Navy aerosol model (NAM) - open ocean type aerosols,

and b) no aerosols. The lower (no-aerosol) curve
shows the typical Rayleigh distribution following
the $1/\lambda^4$ decay, going to zero at approximately 0.9
μm. Superimposed on this curve are the gas
absorption bands. The upper (navy aerosol) curve
shows the combined contribution due to Rayleigh
scattering, gas absorption and aerosols. The
middle curve is the result of subtracting these
two curves. This subtractive technique removes
the Rayleigh scattering, thereby leaving the
radiance due to aerosols. The ratio S_{12} is
calculated after convolving the spectral radiance
with the AVHRR bands. The AVIRIS bands will now
be used in calculations to obtain the optimum band
ratios for describing various types of aerosols.
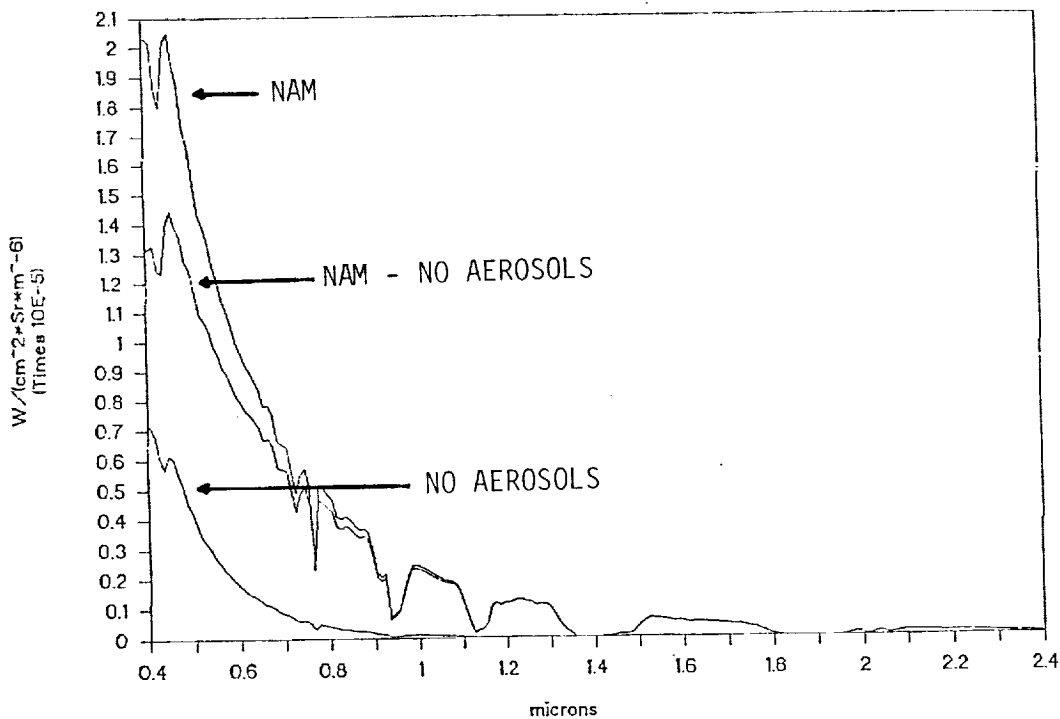
FIG. 1 LOWTRAN CALCULATIONS OF RADIANCE AT ALT =
2KM AND SURFACE ALBEDO = 0 FOR AVIRIS BANDS.

4.0 References:

Durkee, P. A. (1984), The relationship between
marine aerosol particles and satellite-detected
radiance, Ph.D. dissertation, 124pp. Colo. State
University, Fort Collins.

Gathman, Stuart G. (1983), Optical properties of
the marine aerosol as predicted by the Navy
aerosol model, Optical Engineering 22 (1):057-062.

THE SPECTRAL IMAGE PROCESSING SYSTEM (SIPS) - SOFTWARE FOR INTEGRATED ANALYSIS OF AVIRIS DATA

F. A. Kruse [1, 2], A. B. Lefkoff [1], J. W. Boardman [1, 2, 3]
K. B. Heidebrecht [1], A. T. Shapiro [1], P. J. Barloon [1], and A. F. H. Goetz [1, 2]

[1] Center for the Study of Earth from Space (CSES)
Cooperative Institute for Research in Environmental Sciences (CIRES)
University of Colorado, Boulder, Colorado 80309

[2] Department of Geological Sciences
University of Colorado, Boulder, Colorado 80309

1. INTRODUCTION

The Spectral Image Processing System (SIPS) is a software package developed by the Center for the Study of Earth from Space (CSES) at the University of Colorado, Boulder, in response to a perceived need to provide integrated tools for analysis of imaging spectrometer data both spectrally and spatially (Kruse et al., 1992a). SIPS was specifically designed to deal with data from the Airborne Visible/Infrared Imaging Spectrometer (AVIRIS) and the High Resolution Imaging Spectrometer (HIRIS), but has been tested with other datasets including the Geophysical and Environmental Research Imaging Spectrometer (GERIS), GEOSCAN images, and Landsat TM. SIPS was developed using the "Interactive Data Language" (IDL) (Research Systems, 1991). It takes advantage of high speed disk access and fast processors running under the UNIX operating system to provide rapid analysis of entire imaging spectrometer datasets. SIPS allows analysis of single or multiple imaging spectrometer data segments at full spatial and spectral resolution. It also allows visualization and interactive analysis of image cubes derived from quantitative analysis procedures such as absorption band characterization and spectral unmixing. SIPS consists of three modules: SIPS Utilities, SIPS_View, and SIPS Analysis. SIPS version 1.1 is described below.

2. SIPS UTILITIES

The SIPS utilities module contains tools that prepare data for input to SIPS_View, the analysis programs, and other image processing software. These tools are written in IDL and C. Utilities are provided for reading AVIRIS tapes to band sequential (BSQ), band interleaved by pixel (BIP), or band interleaved by line (BIL) format files; creating a wavelength file and a histogram file; calibrating to reflectance; creating spectral libraries; and converting to various output file formats. The utilities all have command line interfaces, and some also have interactive graphical interfaces. A complete list of tools and detailed usage instructions are given in the SIPS User's Guide (CSES 1992).

3. SIPS_VIEW

3.1 GENERAL

SIPS_View is an interactive IDL program that allows the user to visualize and work with imaging spectrometer data both spectrally and spatially. It uses "widgets" such as menus, buttons, and slider-bars along with mouse and keyboard input to create a user-

---

[3] Present address, CSIRO, Division of Exploration Geoscience, N.S.W., Australia 2113

friendly interface. Interaction by the user with a given widget produces an "event" to which the software is able to respond by performing a specific function.

SIPS_View requires a minimum of one image file in any storage order; BSQ, BIP, or BIL. If the same image data is present in more than one storage order, SIPS_View chooses the best file for efficient data extraction. Additional files including wavelength, histogram, bad-bands, and spectral libraries enhance the performance and utility of the program.

3.2 SIPS_VIEW DISPLAY FUNCTIONS

The display functions operate on the image data in its spatial format. The "Image Window" displays the full resolution image in a 512 line x 614 sample window with a default 2% linear contrast stretch applied. The displayed image can be a gray-scale or density-sliced image of a specific band, or a color composite image of three bands. If the image is larger than 512 x 614, SIPS_View displays part of the image at full resolution, and allows scrolling to other parts of the image. Possible actions associated with the Image Window include selecting which band is displayed, selecting the color mode, and saving the current image to a data file or a color PostScript file.

In addition to the main window, SIPS_View creates and manages many other windows throughout its execution. The "Status Window" displays useful information about the current processing status of SIPS_View. The "Zoom Window" contains a subset of the image zoomed from 1 to 16 times. The "Current Spectrum Window" and "Saved Spectra Window" are used for viewing, extracting and saving spectra. Other windows such as "Contrast Stretch", "View Spectra", "Spectral Profiles" and the "SAM Viewer" are created only when accessed by the menu functions.

3.3 SIPS_VIEW SPECTRAL FUNCTIONS

SIPS_View spectral functions are those items that deal with imaging spectrometer data primarily in its spectral format. Spectral functions include browsing, region-of-interest extraction, profile extraction, viewing, and spectral matching.

The browse spectra capability allows the user to roam around the Image window displaying the current spectrum in real-time. The "Class Extraction" function allows the user to interactively define and extract spectral characteristics for user-defined groups of spectra for regions of interest. The mean, standard deviation, minimum, and maximum spectra for each class are displayed in the Saved Spectra window. View Spectra is a utility used for spectral display and analysis. When the View Spectra function is selected, SIPS_View creates a separate window to plot the spectra currently in the Saved Spectra Window as well as access and plot other ASCII and binary library spectra. The user can then manipulate this plot in a number of different ways, produce a PostScript output file of the plot, or import the plotted spectra back into the Saved Spectra Window for subsequent use in other SIPS functions. The "Spectral Angle Mapper" (SAM) is an analysis tool that permits rapid mapping of the spectral similarity of image spectra to reference spectra (Boardman 1992a). The algorithm determines the spectral similarity between two spectra by calculating the "angle" between the spectra, treating them as vectors in a space with dimensionality equal to the number of bands.

4. SIPS ANALYSIS PROGRAMS

The analysis module provides tools that perform complex calculations on an entire image and are too time consuming for interactive use. Currently, only the *unmix* analysis tool which performs linear spectral unmixing is available in this module. A knowledge-based, expert system analysis utility is presently undergoing testing and

revision (Kruse et al., 1992b) and will be released in the next version of SIPS. Other analysis modules are being developed and will be added at a later date.

The SIPS unmixing program, written in IDL, uses a simple linear mixing model. This model assumes that observed spectra can be modeled as linear combinations of endmembers contained in a spectral mixing library (Boardman 1992b). The unmixing approach seeks to determine the fractional abundance of each endmember within each pixel.

5. SOFTWARE AVAILABILITY

SIPS is provided free of charge or royalties. CSES plans, however, to continue development of these programs and retains the title and copyright to the software, documentation, and supporting materials. Recipients of this software are required to execute a Memorandum of Understanding (MOU) provided by CSES that specifies in detail all of the associated conditions. Send requests for an MOU to:

e-mail: sips@cses.colorado.edu
voice: (303) 492-1866
fax: (303) 492-5070

6. ACKNOWLEDGMENTS

7. REFERENCES

Boardman, J. W. (1992a), Spectral angle mapping: a rapid measure of spectral similarity, (in preparation).

Boardman, J. W. (1992b), Sedimentary Facies Analysis Using Imaging Spectrometry: A Geophysical Inverse problem: Remote Sensing of Environment, Special issue on AVIRIS, (in press).

Center for the Study of Earth from Space (CSES), (1992), SIPS User's Guide, The Spectral Image Processing System v. 1.1, 74 p.

Kruse, F. A., Lefkoff, A. B., Boardman, J. B., Heidebrecht, K. B., Shapiro, A. T., Barloon, P. J., and Goetz, A. F. H., 1992a, The Spectral Image Processing System (SIPS) - Interactive Visualization and Analysis of Imaging Spectrometer Data: Remote Sensing of Environment, Special issue on AVIRIS, (in press)

Kruse, F. A., Lefkoff, A. B., and Dietz, J. B. ,1992b, Expert-system based mineral mapping in northern Death Valley, California/Nevada using the Airborne Visible-Infrared Imaging Spectrometer (AVIRIS): Remote Sensing of Environment, Special issue on AVIRIS, (in press).

Research Systems, Inc. (1991), IDL® User's Guide Version 2.2.

FIRST RESULTS FROM ANALYSIS OF COORDINATED AVIRIS, TIMS, AND ISM (FRENCH) DATA FOR THE RONDA (SPAIN) AND BENI BOUSERA (MOROCCO) PERIDOTITES

J. F. MUSTARD[1], S. HURTREZ[2], P. PINET[3], AND C. SOTIN[2]

1) DEPT. GEOL. SCI., BOX 1846, BROWN UNIVERSITY, PROVIDENCE RI, 02912
2) LAB.DE GEOPHYSIQUE, UNIVERSITE DE PARIS-SUD, 91405, ORSAY FRANCE
3) GRGS/OBSERVATOIRE MIDI PYRENEES, 14 AV. EDUARD BELIN, 31400 TOULOUSE FRANCE

Introduction

Ultramafic rocks are relatively rare at the Earth's surface but constitute the vast majority of the Earth by volume. Exposures of ultramafic bodies are therefore crucial for deducing many important processes that occur in the Earth's mantle. An important science question regarding the spatial distribution, abundance, and composition of mafic minerals in ultramafic bodies that can be examined with advanced sensor data is the melting process. When a lherzolite melts, clinopyroxene (cpx) melts first and therefore variations in the modal amount of cpx remaining in the mantle are a reflection of the amount of fractional melting that has occurred. Fe goes preferentially into the melt during melting but a 20% batch melting (i.e. closed system) acquires less Fe relative to 20% fractional melting (i.e. open system). Since the strength and wavelength of diagnostic absorptions is a strong function of Fe content, it is possible to make maps of the variation in Fe:Mg ratios which can be related to the general melting process. Accurate ground-truth information about local mineralogy provides internal calibration and consistency checks. Investigations using imaging spectrometer are very complementary to field studies because advanced sensor data can provide a synoptic view of modal mineralogy and chemical composition whereas field studies focus on detailed characterization of local areas.

Two excellent exposures of ultramafic lithologies are being investigated with visible to mid-infrared imaging spectrometer data: the Ronda peridotite near Ronda, Spain and the Beni Bousera ophiolitic fragment in northern Morocco (Figure 1a). Although separated by the Alboran Sea, these bodies are thought to be related (Bonini et al, 1973, Frey et al, 1985) and represent fertile sub-continental mantle. The Ronda peridotite, shown in Figure 1b, is predominantly spinel lherzolite but grades into harzburgite and shows considerable variation in major and trace element compositions (Frey et al., 1985). Mafic layering and dykes (i.e. olivine gabbro) are also observed. This indicates some sections of the peridotite have experienced greater degrees of partial melting. The Beni Bousera peridotite, shown in Figure 1c, also contains mafic layers and dykes and grades into harzburgite representing similar fundamental shifts in the bulk chemistry of this ultramafic body probably related to an episode of partial melting (Lorand, 1985). The specific mode of emplacement of these bodies is controversial (allocthonous thrust related bodies, Frizon de Lamotte et al, 1990: mantle core complexes, Doblas and Oyazun, 1989; 1990) and important for understanding the tectonic evolution of this region. Our investigations are not necessarily designed to help resolve this controversy. Rather, these exposures provide excellent and unusual examples of fertile mantle which have undergone variable degrees of partial melting.

ISM-AVIRIS Cross Calibration

A significant aspect of the European deployment of the NASA aircraft is the unique opportunity for cross calibration of the ISM and AVIRIS sensors. ISM data were obtained over the Ronda peridotite in July 1991, two weeks before the AVIRIS flight, and were also obtained over the Beni Bousera peridotite. However NASA chose not to fly over any targets in Africa during this deployment. The ISM instrument contains two

arrays of 64 PbS detectors each for the 0.76 to 1.51 μm and 1.63 to 3.16 μm wavelength regions which have spectral resolutions of 12.5 and 24 nm respectively. The instrument has an IFOV of 10' cross track and 40' along track. From a typical flight altitude of 6000 meters this translates to a pixel size of 18 x 75 meters. The scanning mirror has a displacement of ±20° which corresponds to a 4.5 km swath from 6000 meters. Although the instrument is not directly comparable to AVIRIS in spectral and spatial resolution, the predicted signal to noise of ISM is ~500:1 with a 50% reflective target and the ISM wavelength range extends to longer wavelengths. Therefore these instruments have important complementary characteristics.

Data Reduction and Analysis

The calibration and reduction of the AVIRIS, TIMS, and ISM data is just beginning but will proceed in a series of well defined steps. Upon acquisition of AVIRIS data tapes from JPL all bands will be inspected for data quality and channels with unacceptably low signal to noise levels (less than 40:1 for spectrometers A, B, C, and less than 20:1 for spectrometer D) will be identified and removed from the analysis. The precise ground coverage will be determined and a library of field and laboratory spectra for these areas will be assembled for reference. Additional spectra from the extensive RELAB library established in previous investigations (i.e. Moses Rock Dike, Kings-Kaweah ophiolite melange) which are pertinent to this investigation will be included. A sub area from each field site containing several homogeneous targets will be selected for initial calibration and a linear mixing analysis of the raw data will be performed to determine the dimensionality of the raw data. The image endmembers determined from this analysis will be passed through the spectral library to determine a set of gains and offsets to calibrate the raw data to reflectance (e.g. Smith et al, 1990). Estimates of atmospheric scattering determined with the field spectrometer will be compared to the offsets determined by this method. The calibrated AVIRIS data will then be inspected to validate the calibration procedure and compared to field and laboratory spectra. Once we are satisfied with the calibration we will expand the analysis to the entire field site at both locations.

TIMS data are a measure of the surface temperature in the 8-12 μm region. Preliminary analysis of the standard decorrelation stretched images clearly distinguishes the mafic, ultramafic, and felsic rock types exposed in the Ronda peridotite. However, emittance is the parameter that is desired. This will be estimated by assuming an emittance of 0.93 for channel 6 of TIMS (approximately 11.5 μm) for silica rich targets or channel 1 for silica poor targets. Using these assumptions, an estimate of the surface temperature at the other wavelengths can be calculated and the emittance is the difference between the estimated temperature and the TIMS data. This calibration process reduces the number of TIMS channels from 6 to 5. The calibrations will be checked to establish that topography, slope, and other local surface temperature effects are completely removed. These data will then be co-registered with the AVIRIS data.

Cross-calibration of the NASA acquired AVIRIS data with the ISM data acquired by CNES is an important part of this investigation. The ISM data are complementary to the AVIRIS data. Although AVIRIS has a higher spectral resolution (approx. 9.75 nm between 0.4 and 2.45 μm) than ISM (approx. 12.5 between 0.76 and 1.51 μm: 24 nm between 1.63 and 3.16 μm), the signal to noise anticipated from ISM is very high (>500:1). Also, since the spectral range of ISM extends to 3.16 μm, the spectral range of AVIRIS can be extended to the saturated atmospheric water band near 2.7 μm. The ISM instrument is configured with a comparable spatial resolution to AVIRIS from a 6000 meter altitude and data were collected over the Ronda and Beni Bousera peridotites in July of 1991. These data are currently being calibrated in France using internal calibration sources. The AVIRIS and ISM data will then be co-registered and the two calibrations evaluated. Drawing on the strengths of each instrument (higher spectral resolution, greater visible coverage of AVIRIS: higher signal to noise and extended wavelength range

of ISM) we will converge on a consistent set of calibration parameters and a greater understanding of the two instruments.

References

Bonini, W. E., T. P. Loomis, and J. D. Robertson, Gravity anomalies, ultramafic intrusions, and the tectonics of the region around the Strait of Gibraltar, *J. Geophys. Res.*, 78, 1372-1382, 1973.

Doblas, M, and R. Oyarzun, "Mantle core complexes" and Neogene extensional detachment tectonics in the western Betic Cordilleras, Spain: An alternative model for the emplacement of the Ronda peridotite, *Earth Planet. Sci. Letters*, 93, 76-84, 1989.

Doblas, M, and R. Oyarzun, Comment and reply on "Neogene extensional collapse in the western Mediterranean (Betic-Rif Alpine orogenic belt): Implications for the genesis of the Gibraltar Arc and magmatic activity", *Geology* 18, 381-382, 1990.

Frey, F. A., C. J Suen, and H. W. Stockman, The Ronda high temperature peridotite: Geochemistry and petrogenesis, *Geochem. Cosmo. Acta.*, 49, 2469-2491, 1985.

Frizon de Lamotte, D., J-C. Guezou, J. Andrieuz, M-A. Albertini, M. Coulon, A. Poisson, Comment and reply on "Neogene extensional collapse in the western Mediterranean (Betic-Rif Alpine orogenic belt): Implications for the genesis of the Gibraltar Arc and magmatic activity", *Geology* 18, 381-382, 1990.

Lorand, J. P., The behavior of the upper mantle sulphide component during incipient alteration of "Alpine"-type peridotites as illustrated by the Beni Bousera (north Morocco) and Ronda (southern Spain) ultramafic bodies, *Tschermaks. Min. Petr. Mitt.*, 34, 183-209, 1985.

Smith, M. O, S. L. Ustin, J. B. Adams, and A. R. Gillespie, Vegetation in deserts: I. A regional measure of abundance from multispectral images, *Remote Sens. Environ.* 31, 1-26, 1990.
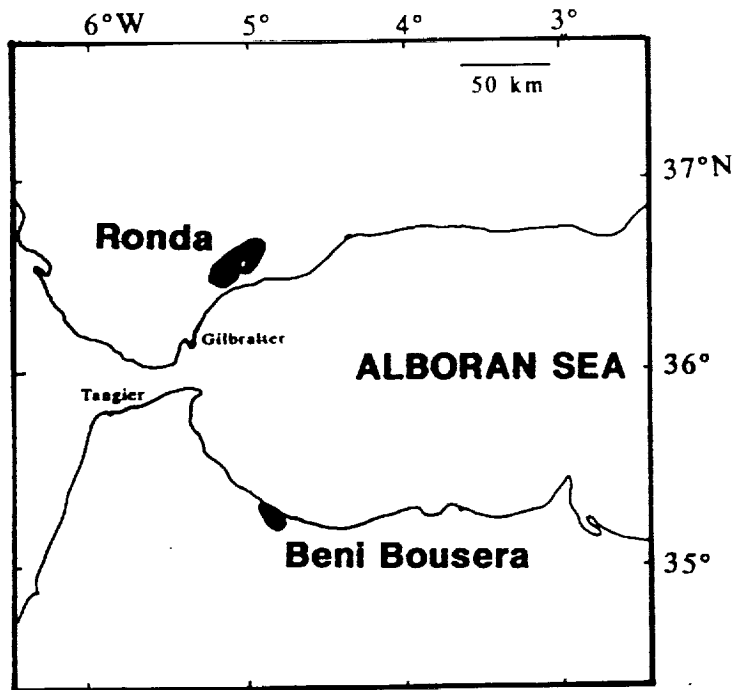
Figure 1. Generalized location map for the Ronda and Beni Bousera peridotite bodies.

AVIRIS STUDY OF DEATH VALLEY EVAPORITE DEPOSITS USING LEAST-SQUARES BAND-FITTING METHODS

By J.K. Crowley[1] and R.N. Clark[2]

[1] U.S. Geological Survey, 927 National Center
Reston, Virginia 22092

[2] U.S. Geological Survey, Box 25046 Federal Center
Denver, Colorado 80225

1. INTRODUCTION

Minerals found in playa evaporite deposits reflect the chemically diverse origins of ground waters in arid regions. Recently, it has been discovered that many playa minerals exhibit diagnostic visible and near-infrared (0.4-2.5 μm) absorption bands that provide a remote sensing basis for observing important compositional details of desert ground water systems (Crowley, 1991). The study of such systems is relevant to understanding solute acquisition, transport, and fractionation processes that are active in the subsurface. Observations of playa evaporites may also be useful for monitoring the hydrologic response of desert basins to changing climatic conditions on regional and global scales. This paper describes ongoing work using Airborne Visible/Infrared Imaging Spectrometer (AVIRIS) data to map evaporite minerals in the Death Valley salt pan. The AVIRIS data point to differences in inflow water chemistry in different parts of the Death Valley playa system and have led to the discovery of at least two new North American mineral occurrences.

Seven segments of AVIRIS data were acquired over Death Valley on July 31, 1990, and were calibrated to reflectance by using the spectrum of a uniform area of alluvium near the salt pan. The calibrated data were subsequently analyzed by using least-squares spectral band-fitting methods, first described by Clark and others (1990). In the band-fitting procedure, AVIRIS spectra are fit compared over selected wavelength intervals to a series of library reference spectra. Output images showing the degree of fit, band depth, and fit times the band depth are generated for each reference spectrum. The reference spectra used in the study included laboratory data for 35 pure evaporite minerals (Crowley, 1991) as well as several vegetation and rock spectra extracted from the AVIRIS image cube. Additional details of the band-fitting technique are provided by Clark and others elsewhere in this volume.

2. RESULTS AND DISCUSSION

Playa minerals occur under a broad range of moisture conditions and accordingly present special remote sensing problems. In particular, it is necessary to distinguish water coatings on grain surfaces from water that is structurally bound in different mineral species. The band-fitting technique can be used to make this distinction for a number of strongly hydrated minerals by examining the shape and position of a reflectance maximum observed near 1.66 μm. Figure 1 shows laboratory spectra in the 1.5- to 1.8- μm wavelength interval for the hydrate minerals antarcticite (CaCl$_2$.6H$_2$O), bischofite (MgCl$_2$.6H$_2$O), and mirabilite (Na$_2$SO$_4$.10H$_2$O) and for anhydrous halite (NaCl). All the samples consist of coarse (~250 μm) powders, and a small amount of water was added to slightly dampen the halite (dry halite is spectrally featureless). The reflectance maximum in mirabilite and bischofite occurs at longer wavelengths and is

narrower than the halite+water feature. The antarcticite reflec-
tance peak lies near the halite+water feature position but again
is somewhat narrower. At Death Valley, mirabilite has been
mapped successfully by careful analysis of the 1.66 μm reflec-
tance feature in the AVIRIS data. Antarcticite and bischofite
were not expected to occur in Death Valley and do not appear to
be present.
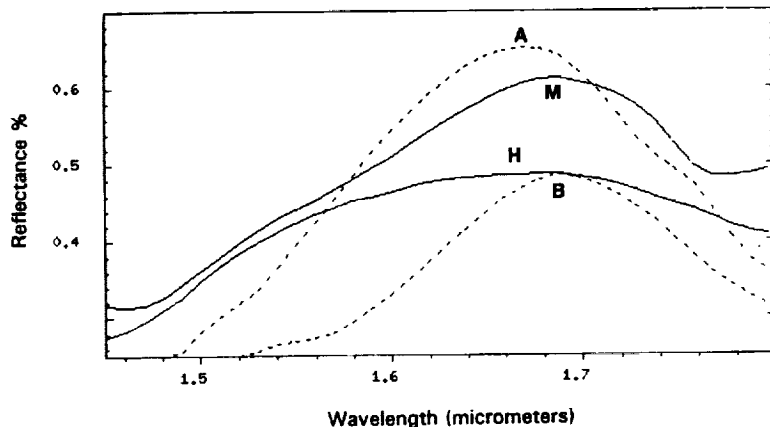
Figure 1. Laboratory reflectance spectra of antarcticite (A),
bischofite (B), mirabilite (M), and damp halite (H).

Reflectance maxima and minima can also be used in combin-
ation to aid in identifying evaporite species. For example,
owing to the signal-to-noise limitations of the AVIRIS "D"
spectrometer, gypsum was not mapped accurately when using only
the gypsum 2.2-μm absorption feature in the band-fitting proce-
dure. However, good mapping results were obtained with the
band-fitting method by using the 2.2-μm band minimum together
with the reflectance maximum near 2.1 μm.

Six different evaporite minerals have been mapped in the
Death Valley salt pan with a reasonable degree of confidence.
The minerals are bloedite ($Na_2Mg(SO_4)_2 \cdot 4H_2O$), gypsum ($CaSO_4 \cdot 2H_2O$),
halite, syngenite ($K_2Ca(SO_4)_2 \cdot H_2O$), rivadavite ($Na_6MgB_{24}O_{40} \cdot 22H_2O$),
and mirabilite. X-ray diffraction analyses of efflorescent crust
samples collected near the old Eagle Borax works indicate the
occurrence of rivadavite and pinnoite ($MgB_2O_4 \cdot 3H_2O$), two rare
magnesium borate minerals. Both minerals are spectrally distinc-
tive (Fig. 2), and neither has been previously reported to occur
in North America.
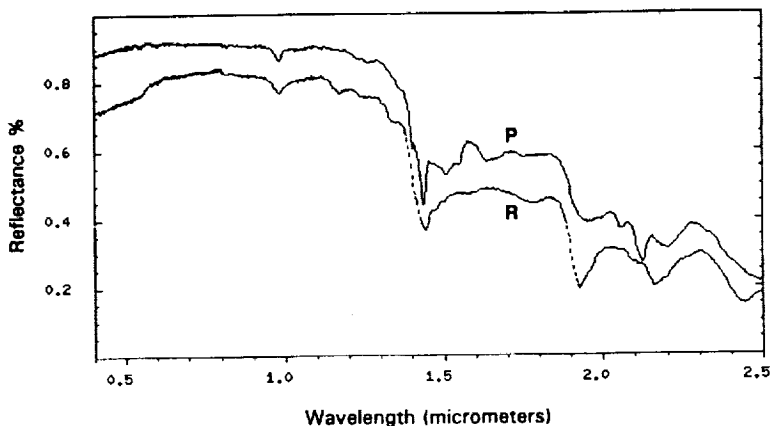
Figure 2. Laboratory spectra of rivadavite (R) and pinnoite
(P).

The Eagle Borax area is one of several spring deposits located along the margins of the Death Valley salt pan. Active springs in Death Valley typically have well-developed efflorescent crusts and mineral assemblages that reflect the water compositions. For example, springs that are relatively low in calcium exhibit thenardite (Na_2SO_4) and mirabilite-rich efflorescent crusts, whereas higher calcium inflow waters generate gypsum-rich crusts. The evaporite assemblages at springs can be quite complex, as at Eagle Borax, where bloedite, gypsum, eugsterite ($Na_4Ca(SO_4)_3 \cdot 2H_2O$), thenardite/mirabilite, rivadavite, and pinnoite occur in various combinations. All of these minerals exhibit diagnostic VNIR spectral bands, and a spectral unmixing study of this area may result in better definition of the mineral distributions. Given the difficulty in studying such deposits with traditional sampling techniques, we believe that the detailed spatial/spectral information provided by imaging spectrometry will improve understanding of evaporite minerals and associated ground water processes in Death Valley and in other arid regions.

3. REFERENCES

Clark, R.N., Gallagher, A.J., and Swayze, G.A., 1990, Material absorption band depth mapping of imaging spectrometer data using a complete band shape least-squares fit with library reference spectra, in Proceedings of the Second Airborne Visible/Infrared Imaging Spectrometer (AVIRIS) Workshop, June 4-5, 1990: Jet Propulsion Laboratory Publication 90-54, p. 176-186.

Crowley, J.K., 1991, Visible and near-infrared (0.4-2.5 μm) reflectance spectra of playa evaporite minerals: Journal of Geophysical Research, v. 96, p. 16231-16240.

A FIELD MEASURE OF THE "SHADE" FRACTION

Alan R. Gillespie, Milton O. Smith and Donald E. Sabol
Department of Geological Sciences, AJ-20
University of Washington
Seattle, WA 98195

"Shade" has a technical definition peculiar to linear spectral mixture analysis of imaging spectrometer data: it is the reduction in radiance from a surface due to lighting conditions and geometry, and includes topographic shading described by photometric functions as well as shadowing at all scales. "Shade" is an important constituent of nearly all remotely sensed images, and is one endmember resolved in spectral mixture analysis, where it is represented as a fraction of the measured radiance and a characteristic spectrum. This spectrum is typically the null vector, provided the data have been corrected for atmospheric and instrument effects: i.e., "shade" is the radiance from an ideal black surface.

In topographic shading, irradiance is reduced -- typically in proportion to cos(i), where i (incidence angle) is the angle between the sun and the local surface normal vectors. Therefore, the radiance is lowered by a multiplicative factor. Shadowing occurs when i>90°, or when sunlight is blocked by adjacent high terrain; the only irradiance is down-welling skylight and bounce light from adjacent terrain. In spectral mixture analysis, "shade" is regarded as an additive term. In this regard, it is an accurate description of the proportion of a scene that consists of ideal shadows ("checkerboard mixing"); however, "shade" represents the multiplicative cos(i) factor as well, and here it should be interpreted as the proportion of shadow that would darken the scene an equivalent amount. In either case, the "shade" fraction is lessened by adjacency effects, because the scene has a non-zero reflectivity instead of the ideal black surface generally assumed.

In spectral mixture analysis, field and laboratory reflectance spectra are utilized to represent endmembers other than "shade." Laboratory measurements are typically made at i≈0°, such that darkening due to shade is minimal. However, field measurements are typically made at greater incidence angles, and are affected by both shading and shadows at a "subpixel" scale, due to roughness of the measured surface. This darkening leads to an underestimation of the scene reflectivity, and this underestimation is related to the "shade" fraction, F_s, sought in spectral mixture analysis. Therefore it appears that field radiance data can be interpreted to yield a reflectance spectrum less affected by "shade," in greater agreement with laboratory measurements, and also to yield F_s, which is a measure of scene roughness at the scale of measurement.

Field spectra are commonly acquired by measuring the radiance from a small (10^1 - 10^3 cm^2) area of natural surface, and comparing this to the radiance from a flat smooth standard, such as halon, of known reflectance and at the same viewing geometry. For the target, assumed to be Lambertian,

$$R_t(\lambda) \approx S(\lambda) \cos(i) \, r_t(\lambda) + D(\lambda) \, r_t(\lambda) \tag{1}$$

where $R_t(\lambda)$ is target radiance at wavelength λ, S is the solar irradiance filtered by the atmosphere, r_t is the target reflectance, and D is the downwelling irradiance from the sky, assumed to be isotropic. When the halon or other standard is placed in front of the spectrometer, the measured radiance is

$$R_h(\lambda) \approx S(\lambda) \cos(i)\, r_h(\lambda) + D(\lambda)\, r_h(\lambda) \tag{2}$$

where r_h is the halon reflectance. For $S(\lambda) \gg D(\lambda)$, it is assumed that

$$r_t(\lambda) \approx r_h(\lambda)\, R_t(\lambda)/R_h(\lambda). \tag{3}$$

However, in the visible spectrum $D(\lambda)$ is variable but may be several percent of $S(\lambda)$, so that this value of $r_t(\lambda)$ is in error. Furthermore, for a textured target "shade" must also be considered. Thus,

$$R_t(\lambda) \approx S(\lambda) \cos(i)\, r_t(\lambda)\, (1 - F_s) + D(\lambda)\, r_t(\lambda). \tag{4}$$

It is clear that, even if $S(\lambda) \gg D(\lambda)$, the apparent value of $r_t(\lambda)$ is reduced in proportion to F_s, such that

$$r_h(\lambda)\, R_t(\lambda)/R_h(\lambda) \approx r_t(\lambda)\, (1 - F_s). \tag{5}$$

Equations (3) and (4) are underdetermined, and it is not possible to calculate both r_t and F_s from them. However, it is possible to do this by making two additional radiance measurements, R_t' and R_h', in the field. For these measurements, the target and halon standard are both shadowed (for instance, by holding up a sheet of cardboard), such that $S(\lambda) = 0$:

$$R_h'(\lambda) \approx D(\lambda)\, r_h(\lambda) \tag{6}$$

$$R_t'(\lambda) \approx D(\lambda)\, r_t(\lambda). \tag{7}$$

Substituting R_h' and R_t' for R_h and R_t in equation (3) produces a more correct estimate of r_t. The "shade" fraction may be also calculated:

$$F_s \approx 1 - R_h'\, (R_t - R_t') / (R_t'\, (R_h - R_h')) \tag{8}$$

where the λ notation has been dropped for simplicity.

It should be noted that the apparent value of F_s will be independent of λ, provided the simplifying assumptions are valid. An important refinement is to consider adjacency factors, which affect primarily the terms containing $D(\lambda)$ but can have an impact of several percent on F_s. We have incorporated a simplistic model of adjacency effects that assumes that: (1) the downwelling skylight is diminished according to i/π (i in radians), and (2) the measured radiance is increased by bounce light from adjacent terrain. It is assumed that the adjacent terrain is flat ($i = 0$) and partially shadowed according to some nominal value F_s^* of F_s (e.g., 10%). The adjusted expression for target radiance is

$$R_t \approx r_t\, S\, (\cos(i)\, (1 - F_s) + r_t\, (1 - F_s^*)\, (i/\pi)\,) + r_t\, D\, (\,(1 - i/\pi) + r_t\, (1 - F_s^*)\,). \tag{9}$$

We have calculated the sensitivity of F_s to measurement error by evaluating the above equations. We have also investigated the effect of viewing geometry on F_s and the magnitude of adjacency effects, using simulated surfaces having different roughness scales. This involved integration over a grid of 2500 cells, for which a digital terrain model was specified by a random number generator. In addition, we have determined F_s for constructed surfaces, using a CCD to measure radiance images. Finally, we have determined F_s in natural field settings.

We discuss the use of F_S in understanding VNIR images. An interesting ramification of this research is that F_S is related to the surface texture at the subpixel level, a difficult characteristic to estimate otherwise. In vegetated terrains such as the Amazon rain forest, F_S determined remotely may be an important parameter for estimating canopy architecture over large areas. It is also possible that the F_S parameter may prove useful in relating VNIR and Radar images.

Measurement of F_S at a range of field scales (i.e., 10^{-3} to 10^0 m) may provide a way to overlap with textural or roughness measurements made by microtopographic or stereometric surveys (10^{-1} to 10^2 m). Such data have been used to characterize surface roughness as a fractal dimension for correlation with Radar backscatter coefficients and use in forward scattering models.

A LINEAR SPECTRAL MATCHING TECHNIQUE FOR RETRIEVING EQUIVALENT WATER THICKNESS AND BIOCHEMICAL CONSTITUENTS OF GREEN VEGETATION

Bo-Cai Gao[1], and Alexander F. H. Goetz[1,2]

[1]Center for the Study of Earth from Space/CIRES, Campus Box 449
[2]Department of Geological Sciences
University of Colorado, Boulder, CO 80309-0449, U. S. A.

1. INTRODUCTION

Over the last decade, technological advances in airborne imaging spectrometers, having a spectral resolution comparable with laboratory spectrometers, have made it possible to estimate biochemical constituents of vegetation canopies. Wessman et al. (1988) have estimated lignin concentration from data acquired with NASA's Airborne Imaging Spectrometer (AIS) over Blackhawk Island in Wisconsin. In this study, a stepwise linear regression technique was used to determine the single spectral channel or channels in the AIS data that best correlated with measured lignin contents using chemical methods. The regression technique does not take advantage of the spectral shape of the lignin reflectance feature as a diagnostic tool nor the increased discrimination among other leaf components with overlapping spectral features.

A nonlinear least squares spectral matching technique (Gao and Goetz 1990) has recently been reported for deriving both the equivalent water thicknesses of surface vegetation and the amounts of water vapor in the atmosphere from contiguous spectra measured with the Airborne Visible/Infrared Imaging Spectrometer (AVIRIS) (Vane, 1987). The same technique has been applied to a laboratory reflectance spectrum of fresh, green leaves (Goetz et al. 1990). The result demonstrates that the fresh leaf spectrum in the 1.0-2.5 μm region consists of spectral components of dry leaves and the spectral component of liquid water. In this paper, we describe a linear least squares spectral matching technique for retrieving equivalent water thickness and biochemical components of green vegetation.

2. METHOD

At present, the prediction of vegetation reflectances based on rigorous radiative transfer modeling and the subsequent retrieval of biochemical components of vegetation are difficult. To simplify the problem, we have assumed that the vegetation reflectance spectrum has the same shape as the transmittance spectrum (Knipling 1970). With the assumption, the reflectance spectrum, $R(\lambda)$, can be expressed as:

$$R(\lambda) = (a + b\,\lambda)\exp\left(-\sum_{i=1}^{i=n} k_i u_i\right) \qquad (1)$$

where n is the total number of end members (such as liquid water, lignin, or cellulose) used in the modeling, k_i is the absorption coefficient of the ith end member, u_i is the absorber amount of the ith end member. The background level of the transmittance spectrum is assumed to be a linear function of wavelength and represented by the term $(a + b\,\lambda)$. This assumption is typically justified for small wavelength intervals (McMahon and Simmons 1980).

Figures 1a-1f illustrate our linear least squares fitting method for retrieving equivalent water thickness and chemical components of vegetation. Fig. 1a shows a reflectance spectrum in the 1.5-1.74 μm wavelength interval. This spectrum was obtained by removing atmospheric effects using the technique described by Gao et al. (1991) from an AVIRIS spectrum measured over an area covered by pine trees in the Oregon Transect on June 1, 1989. Fig. 1b shows the spectrum of the absorptances, the fitted straight line, and the difference spectrum.

Fig. 1c is similar to Fig. 1b but for the end member of liquid water. For clarity, both the minus log curve and the fitted straight line were shifted upward by the same amount in the plot. The water reflectance spectrum was obtained by measuring reflectances of water mixed with glass beads, which have no absorption features near 1.7 μm. Fig. 1d is also similar to Fig. 1b, but for lignin. The lignin reflectance spectrum was supplied by D. Peterson (private communication, 1990).

Fig. 1e shows an example of spectral matching using only water. The solid curve in this figure is the difference spectrum in Fig. 1b. The dashed curve is the fitted spectrum with one end member - water. In this case, the abundance vector, X, has one element. The value of x is the derived equivalent water thickness relative to the liquid water amount from the reflectance spectrum of water mixed with glass beads. The sum of the squared differences between the observed and the fitted spectra is 0.0066. Fig. 1f shows an example of spectral matching with two end members - water and lignin. In this case, the abundance vector, X, contains two elements, the equivalent thicknesses of water and lignin relative to the water spectrum and the lignin spectrum, respectively. The fit between the two curves in the 1.65-1.74 μm region in this figure is better than that in Fig. 1e. The sum of the squared differences between the two curves in Fig. 1f is 0.0036, almost half of that of Fig. 1e.

3. DISCUSSION

In the 1.3-2.5 μm region, absorption features of chemical components, such as lignin and cellulose, overlap (Curran 1989). Because of this, the derived equivalent thickness of lignin, for example, may be affected by other components using our linear spectral matching technique.

Differences do exist in shapes of absorption features of different chemical components (Elvidge 1990). For example, both lignin and cellulose have absorption features near 1.7 μm; the peak positions of the features are slightly offset. Also, the lignin absorption feature is sharper than the cellulose absorption feature. By comparing Figures 1e and 1f, one can see that if water and lignin are included in the fitting of the spectrum over pine trees, the overall fit is improved. This lends some credibility to the derived lignin amount using our technique. Furthermore, if water and cellulose are included in the fitting, the overall fit, particularly in the 1.65-1.75 μm region, is not as good as that with water and lignin.

4. ACKNOWLEDGMENTS

5. REFERENCES

Curran, P. J., Remote sensing of foliar chemistry, *Remote Sens. Env.*, *30*, 271-278, 1989.

Elvidge, C. D., Visible and near infrared reflectance characteristics of dry plant materials, *Int. J. Remote Sens.*, *11*, 1775-1795, 1990.
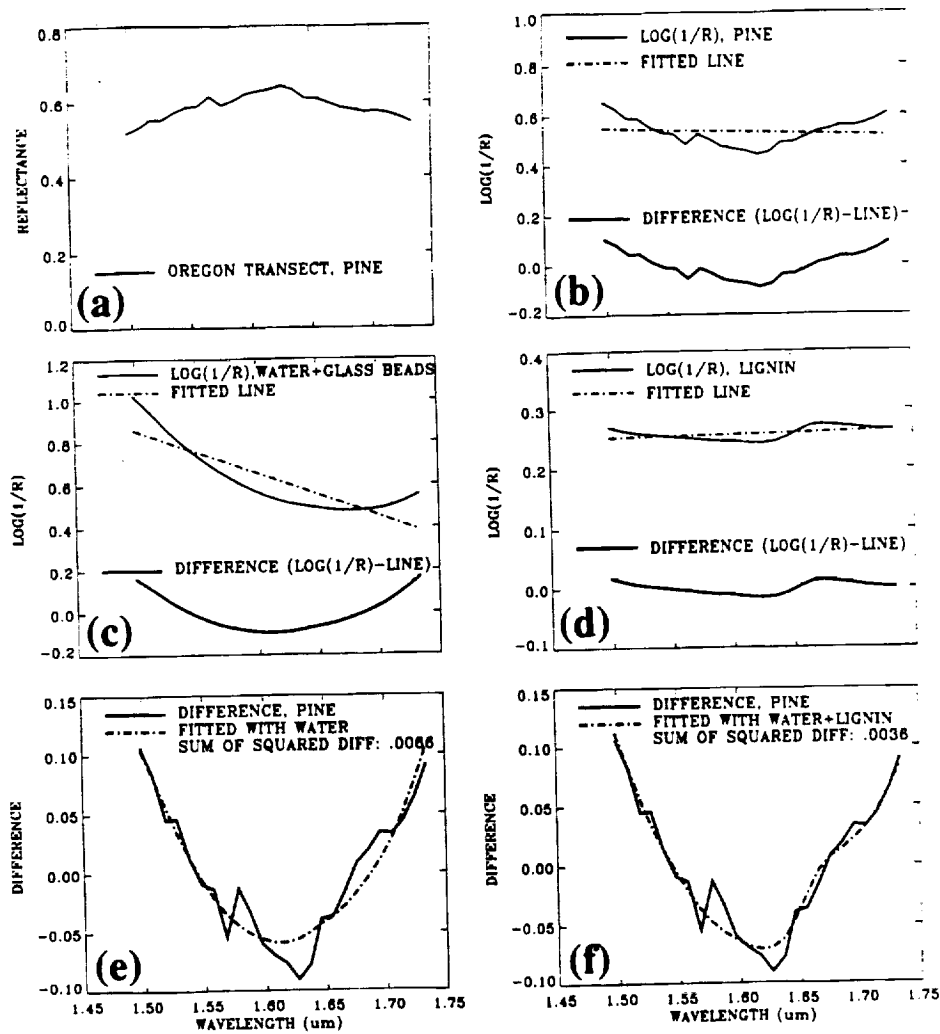
Fig. 1. Illustration of the linear least squares spectral matching technique. See text for details.

Gao, B.-C., and A. F. H. Goetz, Column atmospheric water vapor and vegetation liquid water retrievals from airborne imaging spectrometer data, *J. Geophys. Res.*, *95*, 3549-3564, 1990

Goetz, A. F. H., B.-C. Gao, C. A. Wessman, and W. D. Bowman, Estimation of biochemical constituents from fresh, green leaves by spectrum matching techniques, *IGARSS'90*, *3*, 971-974, 1990.

Gao, B.-C., A. F. H. Goetz, and J. A. Zamudio, Retrievals of surface reflectances from AVIRIS data, *IGARSS'91*, *2*, 669-672, 1991

Knipling, E. B., Physical and physiological basis for the reflectance of visible and near-infrared radiation from vegetation, *Remote Sens. Env.*, *1*, 155-159, 1970.

McMahon, B. B., and E. L. Simmons, Ground-based measurements of atmospheric NO_2 by differential optical absorption, *Nature*, *287*, 710-711, 1980.

Wessman, C. A., J. D. Aber, D. L. Peterson, and J. M. Melillo, Remote sensing of canopy chemistry and nitrogen cycling in temperate forest ecosystems, *Nature*, *335*, 154-156, 1988.

Vane, G. (Ed.), Airborne visible/infrared imaging spectrometer (AVIRIS), *JPL Publ. 87-38*, Jet Propul. Lab., Pasadena, Calif., 1987.

Mapping the Spectral Variability in Photosynthetic and Non-photosynthetic Vegetation, Soils and Shade using AVIRIS

Dar A. Roberts[1], Milton O. Smith[1], Donald E Sabol[1], John B. Adams[1]
and Susan Ustin[2]

1. Department of Geological Sciences, University of Washington, Seattle, WA 98195
2. Department of Land, Air, and Water Resources, University of California Davis, CA 95616

The primary objective of this research was to map as many spectrally distinct types of green vegetation (GV), non-photosynthetic vegetation (NPV), shade and soil (endmembers) in an AVIRIS scene as is warranted by the spectral variability of the data. Once determined, a secondary objective was to interpret these endmembers and their abundances spatially and spectrally in an ecological context.

Primarily, imaging spectrometer data has been viewed as a means for making direct measurements of canopy chemistry, such as protein, lignin and nitrogen (e.g. Wessman et al., 1988). The data also have potential for direct measurements of vegetation liquid water thickness and atmospheric water vapor (Gao and Goetz, 1990; Green et al. 1991).These approaches focus on the presence of subtle absorption features, some of which, in the context of a spectral mixture and canopy complexity, may not be readily detectable in imaging spectrometry data. Furthermore, they neglect much of the information inherent in spectral continua (Gillespie et al., 1990).

In previous papers (Roberts et al. (1990, 1991, 1992)), it was found that most (over 97%) of the spectral variability in an AVIRIS scene collected over Jasper Ridge could be described by 3 or 4 endmembers, GV, soil and shade (with a 4th endmember consisting of NPV). In a three-endmember model, NPV was distinguished from soil based on wavelength-specific residuals attributed to lignin and cellulose. Different types of GV were distinguished on the bases of different degrees of non-linearity, changes in the spectral quality of shade (canopy shade) and changes in the GV fraction when the analysis was applied separately to visible, near-infrared and short-wave-infrared subsets of the total spectrum.

In this paper we report upon a new approach to the problem of interpreting imaging spectrometry data. This is accomplished by extending the spectral mixture concept to allow the endmembers, as well as their abundances, to vary on a pixel-to-pixel basis. This approach has the potential of providing a large suite of ecologically significant variables, including reflectance spectra of multiple types of vegetation (GV and NPV), soil and shade (canopy and photometric) and maps showing the spatial distribution of each endmember type as well as the endmember abundances. It has further advantages over the approach of applying a single suite of endmembers to an entire image in that it provides a greater number of endmembers and optimizes endmember detectability (Sabol et al., 1991,1992).

The new approach was tested on two AVIRIS scenes collected in the vicinity of the Jasper Ridge Biological Preserve on July 27, 1990 and October 3, 1990. The results for the October scene are presented in this paper. A comparison between the July and October data is presented in a companion paper (see Sabol et al., this issue). The AVIRIS

data were calibrated to reflectance using an empirical line calibration and three non-photosynthetic targets to avoid non-linear effects (Roberts et al., 1991). Sets of two and three image endmembers were selected automatically from the scene. Based on two criteria, a RMS threshold of 8 DN and required endmember fractions between 0 and 1, over 92% of the scene was modeled by 12 endmember pairs. The endmember pairs consisted primarily of mixtures of shade and either GV or NPV. The total number of endmember pairs included several shades, GVs, NPVs and soils. Representative GV and NPV spectra are shown in Figures 1A and 1B. The three endmember case provided little additional information above the two endmember case. For most pixels two endmembers were adequate. This result is not surprising considering the analysis was restricted to image endmembers, which themselves can be complex mixtures. The next step is to interpret these image-endmembers in terms of laboratory reference endmembers (see Gillispie et al., 1990 for a description of this procedure).

Spatially, the endmember pairs corresponded to the dominant cover types in the region. As an example, the most abundant pair, which was categorized as a shade-GV mixture, corresponded to Forested Wetland, Evergreen Broadleaf Forest, Conifer Forests and water. In this instance water was a spectral analog of photometric shade. The second most abundant pair, which was categorized as a shade-NPV/GV mixture, corresponded to chaparral and forested/urban areas. In this case the NPV/GV image endmember is most likely a mixture of several photosynthetic and non-photosynthetic materials.

Conclusions

A new spectral mixture approach, in which the endmembers vary from pixel to pixel across an AVIRIS image was tested using data collected over the Jasper Ridge Biological Preserve on October 3, 1990. A preliminary analysis of the image endmembers determined that most of the scene could be described as mixtures of two endmembers, primarily shade and either GV or NPV.The endmember pairs were spatially coherent, varying broadly with community types. Near-term objectives include extending the analysis to reference endmembers and new criteria for selecting endmembers, including the use of wavelength specific-residuals in addition to an RMS error.

References

Gao , B.C. and Goetz, A.F.H., 1990, Column Atmospheric Water Vapor and Vegetation Liquid Water Retrievals From Airborne Imaging Spectrometer Data, *J. Geophys. Res.*, 95, 3549-3564.

Gillespie, A.R., Smith, M.O., Adams, J.B., Willis, S.C., Fischer, A.F. and Sabol, D.E., 1990, Interpretation of Residual Images: Spectral Mixture Analysis of AVIRIS Images, Owens Valley, California, Proc. 2nd Airborne Sci. Workshop: AVIRIS, JPL, Pasadena, CA, 4-5 June, 243-270.

Green, R.O., Conel, J.E., Margolis, J.S., Bruegge, C.J., and Hoover, G.L., 1991, An Inversion Algorithm for Retrieval of Atmospheric and Leaf Water Absorption From AVIRIS Radiance With Compensation for Atmospheric Scattering, Proc. 3rd Airborne Sci. Workshop: AVIRIS, JPL, Pasadena, CA, 20-21, May, 51-61.

Roberts, D.A., Smith, M.O., Adams, J.B., Sabol, D.E., Gillespie, A.R., and Willis, S.C., 1990, Isolating Woody Plant Material and Senescent Vegetation from Green Vegetation in AVIRIS Data, Proc. 2nd Airborne Sci. Workshop: AVIRIS, JPL, Pasadena, CA, 4-5 June, 42-57.

Roberts, D.A., Smith, M.O., Adams, J.B., and Gillespie, A.R., 1991, Leaf Spectral Types, Residuals, and Canopy Shade in an AVIRIS Image, Proc. 3rd Airborne Sci. Workshop: AVIRIS, JPL, Pasadena, CA, 20-21, May, 43-50.

Roberts, D.A., Smith, M.O., and Adams, J.B., 1992, Green Vegetation, Non-Photosynthetic Vegetation and Soils in AVIRIS Data, in press.

Sabol, D.E., Adams J.B., and Smith, M.O., 1992, Quantitative Sub-pixel Spectral Detection of Targets in Multispectral Images, *J. Geophys. Res.*, 97, 2659-2672.

Sabol , D.E., Adams, J.B., Smith, M.O., and Gillespie, A.R., 1991, Target Detection Thresholds Using Imaging Spectrometer Data, Proc. 3rd Airborne Sci. Workshop: AVIRIS, JPL, Pasadena, CA, 20-21, May, 99-108.

Wessman, C.A., Aber, J.D., Peterson, D.L., and Mellilo, J.M., 1988, Remote Sensing of Canopy Chemistry and Nitrogen Cycling in Temperate Forest Ecosystems, *Nature*, 335(8): 154-156.
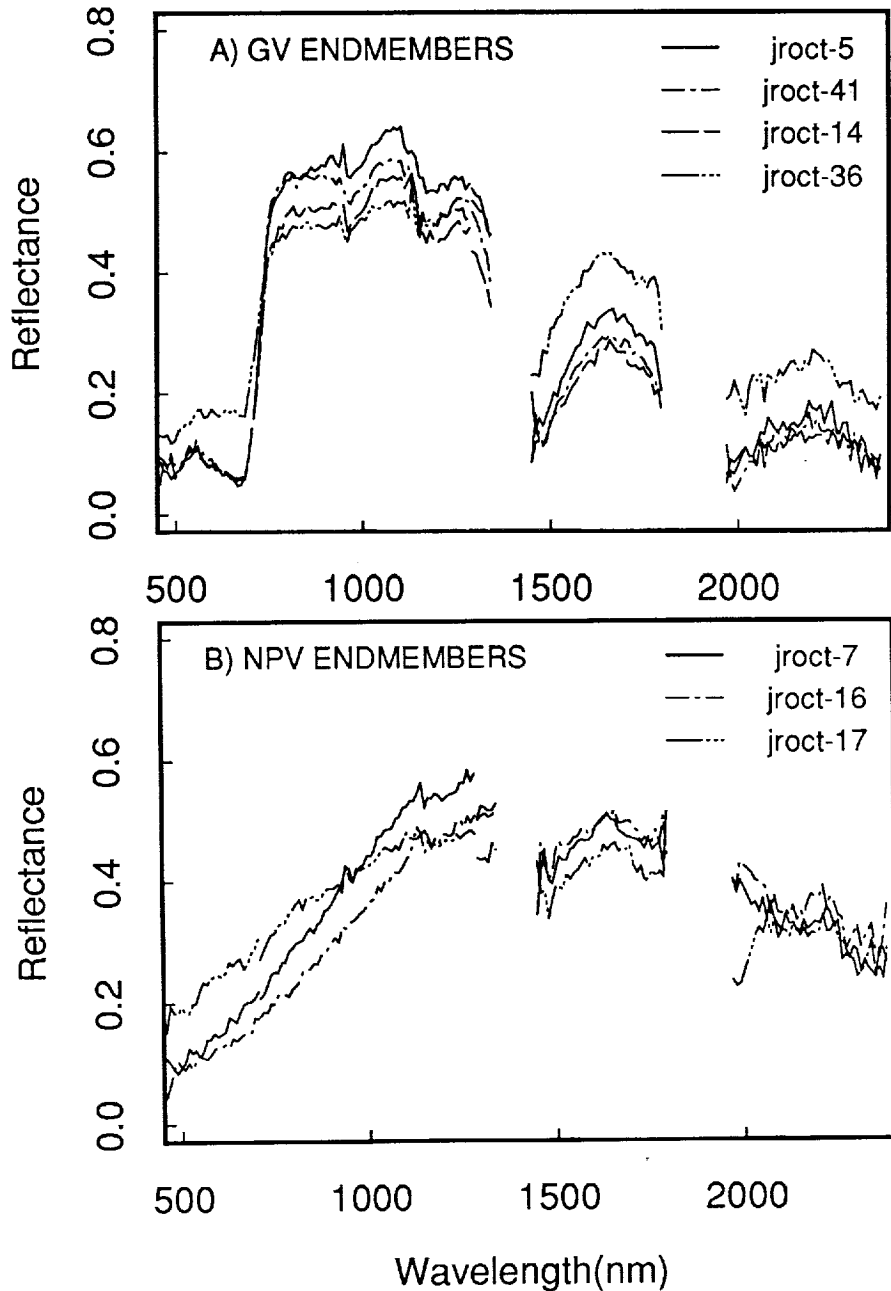
Figure 1 A) Representative GV endmembers automatically selected from the AVIRIS data as part of an endmember pair. B) NPV endmembers selected from the image.

VOLCANIC THERMAL FEATURES OBSERVED BY AVIRIS

Clive Oppenheimer*, David Pieri‡, Veronique Carrere‡, Michael Abrams‡,
David Rothery*, and Peter Francis*

*Department of Earth Sciences, The Open University,
Milton Keynes, MK7 6AA, UK.
‡Jet Propulsion Laboratory, California Institute of Technology,
4800 Oak Grove Drive, Pasadena, CA 91109.

1. INTRODUCTION

In July 1991, AVIRIS was flown over Mount Etna and Stromboli, Italy. Lava-filled vents were then present within summit craters of both volcanoes. Since surfaces at magmatic temperatures radiate strongly over the wavelength ranges of the AVIRIS C- and D-spectrometers, it was hoped that the data collected would reveal clear thermal signatures, even of sub-pixel sized features, as have been observed in the 1.65 and 2.22 μm bands of Landsat Thematic Mapper images (*Rothery et al.* 1988). This would provide an opportunity to explore the potential of imaging spectrometers for deriving temperature distributions of hot volcanic surfaces. Such research has implications for volcano monitoring in the EOS era, and also for any future AVIRIS deployments above active lava flows, lakes and domes, where understanding of their behaviour may be advanced by detailed thermal observations (*Pieri et al.* 1990, *Oppenheimer* 1991).

2. DATA INTERPRETATION

AVIRIS recorded useful data of Stromboli on July 8, 1991 (910708B run 8 segment 1) and Mount Etna on July 19, 1991 (910719B run 7 segment 3). Despite a seven-fold loss of throughput in the D-spectrometer resulting from faulty fiber-optics (R. Green, pers. commun. 1992), there are pronounced thermal responses in this part of the spectrum (1.8-2.45 μm), as well as in the C-spectrometer output (1.2-1.8 μm), to summit features at both volcanoes. No sensor saturation occurred, reflecting the wide dynamic range of AVIRIS (up to about 20 mW cm^{-2} sr^{-1} μm^{-1} for the healthy D-spectrometer).

The radiometrically calibrated data were processed in the following manner. It is assumed that the measured spectral radiance, R_λ, in each AVIRIS channel is the sum of partially transmitted reflected sunlight and skylight, any path radiance, and partially transmitted thermal radiation from one or more components of the surface:

$$R_\lambda = \tau_\lambda \rho_\lambda R_{\lambda,D} + R_{\lambda,U} + \tau_\lambda \sum_i \varepsilon_{\lambda,i} f_i L(\lambda,T_i) \qquad (1),$$

where τ_λ is the atmospheric transmittance at wavelength λ, ρ_λ the spectral reflectivity of the surface, $R_{\lambda,D}$ the downwelling atmospheric radiance, $R_{\lambda,U}$ the upwelling path radiance, $\varepsilon_{\lambda,i}$ the spectral emissivity of the ith surface thermal component, f_i its pixel-filling fraction, and $L(\lambda,T_i)$ the spectral radiance from the ith thermal component with a surface absolute temperature T_i, which is given by the Planck distribution law as follows:

$$L(\lambda,T_i) = \frac{c_1 \lambda^{-5}}{\exp(c_2/\lambda T_i) - 1]} \qquad (2),$$

where c_1 and c_2 have the values 1.19×10^{-16} W m^2 and 1.44×10^{-2} m K, respectively.

For a "hot" pixel, the radiated component of the spectrum was isolated by first subtracting, band-by-band, the spectrum of a neighbouring "cool" pixel. This was deemed to be optimized when the residual spectrum showed the least net signal between 0.4 and 1.2 µm. Next, the "difference" spectrum was divided, band-by-band, by a file containing atmospheric transmission coefficients (obtained using LOWTRAN 7) convolved with the AVIRIS spectral response file. Figure 1 shows a spectrum thus corrected for a single pixel over Stromboli; channels for which the modelled atmospheric transmittance was below 0.5 were excluded. The solid curve shows the best Planck curve fit, found using the Simplex algorithm (*Caceci and Cacheris* 1984), for a single temp-erature hot spot surrounded by ground too cool to radiate significantly in this region of the infrared. The solution represents a pixel containing approximately 12 m^2 (f=3.72% of a nominal 320 m^2 IFOV) of ground at 598 °C (ε=0.95). This would be consistent with a region of recently erupted spatter, or crusted lava inside a small intracrater bocca, both characteristic of Stromboli's activity at the time (*Smithsonian Institution* 1991).
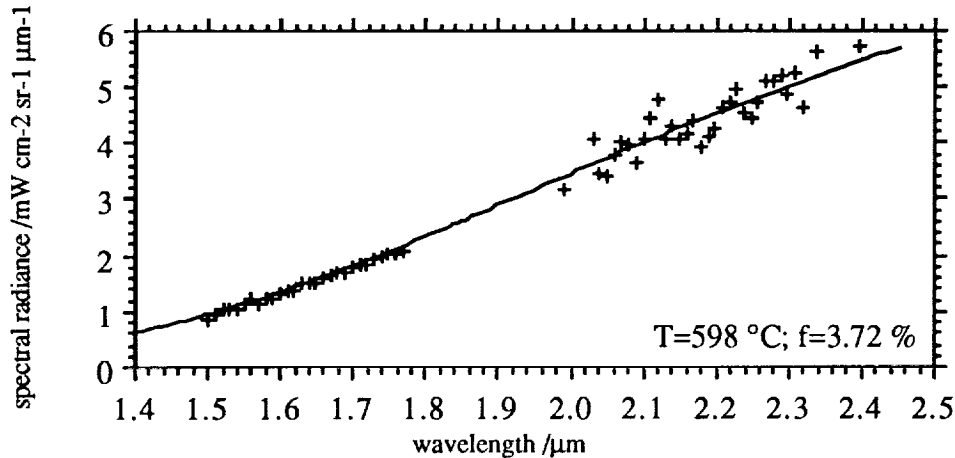
Figure 1. Corrected AVIRIS spectrum and Planck curve fit for a pixel over Stromboli.
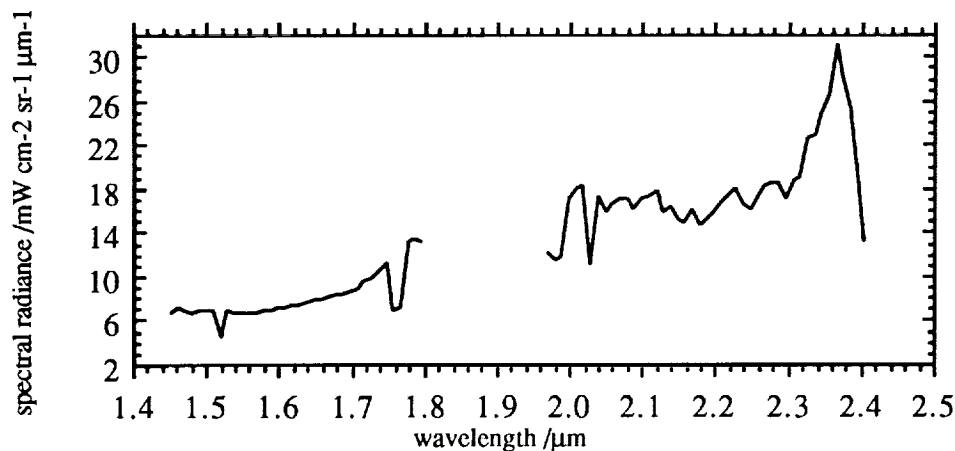
Figure 2. Corrected AVIRIS spectrum for pixel of Northeast Crater, Mount Etna.

Not all the spectra examined have been resolved so convincingly into the sum of Planck radiation curves. Figure 2 shows the most intense thermal anomaly over the Northeast Crater of Mount Etna. This spectrum was derived following the procedure outlined above. Again, the D-spectrometer range is very noisy. Furthermore, the shape of the 1.2-1.8 µm spectrum is not readily interpretable in terms of superposition of different thermal components. In addition to its broadly concave upwards form, there are

marked drops in the spectrum at about 1.52 and 1.76 μm. These could represent either false positive-noise-spike corrections, uncorrected dropouts, or genuine absorption features. At the time the image was recorded, the only hot spot within the Northeast Crater was a funnel-shaped pit on its floor. This vent emitted high temperature gases, glowed, and probably contained magma close to the surface (*Smithsonian Institution* 1991). We note that HCl is infrared-active around 1.76 μm but have yet to calculate the concentrations necessary to attenuate emitted radiation to the extent suggested by the AVIRIS data. We plan also to examine the raw AVIRIS data which could exclude the possibility that a noise-spike correction was applied erroneously.

4.   DISCUSSION

AVIRIS takes 87 μs to record a spectrum in each detector array. This is about 6 orders of magnitude faster than conventional field spectroradiometers. However, even this brief time is equivalent to approximately one cross-track pixel displacement on the ground. This is corrected for by a linear interpolation of the recorded DN in each detector element between adjacent cross-track samples (*Green et al.* 1991). This will tend to blur thermal anomalies in the cross-track direction and, more worryingly, distort the shape of the spectrum according to the size and position of the thermal feature relative to the instrumental instantaneous field of view. Some of the difficulty experienced in fitting Planck radiation curves to the recorded spectra probably reflects this latter point. Unfortunately, going back to the raw image which has not been resampled presents the original problem that each detector element within a given spectrometer has sampled a different piece of ground. However, corresponding detector elements in each spectrometer are nominally spatially coregistered; perhaps by selecting a few neighbouring data points and plotting them along with those at the same position in adjacent detector arrays, one might derive more reliable thermal results. This problem with interband spatial registration should be less significant for large features with uniform surface temperatures. It would be solved altogether by enabling AVIRIS to record all bands simultaneously; such a proposal is under review (R. Green, pers. commun. 1992).

AVIRIS may be in Hawaii in November 1992, which would, in all likelihood, offer a tremendous opportunity to record data above areally extensive lava flow fields and lava ponds. By deriving radiative properties of such features from the AVIRIS data, one might hope to refine models for, and thereby our understanding of, their eruption.

5.   ACKNOWLEDGMENTS

6.   REFERENCES

Caceci, M.S., W.P. Cacheris. Fitting curves to data: the Simplex algorithm is the answer, *Byte*, May issue, 1984, 340-362.

Green, R., S.A. Larson, and H.I. Novack. Calibration of AVIRIS digitized data, Procs. Third AVIRIS Workshop, Ed. R.O. Green, *JPL Publ. 91-28*, 1991, 109-118.

Oppenheimer, C. Lava flow cooling estimated by Landsat Thematic Mapper infrared data: the Lonquimay eruption (Chile, 1989), *J. Geophys. Res.*, 96, 1991, 21865-21878.

Pieri, D.C., L.S. Glaze, and M.J. Abrams. Thermal radiance observations of an active lava flow during the June 1984 eruption of Mount Etna, *Geology*, 18, 1990, 1018-1022.

Rothery, D.A., P.W. Francis, and C.A. Wood. Volcano monitoring using short wavelength infrared data from satellites, *J. Geophys. Res.*, 93, 1988, 7993-8008.

Smithsonian Institution. Stromboli/ Etna, *Bull. Global Volcanism Network*, 16(7), 1991, 18.

RETRIEVAL OF BIOPHYSICAL PARAMETERS WITH AVIRIS AND ISM
- THE LANDES FOREST, SOUTH WEST FRANCE -

Zagolski F.,Gastellu-Etchegorry J.P., Mougin E., Giordano G.,
Marty G., Le Toan T., Beaudoin A.

Centre d'Etude Spatiale Des Rayonnements Université Paul Sabatier, Toulouse.

I. Introduction

This paper presents the first steps of an experiment for investigating the capability of airborne spectrometer data for retrieval of biophysical parameters of vegetation, especially water conditions. AVIRIS and ISM (Table 1) data were acquired in the frame of the 1991 NASA/JPL and CNES campaigns on the Landes, South west France, a large and flat forest area with mainly maritime pines (Le Toan et al., 1991). In-situ measurements were completed at that time; i.e reflectance spectra, atmospheric profiles, sampling for further laboratory analyses of elements concentrations (lignin, water, cellulose, nitrogen,...). All information was integrated in an already existing data base (age, LAI, DBH, understory cover,...). A methodology was designed for (1) obtaining geometrically and atmospherically corrected reflectance data, for (2) registrating all available information, and (3) for analyzing these multi-source informations. Our objective is to conduct comparative studies with simulation reflectance models, and to improve these models, especially in the MIR.

II. Methodology and preliminary results

High resolution reflectance spectra obtained under different experimental configurations (in-situ, laboratory, and remote sensing) are retrieved and compared (Fig. 1).
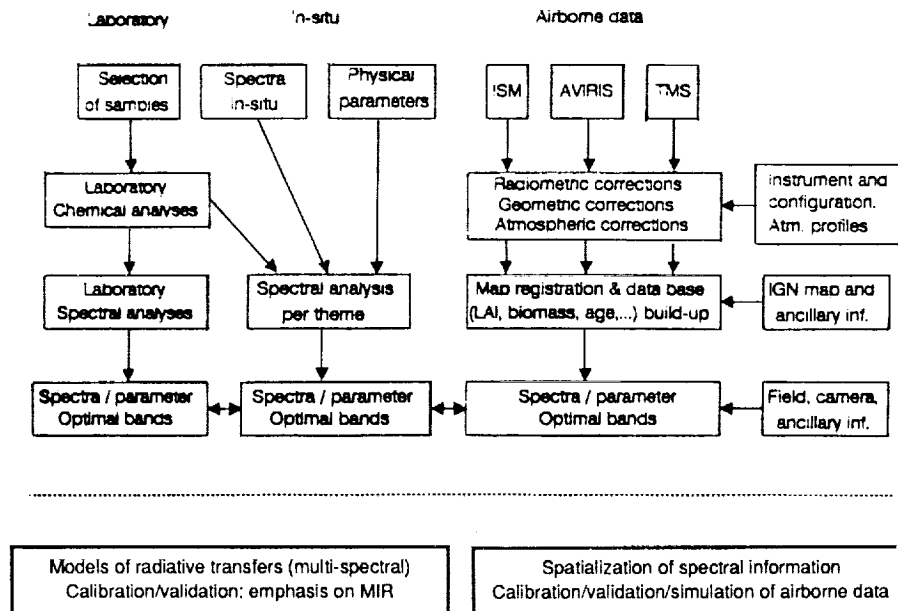
Figure 1: Schematic presentation of the methodology.

- laboratory: spectral analyses (19 bands from 1445 to 2348nm) to assess most valuable wavelengths for biochemical elements of vegetation (dry powder). Stepwise analyses showed that middle infrared bands are mostly efficient (Zagolski et al., 1992).

- in-situ: directional reflectance spectra are displayed on figure 2.

- low to medium altitude (very large to large scale): ISM surveys (Fig. 3) at 700m, 1000m, 2000m and 3000m altitudes, and with different configurations (Zagolski et al., 1992).

- high altitude (medium scale): AVIRIS derived spectral reflectances (Fig. 3) are encouraging in the way they show important differences for different age classes (biomass) of pine stands (Gastellu-Etchegorry, 1991).

Retrieval of biophysical parameters is based on intercalibrated high resolution reflectance spectra. Preliminary steps to obtain these spectra are presented below.

* Radiometric corrections:
- AVIRIS digital counts were transformed into radiance values by calibration coefficients.
- Calibration procedures are being implemented for correction of ISM data.

* Geometric corrections:
- AVIRIS: only corrections of panoramic effects were applied.
- ISM: because surveys took place at low altitude levels geometric corrections are absolutely necessary. These corrections are currently being applied.
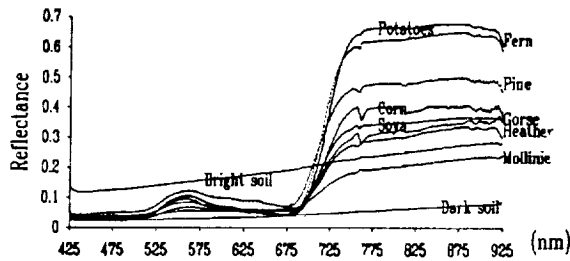
Figure 2 : Directional reflectance spectra measured in the field.
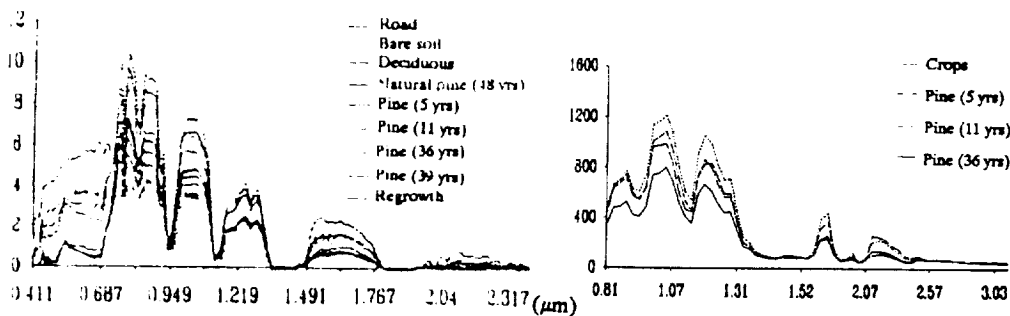
Figure 3:   AVIRIS reflectance spectra.   ISM radiance spectra.

* Atmospheric corrections:

Systematic atmospheric correction of airborne data (Fig. 4), with the inversion of 5S atmospheric model (Tanré et al., 1990), leads to apparent reflectances $\rho \cdot$. A Gauss Seidel based iterative approach leads to convergence with only 5 iterations.

$$\rho \cdot (\theta_s, \theta_v, \phi_v) = \rho_a + \rho_c^* + \rho_e^* = \rho_a(\theta_s, \theta_v, \phi_v) + [\rho_c \cdot \frac{T(\theta_v)}{1-\rho_e \cdot} \cdot e^{-\tau/\mu_v} + \rho_e \cdot \frac{T(\theta_v)}{1-\rho_e \cdot} \cdot t_d(\theta_v)] \cdot T_{gas}$$

with ρ_a: intrinsic atmospheric reflectance,

   ρ_c^*: "direct" apparent reflectance, partly due to the environment,

   ρ_e^*: environment contribution (atm. condition = = > neighborhood of radius 50),

   s and v: for sun and viewing angles, μ_s = cosine(sun zenith angle),

   τ, S, E_s: atmospheric optical depth and albedo, and sun constant,

   $T(\theta_s)/t_d(\theta_v)$: total/diffuse transmission coefficients, independent of T_{gas}.

Radiance: $\rho^{\bullet} \cdot E_s \cdot \mu_s / \pi$

Radio sonde exploration

Intrinsic atmosph radiance removal: $\rho^{\bullet} - \rho_a$

Amospheric model: (ρ_a)

Correction of atmosph. transmission effect:
$\rho^{\bullet} - \rho_a = (\rho^{\bullet} - \rho_a) / T_{gas}$

Atmospheric model: T_{gas}

Initial condition: $\rho_e = 0$

"Overestimate of ρ_c"

Evaluation of ρ_e

Environment function

Computation of $\rho_e^{\bullet}$
Computation of $\rho_c^{\bullet}$

Atmospheric model:
$T(\theta_s)$, S, $e^{-\tau/\mu_v}$, $t_d(\theta_v)$

Evaluation of ρ_c

Yes $\quad |\rho^{\bullet} - \rho_a - (\rho_e^{\bullet} + \rho_c^{\bullet})| > \varepsilon$?

No

ρ_c
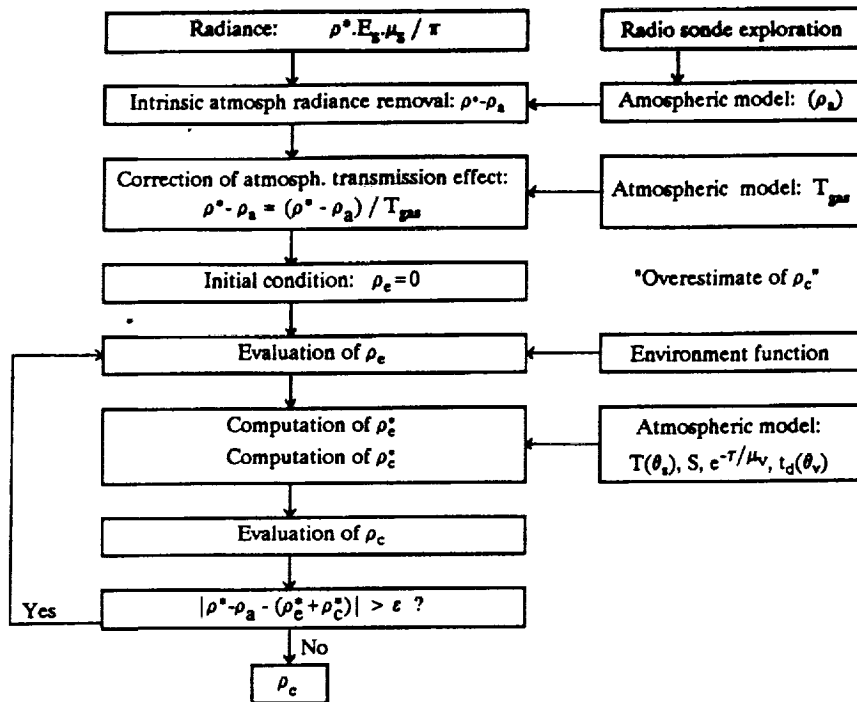
Figure 4: Atmospheric correction of AVIRIS images.

- IFOV (entrance slit)	12' (transverse) / 40' (longitudinal)
- Detector	PbS cooled
- IFOV (Detector) / FOV (selectable)	8' x 8' / ±20°
- Scan unit / Scan rate (selectable)	1' / 341 Hz
- Swath width (at 6 km altitude)	#170 m (12 pixels)
- Spectral coverage: 1st / 2nd band	[0.8-1.6µm] / [1.6-3.2µm]
- Sampling interval: 1st / 2nd band	12.5nm / 25nm
- Number of spectral bands	128
- Digitalization	12 bits
- Integration time	30ms
- Signal/Noise	> 100
- Sun calibration	through optical fiber
- Internal calibration	light (several levels)
- Synchro video registration	Camera

Table 1 :

ISM Operating parameters

IV. Concluding remarks

The 1991 NASA/JPL and CNES campaigns over The Landes test site provide a great opportunity for studying the potential of high spectral resolution for forest areas. Up to now, only basic processings were performed. Preliminary results already show the potential of high spectral resolution for discriminating different classes of vegetation. In a second step, once available information is calibrated and input into a data base, comparative analyses will be conducted for studying how those biophysical parameters that can be spectrally observed in the field and in laboratory can be assessed with airborne spectrometers at different altitude levels. The evolution of information at different spatial and spectral scales will be particularly considered. Our effort will concentrate on the explanation of results with the help of models.

References:

Le Toan et al., 1991, Relating forest parameters to SAR data, Proc. IGARSS 91', 689-692.

Gastellu-Etchegorry J.P. Zagolski F., Retrieval of Vegetation Biophysical Parameters with AVIRIS, TMS and ISM, Proc. IGARSS 92.

Tanré D., Deroo C., Duhaut P., Merman M., Morcrette J.J., Perbos J. & Deschamps P.Y., 1990, Simulation of the Satellite Signal in the Solar Spectrum (5S), Manual, LOA pub.

Zagolski et al., 1992, Preliminary Results of the ISM Campaign - The Landes, IGARSS.

GROUND-TRUTHING AVIRIS MINERAL MAPPING AT CUPRITE, NEVADA

Su-43

189062

P. 3

Gregg Swayze, Roger N. Clark, Fred Kruse[*], Steve Sutley,
and Andrea Gallagher

U.S. Geological Survey
MS 964 Box 25046 Federal Ctn., Denver, CO   80225

[*]Center for the Study of Earth from Space (CSES)
Cooperative Institute for Research in Environmental Sciences (CIRES)
University of Colorado, Boulder, CO   80309-0449
and the Department of Geological Sciences
University of Colorado, Boulder, CO 80309-0250

Mineral abundance maps of 18 minerals were made of the
Cuprite Mining District using 1990 AVIRIS data and the Mul-
tiple Spectral Feature Mapping Algorithm (MSFMA) as dis-
cussed in Clark et al. (1991). This technique uses least-
squares fitting between a scaled laboratory reference spec-
trum and ground calibrated AVIRIS data for each pixel. Mul-
tiple spectral features can be fitted for each mineral and
an unlimited number of minerals can be mapped simultane-
ously. Quality of fit and depth from continuum numbers for
each mineral are calculated for each pixel and the results
displayed as a multicolor image.

Cuprite consists of two acid-sulfate hydrothermal
alteration centers straddling highway 95 in southwestern
Nevada, with alteration involving Tertiary volcanic host
rocks in the eastern center and Cambrian metasedimentary
host rocks in the western center. Cuprite spectral mineral
abundance maps of the area show two elliptical zonation pat-
terns. The western center is zoned progressively inward
from sericite, to halloysite-dickite, kaolinite, Na-alunite,
through K-alunite with halloysite in the interior. While
the eastern center is zoned inward from halloysite to kao-
linite, intermediate alunite, through K-alunite, with a cen-
tral core of siliceous sinter.

Many of these minerals had never been mapped before or
in such detail. We have subdivided kaolinite group minerals
into grades of crystallinity, alunites and montmorillonites
into solid solution endmembers, and have differentiated
between jarosite, goethite, hematite, and ammonium minerals.
We collected 60 field samples using the mineral abundance
maps as guides to locate areas with the strongest mineral
signatures. The PIMA II field spectrometer† was used to do
preliminary mineral identification in the field. Natural
weathered surfaces were marked and were measured, along with
rock chips from sample interiors, in reflectance on a
laboratory Nicolet† 740 Fourier transform IR spectrometer.
In all cases the mineralogy of the interior matched that of

the weathered surface indicating that we are mapping the
rock units themselves. An example of a library reference
and field sample spectra for Dickite at lab and AVIRIS spec-
tral resolution is shown along with an AVIRIS spectrum (avg=
8 pixels) extracted from the collection location of the
field sample (Figure 1). This 2.2-μm feature was used to
identify Dickite with the MSFMA. Twenty-eight field samples
of 17 mineral types were submitted for X-Ray Diffraction
(XRD) analysis to verify or disprove our spectral identifi-
cations (Table 1).
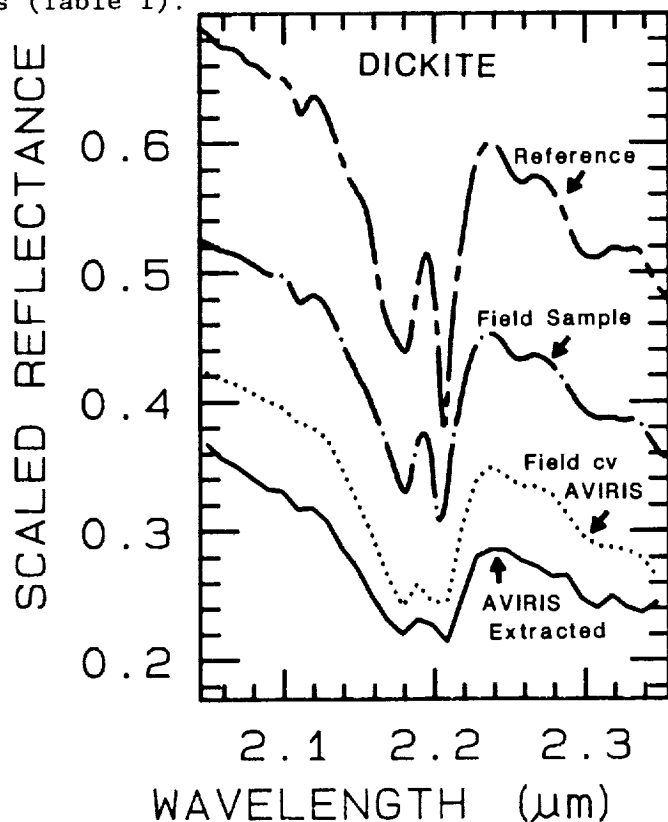
Figure 1. Reflectance spectra of a reference dickite and
field sample, from Cuprite, identified as dickite from
analysis of AVIRIS data. Lab spectra (dash-dot and dash-
dash curves) collected on an Fourier transform IR spectrome-
ter at 4 cm^{-1} resolution. Dotted curve is the field sample
spectrum convolved (cv) to AVIRIS spectral resolution.
Solid curve is an average of eight pixel spectra extracted
from AVIRIS data corresponding in location to the field sam-
ple collection locality. Spectra have been vertically
offset for clarity.

At the time of writing 12 spectrally identified
minerals were confirmed by XRD. Since spectroscopy is more
sensitive for identifying small quantities of Fe-oxides and
clays than XRD, we expect that nontronite is present along
with Fe-Chlorite. Chemical analysis will be used to

determine the cation content of K-alunite and Na-montmorillonite samples. The wavelength position of the 2.2-μm band in muscovite appears to be a function of its Al/Fe ratio (Jim Post, pers. comm.) and may explain why we mapped two different muscovites as Na-montmorillonite and paragonite at some locations in the western center. More details on this will be presented. We have also realized that opal and hydroxyl-bearing chalcedony both have Si-OH bands and that we identified chalcedony instead of opal at Cuprite. Overall, our mineral identifications have proven very accurate in those cases where we have adequate reference spectra. Our difficulties arise from subtle wavelength shifts in spectral features of solid solution series minerals, because the MSFMA is sensitive to small band shifts. Such sensitivity to band position coupled with great sensitivity to band shape indicates that the MSFMA may open up a new frontier in remotely sensing subtle chemical changes in surface materials.

†Any use of trade names is for descriptive purposes only and does not imply endorsement by the U.S. Geological Survey.

Clark, R.N., G.A. Swayze, A. Gallagher, N. Gorelick, and F. Kruse, Mapping with Imaging Spectrometer Data Using the Complete Band Shape Least-Squares Algorithm Simultaneously Fit to Multiple Spectral Features from Multiple Materials, *Proceedings of the Third Airborne Visible/Infrared Imaging Spectrometer (AVIRIS) Workshop*, JPL Publication 91-28, p. 2-3, 1991.

Table 1: Minerals detected by AVIRIS and identified with XRD

AVIRIS Identified	X-Ray Diffraction
K-Alunite	Na-Alunite (submitted for K/Na analysis)
Na-Alunite	Na-Alunite
Buddingtonite	Buddingtonite
Calcite	Not Submitted (occurs as limestone)
Fe-Chlorite	Probably Fe-Chlorite
Dickite	Dickite
Goethite	Goethite
Halloysite	Halloysite (moderately crystallized)
Hematite	Hematite
NH4 Ill/Smectite	Montmorillonite + tr. Illite
Jarosite	K-jarosite
Kaolinite (wxl)	Kaolinite (well crystallized)
Kaolinite (pxl)	Kaolinite (still resolving crystallinity)
Na-Montmorillonite	Ca-Montmorillonite (submitted for anal.)
Ca-Montmorillonite	tr. Smectite and muscovite
Nontronite	Possibly Nontronite
Opal	Quartz (SEM: Qtz + chalcedony*)
Paragonite	K-Muscovite (submitted for analysis)

*Opal and chalcedony are both OH-bearing quartz.

49

EXPLORING THE REMOTE SENSING OF FOLIAR BIOCHEMICAL CONCENTRATIONS WITH AVIRIS DATA

Geoffrey M. Smith and Paul J. Curran.

Department of Geography, University College of Swansea,
University of Wales, Singleton Park, Swansea SA2 8PP, UK.

1. INTRODUCTION

AVIRIS data shows promise for the estimation of foliar biochemical concentrations at the scale of the canopy (Committee on Earth Science 1989, Wessman *et al.* 1988, Curran 1989). There are, however, several problems associated with the use of AVIRIS data in this way and these are detailed in a recent Plant Biochemical Workshop Report (Peterson 1991). The research reported here has concentrated upon three of these problems: field sampling of forest canopies, wet laboratory assay of foliar chemicals and the visualisation of AVIRIS data.

2. STUDY SITES

Two study sites were used in this research. The first is north east of Gainesville, Florida, · is NSF funded and is maintained by the University of Florida (UF). This site is covered by a slash pine (*Pinus elliottii*) plantation and contains 8 fertilised and 8 control plots, each 50m x 50m in size. These were overflown by AVIRIS in March and September 1990, with multiple overpasses on each date (Curran *et al.* 1991). The second study site is around Llyn Brianne in Wales, UK. The upland site is covered by a Sitka spruce (*Picea sitchensis*) plantation with small areas of other plantation species (japanese larch, *Larix kaempferi*; lodgepole pine, *Pinus contorta var. latifolia*) and contains 51, 50m x 50m plots. These were overflown twice by AVIRIS in July 1991 as part of the NASA MAC Europe (Curran and Plummer 1992).

3. PROBLEMS

3.1. Field sampling of forest canopies

The five main stages were: choosing the study site, choosing the study plots, locating the plots, collecting forest mensuration data and finally sampling the foliage. These will be discussed in turn.

The two study sites have a history of environmental research. The site in Florida has a homogeneous canopy on a flat site and the site in Wales has a heterogeneous canopy on a rugged site.

The Florida study site contained established plots. At the Welsh study site the establishment of plots was made difficult by windthrow and drains. In addition, flat areas were seasonally waterlogged and suffered from large variations in tree growth over small distances. Collecting ground data in such

areas would mean sampling virtually every tree within the plot. Therefore, the range of plots chosen to represent relative levels of tree vigour were all on drained, slightly sloping land where neighbouring trees were similar. Sitka spruce plantations afford limited access to their interior and so a network of access paths had to be cut, by the removal of lower branches.

The Global Positioning System (GPS) was to be used to locate the plots. Unfortunately, hand-held systems when used within the forest could not pick up the signals from the GPS transmitters. Any future use of GPS for plot location within forest stands would require an external aerial that could be placed above the canopy. Classical surveying techniques were therefore used to locate the plots on both study sites.

UF collected forest mensuration data for each plot at the Florida study site (Gholz *et al.* 1991). During NASA MAC Europe, a wide range of forest mensuration data (diameter at breast height, leaf area index, tree height) were collected for each plot at the Welsh study site.

The open canopy and lack of low level branches at the Florida study site meant the canopy could be sampled by shooting small branches from the canopy which then fell to the ground. The Sitka spruce at the Welsh study site had a very dense canopy and retains its dead branches on lower whorls preventing sample branches from reaching the ground. Two methods were used to sample this canopy. At some points within the plots the lower dead branches from the tree were cleared until the live canopy was reached. A ladder and pruning pole were then used to remove the selected live branches from the canopy. At other points within the plots a tree was felled. Once the tree was horizontal hand pruners could be used to remove the required parts of the canopy. In total 539 foliage samples were collected, 384 for the study site in Florida and 155 from the study site in Wales.

3.2.   Wet laboratory analysis of foliar chemicals

The sampled foliage was bagged by age class and frozen for return to the University College of Swansea (UCS). The samples were then analyzed using standard wet laboratory techniques for chlorophyll, moisture, lignin, cellulose, nitrogen and carbon, with replication. So far the chlorophyll and moisture analyses have been completed and these show statistically significant differences between the fertilised and control plots at the Florida site and the relative level of tree vigour at the Welsh site.

3.3.   Visualisation of AVIRIS data

The Department of Geography at UCS was oriented towards the analysis of broad band remote sensing data and so initial analysis of the AVIRIS data cube was slow and relatively unproductive. This early processing was divided into two sections: spatial analysis and spectral analysis. The original data cube remained on a VAX 8820 and the required data were displayed spatially on a GEMS image processing system, running GEMSTONE software and spectrally on a 386PC, running in-house software. This separation of the data made it hard to link images and spectra together. Effective processing was achieved using SUN SPARC stations running PV-Wave software which is designed for the visualisation of multi-dimensional data sets. A set of routines is being

developed in the PV-Wave Command Language to perform the necessary processing associated with AVIRIS data.

4. FUTURE RESEARCH

The work described above continues in an effort to better understand the relationships between foliar biochemical concentrations and remotely sensed spectra. The NASA MAC Europe involved other sensors. Broad band multispectral scanners provide estimates of the foliar biomass and the AIRSAR provides estimates of the amount of wood within forest stands. These data sets will be integrated and applied to ecosystem simulation models to derive estimates of net primary productivity at a regional scale.

5. CONCLUSIONS

The remote sensing of foliar biochemical concentrations is an important contribution to the development of ecosystem models on regional to global scales. Field campaigns are vital if it is to be demonstrated that the AVIRIS can provide such information. This paper has emphasised the complexity of such campaigns, in particular the need for meticulous site preparation and a large number of foliar samples, backed up by the facilities necessary for wet laboratory assay and the visualisation of AVIRIS data.

6. REFERENCES

Committee on Earth Sciences, 1989, *Our Changing Planet: The FY1990 Research Plan (The U.S. Global Research Program)*. U.S. Department of Interior, Reston, Va.

Curran, P.J., 1989, The remote sensing of foliar chemistry. *Remote Sensing of Environment*, 29, 271-278.

Curran, P.J., Dungan, J.L. and Smith, G.M., 1991, Increasing the signal-to-noise ratio of AVIRIS imagery through repeated sampling. *Proceedings of the Third Airborne Visible/Infrared Imaging Spectrometer (AVIRIS) Workshop*. R.O. Green. (Ed). JPL Publication 91-28, California Institute of Technology, Pasadena, Ca, 164-167.

Curran, P.J., and Plummer, S., 1992, Remote sensing of forest productivity. *NERC News*, 20, 22-23.

Gholz, H.L., Vogel, S.A., Cropper, W.P.Jr., McKelvey, K., Ewel, K.C., Teskey, R.O. and Curran, P.J., 1991, Dynamics of canopy structure and light interception in *Pinus elliottii* stands, North Florida. *Ecological Monographs*, 61, 33-51.

Peterson, D.L., 1991, *Report on the Workshop Remote Sensing of Plant Biochemical Content: Theoretical and Empirical Studies*. NASA White Paper. NASA Ames Research Center, Ca.

Wessman, C.A., Aber, J.D., Peterson, D.L. and Melillo, J.M., 1988, Remote sensing of canopy chemistry and nitrogen cycling in temperate forest ecosystems. *Nature*, 335, 154-156.

SEASONAL AND SPATIAL VARIATIONS IN PHYTOPLANKTONIC CHLOROPHYLL IN EUTROPHIC MONO LAKE, CALIFORNIA, MEASURED WITH THE AIRBORNE VISIBLE AND INFRARED IMAGING SPECTROMETER (AVIRIS)

John M. Melack and Mary Gastil

Department of Biological Sciences and Marine Science Institute
University of California, Santa Barbara, CA 93106

1.   INTRODUCTION

The principal problem with application of airborne imaging spectrometers to lakes is the weak upwelling signal, especially when narrow spectral bands with high spatial resolution are sought. Furthermore, atmospheric path radiance dominates the signal received from dark targets such as lakes. Once atmospheric effects have been removed from the radiance received at the sensor, semi-empirical relationships can be developed to extract information about phytoplankton pigment concentrations for different underwater optical conditions (Carder, *et al*. 1986). In lakes where concentrations of dissolved organics and suspended detritus may not co-vary with phytoplankton pigments, the many spectral channels of an imaging spectrometer such a AVIRIS are likely to be required to distinguish the various aquasols.

The objectives of our study are two-fold: (1) We estimate the chlorophyll content of a lake with hundred-fold seasonal ranges in chlorophyll concentration using atmospherically corrected upwelling radiances derived from AVIRIS imagery. (2) After reduction of the coherent noise in the imagery by filtering techniques, we examine spatial patterns in chlorophyll.

2.   STUDY SITE

Mono Lake is a large (150 km^2), moderately deep (mean depth, 17 m), hypersaline (total dissolved solids, ca. 90 g L^{-1}) lake lying in the North American Great Basin just east of the Sierra Nevada, California (38°N, 119°W; elevation ca. 1942 m above sea level) (Melack 1983). A decade-long, ongoing limnological study has included examination of spatial variability of the plankton (Lenz 1986) and primary productivity (Jellison and Melack 1988). The phytoplankton is dominated by very small (2-3 μm diameter) coccoid cells that vary in abundance from <1 to ca. 90 mg chlorophyll a m^{-3}. The offshore waters are largely uncontaminated by suspended particles from inflows but contain considerable dissolved organic matter.

3.   METHODS

AVIRIS imagery of western and southern regions of Mono Lake was acquired on four dates: 26 May 1989, 27 March 1990, 10 August 1990 and 30 September 1991. On each date samples were collected at multiple stations for analysis of chlorophyll a and other photosynthetic pigments. Filtered water was obtained for laboratory absorption spectra. Up and downwelling photosynthetically available irradiance (PAR, 400 - 800 nm) was measured on each date.

The radiometrically corrected AVIRIS images were obtained from the AVIRIS project at the Jet Propulsion Laboratory (JPL). Atmospheric corrections were performed with LOWTRAN 7 using a multiple-scattering, mid-latitude, rural model. The atmospheric path radiance spectra, binned to the midpoints of the AVIRIS wavelengths, were subtracted band by band from radiance spectra averaged over subsets of the image containing only water to yield atmospherically corrected radiance spectra.

Chlorophyll a concentrations were estimated using a CZCS-type algorithm developed for coastal waters. To identify and reduce coherent noise, along-track and across-track power spectra were calculated for selected bands.

4.   RESULTS

In-situ measurements of chlorophyll a concentrations ranged widely among dates and within the lake on individual days: 26 May 1989, 13 - 31 mg m^{-3}; 23 March 1990, 28 - 91 mg m^{-3}; 10 August 1990, 1 - 4 mg m^{-3}; 30 September 1991, 3 - 7 mg m^{-3}. Application of CZCS-type algorithms underestimated chlorophyll concentrations by a factor of about 2 for concentrations above 20 mg m^{-3}. Further research in progress will utilize more spectral information to develop new algorithms appropriate for eutrophic lakes.

Atmospherically corrected reflectance spectra have a signature for chlorophyll a when concentrations are above about 20 mg m^{-3}. However, the conspicuous reflectance maximum at about 570 nm and distinct minima at about 680 nm and 480 nm reported by Melack and Pilorz (1990) were less well defined for the other scenes.

Radiances from the surface as measured at the sensor, for bands near 570nm, were low (1 - 3 μW cm^{-2}nm^{-1}sr^{-1}) as expected for inland waters. Coherent noise in the form of 0.1 to 0.2 μW cm^{-2}nm^{-1}sr^{-1} undulations oriented diagonally to the flight line were present in the 26 May 1989 image. Removal of most of the coherent noise by a simple ratio of two spectral bands revealed regional variation in brightness possibly related to differences in chlorophyll content. Coherent noise was detected in the other images and removal by ratioing and filtering is progressing. Hence, measurements of spatial patterns of chlorophyll concentrations are most likely obtainable.

5.   REFERENCES

Carder, K.L., R.G. Steward, J.H. Paul and G.A. Vargo, "Relationships between chlorophyll and ocean color constituents as they affect remote-sensing reflectance models," Limnol. Oceanogr., 31, 403-412, 1986.

Melack, J.M., "Large, deep salt lakes: a comparative limnological analysis," Hydrobiologia, 105, 223-230, 1983.

Lenz, P.H., S.D. Cooper, J.M. Melack and D.W. Winkler, "Spatial and temporal distribution patterns of three trophic levels in a saline lake," J. Plankt. Res., 8, 1051-1064, 1986.

Jellison, R. and J.M. Melack, "Photosynthetic activity of phytoplankton and its relation to environmental factors in hypersaline Mono Lake," Hydrobiologia, 158, 69-88, 1988.

Melack, J.M. and S.H. Pilorz, "Reflectance spectra from eutrophic Mono Lake, California, measured with the Airborne Visible and Infrared Imaging Spectrometer

(AVIRIS)," Imaging Spectroscopy of the Terrestrial Environment, SPIE, 1298, 202-212, 1990.

S/9-48
/89065

p. 4

AVIRIS CALIBRATION AND APPLICATION
IN COASTAL OCEANIC ENVIRONMENTS
by

Kendall L. Carder

Department of Marine Science
University of South Florida
140 Seventh Avenue South
St. Petersburg, Florida 33701

1. OVERVIEW

The Airborne Visible-Infrared Imaging Spectrometer (AVIRIS) is a test-bed for future spacecraft sensors such as the High-Resolution Imaging Spectrometer and the Moderate-Resolution Imaging Spectrometers planned for the Earth Observing System. To use this sensor for ocean applications, S/N was increased by spatial averaging of images. Post-flight recalibration was accomplished using _in situ_ the water-leaving radiance measured at flight time, modelling radiance transmission to the aircraft, and adding modelled atmospheric radiance to that value. The preflight calibration curve was then adjusted until aircraft and modelled total radiance values matched. Water-leaving radiance values from the recalibrated AVIRIS imagery were consistent with _in situ_ data supporting the validity of the approach. Imagery of the absorption coefficient at 415 nm and backscattering coefficient at 671 nm were used to depict the dissolved and particulate constituents of an ebb-tidal esturance plume on the West coast of Florida.

2. METHODS

Sixteen AVIRIS data scenes were collected at about 1515 Eastern Standard Time on 4 March 1990 on a flight line across the west Florida shelf into the mouth of Tampa Bay. The following parameters were measured on the same transect covered the same day by the R/V BELLOWS of the Florida Institute of Oceanography: Chlorophyll a, pheophytin a, remote sensing reflectance R_{rs}, above-water downwelling irradiance $E_d(0^+)$, subsurface downwelling irradiance $E_d(z)$, and subsurface upwelling irradiance $E_u(z)$ and radiance $L_u(z)$ data. Particle absorption coefficients (Mitchell 1990), detritus absorption coefficients (Roesler et al. 1989), and absorption coefficient

due to colored dissolved organic matter (Bricaud
et al. 1981) were determined.

Remote-sensing reflectance measurements
(Carder and Steward 1985, Peacock et al. 1990)
provided measurements which, when multiplied with
modelled (Lowtran 7) total irradiance entering the
sea, resulted in water-leaving radiance L_w
calculations that were consistent with the Lowtran
7 solar and atmosphere parameters. These modelled
data were atmospherically attenuated and combined
with radiance contributions due to reflected
skylight, direct-path radiance and path radiance
scattered from reflected sunlight as would be
viewed by the aircraft, all calculated using
Lowtran 7 code.

Diffuse transmissivity t_d of ocean scenes
from the surface to altitude can be calculated
using gas absorption plus molecular and aerosol
backscattering (Gordon et al. 1983). These were
calculated using Lowtran 7 multiple-scattering
code with a marine aerosol and a horizontal-path,
boundary-layer visibility of 70 km. Direct
atmospheric path radiance, $L_p(\theta_-,\lambda)$, skylight that
is specularly reflected by the sea surface and
diffusely transmitted to the sensor,
$\rho(\theta)t_d(\theta,\lambda)L_{pr}(\theta_+,\lambda)$, and path radiance scattered
from specularly reflected, diffusely transmitted
solar irradiance, $\rho(\theta_o)t_d(\theta_o,\lambda)L_{pr}(\theta_+,\lambda)$, were also
calculated using Lowtran 7. These were summed to
provide the calculated total radiance L_t available
at AVIRIS:

$$L_t(\theta,\lambda) = L_{pr}(\theta_+,\lambda)\{\rho(\theta)t_d(\theta,\lambda) + \rho(\theta_o)t_d(\theta_o,\lambda)\} \quad (1)$$
$$+ t_d(\theta,\lambda)L_w(\theta,\lambda) + L_p(\theta_-,\lambda)$$

where $\rho(\theta)$ and $\rho(\theta_o)$ are the Fresnel reflectance
values of the sea surface for reflected skylight
and sunlight, respectively, and θ_o, the solar and
θ pixel-sensor zenith angles, respectively. $\theta_{+/-}$
are the forward (+) and backward (-) scattering
angles involved in viewing reflected skylight and
direct path radiance, respectively. Note that the
observation geometry must be chosen to avoid
direct sun glint into the sensor.

The reflected skylight reaching AVIRIS was
determined by applying Lowtran 7 as if the sensor
were on the ocean, viewing space at a zenith angle
θ. The reflected, downwelling path radiance,
$L_{pr}(\theta_+,\lambda)$, viewed from this configuration is due to
forward scattering through an angle θ_+ relative to
the downwelling sunlight. This radiance was

subsequently reduced by specular reflectance and diffuse transmittance before reaching the AVIRIS. The upwelling skylight scattered from specularly reflected sunlight is also due to forward scattering. It is similar to reflected skylight reaching AVIRIS except that it has been reduced by diffuse transmittance of the downwelling solar irradiance and by its specular reflectance prior to being scattered as path radiance to AVIRIS.

The total radiance measured by AVIRIS, $L_{tm}(St.3)$, at Station 3 was adjusted to correspond to the radiance calculated, $L_{tc}(St.3)$, at Station 3 by multiplying by a calibration adjustment factor CAL. At all other stations AVIRIS radiance values $L_{tm}(\lambda)$ were multiplied by CAL, where

$$CAL(\lambda) = L_{tc}(St.3,\lambda)/L_{tm}(St.3,\lambda).\qquad(2)$$

The water-leaving radiance for each pixel in each scene was calculated by solving Eq.1 for $L_w(\lambda)$, using $L_{tm}(\lambda)*CAL(\lambda)$ for $L_t(\lambda)$. Lowtran 7 parameters determined at St.3 for the atmosphere were used along the entire flight line to provide the atmospheric correction terms. The water-leaving radiance values determined for wavelengths greater than 800 nm were examined to ensure that these values did not differ significantly from zero. Had non-zero values occurred, they would have suggested that a change in visibility or aerosol optical thickness had occurred, since with water molecular absorption coefficients greater than 2.4 m^{-1} for these wavelengths (Smith and Baker 1981), negligible radiance leaves the water except under unusually turbid conditions.

Applications of this method will be illustrated and results shown.

REFERENCES

Bricaud, A., Morel A., and Prieur, L. (1981), Absorption by dissolved organic matter in the sea (yellow substance) in the UV and visible domains, Limnol. Oceanogr., 26: 43-53.

Carder, K.L., and Steward, R.G., (1985), A remote-sensing reflectance model of a red tide dinoflagellate off west Florida, Limnol. Oceanogr., 30: 286-298.

Gordon, H.R., and Morel, A., (1983), Remote assessment of ocean color for interpretation of

satellite visible imagery: A review, Springer.

Mitchell, B.G., (1990), Algorithms for determining the absorption coefficients for aquatic particulates using the Quantitative Filter Technique, In Ocean Optics X, Proc. SPIE, 1302: 137-148.

Peacock, T.P., Carder, K.L., Davis, C.O., and Steward, R.G., (1990), Effects of fluorescence and water Raman scattering on models of remote sensing reflectance, In Ocean Optics X, Proc. SPIE, 1302: 303-319.

Roesler, C.S., Perry, M.J., and Carder, K.L., (1989), Modelling in situ phytoplankton absorption from total absorption spectra in productive inland marine waters, Limnol. Oceanogr., 34: 1510-1523.

Smith, R.C., and Baker, K.S., (1981), Optical properties of the clearest natural waters (200-800 nm), Appl. Opt., 20, 177-184.

Mapping Vegetation Types with the Multiple Spectral Feature Mapping Algorithm in Both Emission and Absorption

Roger N. Clark, Gregg A. Swayze, Christopher Koch,
and Cathy Ager

U. S. Geological Survey, MS 964
Box 25046 Federal Center
Denver, Colorado 80225

Vegetation covers a large portion of the Earth's land surface. Remotely sensing quantitative information from vegetation has proven difficult because in a broad sense, all vegetation is similar from a chemical viewpoint, and most healthy plants are green. Plant species are generally characterized by the leaf and flower or fruit morphology, not by remote sensing spectral signatures. But to the human eye, many plants show varying shades of green, so there is direct evidence for spectral differences between plant types. Quantifying these changes in a predictable manner has not been easy. We have applied the Clark et al., (1990, 1991) spectral features mapping algorithm to mapping spectral features in vegetation species.

The human eye sees different plant leaves as shades of green, as characterized by the "green peak" in reflectance spectra (Figure 1). The eye/brain color system is able to differentiate shades of green under different lighting conditions. For example under indoor incandescent light there is a strong red slope to the spectral signal received by the eye due to the red spectral shape of the light source (as compared to the same plant in direct sunlight), but we are still able to distinguish the plant as green and distinguish different plants as various shades of green.

The spectral feature mapping algorithm referenced above has been extended to map simultaneously both absorption and emission features. Strictly speaking, in reflectance spectra of rocks, soils, and vegetation in the 0.4 to 2.5 μm region, there are no emission features. However, there are "relative reflectance maxima," hereafter called "emission" features. Thus the reflectance spectrum of any material can be thought of as a combination of absorption and "emission" features.

We consider the green peak in vegetation spectra to be an "emission" feature (Figure 1). A continuum is drawn at the minimum on each side of the peak, and the continuum

removed by division. Removal of a continuum reduces the effects of background materials in the pixel analyzed. To further characterize the vegetation, additional features in the vegetation spectrum are analyzed (e.g. Figure 1, features B, C and D). We have found that the spectral feature mapping algorithm is very sensitive to the shape of the features and has the potential to distinguish more subtle differences in the visible spectrum of plants than can the human eye. An example of the variation in the shape of the "green peak" is illustrated in Figure 2. With the additional information in the near infrared, the algorithm can be used to differentiate the subtle spectral differences between them.

We have applied this method, along with reference spectra of plants, to map vegetation in AVIRIS scenes.
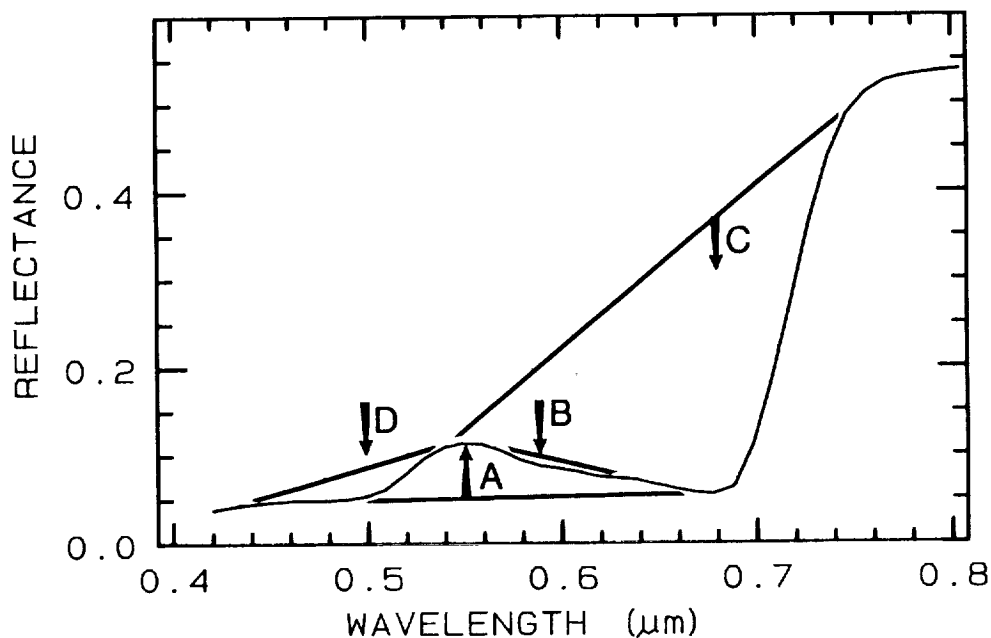
Figure 1. Example spectrum of green vegetation. Sample continua used to define "emission" (A) and absorption (B, C, and D) features.
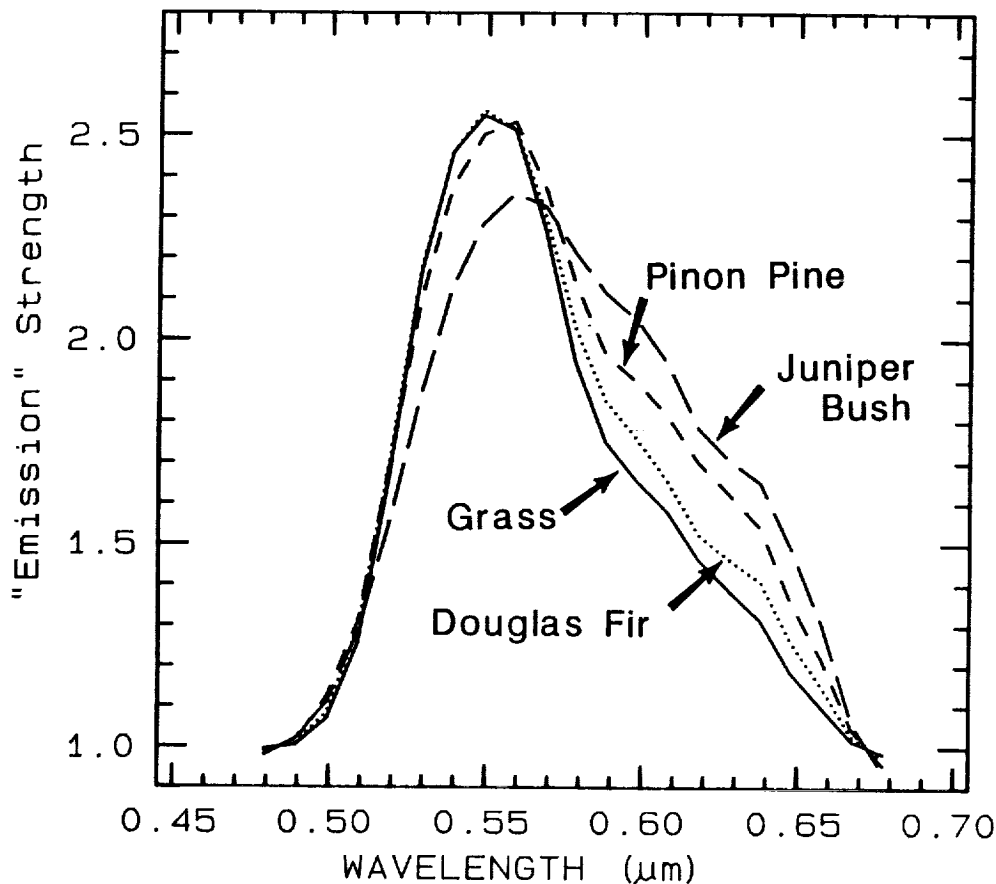
Figure 2. The normalized "emission" strengths of the green peak in 4 plant species are shown. The Douglas fir, pinon pine, and juniper are all in the Pine family and grow in the same area, yet have spectral structure that may be used to distinguish between them. The spectra are at AVIRIS spectral resolution.

References

Clark, R.N., A.J. Gallagher, and G.A. Swayze, Material Absorption Band Depth Mapping of Imaging Spectrometer Data Using a Complete Band Shape Least-Squares Fit with Library Reference Spectra, *Proceedings of the Second Airborne Visible/Infrared Imaging Spectrometer (AVIRIS) Workshop.* JPL Publication 90-54, 176-186, 1990.

Clark, R.N., G.A. Swayze, A. Gallagher, N. Gorelick, and F. Kruse, Mapping with Imaging Spectrometer Data Using the Complete Band Shape Least-Squares Algorithm Simultaneously Fit to Multiple Spectral Features from Multiple Materials, *Proceedings of the Third Airborne Visible/Infrared Imaging Spectrometer (AVIRIS) Workshop,* JPL Publication 91-28, 2-3, 1991.

MULTIPLE DATASET WATER-QUALITY ANALYSES
IN THE VICINITY OF AN OCEAN WASTEWATER PLUME

Michael Hamilton, Curtiss O. Davis,
W. Joseph Rhea, and Jeannette van den Bosch

Jet Propulsion Laboratory, California Institute of Technology
4800 Oak Grove Drive, Pasadena, CA 91109

1.   INTRODUCTION

The White's Point ocean outfall is the method of disposal for approximately 374 millon gallons of treated wastewater per day from Los Angeles County. The photosynthetic characteristics and particle distributions have well-defined properties that can be exploited to yield information on transport of the plume, mixing dynamics, and resuspension of bottom sediments during periods of bottom current velocity in excess of ca. 0.1 m/s. This plume of particles serves as a conservative tracer, which has been studied using a number of sampling platforms and strategies, including underway sawtooth, or "tow-yo" sampling, moored arrays of instruments, stationary profiling, and now for the first time with remotely-sensed multispectral color imagery.

Research in this area has previously focused on examination of the plume as it relates to the local current field and transport of particles, and on the resuspension of bottom sediments during periods of increased currents (Washburn et al, 1992). In addition, Wu et al (unpublished graduate work) have elucidated techniques for separating the particle signal into photosynthetic and nonphotosynthetic components, based on the beam attenuation to chlorophyll fluorescence ratio. High-frequency time series measurements of the current field and bio-optical characteristics at a site close to the waste diffusers have also been collected. These are being analyzed for the spectral characteristics of the longer-timescale variability, in order to predict particle transport through simple meteorological measurements (Dickey et al., unpub.). With the advent of high spectral and spatial resolution imaging spectrometers such as AVIRIS, it is now possible to construct causal relationships between particle distributions and signature of the upwelled radiance from the surface. The availability of a constant and well-characterized source of material lends itself well to models which predict upwelled light as a function of particle distributions, photosynthetic pigments, colored dissolved organic material, and detrital and degradation products of photosynthesis. In addition, the spatial coverage provided by the tow-yo sampling device, combined with the profile measurements of the light field, should facilitate the best inverse modeling attempts possible thus far.

2.   STUDY SITE

The White's Point/San Pedro Channel data were collected March 21, 1991, between the Palos Verdes Peninsula and Catalina Island off the coast of Southern California, at 33° 41.2' N, 118° 20.41' W. The day of the overflight was subsequent to several days of storms, and the sea state was somewhat rough. A few clouds are observed in the images, but overall visibility was quite

good. For this analysis, only the two images closest to White's Point are examined, for a total of 805 lines of image data.

3. *IN-SITU* MEASUREMENTS

The primary in-water instrument was a "tow-yo" platform operated by researchers at USCB and USC. Towed behind a ship, it is constantly raised and lowered to produce a sawtooth sampling pattern. Data collected in this manner can be interpolated to produce a grid of sampled points, at a spatial resolution that coincides with the SNR requirements of the analyses. Measurements collected with this instrument are: percent attenuation of a collimated beam of light at 660nm (transformed to beam attenuation coefficient, hereafter beam c), which is proportional to the concentration of particles in the size range 1-50μm; stimulated fluorescence of chlorophyll (chl-fl), where chl-containing particles in the sample volume are excited by a blue-green light, after which the emission of red light is collected and is proportional to the concentration of chl and chl-like pigments; photosynthetically available radiation (PAR), or broadband spectral irradiance, integrated from 400 to 700nm; microconductivity, used as a measure of small-scale turbulent processes that are proportional to the rate and intensity of mixing; and the underway current field.

Shipboard measurements were simultaneously carried out by a team from the Jet Propulsion Laboratory. Their measurements included the downwelling irradiance at 13 wavelengths, upwelling irradiance at 8 wavelengths, and upwelling radiance at 8 wavelengths, using a Biospherical Instruments MER-1048 bio-optical profiling system. Additional profiled measurements were PAR, chl-fl and beam c. Bottle samples for HPLC determination of chlorophyll and accessory pigments were collected for later analysis.

For the two months preceding the overflight, a physical and bio-optical mooring was placed near the location of the outfall by the USC Ocean Physics Group, with four instrument packages placed from 10m to 50m in the water column. The instrument packages contained suites of sensors measuring beam c, chl-fl, conductivity, dissolved oxygen, and orthogonal components of current. Each instrument at each depth collected a datapoint once per minute. Additionally, archived meteorological data were obtained from several sources for parameterization of the atmospheric correction to the images.

4. ANALYSES AND RESULTS

The images were processed by first modeling the propagation of surface measurements of water-leaving radiance to the aircraft, and determining recalibration coefficients that overcome the limitations of the laboratory calibration in the blue end of the spectrum (e.g. Carder et al., in press). The recalibrated images were then corrected for the effects of the atmosphere, using a combination of the CIBR (Carrere et al. 1990) water vapor parameterization, and the aerosol parameterization of Gordon et al. (1980). The SNR of the scenes was then increased by spatial averaging, depending on the requirements of the different analyses.

The *in-situ* data were resampled to a 100m X 100m grid of surface concentrations of particles, PAR, and chlorophyll. This grid was then used to either condition empirical models, parameterize an inverse model, or provide control to independent model estimates. Mooring data were examined to judge

the effect of ~48 h current history on observed oddities in the spatial distribution of suspended particle load.

The analyses then carried out describe the characteristics of a particle front in terms of its photosynthetic versus nonphotosynthetic components, separation of co-absorbing chlorophyll and colored dissolved organic matter, and the variation in the diffuse attenuation coeffient. Good agreement between measurements and model estimates was achieved, and strategies for improving the models were determined.

5.   REFERENCES

K.L. Carder, P. Reinersman, R. Chen, and F. Muller-Karger, "AVIRIS Calibration and Application in Coastal Oceanic Environments", *Remote Sensing of Environment*, in press.

V. Carrere, J. Conel, R. Green, C. Bruegge, J. Margolis, and R. Alley, "Analysis of Atmospheric Water Vapor Maps from AVIRIS at Salton Sea, California: Part I, Experiments, Methods, Results, and Error Budgets," in Proceedings of the Second AVIRIS Workshop, R. Green, ed., JPL 90-54, 107-128, 1990.

H. Gordon, J. Mueller, and R. Wrigley, "Atmospheric Correction of Nimbus-7 Coastal Zone Color Scanner imagery," in Remote Sensing of Atmospheres and Oceans, A. Deepak, ed. (Academic, New York, 1980), 457-483.

L. Washburn, B. Jones, A. Bratkovich, T. Dickey, and M. Chen, "Mixing, Dispersion, and Resuspension in Vicinity of Ocean Wastewater Plume," Journal of Hydraulic Engineering, 118(1), 38-58, 1992.

522-43

189068

P 3

MAC Europe 91: Evaluation of AVIRIS,
GER Imaging Spectrometry Data for the Land Application
Testsite Oberpfaffenhofen.

F. Lehmann, R. Richter, H. Rothfuss, K. Werner,
P. Hausknecht, A. Müller, P. Strobl.

During the MAC Europe 91 Campaign the area of Oberpfaffenhofen including the land application testsite Oberpfaffenhofen was flown by the AVIRIS imaging spectrometer, the GER II imaging spectrometer (63 band scanner), and two SAR systems (NASA/JPL AIRSAR and DLR E-SAR).

In parallel to the overflights ground spectrometry (ASD, IRIS M IV) and atmospheric measurements were carried out in order to provide data for optical sensor calibration.

Ground spectrometry measurements were carried out in the runway area of the DLR research center Oberpfaffenhofen. This area was used as well during the GER II European flight campaign EISAC 89 (ref 1,3) as a calibration target (ref 2).

The land application testsite Oberpfaffenhofen is located 3 km north of the DLR research center. During the MAC Europe 91 Campaign a ground survey was carried out for documentation in the ground information data base (vegetation type, vegetation geometry, soil type, soil moisture). Crop stands analysed were corn, barley and rape.

The DLR runway area and the land application testsite Oberpfaffenhofen were flown with the AVIRIS on July 29 and with the GER II on July 12, 23 and Sept. 3.

AVIRIS and GER II scenes have been processed and atmospherically corrected for optical data analysis and integrated analysis of optical and radar data.

For the AVIRIS and the GER II scenes SNR estimates have been calculated (ref 4,5,6). Fig. 1 gives an example of the reflectance of 6 calibration targets inside a GER II scene of Oberpfaffenhofen. SNR values for the GER II for a medium albedo target are given in Fig. 2.

The integrated analysis for the optical and radar data has been carried out in cooperation with the DLR Institute for Microwave Technologies.
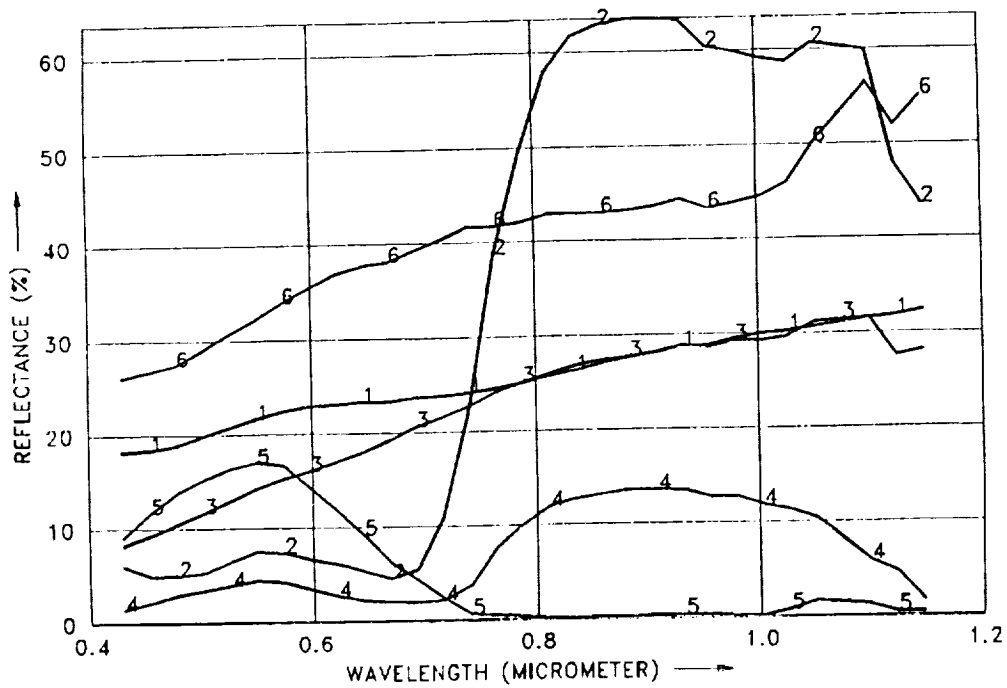
Figure 1: **GER reflectance spectra of selected targets**
1 = concrete airport DLR, 2 = meadow, 3 = bare soil,
4 = spruce, 5 = lake, 6 = concrete (AWA).
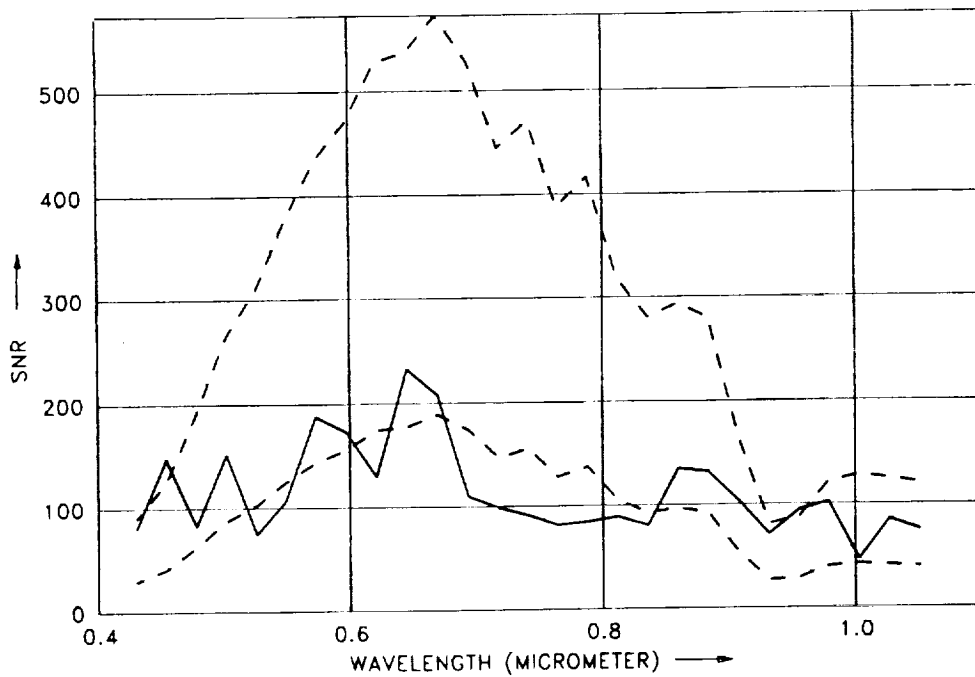
Figure 2: **SNR values of GER II**
Solid line: GER II measurement
lower dashed line: scene noise selected to match measurement
upper dashed line: scene noise reduced by a factor 3

References

1. F. Lehmann, H. Rothfuss, K. Werner, "Imaging Spectrometry Data Used for Geological and Environmental Analysis in Europe", Proceedings of the Third AVIRIS Workshop, NASA JPL Publication 91-28, 62 - 72, (1991).

2. F. Lehmann, S. Mackin, R. Richter, H. Rothfuss, A. Walbrodt, "The European Imaging Spectrometry Airborne Campaign 1989 (EISAC) - Preprocessing, Processing and Data Evaluation of the GER Airborne Imaging Spectrometer Data", Progress Report to the European Community, JRC, Ispra. DLR, Oberpfaffenhofen, (1989).

3. "Imaging Spectroscopy" - EARSEL Advances in Remote Sensing, Volume 1, No.1, ISBN 2-9088865-00-X, (1991).

4. R. Richter, "A fast atmospheric correction algorithm applied to Landsat TM images", Int. J. Remote Sensing, Vol. 11, 159 - 166, (1990).

5   F. X. Kneizys et al., "Users Guide to LOWTRAN 7", AFGL-TR-88-0177, Air Force Geophysics Laboratory, Bedford MA, (1988).

6. R. Richter, "Model SENSAT-4" DLR-IB 552-01/92, Wessling, (1992).

USING ENDMEMBERS IN AVIRIS IMAGES TO ESTIMATE CHANGES IN VEGETATIVE BIOMASS

Milton O. Smith[1], John B. Adams[1], Susan L. Ustin[2], and Dar A. Roberts[1]

1 Department of Geological Sciences, University of Washington
Seattle, Washington 98195
2 Department of Land, Air, and Water Resources, University of California
Davis, California 95616

Field techniques for estimating vegetative biomass are labor intensive, and rarely are used to monitor changes in biomass over time. Remote-sensing offers an attractive alternative to field measurements; however, because there is no simple correspondence between encoded radiance in multispectral images and biomass, it is not possible to measure vegetative biomass directly from AVIRIS images. We are investigating ways to estimate vegetative biomass by identifying community types and then applying biomass scalars derived from field measurements.

Field measurements of community-scale vegetative biomass can be made, at least for local areas, but it is not always possible to identify vegetation communities unambiguously using remote measurements and conventional image-processing techniques. Furthermore, even when communities are well characterized in a single image, it typically is difficult to assess the extent and nature of changes in a time series of images, owing to uncertainties introduced by variations in illumination geometry, atmospheric attenuation, and instrumental responses.

Our objective is to develop an improved method based on spectral mixture analysis to characterize and identify vegetative communities, that can be applied to multi-temporal AVIRIS and other types of images. In previous studies we analyzed multi-temporal data sets (AVIRIS and TM) of Owens Valley, CA (Smith et al., 1990) and (TM) of Manaus, Brazil (Adams et al., 1990, and in prep), and defined vegetation communities in terms of fractions of reference (laboratory and field) endmember spectra. An advantage of converting an image to fractions of reference endmembers is that, although fractions in a given pixel may vary from image to image in a time series, the endmembers themselves typically are constant, thus providing a consistent frame of reference.

In the Owens Valley we found that several shrub, riparian and conifer communities could be characterized by the fractions of two types of green vegetation and of shade, in addition to two types of soil. On the shrub-covered bajada the fraction of vegetation (GVF) and the fraction of shade correlated linearly with vegetation cover and with biomass, as determined on the ground. However, the fractions of these endmembers also varied predictably with seasonal changes, emphasizing that any estimates of biomass from AVIRIS or TM images must take into account the season of measurement.

In TM images of Manaus we found that several vegetation communities could be identified by the fractions of the endmembers green vegetation, non-photosynthetic vegetation (NPV), shade and soil. For example, primary forest has a high proportion of NPV (from branches and stems exposed in the canopy) and shade (from shade and shadow associated with canopy roughness). Using fractions of reference endmembers, we were able to consistently identify vegetation communities and changes in communities in TM images over time. The importance of NPV endmembers was further demonstrated in an analysis of AVIRIS images of Jasper Ridge, CA (Roberts et al.,1992).

To further test the identification of a range of vegetation communities using fractions of reference endmembers (Figure 1), we analyzed two sets of multi-temporal

AVIRIS images, one of Jasper Ridge, CA (see Roberts et al., this volume) and Shasta, CA (see Ustin et al., this volume). Six images of the same area near Shasta were obtained on one day at 45 minute intervals about solar noon, providing an opportunity to test how endmember fractions behaved with changing illumination geometry.

In addition to studying multi-temporal AVIRIS data sets we have developed a way to expand the number of endmembers applied to AVIRIS images. In previous analyses we have characterized all of a scene by a few (usually 3-5) endmembers and the residuals for each pixel (e.g. Gillespie et al., 1990). We have now applied a new technique to the above AVIRIS scenes that produces different sets of endmembers for each pixel, in addition to the residuals. This approach expands the potential number of endmembers, while at the same time specifying no more than the number of endmembers needed to fit each pixel. (Sabol et al, 1992 have shown that fitting image data with endmembers that are not present introduces noise and lowers detectability.) The multiple-endmember approach has significantly improved our ability to characterize vegetation communities in AVIRIS and other images. Different communities are fit by different endmembers and by different numbers of endmembers. For example, a pine-forest community near Shasta is fit by spectral mixtures of green vegetation, woody material and shade. In the same scene, shrub and grass communities are fit by the spectra of different green vegetation, NPV and shade, and by characteristic fractions of these endmembers.

Although the fraction of green vegetation in images of the Owens Valley shrubland correlated well with cover and biomass, we emphasize that in general, single parameters such as the fraction of green vegetation, or proxies for the green vegetation fraction (e.g., the normalized-difference vegetation index, NDVI), are not always reliable indicators of biomass. For example, a green pasture and a closed-canopy forest both have high fractions of green foliage but differ substantially in biomass. However, our recent results using reference endmembers indicate that many types of vegetation communities can be identified in sets of AVIRIS images, independent of illumination geometry, and atmospheric and instrumental effects. Measurements of biomass in the field can be linked to vegetation communities that are well characterized by fractions of different types of green foliage and NPV. In addition, the shade fraction is influenced by plant size, spacing and architecture, and can assist in defining the community type.

References.

Adams J.B., Kapos V., Smith M.O., Almeida Filho R., Gillespie A.R., and Roberts D.A., 1990, A new Landsat view of land use in Amazonia, Proc. Int. Symp. on Primary Data Acquisition. ISPRS. Manaus. 1990; 28, part 1,177-185.

Gillespie A.R., Smith M.O., Adams J.B., Willis S.C., Fischer A.F. III, and Sabol D.E., 1990, Interpretation of residual images: Spectral mixture analysis of AVIRIS images, Owens Valley, California, Proc. Second Airborne Visible/Infrared Imaging Spectrometer (AVIRIS) Workshop, JPL Pub. 90-54, 243-270.

Roberts D.A., Smith M.O., and Adams J.B., 1992, Green vegetation, non-photosynthetic vegetation and soils in AVIRIS data, Remote Sensing of Environ., in press.

Sabol D.E., Adams J.B., and Smith M.O., 1992, Quantitative sub-pixel spectral detection of targets in multispectral images, J. Geophys. Res.97, 2659-2672.

Smith M.O., Ustin S.L., Adams J.B., and Gillespie A.R., 1990a, Vegetation in deserts: I. A regional measure of abundance from multispectral images, Remote Sensing of Environ.31, 1-26.
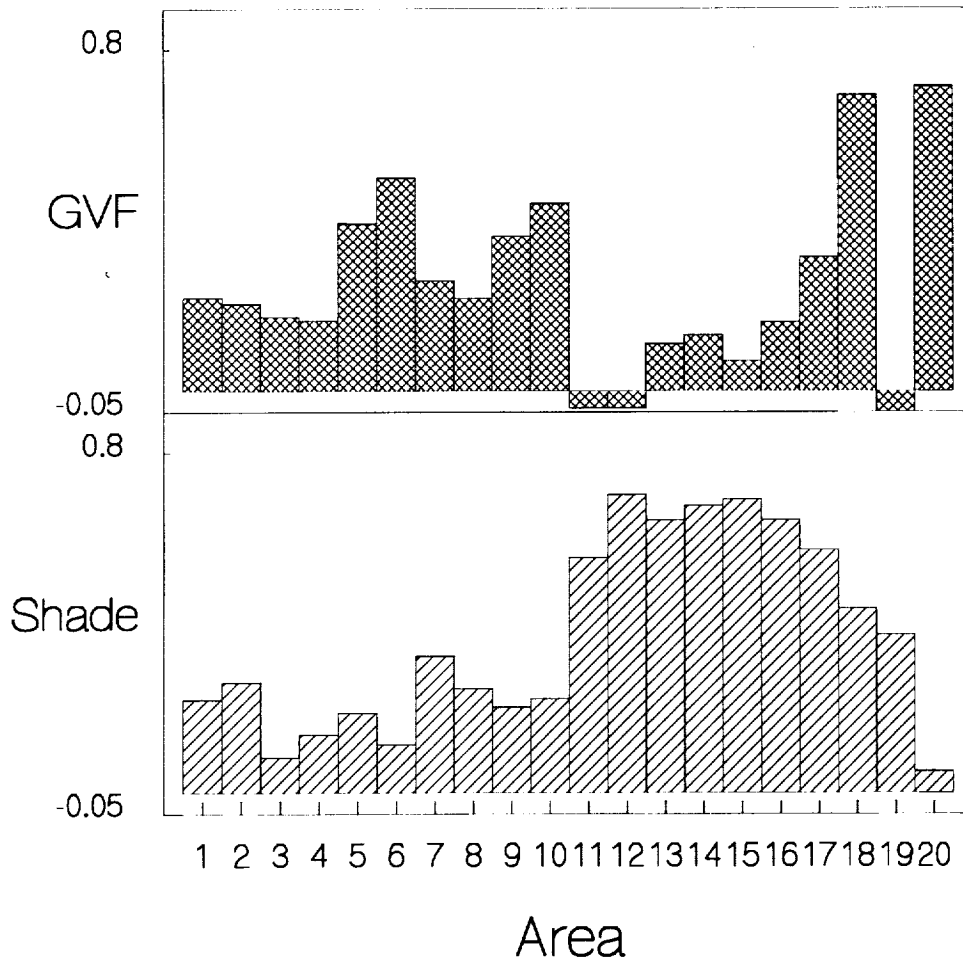
Figure 1.
The G_{vf} and shade fraction for 20 areas of diverse vegetation communities of AVIRIS images of Jasper Ridge and Shasta, CA. The areas are 1) 1st clear cut area 2) 2nd clear cut area 3) 1st recent clear cut area 4) 2nd recent clear cut area 5) second growth ponderosa pine plantation 6) 1st mature ponderosa pine forest 7) 2nd mature ponderosa pine forest 8) 2nd young second growth ponderosa pine stand 9) 1st young second growth stand 10) meadow 11) ungrazed non serpentine drygrass, 12) serpentine grassland, 13) serpentine chaparral, 14) nonserpentine chaparral, 15) nonserpentine chaparral with dieback, 16) blue oak ,17) evergreen oak, 18) forest wetland, 19) grassland at Webb ranch, and 20) golf course. The G_{vf} does not provide a reasonable estimate of biomass over all communities. The vegetation fractions do not correspond to a ranking that coincides with the biomass. The meadow, for example, has a higher vegetation fraction than any of the forested areas but has a lower biomass. Even when shade is normalized out of the remainder of fractions the forest contains other nonphotosynthetic endmembers not part of the G_{vf}.

$524-48$
189070
$P.5$

ATMOSPHERIC CORRECTION OF AVIRIS DATA IN OCEAN WATERS

Gregory Terrie and Robert Arnone
Naval Research Laboratory, Stennis Space Center

1. INTRODUCTION

Hyperspectral data offers unique capabilities for characterizing the ocean environment. The spectral characterization of the composition of ocean waters can be organized into biological and terrigenous components. Biological photosynthetic pigments in ocean waters have unique spectral ocean color signatures which can be associated with different biological species (Arnone et al, 1986). Additionally, suspended sediment has different scattering coefficients which result in ocean color signatures. Measuring the spatial distributions of these components in the maritime environments provides important tools for understanding and monitoring the ocean environment. These tools have significant applications in pollution, carbon cycle, current and water mass detection, location of fronts and eddies, sewage discharge and fate etc.

Ocean color has been used from satellite for describing the spatial variability of chlorophyll, water clarity (k_{490}), suspended sediment concentration, currents etc. Additionally, with improved atmospheric correction methods, ocean color results have produced global products of spectral water leaving radiance (L_w) (Feldman 1989). Ocean color results have clearly indicated strong applications for characterizing the spatial and temporal variability of bio-optical oceanography (Arnone et al, 1991).

These studies have been largely the results of advanced atmospheric correction techniques applied to multispectral imagery. The atmosphere contributes approximately 80% - 90% of the satellite received radiance in the blue-green portion of the spectrum. In deep ocean waters, maximum transmission of visible radiance is achieved at 490nm. Conversely, nearly all of the light is absorbed by the water at wavelengths greater than about 650nm and thus appears black. These spectral ocean properties are exploited by algorithms developed for the atmospheric correction used in satellite ocean color processing.

The objective of this study was to apply atmospheric correction techniques that were used for processing satellite Coastal Zone Color Scanner (CZCS) data to AVIRIS data. Quantitative measures of L_w from AVIRIS will be compared with ship ground truth data and input into bio-optical models.

2. METHODS

Atmospheric correction of CZCS assumes a linear summation of the total radiance, $L_t(\lambda)$, sensed at the sensor (Gordon et al, 1983, Gordon and Clark, 1979). The atmospheric contribution is divided into the Rayleigh, $L_r(\lambda)$, component (molecular scattering) and the aerosol, $L_a(\lambda)$, component (Mie scattering). The volume scattering of the water, $L_w(\lambda)$ (ocean color) is transmitted through the air sea interface, $t(\lambda)$. All of these parameters are related to the total radiance, $L_t(\lambda)$ by

$$L_t(\lambda) = L_r(\lambda) + L_a(\lambda) + t(\lambda)L_w(\lambda). \qquad (1)$$

Assuming that the signal at 670nm is due entirely to atmospheric effects and the aerosol optical thickness $\tau_a(670)$ is proportional to $\tau_a(\lambda)$, equation (1) can be written in terms of $L_w(\lambda)$, at nadir, by

$$tL_w(\lambda)=L_t(\lambda)-L_r(\lambda)-\frac{F_0(\lambda)}{F_0(670)}(\frac{\lambda}{670})^n(L_t(670)-L_r(670)), \qquad (2)$$

where F_0 is the solar flux and n is the angstrom coefficient.

This relationship was applied to AVIRIS data by expanding this generalized nadir equation to account for the angular atmospheric path radiance from the sensor altitude. The rayleigh component $L_r(\lambda)$ was computed using a multiple scattering model (Gordon et al, 1988). Both solar and sensor zenith and azimuth angles were computed for each pixel in the scene according to the date, time and location of data collection. The solar fluxes were assumed constants and the angstrom coefficient was varied.

Four spectral channels were used in processing CZCS ocean color data which were centered at 443nm, 520nm, 550nm, and 670nm with a bandwidth of 20 nm. The 443nm channel represents the chlorophyll absorption wavelength which is inversely proportional to concentration (Clark 1980). The 520nm and 550nm channels characterize the hinge point in bio-optical ocean waters and are related to sediment scattering. These bands were simulated using AVIRIS bands by averaging the two adjacent bands for each wavelength. Additionally, a 750nm channel, analogous to the CZCS 750nm band, was used as the atmospheric reference channel because of a problem with bottom reflectance at 670nm, especially in the shallow coastal regions. Each of the channels were calibrated for spectral radiance and for vignetting effects using the supplied correction data.

The atmospheric model was applied to an AVIRIS scene collected off Tampa Bay on April 3, 1990. This image has many different ocean regimes characterizing, shallow coastal waters with a uniform bottom reflectance, suspended sediment in the water, absorbing "yellow substance", and variability of coastal phytoplankton and clear waters. Ship measurements were collected by the University of South Florida (Carder et al, 1991) coincident with the overflight at three stations in which $L_w(\lambda)$, chlorophyll, and the diffuse attenuation coefficient were measured.

3. RESULTS

The 443nm channel is severely contaminated by the atmosphere and sensor noise such that little ocean features are observed. Atmospheric scattering diminishes in the 520nm and 550nm channels and ocean features can be recognized although not quantitative. Atmospheric correction using the 670nm channel as the reference was applied to the scene ranging from clear waters to the coastal environments. In the near shore coastal waters, the AVIRIS data was shown to be correlated with the bathymetry since the reflectivity of the white bottom clearly dominated the water leaving radiance signal. The 670nm channel was shown to be correlated with bottom reflectivity and therefore is not a good channel for only characterizing the atmosphere. Because of these non-zero 670nm components, these is an overcorrection for the atmosphere. This results in negative radiance in areas where the bottom reflectance dominates the 670nm channel. Since this is not possible the images were processed and negative values clipped to zero. The

resulting atmospheric corrected 443 radiance was significantly improved and agreed favorably with the ship radiance data. Similarly, the 520nm and 550nm radiances were clipped to zero radiances in the shallow coastal waters. Comparison with the ship ground truth showed comparable results. Use of the 750nm channel for aerosol correction in the coastal waters showed improvement versus the 670nm.

The atmospherically corrected data was then used to compute chlorophyll and k_{490} distributions. Results compared favorably with ship data and spatial distribution is clearly evident.

4. CONCLUSIONS

Because the atmosphere contributes a high percentage of the signal, the low signal to noise of AVIRIS limits the atmospheric removal process for deep ocean waters. The atmospheric correction techniques on CZCS can be applied to AVIRIS imagery to obtain quantitative estimates of the water leaving radiance. These results appear comparable with ship measurements. The high bottom reflectance observed in shallow waters severely restricts the conventional atmospheric correction technique of CZCS processing. Improved techniques are required to separate the volume scattering ocean color and the bottom reflectance radiance. The removal of the atmospheric contamination using the CZCS techniques can be improved substantially by using other spectral channels which are available using AVIRIS. Future efforts are focused on identifying optimal channels for atmospheric removal.

5. ACKNOWLEDGEMENTS

6. REFERENCES

Arnone R.A, Bidigare R.R, Trees C.C. and Brooks J. "Comparison of the attenuation of spectral irradiance and phytoplankton pigments within frontal zones." *Ocean Optics VII, Proc. SPIE*, **637**: 126-130. 1986

Arnone R.A, and Elenbass W. "Optical variability off the East coast using CZCS data", *EOS Trans.* **72**(17), 1991.

Carder K., P. Reinersman, R. Chen, F. Muller-Karger, C. Davis, and M. Hamilton. "AVIRIS Calibration and Application in Coastal Oceanic Environments". Submitted to *Remote Sensing of the Environment*, (1992).

Clark, D.K. "Phytoplankton Pigment Algorithms for the Nimbus-7 CZCS", *Oceanography from Space*, J.R.F. Gower, Ed. (Plenum, NY, 1981), pp 227-238.

Feldman, C, N. Kuring, C. Ng, W. Esaias, C. McClain, J. Elrod, N. Maynard, D. Endres, R. Evans, J. Brown, S. Walsh, M. Carle, and G. Podesta. "Ocean color: Availability of the global data set",*EOS*,**70**(23), 634-641, 1989.

Gordon H.R. and D. Clark. "Atmospheric Effects in the Remote Sensing of Phytoplankton Pigments", *Boundary-Layer Meteorology* **18** (1980), 299-313.

Gordon H.R., J.W. Brown, and R.H. Evans. "Exact Rayleigh scattering calculations for use with the Nimbus-7 Coastal Zone Color Scanner", *Applied Optics* **27**(5), 862-871, 1988.

THE 1991 AVIRIS/POLDER EXPERIMENT IN CAMARGUE, FRANCE

N 9 4 - 1 6 6 9 1

F. Baret[1], C. Leprieur[2], S. Jacquemoud[1], V. Carrère[3], X.F. Gu[1], M. Steven[4],
V. Vanderbilt[5], J.F. Hanocq[1], S. Ustin[6], G. Rondeaux[5], C. Daughtry[7], L. Biehl[8],
R. Pettigrew[5], D. Modro[5], H. Horoyan[1], T. Sarto[5], C. Despontin[1],
H. Razafindraibe[1]

[1]INRA Bioclimatologie, BP 91 , 84140 Montfavet Cedex, France,
[2]LERTS, 18 Av. Ed. Belin, 31 055 Toulouse cedex, France,
[3]JPL, MS 180-701, 4800 Oak Grove Drive, Pasadena CA 91109, USA,
[4]Nottingham university, Dept. Geog., NG7 2RD, Nottingham, England,
[5]NASA/Ames R.C., MS 242-4, Moffet Field, CA 94 035, USA,
[6]Dept. Land Air Water Res., Unic. Calif. Davis, 95 616, USA,
[7]USDA/ARS, RSL., Buid. 1, BARC-West, Beltsville, Maryland 20705, USA,
[8]Purdue University, West Lafayette, Indiana 47907, USA.

1. INTRODUCTION.

Airborne campaigns during the eighties have provided high spectral resolution data, collected with imaging instruments such as AIS, AVIRIS, FLI, CAESI and ISM, in order to investigate the relationship with canopy biophysical characteristics. The statistical approaches used to analyze these data do not allow investigation of the causality and the applicability of the observed correlations. Further, statistical studies have demonstrated the high degree of redundancy of the spectral information (Ferns et al, 1984; Price, 1991 amongst many others). And for retrieving vegetation biophysical characteristics, few results demonstrate the real information gain attributable to the high spectral resolution capability as compared to the use of a few wide wavelength bands.

With several new imaging spectrophotometers scheduled for launch during the next 10 years (MERIS, MODIS, HIRIS), progress in the description and understanding of the mechanisms that drive the spectral variation of canopy reflectance is required. Most of these new sensor systems will also have the capability to observe the target under differing view directions. The problem of the combination and the use of the synergy between both the spectral and the directional sources of canopy reflectance variations has to be addressed.

Apart from the atmospheric effects, the spectral variation of the light reflected by canopies originates from the leaves, the soil or the other vegetation elements such as branches and fruits. At leaf level, both diffuse reflectance and transmittance may be simulated by simple models (Jacquemoud and Baret, 1990), although no accurate information exists on the absorption features of the biochemicals (except water) in the 900-2500nm wavelength range. Many models mimic the directional variability of canopy reflectance at a given wavelength (see the review by Goel, 1988 for example). Combining a leaf spectral model with a canopy directional model provides a powerful tool to analyze this problem. Some of us have initiated such a study (Baret et al, 1991, Jacquemoud, 1992), but our approach and theory remain to be tested using canopy data with their complexity, associated experimental error, and atmospheric effects.

The main objective of the 1991 POLDER/AVIRIS experiment in Camargue was to provide a consistent data set over various canopies in order to test the applicability of the theory. The experiment, part of the 1991 MAC Europe experiment, involved simultaneous data collection using two sensors: AVIRIS (Vane, 1987) and POLDER (Deschamps et al, 1990) which measures the bidirectional and polarization properties of the targets at 670 and 880nm wavebands.

3. THE EXPERIMENT

The topographically flat flightline, located near the Camargue region in the south of France, included diverse crops planted in fields having dimensions from 100 to 500m.
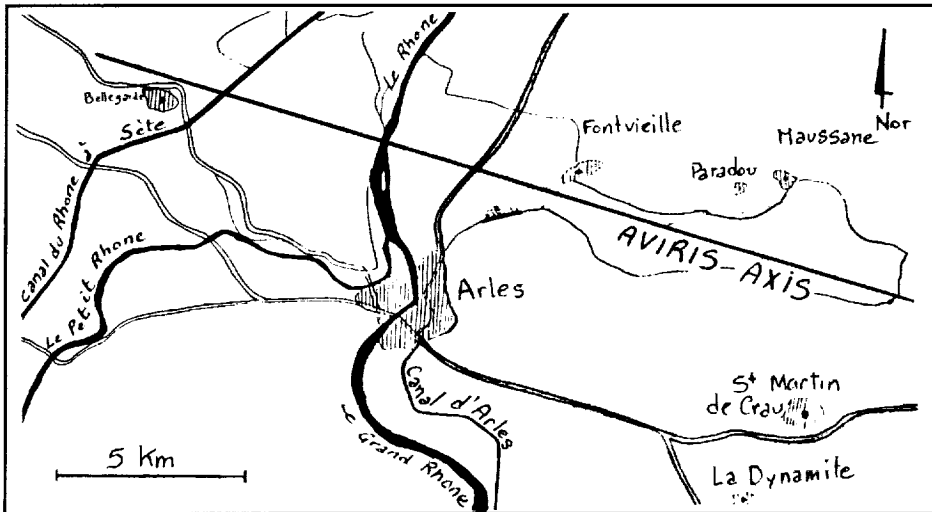
3.1. The flights

The altitude of each sensor, 20,000m for AVIRIS flown on the NASA ER-2 and 3,000m for POLDER on the ARAT airplane, provided a ground spatial resolution of approximately 20m for each sensor. Simultaneous data were collected on June 24, 1991. In addition POLDER data were collected on 18, 19, and 21 June 1991 and AVIRIS data on July 16, 1991. The POLDER flights were designed to sample the directional variability due to both sun and view orientation.

3.2. The ground measurements.

The characteristics of the atmosphere, monitored during collection of aircraft data, will allow retrieval of calibrated reflectance values. Retrieval will be facilitated by the availability of additional atmospheric data collected at the AVIRIS/SPOT calibration experiment at La Crau (about 30Km distance from our test sites). Three types of sunphotometers (Reagan, Cimel, spectral hygrometer) were used to measure solar irradiance throughout the day. During AVIRIS flights, the reflectance of two contrasted fields was recorded using SPOT simulation Cimel radiometers and a spectrophotometer. These measurements will provide tests of the accuracy of atmospherical corrections.

The ground measurements were designed to provide information about canopy biophysical parameters. Two data sets were gathered:

One **intensive data set** included 28 individual fields planted primarily in sunflower, corn, sorghum and rice. On each field, the leaf area index, the fresh and dry

biomass and its partition between leaf and stem were measured. A subsample of the leaves was later analyzed for chlorophyll, accessory pigments and biochemical constituents such as lignin, starch and proteins. Other characteristics such as the plant height, row orientation, vegetation coverage, soil surface characteristics were also noted. On 21 of the 28 plots, the zenithal variation of the gap frequency was evaluated using the LAI2000 device developed by LiCor. This measurement is particularly important in radiative transfer models and allows computation of the PAR balance for the canopies. Except for sunflower canopies, the leaf area index computed from gap frequency data showed good agreement with LAI values which were directly measured. (The heliotropism common to sunflower canopies might violate the hypotheses that leaves are distributed randomly in azimuth.) Optical properties of the leaves were measured using both laboratory (Varian Cary D17) and field portable spectrophotometers.

The second, **extensive data set,** which includes per field species information for the entire flightline, was developed during an exhaustive, ground level enquiry. This information will be available for resolving questions linked to the spatial scale.

5. CONCLUSION

This experiment will provide a consistent data set which includes the spectral, directional and polarization variations of canopy reflectances. The next step in the data processing is to build a data base for the 28 plots which contains the atmospherically corrected ground level reflectances linked to the biophysical measurements of the canopies. This will permit us to apply and test the relationships, developed during model simulation, to aircraft data. Ultimately, results from this experiment will allow better estimates of plant canopy biophysical properties through improved extraction of the spectral, directional and polarization information contained in data collected by spaceborne sensors.

6. REFERENCES

Baret F., Jacquemoud S., Leprieur C., Guyot G., **1992**. Modelled analysis of the biophysical nature of spectral shifts. Accepted for Remote Sens. Environ.

Deschamps P.Y., Herman M., Podaire A., Leroy M., Laporte M., Vermande P., **1990**. A spatial instrument for the observation of polarization and directionnality of earth reflectances: POLDER. in IGARSS'90 conf. proc., Washington D.C., USA.

Ferns, D.C., Zara J.C., Barber J., **1984**. Application of high resolution spectroradiometry to vegetation. Photogram. Eng. Remote Sens., 50(12):1725-1735.

Goel N.S., **1988**. Models of vegetation canopy reflectance and their use in estimation of biophysical parameters from reflectance data. Remote Sens. Reviews, 4(1).

Jacquemoud S., Baret F., **1990**. PROSPECT: a model of leaf optical properties spectra. Remote Sens. Environ. 34:75-91.

Jacquemoud S., Baret F., **1991**. Estimation des parametres biophysiques d'un couvert vegetal par inversion d'un modele de reflectance sur des donnees haute resolution spectrale. Workshop "Structure du couvert vegetal et climat lumineux. Methodes de caracterisation et applications", 23-27 Sept.,Chateau de Saumane, France.

Price J.C., **1990**. On the information content of soil spectra. Remote Sens, Environ. 33:113-121.

Vane G., **1987**. Airborne Visible/Infrared Imaging Spectrophotometer: Description of the sensor, ground data, processing facility, laboratory calibration and first results. JPL publication 87-38.

AVIRIS:
RECENT INSTRUMENT MAINTENANCE, MODIFICATIONS AND 1992 PERFORMANCE

Thomas G. Chrien

Jet Propulsion Laboratory
4800 Oak Grove Drive, Pasadena California, 91109

1. INTRODUCTION

Over the past five years the AVIRIS engineering team has worked to improve the performance, reliability and calibration accuracy of the AVIRIS sensor. Recent modifications to the instrument include a new tape recording subsystem and an improved blocking filter for the D spectrometer. Maintenance activities during the 1992 engineering cycle include the recoating of the spectrometer spherical mirrors, replacement of the fiber optic harness and routine noise reduction tuning and optical alignment.

2. TAPE RECORDER UPGRADE

The Ampex AHBR 1700 tape recorder system has been replaced by a Metrum VLDS. The VLDS provides a number of advantages over the old Ampex unit. The lower cost of the VLDS has made it possible to purchase a field replaceable spare. The T120 VHS cassette tape format eliminates the need for preflight tape threading. The 10 Gigabyte storage capacity enables the acquisition of approximately 70 AVIRIS scenes per flight.

3. SIGNAL THROUGHPUT

The AVIRIS scan mirror has been re-coated. The new coating has a 10% improvement in reflectivity at 400 nanometers. A new fiber harness has been installed and will return the D spectrometer to full service. A new, more resilient IR fiber material was used. An additional anti-reflection coating has been added at the foreoptics end of the new fiber harness. The recoating of the spherical spectrometer mirrors has increased signal throughput and eliminated the scattering caused by a previous incident of water damage.

A new blocking filter has been installed in the D spectrometer. The old blocking filter impacted the signal level of the last five spectral channels. The new blocking filter will enable good signal out to 2500 nanometers. The channel positions will be shifted to take advantage of this fact. The new filter also has a 20% better transmittance in the pass band.

4. SYSTEM NOISE

A detailed study of sensor related noise was useful in identification of a number of noise reduction actions. The result is reduced system noise and

better external noise rejection. Modifications include (1) timing signal opto-isolators with lower jitter, (2) nested timing of the clock driver signals, (3) RFI shielded timing cables, (4) better routing of dewar internal wiring, and (5) rerouting of the focal plane temperature sensor wiring.

5. PREDICTED PERFORMANCE

The current instrument performance as assessed by the preseason laboratory calibration and inflight calibration experiment will be presented. Performance will be stated in terms of signal-to-noise ratio for a standard reference radiance and in terms of noise equivalent radiance for each of the spectral channels.

6. FUTURE MAINTENANCE WORK

The primary maintenance activity for the 1993 engineering cycle will be the replacement of the focal plane arrays. The A spectrometer FPA experienced a wire debond immediately after the 1991 flight season. Other FPAs have shown an increase in the number of noisy pixels. Each FPA has over 1000 liquid nitrogen cool down cycles in which the temperature goes from 300 K to 77 K in less than one minute.

7. REFERENCES

Vane, Airborne Visible/Infrared Imaging Spectrometer, JPL pub 87-38, Nov. 15, 1987.

Vane, Proceedings of the Airborne Visible/Infrared Imaging Spectrometer Performance Evaluation Workshop, JPL pub. 88-38, June 6, 1988.

Green, Proceedings of the Second Annual Airborne Visible/Infrared Imaging Spectrometer Workshop , JPL pub. 90-54, June 4, 1990.

Green, Proceedings of the Second Annual Airborne Visible/Infrared Imaging Spectrometer Workshop, JPL pub. 91-28, May 20, 1991.

8. ACKNOWLEDGMENTS

AVIRIS GROUND DATA PROCESSING SYSTEM

Earl G. Hansen, Steve Larson, H. Ian Novack, Robert Bennett

Jet Propulsion Laboratory, California Institute of Technology
4800 Oak Grove Drive, Pasadena, California 91109

1. INTRODUCTION

During the last year and a half, February, 1991 to June, 1992, a major upgrade of the AVIRIS ground data processing system has taken place. Both the hardware and software components have been changed significantly to improve the processing capacity and performance and to structure a data facility capable of handling the projected work load into the near future.

This paper will provide a summary report of these changes and some projections for the future.

2. OBJECTIVES

The objectives of the AVIRIS data facility are to decommutate and archive AVIRIS data and to provide raw or radiometrically calibrated data products to the science investigator. These primary objectives have not changed from the initial concepts (Reimer et al. 1987). The upgrade effort has greatly improved the processing system. These objectives can now be accomplished in a more timely fashion at a reasonable cost and there is sufficient capacity to manage the current processing load and provide for future growth. The method of implementation has added the flexibility to provide better service to the investigator and allow for future changes.

3. HARDWARE DESCRIPTION

The data facility hardware system has been changed significantly. The original system was a VAX 11/780 processor with 2.4 GB of disk, two 1/2 inch tape drives, a 35mm camera for quicklook production and an AMPEX HBR3000 high density tape drive for playback of the instrument tape. This system became too slow to handle the processing load in a timely manner.

The new system consists of two UNIX based server platforms and two UNIX based workstations. The archiving process runs on a SUN 4/490 server with 32 MB of memory, 8 GB of disk, two 4mm DAT tape drives, one 8 mm tape drive, a Kodak XL7700 image printer, and a Metrum VLDS tape subsystem to provide playback of the instrument tape. The 4mm DAT tape drives are used as the archive media and the Kodak image printer replaces 35mm photography prints as the quicklook production method.

The hardware system for retrieval processing is a Solbourne 5E/900 server with two SPARC processors running in a symmetric multiprocessing mode. This system has 128 MB of memory, 8 GB of disk, two 1/2 inch tape drives, three 4mm DAT tape drives, two 8mm tape drives, and two IVAS image processing subsystems. The 1/2 inch, 4mm DAT, and 8mm tape drives provide the means to deliver data

products to the investigators. The IVAS processors are used as analysis display devices providing 24-bit color capability. This system also serves as the host for the RDBMS which stores the archive catalog, the retrieval audit trail and quality control tables and the instrument performance statistical tables.

Two SUN SPARC 1 workstations provide the software maintenance and testing capabilities. In addition these workstations support the calibration process, data analysis and scientific visualization.

4. OPERATION

The major impacts the upgrade has made on operations are in the areas of performance and capacity. The archival process has been improved to perform the archiving of one scene in twenty minutes with the production of quicklooks on the same day as archiving using the image printer. The use of a dedicated server allows the archiving of AVIRIS data in quantities of runs, as it is acquired. Each run can be archived in one to two hours depending on the run size. This makes possible the archiving of four to eight runs per day. The quicklooks for these runs are available for mailing the next day. The system as implemented has a capacity to archive 3600 scenes per year allowing for system maintenance and down time. It will also provide for a one week time span from data acquisition to delivery of quicklooks.

Retrieval processing performance has also been improved. The system as implemented permits processing of each scene in thirty to forty minutes depending upon the processing options. This new system will allow two retrievals to be run concurrently. The capacity of the new system is then comparable to the archiving system, capable of producing 3600 retrieval data products annually. In addition, the new system will permit the creation of data products on additional media and in UNIX format. Retrieval products will be available on 1/2 inch, 8mm, or 4mm DAT tapes and in both VAX and UNIX formats.

5. FUTURE PLANS

With the implementation of the new data processing system a major improvement in the data handling capabilities for AVIRIS has been accomplished. This system should provide a stable, flexible and maintainable facility for processing AVIRIS data today and into the near future.

Additional improvements are being explored and will be implemented as they are approved. Next to be explored is the possible use of CD-ROM as a delivery media for retrievals. In the near future the means to master CD-ROM disks in the data facility will become available at reasonable cost and performance. This media would be added to the choices for data product delivery.

We look forward to supporting the science community in delivering high quality data in a timely fashion and ask that any suggestions on how we can improve our service to you, the investigator, be forwarded to the AVIRIS support team.

6. REFERENCES

W. M. Porter, T. G. Chrien, E. G. Hansen, C. M. Sarture, "Evolution of the Airborne Visible/Infrared Imaging Spectrometer (AVIRIS) Flight and Ground Data Processing System," *Imaging Spectroscopy of the Terrestrial Environment, Proceedings of SPIE,*

Volume 1298, pp. 11-17, 1990.

J. H. Reimer, J. R. Heyada, S. C. Carpenter, W. T. S. Deich, M. Lee, "AVIRIS Ground Data Processing System," *Imaging Spectroscopy II, Proceedings of SPIE,* Volume 834, pp. 79-90, 1987.

SIMULATION OF ASTER DATA USING AVIRIS IMAGES

Michael Abrams

Jet Propulsion Lab/California Institute of Technology
4800 Oak Grove Dr.
Pasadena, California 91109

The Advanced Thermal Emission and Reflectance
Radiometer (ASTER) is a joint Japanese/US imaging in-
strument scheduled to fly on the first EOS platform in
1998. The complement of scanners includes a visible, three
channel module with forward-looking stereo capability, a
six channel short wavelength infrared module, and a five
channel thermal module. As part of the definition phase
for the instrument design, we used AVIRIS data to simu-
late the SWIR bands to investigate the effects of widening
two of the bands to increase the signal-to-noise ratio
(SNR) versus loss of spectral separability due to uncertain-
ty in the post-launch band positions.

The six SWIR bands (channels 4 to 9) are located in
the region between 1.60 and 2.43 µm. The nominal band
positions and widths (FWHM) are shown in Table 1. These
bands were selected to maximize separability of certain
important minerals or mineral groups. Band 8, for exam-
ple, is centered over a major absorption feature for car-
bonates. Bands 5, 6 and 7 are located to allow separation of
absorption features of hydrous minerals: alunite in band 5,
sericite/montmorillonite in band 6, kaolinite in bands 5
and 6, and chlorite in band 7, for example. At the time of
this study, there was still freedom to modify the widths of
bands 5 and 6. Increasing the widths from 40 to 50 nm
would increase the SNR by about 25%, but would cause
increased overlap between the bands, and hence a decrease
of spectral separability for minerals whose major absorp-
tion features were in these two bands. In addition, there is
a potential post-launch uncertainty of ±7 nm in the band
positions, so they could possibly overlap even more than
from just widening.

AVIRIS data over Cuprite, Nevada were chosen to
create simulated ASTER bands to study the trade-off
between SNR and spectral separability. These data were
flown on July 19, 1990.

Four simulations of the ASTER bands were created:
nominal bands, wider bands, and each of these shifted 7

nm closer together (the worst cases). ASTER bands were produced by fitting gaussian band shapes to the AVIRIS channels, then amalgamating the appropriate number of AVIRIS bands. SNR was calculated by a similar procedure using the dark current file for the noise, and locating areas on the images for signal computation.

Simulated images were processed using ratioing, principal components, etc. for visual examination and evaluation. Additionally, known mineralogically homogeneous area were extracted from the images, and the point spectra plotted for evaluation of spectral separability. These examples will be shown during the presentation.

The results of this study confirm that widening bands 5 and 6 from 40 to 50 nm would increase the SNR by about 25%. On the other hand, spectral separability of kaolinite and sericite suffers as a result of the combined effects of widening the bands and the (worst case scenario) further overlap caused by a 7 nm shift in band positions. The recommendation was made to maintain the bands at 40 nm width to maximize spectral separability, at the expense of increased SNR.

Table 1. ASTER nominal SWIR bands

Band	Range (μm)	Width (nm)
4	1.600-1.700	100
5	2.145-2.185	40
6	2.185-2.225	40
7	2.235-2.285	50
8	2.295-2.365	70
9	2.360-2.430	70

USE OF AVIRIS DATA TO THE DEFINITION OF OPTIMISED SPECIFICATIONS FOR LAND APPLICATIONS WITH FUTURE SPACEBORNE IMAGING SPECTROMETERS

J. Bodechtel

AGF am Institut für Allgemeine und Angewandte Geologie
Ludwig-Maximilians-Universität München
Luisenstraße 37, W-8000 München 2

Recent experience with airborne imaging spectrometers has demonstrated the advantages of narrow band sensors over broad band scanners for characterising the nature, extent and physical status of typical land surfaces. Information on key spectral features associated with various land surfaces can be obtained from the data of such instruments, which can be used to simulate spaceborne imaging spectrometer data and to assess their information content if comprehensive underpinning is provided by ground data.
The collection of such information has been an issue of airborne imaging spectrometer campaigns like the NASA MAC-Europe 1991.
In the presented study airborne and ground data obtained from different test sites in Europe are utilised for a comparative analysis of the spectral signatures of various land surfaces (vegetation, bare soils and rocks, mixed soil/rock - vegetation) as seen from different imaging spectrometers like AVIRIS, GERIS 63 band scanner and CASI. The following items are discussed:

- the significance of different spectral regions within the wavelength interval between 0.4 m and 2.5 m for the differentiation of different land units.

- recommendations on the optimum band selection and band-widths to be used for the application of future satellite-based imaging spectrometers for land applications.

- the boundaries for the detection of plant features in mixed-soil plant spectra and the influence of different soil properties on the mixture of the spectra.

- recommendations on the optimum spatial resolution and recording dates for the discrimination of spectral features of various surface types.

- evaluation of different data compressing techniques for the optimum extraction of spectral information from imaging spectrometry data.

PRIMARY STUDIES OF TRACE QUANTITIES OF GREEN VEGETATION IN MONO LAKE AREA USING 1990 AVIRIS DATA[**]

Zhikang Chen, Chris D. Elvidge

Biological Sciences Center
Desert Research Institute
University of Nevada System
7010 Dandini Blvd.
Reno, Nevada 89512

David P. Groeneveld

Inyo County Water Department
163 May Street
Bishop, California 93514

Our primary results in Jasper Ridge Biological Preserve indicate that high spectral resolution AVIRIS data may provide a substantial advantage in the detection of trace quantities of green vegetation, based on the chlorophyll red edge feature from 700-780 nm. The chlorophyll red edge was detected for green vegetation cover as low as 4.8%. The objective of our studies in Mono Lake area is to continue the experiments performed in Jasper Ridge and to examine the persistence of red edge feature of trace quantities of green vegetation for different plant communities with non-uniform soil backgrounds.

Mono Lake area contains a wide variation in both rock and soil spectral signatures and vegetation density levels, ranging from sparse desertscrub to pine forests and dense canopies of riparian corridors. High quality AVIRIS data of this area was acquired in 1990. Low altitude aerial photography was used to assist in the location of the field sites in the field and on the AVIRIS data sets. Two types of field sites were selected for the investigation: calibration targets and vegetation test sites. A series of calibration targets covers a spread in ground reflectance from about 0% in NIR (open water) to nearly 70% (salt shell on open sediment) over the AVIRIS bands. The vegetation test sites chosen have all major

[**] Presented at the Third JPL Airborne Geosciences Workshop, Pasadena, California, June 1-5, 1992.

backgrounds versus vegetation combination present in the AVIRIS flight area. The AVIRIS DN spectra for each test site were calibrated to ground reflectance by using an empirical linear regression equation: Reflectance=A+B*DN. The coefficients of A, B were generated from calibration targets. The primary results of this research have shown that the red edge magnitude persistently decrease as green cover densities decrease. But this research is still underway. The detailed results and analyses will be available later.

REFERENCES

Collins, W. (1978), Remote sensing of crop type and maturity, Photogramm. Eng. Remote Sens. 44:43-55.

Elvidge, C.D. and Lyon, R.J.P. (1985), Influence of rock-soil spectral variation on the assessment of green biomass, Remote Sens. Environ. 17:265-279.

Elvidge, C.D. (1988), Vegetation reflectance features in AVIRIS data, in Proc. Int. Symp. Remote Sens. Environ., 6th Thematic Conf: Remote Sensing for Exploration Geology, Houston, TX, p.169-178.

Elvidge, C.D. and Mouat, D.A. (1989), Analysis of green vegetation detection limits in 1988 AVIRIS data, in Proc. Int. Symp. Remote Sens. Environ., 7th Thematic Conf: Remote Sensing for Exploration Geology, Calgary, Alberta, Canada, 16p.

Huete, A.R., Jackson, R.D. and Post, D.F. (1985), Spectral response of a plant canopy with different soil backgrounds, Remote Sens. Environ. 17:37-53.

Peterson, D.L., Aber, J.B., Matson, P.A., Card, D.H., Swanberg, N., Wessman, C. and Spanner, M. (1988), Remote sensing of forest canopy and leaf biochemical contents, Remote Sens. Environ. 24:85-108.

Rock, B.N., Hoshizaki, T. and Miller, J.R. (1988), Comparison of in situ and airborne spectral measurements of the blue shift associated with forest decline, Remote Sens. Environ. 24:109-127.

Tucker, C.J. (1979), Red and photographic infrared linear combinations for monitoring vegetation, Remote Sens. Environ. 8:127-150.

JPL ACTIVITIES ON DEVELOPMENT OF ACOUSTO-OPTIC TUNABLE FILTER IMAGING SPECTROMETER

Li-Jen Cheng, Tien-Hsin Chao, and George Reyes
Center for Space Microelectronics Technology
Jet Propulsion Laboratory
California Institute of Technology
Pasadena, California 91109

This paper reports recent activities of JPL in the development of a new type of imaging spectrometers for earth observation and planetary exploration. This instrument uses the acousto-optic tunable filter (AOTF) as high resolution and fast programmable bandpass filter. AOTF operates in the principle of acousto-optic interaction in an anisotropic medium. This filter can be tuned in sequential, random, and multiwavelength access modes, providing observational flexibility. The diffraction process in the filter generates two diffracted monochromatic beams with polarization orthogonal to each other, creating a unique capability to measure both polarimetric and spectral properties of the incoming light simultaneously with a single instrument. The device gives wide wavelength operations with reasonably large throughput. In addition, it is in a compact solid-state structure without moving parts, providing system reliability. These attractive features give promising opportunities to develop a new generation of airborne/spaceborne and ground, real-time, imaging spectrometer systems for remote sensing applications.

The operation principle of the AOTF imaging spectrometer is different from that of current airborne multispectral imaging instruments, such as the airborne visible/infrared imaging spectrometer (AVIRIS). The AOTF instrument gives a two-dimensional image at a desired wavelength at one time, whereas AVIRIS takes a spectrum over a predetermined wavelength range at one pixel at a time and the image is constructed later. Each technique has its own merit. AVIRIS is an excellent tool for high spectral resolution remote sensing of earth. AOTF instrument has its unique properties. For example, AOTF allows observations to be tailored in real time to perform the desired experiments and to collect only required data. For example, an AOTF imaging spectrometer has the potential to monitor distributions of several gaseous

pollutants in air and its time variation in real time. In addition, the flexibility enables the instrument to address a wide range of objectives and permits the observation parameters to be modified in flight as new objectives are developed. Consequently, the performance in each mission can be increased with minimal resources.

Up to now, two microcomputer-controlled AOTF multispectral imaging breadboards were designed, assembled, and demonstrated at Jet Propulsion Laboratory(JPL) (Chao, et al. 1990; Yu, et al, 1990; Chao, et al.1991; Cheng, et al. 1992). One operates in the wavelength range of 0.48-0.76 microns and the other between 1.2 and 2.5 microns. The optical system of the visible/near-infrared breadboard has foreoptics, an AOTF, imaging optics, and a silicon charge coupled device (CCD) camera. An ordinary camera zoom lens is used for foreoptics. A field lens is placed behind the AOTF. The combination of the field lens and the camera lens generates the diffracted image at the CCD detector array. The optical system design and analysis of this breadboard were reported previously. Two types of the CCD cameras are used in the system, an electrical-ly cooled integrating CCD camera for precision measurements in the laboratory and an ordinary CCD video camera for real-time observations. The breadboard system consists of a 386 IBM-PC compatible computer for control and data acquisition, a RF generator, a RF power supply, and an image grabber.

Several experiments to demonstrate the feasibility of using the visible/near-infrared AOTF-based breadboard for a number of applications were done. They include: identification and mapping of mineral contents; observations of botanical objects; demonstration of using optical fiber bundle to make observational flexibility; real-time spectral imaging at the video rate; and measurements of polarized signatures.

The optical system architecture of the infrared breadboard is the same as that of the visible/near-infrared breadboard, except that a liquid nitrogen-cooled HgCdTe detector array and a set of ZnSe lenses are used. Limited experiments using this breadboard system were carried out. They included identification and mapping of mineral contents as well as observation of botanical objects.

In this workshop presentation, results of experiments with the objective to demonstrate potentials of the AOTF instrument for remote sensing applications will be presented. The technology issue associated with the development of AOTF imaging spectrometers will be addressed. Finally, current JPL activities on the subject will be given.

T. Chao, J. Yu, L. Cheng, and J. Lambert, "Acousto-Optic Tunable Filter Imaging Spectrometer for NASA Applications: Breadboard Demonstration", in "Optical Information Processing Systems and Architectures II", SPIE Proceedings, Vol. 1347, p.655 (1990).

T. Chao, J. Yu, G. Reyes, D. Rider and L. Cheng, "Acousto-Optic Tunable Imaging Spectrometers", Proceedings of 1991 International Geoscience and Remote Sensing Symposium, Helsinki, Espoo, FINLAND, June, 1991 (IEEE 91CH2971-0), p. 585.

L. Cheng, T. Chao, and G. Reyes, "Acousto-Optic Tunable Filter Multispectral Imaging System", Proceedings of AIAA Space Programs and Technologies Conference, March 24-27, 1992, Huntsville, AL.

J. Yu, T. Chao, and L. Cheng, "Acousto-Optic Tunable Filter Imaging Spectrometer System for NASA Applications: System Issues", in "Optical Information Processing Systems and Architectures II", SPIE Proceedings, Vol. 1347, p.644 (1990).

MEASURING DRY PLANT RESIDUES IN GRASSLANDS:
A CASE STUDY USING AVIRIS

By

MICHAEL FITZGERALD, ATAC, INC.,
HIGH ALTITUDE AIRCRAFT PROGRAM,
NASA AMES RESEARCH CENTER, MS 240-6,
MOFFETT FIELD, CALIFORNIA 94035
and
SUSAN L. USTIN, DEPARTMENT OF LAND, AIR, AND WATER
RESOURCES, UNIVERSITY OF CALIFORNIA, DAVIS, CALIFORNIA 95616

INTRODUCTION

Grasslands, savannah, and hardwood rangelands are critical ecosystems and sensitive to disturbance. Approximately 20% of the Earth's surface are grasslands and represent 3 million ha. in California alone. Developing a methodology for estimating disturbance and the effects of cumulative impacts on grasslands and rangelands is needed to effectively monitor these ecosystems. Estimating the dry biomass residue remaining on rangelands at the end of the growing season provides a basis for evaluating the effectiveness of land management practices. The residual biomass is indicative of the grazing pressure and provides a measure of the system capacity for nutrient cycling since it represents the maximum organic matter available for decomposition, and finally, provides a measure of the erosion potential for the ecosystem.

Remote sensing presents a possible method for measuring dry residue. However, current satellites have had limited application due to the coarse spatial scales (relative to the patch dynamics) and insensitivity of the spectral coverage to resolve dry plant material. Several hypotheses for measuring the biochemical constituents of dry plant material, particularly cellulose and lignin, using high spectral resolution sensors have been proposed. We have investigated the use of AVIRIS to measure dry plant residues over an oak savannah on the eastern slopes of the Coast Range in central California and have asked what spatial and spectral resolutions are needed to quantitatively measure dry plant biomass in this ecosystem.

MEASUREMENTS

The study site is located west of Winters, CA (38°30'N lat, 122°00'W long.) near Lake Berryessa on 260ha. private land that is part of an undeveloped block that includes the University of California Stebbins Preserve and the Quail Ridge Nature Conservancy. Although historically grazed, these lands are currently managed to promote native perennial grasslands. Other private lands within the scene are currently grazed. The study area was stratified by aspect (principally NE and SE facing slopes), soil type (three soil units identified on 1:24,000 maps), and position (lower, mid, and upper elevation) on the hillside and 45 sites were chosen for sampling. Aboveground biomass (fresh and dry weights) on 3m x 3m plots were harvested in spring (at peak growth) and in late summer, 1991. Spring biomass ranged between 27 and

7757 g. on the plots, late summer residue from 13 to 2457 g.. Spring biomass was a poor predictor of late summer residue (r^2=0.12). Locations of plots were recorded using a Trimble Navigation Pathfinder Basic and Pathfinder Professional base station. Nominal slope and aspect were recorded with field measurements, correlated with a DEM created by scanning contours, then used to correct the data. Mean (n=20) field spectra (450-850nm) of about 1.5 m resolution were obtained adjacent to each plot using an Analytical Spectral Devices Perspec II in fall of 1991. Additional spectra of soils, dry plant litter, and green foliage were measured to obtain library endmember spectra. In addition, soil (n= 20) and litter (n=8) samples were analyzed in the lab (400-2500nm) using a Perkin-Elmer Model 330 spectrophotometer with 1nm wavelength resolution.

Two nonradiometrically and nongeometrically corrected AVIRIS scenes of the area were acquired on August 20, 1992 (910820, run 5 scenes 1,2) with a nominal pixel resolution of 20m. The fourth (D) spectrometer was not functioning at the time of acquisition. Images were nominally radiometrically calibrated using Modtran and spectral mixture analysis. Additional AVIRIS images were available from 23 March 1990, 31 July 1990 and used for comparisons. For all AVIRIS scenes, coincident high spatial resolution CIR photos using the RC-10 camera were obtained. Additionally, low alititude aerial CIR photography was obtained at 3665m elevation from NASA C-130 aircraft with a Zeiss camera concurrent with a NS001 (TMS) on 31 May 1991. All aerial photographs were digitized using the Eikonix model EC 78-99 scanner creating a 4096 x 4096 RGB image.

COMPARISONS

AVIRIS images were analyzed using GenIsis and IDIMS software for pixel extractions and exploratory comparisons. Spectral mixture analysis software was provided by J. Adams and M. Smith of the University of Washington.

Spatial patterns

Field plots were identified in the low altitude scanned photos and corresponding AVIRIS pixels were selected for analysis by manual interpretation without resampling. Numerous distinct ground targets made it possible to visually locate points without coregistration. The analysis was repeated after registering the AVIRIS image to a map base, integrating the GPS coordinates, and then examining the effects of resampling. This low altitude scanned photo was later degraded to 10 and 20 m pixels to permit comparisons between spatial resolutions of the other sensors. Scanned CIR photos at 10m resolution closely approximated the NS001 band 4 and at 20 m resolution a synthetic AVIRIS NIR band. The topographically determined major features related to larger scale patterns are maintained throughout the spatial degredation from 1 to 20m although the fine-scale variance related to tree shape and bare patches was lost.

In late summer, annual grasslands in the area are completely dormant and NDVI values are low and indistinguishable from patches of bare soil. Albedo variation was due principally to topography. Irriadiance was adjusted for local slope and aspect using a cosine correction and regressed against biomass during late summer.

Spectral patterns

AVIRIS spectral signatures from each of the sample sites were analyzed using GenIsis software. Similiarity indexes were generated from these signatures and the spectral homogeneity of the study area was mapped and compared to field measures.

Several SWIR wavelengths have been shown in previous studies to be useful for identifying cellulose. We have begun to investigate the use of wavebands in the third (C) spectrometer as predictors of dry plant biomass through regressions against field measurements. These results will be contrasted with those derived from mixture modeling. We have used spectral mixture analysis to identify the dominant scene components as an alternative method for identifying and quantifying dry plant material in the AVIRIS images. We examined the AVIRIS images under two mixture models; a three member model of soil, green vegetation and shade and examined high residuals at wavelengths indicating presence of dry plant material (e.g., lignin and cellulose features) and a four endmember mixture model that included dry vegetation. Preliminary analysis indicates that we are able to derive a better relationship using spectral mixture analysis although many uncertainties remain. We contrast the results of this study with those of Jasper Ridge, CA presented by Roberts et al. , Gamon et al. and Ustin et al., in this workshop, to evaluate the consistency of green and dry biomass predictions using images acquired in different seasons over savannah landscapes composed of similar ecosystems.

ANALYSIS OF AVIRIS SAN PEDRO CHANNEL DATA:
METHODS AND APPLICATIONS

Richard B. Frost

NCCOSC, RTD&E Division
Electro-Optics Branch, Code 754
271 Catalina Boulevard
San Diego, California 92152-5000

The U.S. Navy has and/or is developing imaging spectrometers for remote sensing of deep ocean and coastal waters. The AVIRIS test program provides a unique opportunity to evaluate the performance of so-called hyper–spectral systems in marine environments. Data used for this study were collected over San Pedro, California in March 1991 and obtained from the Oceanography Group at the Jet Propulsion Laboratory in Pasadena. Much of what will be presented here is work in progress. Technical pre-prints and software tools will be available from the author at conference time.

Remote sensing of marine environments can be significantly more challenging than surveillance of terrestrial phenomena. This is primarily due to the coupling of low contrast targets and complicated hydro–optic interactions. Therefore, a successful maritime program requires high signal–to–noise ratios, a realistic atmospheric correction, and suitable metrics for hydro-optic analysis.

The initial calibration of AVIRIS data depends upon dark current, vignetting, navigation, and spectral response data. Each is a potential source of error, particularly if the calculation is performed in the domain of integers. Further, the numerical resolution of these data are poor—although proposed sensor upgrades offer substantial improvements. A calibration method based upon dark current smoothing, vignetting curve fits, navigational aberration, spectral overlap, and standard calibration data will be presented.

There are currently many efforts underway to model atmospheric effects in AVIRIS data. Here we present a unique approach involving the recursive tuning of unknown atmospheric parameters via simulated annealing while holding fixed those few parameters measured in situ. This method has potential use for measurements involving joint radar and long–wave IR data *sans* ground truth.

Hydro-optic metrics related to suspended sediment content and other marine phenomena require signal–to–noise ratios near 300:1 at spatial resolutions less than 100 meters. To meet these requirements, neighboring pixels were ganged together in both the spatial and spectral directions. The variance spectra of turbulent structures and chlorophyll concentrations are then compared to previous studies. The ability of AVIRIS to meet marine sensing requirements and implications for HIRIS will also be discussed.

TRACKING PHOTOSYNTHETIC EFFICIENCY WITH NARROW-BAND SPECTRORADIOMETRY*

John A. Gamon[1] and Christopher B. Field[2]

[1]California State University, Los Angeles
Department of Biology
5151 State University Drive
Los Angeles, CA 90032

[2]Carnegie Institution of Washington
Department of Plant Biology
290 Panama Street
Stanford, CA 94305

1. BACKGROUND

Narrow-waveband spectroradiometry presents the possibility of detecting subtle signals closely related to the current physiological state of vegetation. In this paper we discuss one such signal related to the epoxidation state of the xanthophyll cycle pigments, violaxanthin, antheraxanthin and zeaxanthin. Recent advances in plant ecophysiology have demonstrated a close relationship between these pigments and the regulatory state of photosystem II in photosynthesis (Demmig-Adams 1990). Our recent field studies of sunflower (*Helianthus annuus*) and oak (*Quercus agrifolia*) have demonstrated that a "xanthophyll signal" can be isolated from the diurnal reflectance spectra of intact canopies. Furthermore, the xanthophyll signal can be used to derive a "physiological reflectance index" (PRI) that closely correlates with the actual photosynthetic efficiency (defined as the photosynthetic rate divided by the incident PAR) in closed canopies (Gamon et al. *in press*). If these signals were detectable in AVIRIS images, they could lead to improved remote estimates of photosythetic fluxes.

2. MATERIALS AND METHODS

Spectral reflectance was measured by positioning a Spectron spectroradiometer with 15 degree FOV optics (model SE590 with detector model CE390WB-R, Spectron Engineering, Denver, CO) approximately 4 meters above intact sunflower or 2 meters above oak canopies. Reflectance was presented as a "physiological reflectance index" (PRI) analogous in formulation to NDVI, for comparison with physiological measurements.

$$PRI = (R_{531} - R_{ref}) / (R_{531} + R_{ref}) \qquad (1)$$

Where "R" indicates reflectance, the subscript "531" indicates the wavelength (in nm) of the xanthophyll signal, and the subscript "ref" indicates a reference wavelength (either 550 or 570 nm).

Physiological assays included leaf-level gas exchange (LI-6200, Li-Cor Inc., Lincoln Nebraska) and chlorophyll and carotenoid determinations by HPLC. Incident photosynthetic photon flux density (PFD) was used to calculate photosynthetic efficiency from net CO_2 uptake rates.

$$\text{Photosynthetic efficiency} = \text{Net } CO_2 \text{ uptake rate / incident PFD} \qquad (2)$$

Methods are further described in Gamon et al. 1990 and Gamon et al. *in press*.

3. RESULTS AND DISCUSSION

The PRI correlated well with photosynthetic efficiency in both sunflower and oak (Fig. 1). Photosynthetic efficiency, analogous to the photon (quantum) yield of photosynthesis or the conversion efficiency of PAR to biomass (Monteith 1977), is an indicator of the short-term efficiency of converting PAR to fixed carbon through photosynthesis. This reflectance index may be useful in remotely detecting conditions of reduced photosynthetic activity associated with a number of stresses.

Narrow waveband spectroradiometry could also be used to assess other aspects of physiologically important plant pigments (e.g. chlorophylls, carotenoids and anthocyanins). For example, subtle changes in chlorophyll to carotenoid ratios associated with reduced photosynthetic performance could be detectable with narrow-band reflectance. Narrow-waveband indices of vegetation function may be particularly useful in conditions where broad-band indices are insensitive to current physiological status (e.g. in evergreen vegetation lacking strong diurnal or seasonal changes in canopy display).

Estimation of pigment content from AVIRIS images could lead to improved estimates of photosynthetic fluxes at the landscape scale. In AVIRIS images, pigment contents may be accessible via reflectance indices analogous to the PRI; another approach would be to use a mixture model to isolate component and residual images (Ustin et al. *in press*), which could then be compared with pigment spectra.

In our ground-based studies, validation of physiological interpretations required detailed physiological assays (e.g. of pigment content and photosynthetic flux) that were both expensive and time consuming. These direct "physiological calibrations" of spectral reflectance would be even more difficult at the 20 m scale of the AVIRIS pixel, and atmospheric effects may further obscure relationships between photosynthetic fluxes and spectral reflectance. Ground validation of possible physiological signals in AVIRIS imagery should include flux and reflectance measurements at a range of scales between the leaf and the landscape.

4. ACKNOWLEDGEMENTS

5. REFERENCES

Demmig-Adams, B. (1990) Carotenoids and photoprotection in plants: a role for the xanthophyll zeaxanthin. Biochimica et Biophysica Acta 1020:1-24.

Gamon J.A., Field C.B., Bilger W., Bjorkman O., Fredeen A.L., and Penuelas J. (1990) Remote sensing of the xanthophyll cycle and chlorophyll fluorescence in sunflower leaves and canopies. Oecologia 85:1-7.

Gamon JA, Penuelas J, Field CB (In press) A narrow-waveband spectral index that tracks diurnal changes in photosynthetic efficiency. Remote Sensing of Environment.

Monteith JL (1977) Climate and the efficiency of crop production in Britain. Phil. Trans. R. Soc. Lond. B. 281:277-294.

Ustin SL, Smith MO, Adams JB (In press) Remote sensing of ecological processes: a strategy for developing and testing ecological models using spectral mixture analysis. In: Ehleringer JR, Field CB (eds) Ecological Scaling from the Leaf to the Landscape. Academic Press, San Diego.
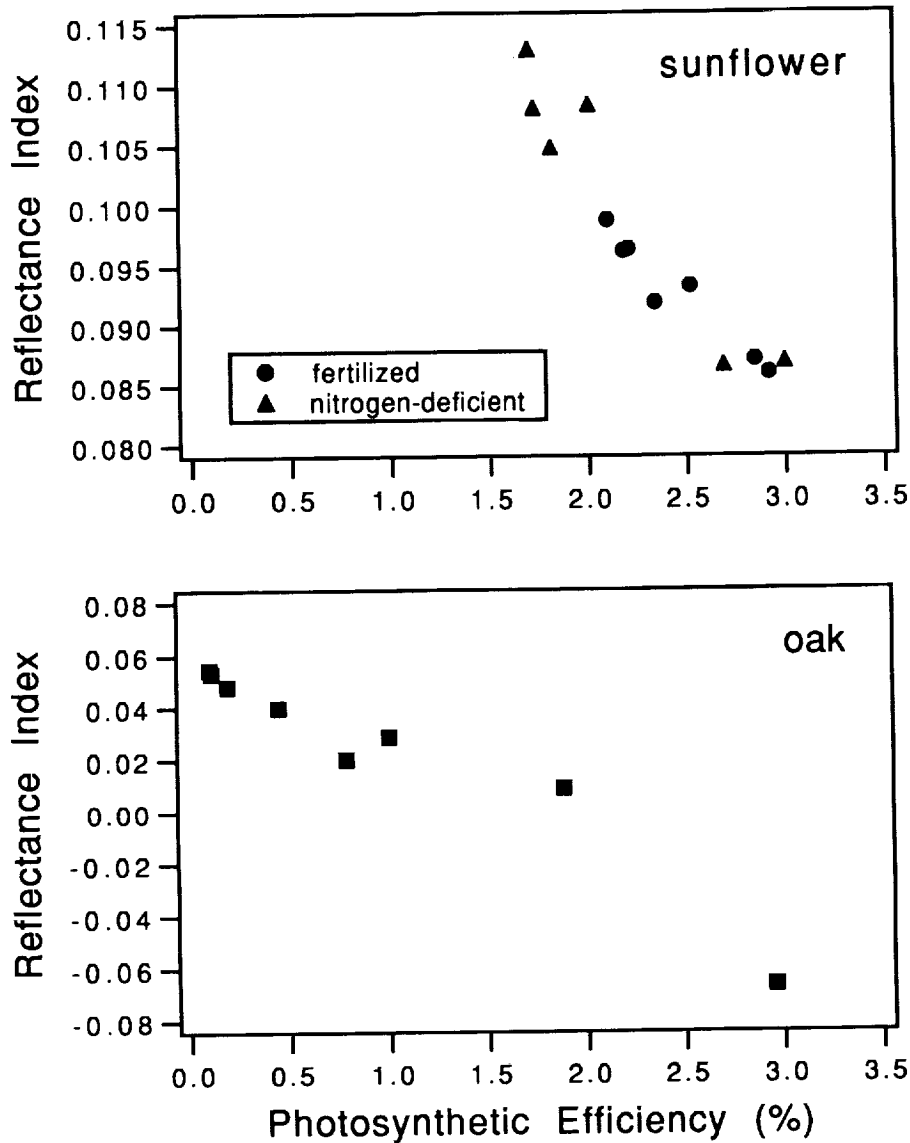
Fig. 1.

Comparison of the physiological reflectance index (PRI; eq. 1) with photosynthetic efficiency (eq. 2) for sunflower (± nitrogen) and oak. Reference wavelengths were 550 and 570 nm for sunflower and oak, respectively. Points represent measurements taken at different times in a single day.

SEPARATION OF CIRRUS CLOUD FROM CLEAR SURFACE FROM AVIRIS DATA USING THE 1.38-μm WATER VAPOR BAND

Bo-Cai Gao[1], and Alexander F. H. Goetz[1,2]

[1]Center for the Study of Earth from Space/CIRES, Campus Box 449
[2]Department of Geological Sciences
University of Colorado, Boulder, CO 80309-0449, U. S. A.

1. INTRODUCTION

Cirrus clouds play an important role in climate systems because of their large area coverage, persistence and radiative effects (Starr 1987). Thin cirrus clouds are difficult to detect in visible images and infrared images in the 10-12 μm atmospheric window region, particularly over land, because these clouds are partially transparent. Ackerman et al. (1990) have recently developed a method for detecting cirrus clouds using three narrow channels centered near 8, 11, and 12 μm, respectively, based on the analysis of IR emission spectra measured with a high spectral resolution interferometer. Barton (1983) has also described a method for estimating cirrus cloud height and amount from measurements with two narrow channel radiometers of the Selective Chopper Radiometer on Nimbus 5. Both channels are located within the strong 2.7 μm water vapor band absorption region. One of the channels includes additional carbon dioxide absorption. A differential absorption technique with sets of empirical coefficients has been used in the estimation of cirrus cloud heights and amounts.

In this paper a technique using narrow channels in the strong 1.38 μm water vapor band absorption region for detecting cirrus clouds from spectral imaging data acquired by the Airborne Visible/Infrared Imaging Spectrometer (AVIRIS) (Vane 1987) on December 5, 1991 during the FIRE (The First International Satellite Cloud Climatology Project (ISCCP) Regional Experiment) Phase II Field Experiment (Starr 1987) is described.

2. METHOD

The method for the detection of cirrus clouds using channels near the center of the strong 1.38 μm water vapor band is straight forward. Cirrus clouds are typically located at altitudes greater than 6 km. Most of the atmospheric water vapor is located below 6 km. AVIRIS channels near 1.38 μm receive little radiance resulting from scattering of solar radiation by the surface, because the solar radiation is mostly absorbed by water vapor in the lower atmosphere. When cirrus clouds are present, however, the AVIRIS channels near 1.38 μm receive a large amount of radiance resulting from scattering of solar radiation by the cirrus clouds. The radiance contrast in AVIRIS images near 1.38 μm allows the detection of cirrus clouds.

3. RESULTS

The method described above has been applied to AVIRIS data measured over Coffeyville in the southeastern part of Kansas and over the Gulf of Mexico on December 5, 1991 during the FIRE Phase II Field Experiment. Figure 1 shows a 0.56 μm AVIRIS image over Coffeyville. The surface area covered by the image is approximately 12x17 km. Various types of surface features are seen. For example, the town of Coffeyville in the upper left, triangular runways of the Coffeyville Airport in the middle left, and roads and rivers in several parts of the image are all seen. At the time of the AVIRIS overflight, thin cirrus clouds were seen from the ground. Figure 2 shows a 1.37 μm

Fig. 1: A 0.56 μm AVIRIS image over Coffeyville, Kansas. Surface features are seen in this figure.

Fig. 2: A 1.37 μm AVIRIS image over the same area as that of Figure 1. Only cirrus clouds are seen in this figure.

Fig. 3: A 0.56 μm AVIRIS image over the Gulf of Mexico. Both the upper level extensive cirrus clouds and the lower level smaller cumulus clouds are seen.
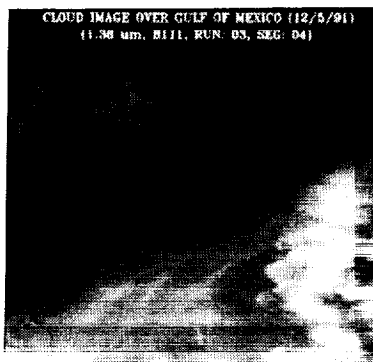
Fig. 4: A 1.38 μm AVIRIS image over the Gulf of Mexico. Only the upper level extensive cirrus clouds are seen.

AVIRIS image over the same area as that of Figure 1. Cirrus clouds are seen clearly in this figure. The surface features visible in Figure 1 disappear completely in this figure. This demonstrates that the 1.37 μm channel is useful for detecting thin cirrus clouds.

Figure 3 shows a 0.56 μm AVIRIS image over the Gulf of Mexico. Extensive cirrus clouds in the upper level and smaller cumulus clouds in the lower level are seen. Figure 4 shows a 1.38 μm AVIRIS image over the same area. The smaller cumulus clouds disappear completely in this figure. Only cirrus clouds are seen. This demonstrates again the usefulness of channels located near the center of the strong 1.38 μm water vapor band for detecting cirrus clouds.

4. DISCUSSION

Figures 1 and 3 show that the visible channels are contaminated by reflection from land surfaces and from lower level clouds when viewing thin cirrus clouds. This implies that it is difficult to derive accurate optical parameters of thin cirrus clouds from measurements with visible channels.

The availability of AVIRIS data allowed us to find the usefulness of detecting cirrus clouds using narrow spectral channels near the center of the strong 1.38 μm water vapor band, as demonstrated in Figures 2 and 4. These channels are also expected to have small sensitivity to mid-level clouds with top altitudes between approximately 4 and 6 km.

The 1.38 μm channel has some advantages over the 2.7 μm channels described by Barton (1983). The solar energy at 1.38 μm is 10 times as great as that at 2.7 μm. The ice particle absorption near 1.38 μm is significantly smaller than that near 2.7 μm. Also, the 1.38 μm region is not affected by emission from the Earth, while the 2.7 μm region is slightly contaminated by Earth's emission. The 8, 11, and 12 μm narrow IR channels described by Ackerman et al. (1990) have been proposed for a future polar-orbiting satellite for monitoring clouds. This IR emission technique has an advantage that it works both day and night. A disadvantage is that it requires a large field of view because of the weakness of the atmospheric and surface emission.

5. CONCLUSION

Narrow spectral channels near the center of the 1.38 μm strong water vapor band are useful for monitoring cirrus clouds. It is expected that our ability to determine cirrus cloud amounts using space-based remote sensing will be improved if channels near the center of the 1.38 μm water vapor band are added to future satellites.

6. ACKNOWLEDGMENTS

7. REFERENCES

Ackerman, S. A., W. L. Smith, J. D. Spinhirne, and H. E. Revercomb, "The 27-28 October 1986 FIRE IFO cirrus case studies: Spectral properties of cirrus clouds in the 8-12 μm window", *Mon. Wea. Rev., 118*, 2377-2388, 1990.

Barton, I. J., "Upper level cloud climatology from an orbiting satellite", *J. Atmos. Sci., 40*, 435-447, 1983.

Starr, D. O'C., "A cirrus cloud experiment: Intensive field observations planned for FIRE", *Bull. Amer. Meteoro. Soc., 67*, 119-124, 1987.

Vane, G. (Ed.), "Airborne visible/infrared imaging spectrometer (AVIRIS)", *JPL Publ. 87-38*, Jet Propul. Lab., Pasadena, Calif., 1987.

SOFTWARE FOR THE DERIVATION OF SCALED SURFACE REFLECTANCES FROM AVIRIS DATA

Bo-Cai Gao[1], Kathleen Heidebrecht[1], and Alexander F. H. Goetz[1,2]

[1]Center for the Study of Earth from Space/CIRES
[2]Department of Geological Sciences
Campus Box 449, University of Colorado
Boulder, Colorado 80309-0449, U.S.A.

1. INTRODUCTION

An operational software program is now available for deriving "scaled surface reflectances" from spectral data collected by the Airborne Visible/Infrared Imaging Spectrometer (AVIRIS) (Vane, 1987). The program simulates both the atmospheric scattering and absorption effects. Brief descriptions of the algorithm, inputs, outputs, the limitations of the software, and procedures for obtaining the software are given.

2. FUNCTIONAL OVERVIEW

The program derives scaled surface reflectances using an approximate atmospheric radiative transfer model. Horizontal surfaces having Lambertian reflectances are assumed. The scaled surface reflectances can be converted to the real surface reflectances if the slopes and aspects of the surfaces are known. For simplicity, the scaled surface reflectances are referred to as "surface reflectances" in this document.

The atmospheric scattering effects are modeled using the Simulation of the Satellite Signal in the Solar Spectrum (5S) code (Tanre et al. 1986). The transmittances of seven gases are calculated based on an assumed atmospheric model, the solar and observational geometries, and using the Malkmus (1967) narrow band spectral model. Water vapor values are derived from AVIRIS data in the 0.94 μm and 1.14 μm regions using a 3-channel ratioing technique and a look-up table procedure. The derived water vapor values are used in the process of removing atmospheric gaseous absorption effects from AVIRIS data. Fig. 1a shows an AVIRIS spectrum over a vegetated area. Fig. 1b shows the corresponding derived surface reflectance spectrum.

3. INPUT DATA

The program requires an input file containing information on the AVIRIS scene including geometric parameters, spectral parameters, atmospheric parameters, and input/output parameters. Table 1 shows a sample input file. The input values are based on information provided with the AVIRIS data and knowledge of the aerosol condition when the data were collected. The program can be executed without the need of any field measurements as inputs. However, a measurement of the aerosol optical depth when the AVIRIS data were collected will improve the accuracy of the derived surface reflectances. The input data are described further below:

1. Geometric Parameters
   - Date and Time: the date and time in GMT that the AVIRIS data was measured.
   - Latitude and Longitude: the latitude and longitude of the center position of the AVIRIS scene.

2. Spectral Parameters
   - Wavelength File: the name of the AVIRIS wavelength file.
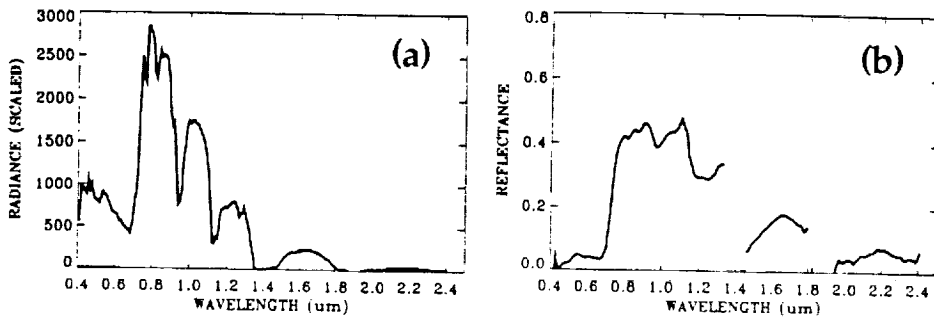
Figure 1. (a): An AVIRIS spectrum over a vegetated area, and (b) the corresponding derived surface reflectance spectrum.

Table 1. An example input file.

Input	Comment
07 23 1990 20 58 32	date and time
37 30 08	latitude
N	hemisphere of the earth (N or S)
117 13 17	longitude
W	hemisphere of the earth (E or W)
/tmp/aviris.wav	wavelength file
10.	spectral resolution of AVIRIS data
1	channel ratio parameters (if "0", defaults used)
0.8630 1.0550 3 3 0.9398 7	
1.0550 1.2470 3 3 1.1414 7	
2	atmospheric model number
1 1 1 1 1 1 1	gas selectors
0.34	total column ozone amount (atm-cm)
1 100	aerosol model and visibility
1.5	average elevation of the surface scene
/tmp/aviris.cub	input AVIRIS data
0	input AVIRIS dimensions
/tmp/aviris_atm.cub	output image file
10.	output data resolution
/tmp/aviris.vap	output water vapor file
/tmp/aviris.lib	output spectral library file

- Spectral Resolution: the AVIRIS spectral resolution in nanometers.
- Channel Ratio Parameters: the center positions and widths of window channels and absorption channels for the 0.94-μm and the 1.14-μm water vapor bands.

3. Atmospheric Parameters
- Atmospheric Model: a model atmosphere close to the measurement condition.
- Gas Selectors: indicators for determining which of the seven gases that have absorption features in the 0.4-2.5 μm will be included in atmospheric gaseous transmission calculations. The seven gases are water vapor, carbon dioxide, ozone, nitrous oxide, carbon monoxide, methane, and oxygen.
- Total Ozone: the vertical column amount of ozone (in units of atm-cm) that is contained in the atmosphere (typically 0.34 atm-cm).
- Aerosol Model and Visibility or Optical Depth at 0.55 μm: a model of the aerosol conditions and the visibility or the optical depth at 0.55 μm when the AVIRIS measurements were made.

• Average Elevation: the average elevation (in units of km) of the scene.

4. Input/Output Parameters
   • Input AVIRIS Image: the path and file name of the input AVIRIS data.
   • Input AVIRIS Image Dimensions: the dimensions of the input AVIRIS image including the header size in bytes, the number samples, the number of lines, the number of channels, and the storage order.
   • Output Image File: the path and file name of the output surface reflectance data.
   • Output Spectral Resolution: the desired resolution of the output spectra in nanometers. If the output spectral resolution is coarser than the input spectral resolution, then the output spectra will be smoothed using a gaussian function.
   • Output Water Vapor File: the path and file name of output water vapor image file.
   • Output Spectral Library File: the path and file name of output spectral library file.

4. OUTPUT DATA

1. Surface Reflectance Image
   a surface reflectance image that has the same size as the input AVIRIS image.
2. Water Vapor Image
   a single spatial image containing the column water vapor amount at each pixel.
3. Transmittance Lookup Table
   a file containing atmospheric transmittance spectra and band ratios for each of the 60 column water vapor values.

5. LIMITATIONS

The elevations within an image are not allowed to vary. As a result, the program is mostly applicable to images with surface elevation variations less than about 1 km. The atmospheric adjacency effect and the topographic adjacency effect are not modeled. When using our program for surface reflectance retrievals, the band positions between observed and calculated spectra must be matched to 0.5 nm or better.

6. SOFTWARE AVAILABILITY

The source code and user documentation is provided free of charge or royalties. However, CSES retains the title and copyright to the software and documentation. Recipients of this software are required to execute a memorandum of understanding (MOU) provided by CSES that specifies in detail all of the associated conditions. Send requests for an MOU to:

e-mail:	sips@cses.colorado.edu
voice:	(303) 492-1866
fax:	(303) 492-5070

7. ACKNOWLEDGEMENTS

8. REFERENCES

Malkmus, W., Random Lorentz band model with exponential-tailed S line intensity distribution function, *J. Opt. Soc. Am.*, *57*, 323-329, 1967.

Tanre, D., C. Deroo, P. Duhaut, M. Herman, and J. J. Morcrette, J. Perbos, and P. Y. Deschamps, Simulation of the Satellite Signal in the Solar Spectrum (5S), User's Guide (U.S.T. de Lille, 59655 Villeneuve d'ascq, France: Laboratoire d'Optique Atmospherique), 1986.

Vane, G. (Ed.), Airborne visible/infrared imaging spectrometer (AVIRIS), *JPL Publ. 87-38*, Jet Propul. Lab., Pasadena, Calif., 1987.

INTEGRATING REMOTE SENSING TECHNIQUES AT CUPRITE, NEVADA: AVIRIS, THEMATIC MAPPER, AND FIELD SPECTROSCOPY

Bradley Hill, State of Utah, Dept. of Natural Resources, Division of Oil, Gas, and Mining; Greg Nash, and Merrill Ridd, University of Utah Research Institute, Research Park, Salt Lake City, Utah; Phoebe Hauff, Spectral Research, Lafayette, Colorado; Phil Ebel, Earth Search Sciences, Inc., Salt Lake City, Utah.

1.0 Introduction

The Cuprite mining district in southwestern Nevada has become a test site for remote sensing studies with numerous airborne scanners (Abrams et al. 1977; Nobel et al. 1984; Goetz and Srivastava 1985; Carrere 1989; Kruse et al. 1990; and Hook and Rast 1990) and ground sensor data sets (Goetz and Curtiss, personal communication; Shipman and Adams 1987; and Kruse et al. 1990) collected over the past fifteen years.

Structurally, the Cuprite region can be divided into two areas with slightly different alteration and mineralogy. These zones lie on either side of a postulated low-angle structural discontinuity that strikes nearly parallel to US Route 95. Hydrothermal alteration at Cuprite has been classified into three major zones: silicified, opalized, and argillized (Hook and Rast 1990). These alteration types form a bulls-eye pattern east of the highway and are more linear on the west side of the highway making a striking contrast from the air and the imagery. Cuprite is therefore an ideal location for remote sensing research as it exhibits easily identified hydrothermal zoning, is relatively devoid of vegetation, and contains a distinctive, spectrally diagnostic mineral suite including the ammonium feldspar buddingtonite, several types of alunite, different jarosites, illite, kaolinite, smectite, dickite, and opal.

This present study brings a new dimension to these previous remote sensing and ground data sets compiled for Cuprite. The development of a higher resolution field spectrometer now provides the capability to combine extensive in-situ mineralogical data with a new geologic field survey and detailed AVIRIS images. This paper discusses the various data collection methods and the refinement of the integrated techniques.

2.0 AVIRIS Data

AVIRIS data from the 1990 season were evaluated utilizing GenIsis© and ERDAS© software on a personal computer. False color composite images and principal component images were generated using bands selected for optimum mineralogic discrimination. Bands were interactively selected by examination of the AVIRIS spectra on a pixel by pixel basis. Spectra of individual pixels in known altered areas were examined for diagnostic mineral absorption features. Bands were selected which showed maximum variation between alunite, kaolinite, buddingtonite, illite, and iron absorption features. Good mineralogic differentiation can be seen on both the false color composite and the principal component images. Similarity Index maps of alunite, kaolinite, buddingtonite, illite, and iron stained rocks were generated using GenIsis©. The Similarity Index maps gave a more specific indication of the distribution of each mineral and greatly aided the selection of field sampling sites. Figure 1 shows a Similarity Index map of alunite occurrences in the study area.
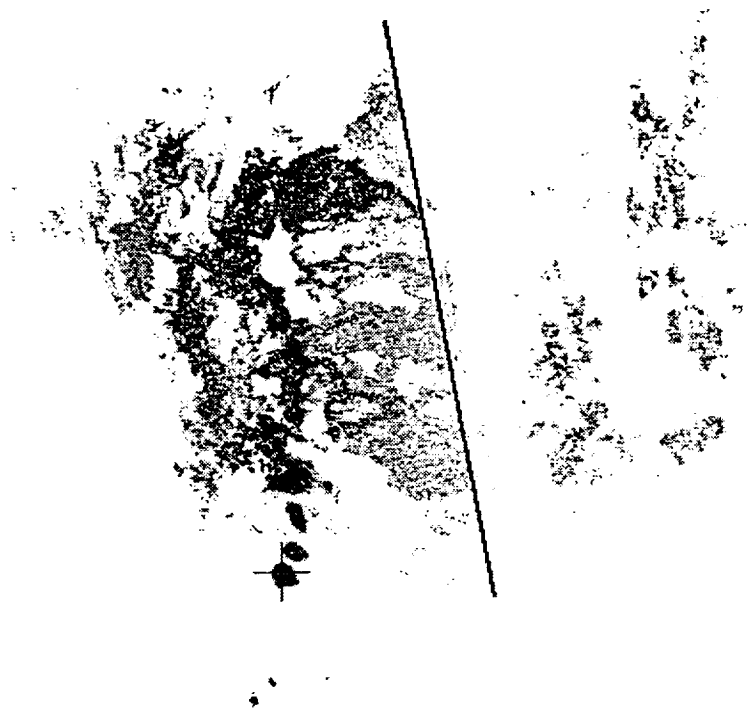
Fig. 1. Similarity Index for Alunite, Cuprite, NV - Darker
Values Indicate Increasing Alunite.

3.0 Geologic Alteration Mapping and Sampling

The field sampling for this project was carried out in two separate phases.
Thematic Mapper (TM) data were utilized to guide the first phase of sampling. A
color ratio composite (CRC) was generated using TM ratios TM5/7, TM5/4 and
TM3/1. Scatter plots were generated from TM5/7 vs. TM5/4 and TM5/4 vs. TM3/1.
The scatter plots were used as an aid in the classification of the CRC data. A GIS
character print map was then generated showing the areas most likely to contain
hydrothermal alteration types. The sites delineated in the GIS were then visited and
sampled.

AVIRIS data were used to guide the second phase of the field sampling.
False color composite images, principal component images, and Similarity Index maps
generated from the comparison of spectral plots derived from the AVIRIS data and
those in the spectral library were used to guide the sampling to localities showing
specific alteration assemblages.

The samples collected from the field visit were analyzed by three different
methods. These include spectral analysis utilizing the PIMA-II spectrometer, thin
section analysis, and x-ray diffraction.

The analytical results, combined with further field checks and field mapping,
were used as an aid in the interpretation of the AVIRIS data. This allowed a refined
geologic and mineralogic map of the alteration zones to be created which delineates
the mineralogy in a detail not previously presented.

105

4.0 Field Spectroscopy Data

Spectral ground truthing was done at Cuprite using the PIMA-II portable spectrometer. With an internal light source and 5-7nm resolution, PIMA-II provides near-laboratory quality spectra within minutes and can be used exclusive of solar illumination and under most weather conditions. Therefore, the atmospherically masked bands, at $1.4\mu m$ and the $1.9\mu m$, which provide invaluable information on hydroxyl and water content, can now be utilized.

With the field spectrometer, crystalline examples of alunite, buddingtonite, kaolinite, smectite, illite, and opal were observed in the eastern alteration zone, while spectra of illite, dickite, natro-alunite, and jarosite, among other minerals, were collected from the western alteration zone. This method is unique as it provides detailed mineralogy and multiple phase identification capabilities easily and almost instantly in the field. An example of this is shown in Figure 2. Spectrum (A) was collected from the "Buddingtonite Bump" and contains kaolinite, alunite, illite, and buddingtonite, all of which have identifiable features. Spectrum (B) is from the western alteration zone and shows dickite and natro-alunite. The ability to differentiate numerous species and solid solution phases, with confidence, has not been possible in-situ before now.
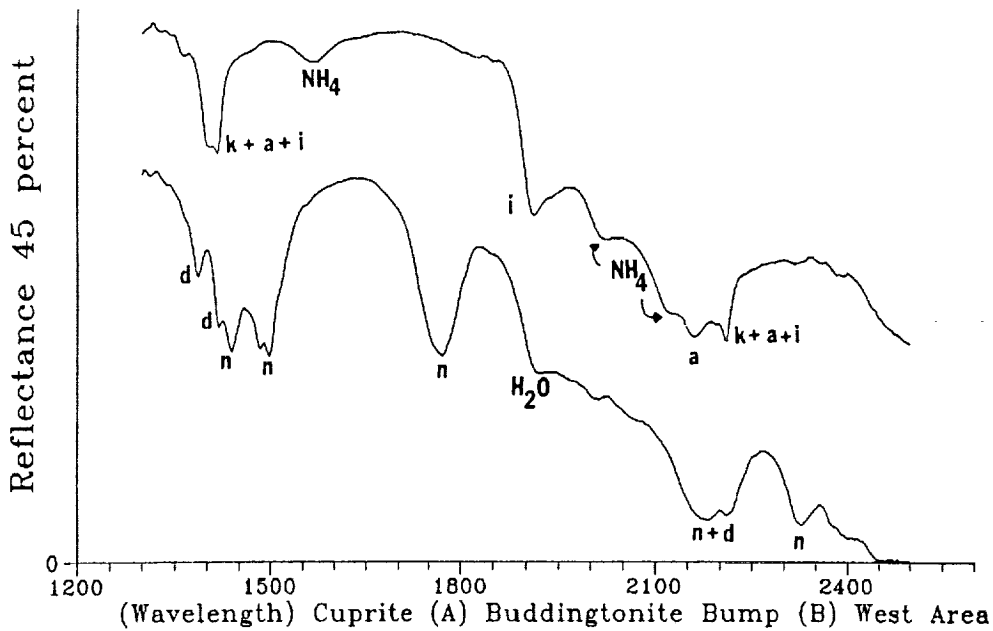
Fig. 2. PIMA-II Spectra from Cuprite, NV. (A) is from the Buddingtonite Bump; (B) from the Alteration Zone West of U.S. Highway 95. Key for the Minerals in the Spectra: K = Kaolinite, A = Alunite, N = natro-alunite, D = dickite, I = Illite. Spectra Collected with the PIMA-II Portable Short Wave Infrared (SWIR) Spectrometer, *Integrated Spectronics, Pty Ltd., Sydney, Australia.*

5.0 Discussion

The field spectrometer provided the ability to investigate the alteration zones distribution and subtle mineralogical changes at Cuprite, in detail not documented before. The ability to discriminate, in the field, ordering and chemical substitution within the mineral series, such as kaolinites and alunites, coupled with the hyperspectral data from AVIRIS and TM alteration mapping offers the field geologist an invaluable tool for sampling, geological interpretation, and exploration.

6.0 References

Abrams, M.J., R.P. Ashley, L.C. Rowan, A.F.H. Goetz, and A.B. Kahle, 1977, Use of imaging in the .46-2.36μm spectral region for alteration mapping in the Cuprite mining district, Nevada: USGS Open-File Report 77-585.

Ashley, R.P., 1974, Goldfield mining district, in Guidebook of four Tertiary volcanic centers in central Nevada: Nevada Bureau of Mines and Geology Report 19, 49-66.

Carrere, V.,1989, Mapping alteration in the Goldfield mining district, Nevada, with the Airborne Visible/ Infrared Imaging Spectrometer (AVIRIS), Proceedings, 7th Thematic Conference on Remote Sensing for Exploration Geology, Calgary, Alberta, Canada, October 2-6, 365-372, ERIM, Ann Arbor, MI.

Goetz, A.F.H., and V. Srivastava. 1985, Mineralogical mapping in the Cuprite mining district, Nevada: in Vane, G., and Goetz, A.F.H. Eds., Proceedings Airborne imaging spectrometer data analysis workshop, JPL Publication 85-41, 22-31.

Hook, S.J. and M. Rast, 1990, Mineralogic mapping using Airborne Visible Infrared Imaging Spectrometer (AVIRIS) Shortwave Infrared (SWIR) data acquired over Cuprite, Nevada: in Green, R.O., Ed., Proceedings of the second Airborne Visible/Infrared Imaging Spectrometer (AVIRIS) workshop, JPL Publication 90-54, 199-207.

Kruse, F.A., K.S. Kierein-Young, and J.W. Boardman, 1990, Mineral mapping at Cuprite, Nevada with a 63-channel imaging spectrometer: Photogrammetric Engineering and Remote Sensing, 56(1), 83-92.

Nobel, D.C., T. Vogel, S. Erwin, E.McKee, and L.Younker, 1984, Stratigraphic relations and source areas of ash flows of the Black Mountain and Stonewall Mountain volcanic centers, Nevada: Journal of Geophysical Research, 89(B10), 8593-8602.

Shipman, H. and Adams, J.B., 1987, Detectability of minerals on desert alluvial fans using reflectance spectra: Journal of Geophysical Research, 92(B10), 10,391-10,402.

EVALUATION OF AVIRISwiss-91 CAMPAIGN DATA

K.I.Itten*, P.Meyer*, K.Staenz**, T.Kellenberger* and
M.Schaepman*

* Remote Sensing Laboratories/RSL, University of Zurich-Irchel,
CH-8057 Zurich, Switzerland
** Canada Centre for Remote Sensing, Ottawa, Canada K1A 0Y7

1. INTRODUCTION

On 5th of July 1991 at 2.10 p.m. the multidisciplinary testsite Rigi in Central Switzerland was covered by the ER-2 and its sensors, the AVIRIS, TMS and RC-10 within the NASA MAC Europe 1991 deployment.

Our focus of research is the evaluation of the applicability of hyperspectral data over rugged alpine terrain. The utility of imaging spectrometry under highly complicated terrain and atmospheric conditions shall be investigated with a team that has some experience in high precision adoption of airborne and satellite data through geometric and radiometric corrections and subsequent task-adapted classification procedures.

2. SUPPORTING MEASUREMENTS

A multidisciplinary team of specialists in remote sensing, image processing, geography, landuse, agronomy and botany, forestry, limnology and atmospheric research enabled a multitude of parallel measurements concurrent to the AVIRIS overflight. Synergism with an athmospheric research project "POLLUMET" which took place at the same time, and within the same area, yielded a wealth of measurements of meteorological and atmospheric parameters.

Concurrent to the ER-2 overflight, for instance vertical spectroradiometric profiles of the atmosphere were measured from helicopter descending from 3000 m GND to water level, and at the same time subsurface underwater spectroradiometric profiles were taken as well. Simultaneously hundreds of water samples were taken and measurements of chlorophyll, phytoplankton concentration, optical thickness of the water, acidity etc. acquired. Several teams were active assessing horizontal visibility along mountain profiles. Agrarian landuse mapping was carried out at specific testsites totalling 124 fields. Soil samples as well as forest cuttings were taken and stored for laboratory tests. This brief summary of course cannot give an indepth insight into all the gathered information and the extensive activities of the involved approximately one hundred specialists on the ground.

The following table gives an overview on the activities in data capturing for the AVIRISwiss-91 campaign.

Table 1: Instruments and Data Collection during the AVIRISwiss'91 Campaign

Platform	System	Instrument	Target	Measurement	Use
Satellite	SPOT	HRV-PAN	central Switzerland	1 band, VIS	landuse
		HRV-XS	central Switzerland	3 bands, VIS, NIR	landuse
	Landsat	TM	central Switzerland	7 bands VIS, NIR,IR	landuse
	NOAA	AVHRR	central Switzerland	5 bands	meteorology
Aircraft	ER-2	AVIRIS	Rigi testsite	220 bands VIS, NIR	applied imaging spectrometry
		TMS	Rigi testsite	12 bands, VIS, NIR,IR	cross referencing to AVIRIS
		RC-10	Rigi testsite	color IR	photogrammetry
	engine powered glider	by MetAir	central Switzerland	$P, T, M, O_3, NO_2, H_2O_2$	atmospheric constituents
Balloon / Sonde	radiosonde	by LAPETH	testsite atmosphere	T, WD, WV	atmospheric parameters
	captive balloon	by KLIMET	testsite atmosphere	WD, WV, P, T, M, O_3	atmospheric parameters
	constant level balloon	by PSI	atmosphere	P, T, M, WD	atmospheric parameters
Helicopter	spectrometer	Spectron SE-590	selected test-areas	256 bands	spectral radiometry of targets and atmosphere
	photography	video (VHS)	selected areas	color	referencing
		camera	selected targets	color	referencing
Radar	ground radar	ADOUR	ER-2	2 frequency C-band	tracking of the ER-2 flight line
Ground	spectrometer	GER IRIS Mark V	selected reference targets	875 bands	target spectral radiometry, calibration
		LI-COR Li-1800		161 bands	
		Spectron SE-590		256 bands	
	analysts	Magellan GPS	selected targets, fields, etc.	landuse, cover state	classification
Boat	underwater spectrometer	LI-COR UWLi-1800	water	161 bands	optical properties
	Seccidisk	disk	water	% of light	optical thickness
	specific sondes	ME, WTW	water	T, Tr, Vis, Att, Chl	water chemistry

Legend: P = Pressure, T = Temperature, M = Moisture, Tr= up/down trans, WD = Wind Direction, WV = Wind Velocity, Vis = Visibility, Att = Attenuation, Chl = Chlorophyll (Scor)

3.   ANALYSIS APPROACH

A fully integrated analysis approach is pursued in handling all datasets, sensor data as well as ground truth measurements, in a digital database. For this purpose most of the ground truth is already converted into digital form and ready for modelling.

A first analysis step is a thorough data quality assessment where sensor and scene related effects are investigated. Among them geometric factors such as distortions and errors are handled and radiometric influences due to blurring, striping and calibration problems etc. are analyzed and corrected as a preprocessing step. Scene related factors such as the ones due to sensor geometry and terrain as well as radiometric effects due to topography, viewing angle and atmosphere are investigated and removed using a high precision DEM (*Itten et al. 1992*). Georegistration in a mountainous environment is a challenge in itself, and slope-aspect corrections as well as atmospheric modelling, using 5S, LOWTRAN and MODTRAN, are tested.

In processing we propose an information based approach with a general broad aim in mind to considerably improve landuse mapping and detailed land cover state analysis. New ways for classifying scenes are foreseen by using an information based approach (*Meyer 1992*). Symbolic description is applied in spatial and spectral modes; segmentation procedures will be tested and rules generated for an application oriented automatic feature extraction.

Teams of hydrologists, botanists, geographers, foresters, agrarian engineers, climatologists as well as image processing and remote sensing specialists are actively involved. Since corrected data have only been received by the end of March'92, the investigation based on the RSL-DIPS and IDL/SIPS (by CSES/CIRES University of Colorado, Boulder) on a DECStation 5000 workstation is in full progress.

4.   ACKNOWLEDGEMENTS

5.   REFERENCES

ITTEN K.I., MEYER P., KELLENBERGER T., LEU R., SANDMEIER St., BITTER P. and SEIDEL K., 1992: "Correction of the impact of topography and atmosphere on Landsat-TM forest mapping of alpine regions", Remote Sensing Series Vol.18, RSL, University of Zurich, 48 pp.

MEYER P., 1992: "Segmentation and symbolic description for a classification of agricultural areas with multispectral scanner data," IEEE Trans. GRS, Vol. 30/3, 8 pp.

AVIRIS INVESTIGATOR'S GUIDE

Howell Johnson

Jet Propulsion Laboratory
4800 Oak Grove Drive, Pasadena, California, 91109

1. INTRODUCTION

The purpose of the AVIRIS Investigator's Guide is to provide Investigators with a uniform, structured approach to conducting AVIRIS experiments and interacting with the AVIRIS project. It is not a guide for designing experiments; rather, it is simply a guide for planning these experiments and carrying them out.

The motivation for writing this guide stems from an ever-increasing demand for experiments with the AVIRIS instrument. The guide will introduce new investigators to the fundamentals of AVIRIS activities in the domains of science, engineering, and operations. It will also serve as a useful reference for "old-timers," as it will contain background information on the instrument, data processing facility, and the ER-2 aircraft. As a reference, it will also serve as a written description of the roles and responsibilities of investigators in their interaction with the AVIRIS project.

2. APPROACH

The growing necessity for simultaneous ground truth measurements, combined with the random nature of operations dictated by weather conditions, creates a serious challenge for an investigative team to carry out an experiment with limited resources. For this reason a major portion of the Investigator's Guide will be devoted to the planning and logistics of field measurements that must be coordinated with the ER-2 aircraft.

This aspect of AVIRIS operations - the coordination of field measurements with the aircraft - has been a source of friction between investigators, the AVIRIS project, and the High Altitude Missions group. This situation can be improved only by educating people on the realities of aircraft operations and establishing sound, secure agreements that address the needs of each party involved.

The remainder of the guide will be devoted to technical descriptions of the instrument and aircraft, background information on operations and weather prediction, and tips on filling out paperwork associated with flight requests and retrieval of AVIRIS data.

3. CONTENT

The guide will be divided into five sections:

1) <u>Background information</u> - descriptions of those aspects of the instrument, the aircraft, and operations that are most pertinent to investigators. This information will give some idea of the complexity of aircraft operations and hopefully provide insight into the reasons why events unfold as they do during and after a deployment.

2) <u>Requesting acquisition of AVIRIS data</u> - guidelines on properly filling out a flight request form for AVIRS/ER-2 experiments.

3) <u>Preparing for data acquisition</u> - how to plan for successful field operations that will maximize scientific objectives at minimum cost. This information will culminate the techniques of the most successful investigators and point out common errors that result in failure or compromised objectives.

4) <u>Data acquistion</u> - what to expect during a deployment, daily procedures, communications protocols for investigators, role of AVIRIS experiment coordinator during deployment.

5) <u>Requesting AVIRIS data</u> - how to request a retrieval of AVIRIS data from the archive after receiving quick-look data products.

5) <u>Appendices</u> - detailed information on characteristics and performance of the AVIRIS instrument and the ER-2 aircraft. Fundamentals of visible and near-infrared remote sensing through the atmosphere. Calibration of the AVIRIS instrument. Recommendations for ground truth measurements and instrumentation.

4. GENERAL

The Investigator's Guide will be available for distribution prior to the Airborne Geoscience Workshop and may differ slightly from the format indicated in this summary. It will be distributed as a loose-leaf booklet booklet in which sections may be augmented or updated over time.

OREGON TRANSECT: COMPARISON OF LEAF-LEVEL REFLECTANCE WITH CANOPY-LEVEL AND MODELLED REFLECTANCE

Lee F. Johnson
TGS Technology, Inc.
NASA/Ames Research Center 242-4
Moffett Field, California 94035

Frederic Baret
INRA Bioclimatologie
Avignon, France

David L. Peterson
NASA/Ames Research Center 242-4
Moffett Field, California 94035

1. INTRODUCTION

The Oregon Transect Ecosystem Research (OTTER) project involves the collection of a variety of remotely-sensed and in-situ measurements for characterization of forest biophysical and biochemical parameters. The project includes nine study plots located along an environmental gradient in west-central Oregon, extending from the Pacific coast inland approximately 300km. These plots represent a broad range in ecosystem structure and function. Within the OTTER project, the sensitivity of the AVIRIS signal to absorption by foliar biochemicals is being examined *(Johnson and Peterson, 1991)*. AVIRIS data were acquired over all plots in conjunction with four OTTER Multi-sensor Aircraft Campaigns spanning the growing season. Foliage samples were gathered during each campaign for biochemical determination (at Ames Research Center), to estimate stand-level constituency at each plot.

Directional-hemispheric leaf reflectance throughout the 400-2400nm region was measured in the laboratory as an aid to interpreting concurrent AVIRIS data. Obtaining leaf spectra in this manner reduces or eliminates the confounding influences of atmosphere, canopy architecture, and reflectance by woody components, understory, and exposed soils which are present in airborne observations. These laboratory spectra were compared to simulated spectra derived by inverting the PROSPECT leaf-level radiative-transfer model *(Jacquemoud and Baret, 1990)*, and to canopy reflectance derived from AVIRIS data by use of the LOWTRAN-7 *(Kneizys et al., 1989)* atmospheric radiative-transfer model.

2. LEAF REFLECTANCE MEASUREMENT

Five foliage samples were collected by shotgun or pruning pole from mid-to-upper canopy at each of four OTTER plots in early June, 1991. Red alder (*Alnus rubra*), a broadleaf, was collected at one plot; the other plots contained western hemlock (*Tsuga heterophylla*), a conifer. Each sample was divided into two sub-samples, one for biochemical analysis and another for spectral analysis.

The biochemistry sub-samples were maintained in a frozen state until analysis. These samples were assayed by wet chemical techniques for total nitrogen, total phosphorus, total chlorophyll, amino acids, sugar and starch. Specific leaf area (cm^2 leaf area/g dry wt) was also measured.

Each spectral sub-sample was immediately inserted into an airtight transparent plastic bag along with a moist paper towel. These bags were grouped and placed inside a black bag to shield from light exposure, and refrigerated for a period of 10-14 days.

Reflectance measurement (bandwidth 6 nm, sampling interval 2 nm) was performed on a Perkin-Elmer 330 spectrophotometer (Norwalk CT), resident at Ames Research Center. For each conifer sample, several needles attached to twig were placed in the instrument sample holder, and scanned. For the broadleaf samples, one entire leaf without woody material was scanned. Calibration standards were used to convert raw channel response into absolute reflectance and to verify accuracy of spectral response to within $\pm 2nm$.

3. LEAF REFLECTANCE VS. SIMULATED REFLECTANCE

The PROSPECT model simulates leaf reflectance (and transmittance) in the 400-2400nm region as a function of chlorophyll concentration ($\mu g/cm^2$) and water content (equivalent water thickness). The model was inverted to estimate chlorophyll concentration by fitting to the diffuse leaf reflectance component of each measured spectrum. Predictions from inversions with low root mean square error between the simulated and measured spectra were significantly (.01 level) correlated with assay values (r=0.93, n=6, se=4.2 $\mu g/cm^2$). Measured reflectance was consistently lower than modelled reflectance in the 1500-1800nm region, possibly as a result of biochemical absorption, with the largest residuals occurring between 1690 and 1710nm.

4. LEAF REFLECTANCE VS. CANOPY REFLECTANCE

The LOWTRAN-7 code was used to convert AVIRIS at-sensor radiance acquired 22-May-91 into canopy reflectance. Total atmospheric optical depth at each plot at or near the time of AVIRIS overflight was measured by sun-photometer. These

optical depths were used to estimate horizontal visibility by fitting to LOWTRAN-calculated total transmittance throughout the 400-1000nm range *(Green, 1990)*. Using this visibility, the Continuum Interpolated Band Ratio technique *(Carrere et al., 1990)* was then applied to the 940nm absorption feature to estimate water vapor abundance. Subsequently, canopy reflectance (ρ) was retrieved from at-sensor radiance (after Green, 1990) by:

$$\rho = (L_r/L_{r\alpha})\alpha \tag{1}$$

where L_r is the net canopy-reflected radiance in the AVIRIS signal, and $L_{r\alpha}$ is the modelled radiance reflected from a surface with albedo α for the given solar zenith and surface elevation.

These spectra were compared with the mean leaf spectra at each site. The canopy spectra are similar in shape to the measured leaf spectra for both broadleaf and conifer. The degree of similarity increases with greater leaf-area-index (LAI), as background exerts less influence on the signal. Conifer leaf reflectance exceeds canopy reflectance by a factor of two along the NIR plateau, and by a factor of three in the shortwave IR. Less disparity is observed in the alder, where leaf reflectance exceeds canopy reflectance by a factor of less than two along the NIR plateau, and by a factor of two in the shortwave IR. AVIRIS reflectance spectra from canopies with high LAI will be used to test an adaptation of the PROSPECT model to canopy level simulation.

5. REFERENCES

Carrere, V., J. Conel, R. Green, C. Bruegge, J. Margolis, and R. Alley, "Analysis of Atmospheric Water Vapor Maps from AVIRIS at Salton Sea, California," Proc. Second AVIRIS Workshop, JPL Publication 90-54, pp. 107-128, 1990.

Green, R., "Retrieval of Relectance from Calibrated Radiance Imagery Measured by the Airborne Visible/Infrared Imaging Spectrometer," Proc. Second AVIRIS Workshop, JPL Publication 90-54, pp. 167-175, 1990.

Jacquemoud, S. and F. Baret, "PROSPECT: A Model of Leaf Optical Properties Spectra," Remote Sensing Environment 34:75-91, 1990.

Johnson, L. and D. Peterson, "AVIRIS Observation of Forest Ecosystems Along the Oregon Transect," Proc. Second JPL Airborne Geoscience Workshop, JPL Publication 91-28, pp. 190-199, 1991.

Kneizys, F., E. Shettle, G. Anderson, L. Abrew, J. Chetwynd, J. Shelby, and W. Gallery, "Atmospheric Transmittance/Radiance; Computer Code Lowtran 7," AFGL, Hanscom AFB, MA, 1989.

AVIRIS AS A TOOL FOR CARBONATITE EXPLORATION: COMPARISON OF SPAM AND MBANDMAP DATA ANALYSIS METHODS

Marguerite J. Kingston and James K. Crowley
U.S. Geological Survey, Reston, VA 22092

INTRODUCTION

Data acquired with the Airborne Visible/Infrared Imaging Spectrometer (AVIRIS) of the Mountain Pass, San Bernadino County, California, area were analyzed to evaluate the use of narrow-band imaging data for carbonatite exploration. Carbonatites are igneous carbonate-rich rocks that are economically important in part because they are the major source for rare-earth minerals. Because the 224 AVIRIS spectral channels have a nominal spectral resolution of 10 nm, narrow absorption features such as those displayed by the rare-earth elements neodymium (Nd) and samarium (Sm) may be detected.

The Mountain Pass region encompasses a well-exposed sequence of sedimentary, metamorphic, and igneous rocks, including an alkalic carbonatite intrusion. The carbonatite was emplaced in Precambrain granitic rocks that are fault bounded by a thick suite of Paleozoic sedimentary rock, predominantly dolomite. The carbonatite stock, the major source of light rare-earth elements (REE) in the United States, affords the opportunity to test AVIRIS capabilities for detecting REE absorption features. Nd-bearing minerals display narrow, sharp and distinctive spectral features at 580, 740, 800, and 870 nm (Kingston, 1989). Minerals bearing Sm display similarly sharp features near 1090, 1250, 1410, and 1550 nm. The more common REE, lanthanum and cerium, do not display absorption features in the visible/near-infrared region in their natural oxidation states.

RESULTS AND DISCUSSION

This study compares two "curve-matching" techniques designed to locate spectrally similar pixels in an AVIRIS image cube (lines, pixels, channels). The two techniques are the SPectral Analysis Manager (SPAM) binary-encoding approach developed at the Jet Propulsion Laboratory (Mazer et al., 1988) and Mbandmap (multiple band mapping), a least squares band-fitting method recently developed at the U.S. Geological Survey (Clark et al., 1990).

The SPAM software program uses a binary-encoding algorithm to classify materials present in the scene by comparing amplitude and slope similarity of spectral curves point by point. Digital numbers above and below the mean for each reference spectrum are stored as binary values 0 or 1. The spectrum for each pixel is encoded in the same way and compared to the reference spectrum. Materials may be mapped by matching image spectra to plots extracted from the image or to plots selected from a spectral library. Noise in AVIRIS data imparts a sawtooth pattern in the spectra, which commonly leads to spectral mismatches when the binary-encoding technique is used. This sawtooth effect can be reduced by smoothing; however, smoothing seriously reduces the spectral contrast of narrow absorption features, such as the Nd features. At Mountain Pass, the SPAM algorithm was effective for mapping distributions of some materials, like carbonates, which have broad absorption features, but mapping of REE-bearing materials was less successful, being limited to a few of the major mine dumps.

The Mbandmap program allows the discrimination of spectrally unique materials by use of a least squares band-fitting method. Mbandmap clusters materials by fit-comparing calibrated AVIRIS spectra to selected image spectra or to library reference spectra. Multiple absorption bands for each mineral may be compared in a single mapping run. Images showing band depth, degree of fit, and band depth fit are generated. Clark and others discuss details of this technique elsewhere in this volume.

Prior to Mbandmap analysis, AVIRIS radiance digital numbers were converted to approximate ground reflectance by use of laboratory reflectance measurements of samples collected from a highway borrow pit that was easily identified on the image. The Mbandmap reference library consists of laboratory reflectance data of pure minerals as well as representative rock and soil samples collected in the field area. The REE reference sample is a Mountain Pass REE-enriched sample from the U.S. National Museum Collection. The composition of two REE-bearing minerals in this sample, bastnaesite and synchysite, was determined by microprobe analysis. Weight percent Nd averaged 9% in bastnaesite and 8% in synchysite. Because of the lack of a Sm standard, that element could not be examined by microprobe. Comparison of laboratory spectral reflectance measurements of the samples with Nd_2O_3 and Sm_2O_3 spectra corroborated the Nd and Sm composition.

By using Mbandmap, several areas of rare-earth enrichment not previously discriminated by AVIRIS data were identified in the Mountain Pass mine area. One small area of REE response occurs south of the active mining area and may correspond to a carbonatite dike. Spectra extracted from the mapped area display the four distinctive Nd bands between 580 nm and 870 nm. Some of the spectra also displayed Sm bands between 1090 and 1550 nm, although these occur in a wavelength region of greater atmospheric interference. Dolomite, calcite, and muscovite-bearing granite in rocks near the carbonatite were also mapped.

CONCLUSION

SPAM provides the capability to classify spectrally similar materials by comparing image spectra to reference spectra, but it is relatively insensitive to narrow features and to subtle band shape differences. As a result, only high concentrates of Nd-bearing minerals could be identified in the Mountain Pass mine area. However, SPAM is particularly useful for mapping materials that can only be discriminated by overall curve shape, including the relatively featureless alkalic rocks associated with carbonatites. Mbandmap allows improved mapping of carbonate and REE minerals characteristic of carbonatites because shapes and depths of multiple features can be compared simultaneously.

For remote sensing detection of specific REE-absorption features, Mbandmap alone was highly effective. When a more general spectral classification of surface materials is the objective, a combination of the SPAM and the Mbandmap methods should provide increased information.

REFERENCES

Clark, R.N., Gallagher, A.J., and Swayze, G.A., 1990, Material absorption band depth mapping of imaging spectrometer data using a complete band shape least-squares fit with library reference spectra: in Proceedings of the Second Airborne Visible/Infrared Imaging Spectrometer (AVIRIS) Workshop, June 4-5, 1990, Jet Propulsion Laboratory Publication 90-54, p. 176-186.

Kingston, M.J., 1989, Spectral reflectance features of kimberlites and carbonatites: implications for remote sensing for exploration: in Kimberlites and Related Rocks, v.2, Proceedings of the Fourth International Kimberlite Conference, Perth 1986, Geological Soc. of Australia Special Publication No. 14, pp. 1135-1146.

Mazer, A.S., Martin, M., Lee, M., Solomon, J.E., 1988, Image Processing Software for Imaging Spectrometry Data Analysis, Remote Sensing of Environment v. 24, pp. 201-210.

EXPERT SYSTEM-BASED MINERAL MAPPING USING AVIRIS

F. A. Kruse [1,2] A. B. Lefkoff [1] and J. B. Dietz [1]

[1] Center for the Study of Earth from Space (CSES)
Cooperative Institute for Research in Environmental Sciences (CIRES)
University of Colorado, Boulder, Colorado 80309-0449

[2] Department of Geological Sciences
University of Colorado, Boulder, Colorado 80309-0250

1. INTRODUCTION

Integrated analysis of imaging spectrometer data and field spectral measurements were used in conjunction with conventional geologic field mapping to characterize bedrock and surficial geology at the northern end of Death Valley, California and Nevada. A knowledge-based expert system was used to automatically produce image maps from Airborne Visible/Infrared Imaging Spectrometer (AVIRIS) data showing the principal surface mineralogy. The imaging spectrometer data show the spatial distribution of spectrally distinct minerals occurring both as primary rock-forming minerals and as alteration and weathering products. Field spectral measurements have been used to verify the mineral maps and field mapping has been used to extend the remote sensing results. Geographically referenced image-maps produced from these data form new base maps from which to develop improved understanding of the processes of deposition and erosion affecting the present land surface.

The "northern Grapevine Mountains" (NGM) study area has been reported on in numerous papers (Kruse et al., 1992, and references therein). This area is an unnamed northwestward extension of the range. Most of the research here has concentrated on mapping of Jurassic-age plutons and associated hydrothermal alteration (Wrucke et al., 1984; Kruse, 1988), however, the nature and scope of these studies is much broader, pertaining to the geologic history and development of the entire Death Valley region.

AVIRIS data for the NGM site were obtained during May 1989. Additional AVIRIS data were acquired during September 1989 as part of the Geologic Remote Sensing Field Experiment (GRSFE) (Evans and Arvidson, 1990). The area covered by these data overlaps slightly with the May 1989 data. Three and one-half AVIRIS scenes total were analyzed.

2. MINERAL MAPPING WITH AN EXPERT SYSTEM

Many naturally occurring materials can be identified and characterized based on their reflected-light spectral characteristics. In geology, the exact positions and shapes of visible and infrared absorption bands are different for different minerals, and reflectance spectra allow direct identification. The objective of this work was to use an expert system approach based on known mineral absorption bands to perform automated mineral mapping using AVIRIS as the first step to detailed geologic mapping and analysis.

Because of the large volume of data that is generated by imaging spectrometers and its unique spectral/spatial nature, development of automated data reduction and analysis capabilities is required to allow extraction of useful information. As part of the research described here, an expert system was developed that allowed automated identification of Earth surface materials based on their spectral characteristics in imaging spectrometer data. A spectral library of laboratory spectral reflectance measurements was

used to develop a generalized knowledge base for analysis of visible and infrared reflectance spectra. Spectral features were digitally extracted from a spectral library containing a suite of 28 common minerals (Kruse, unpublished data) and both green and dry vegetation. Numerical analysis and characterization of the digital reflectance measurements were used to establish quantitative absorption band criteria (wavelength position, band depth, FWHM, and asymmetry) for identifying minerals, mineral mixtures, and vegetation. These procedures are described in detail in Kruse (1990).

The expert system was used to analyze the AVIRIS data to automatically identify minerals and to map their spatial distributions. The absorption feature positions and shapes of each reflectance spectrum for each pixel were characterized using the automated techniques. The features attributed to a specific mineral were assigned weighting factors between 0 and 1 depending upon whether they were required to identify the mineral (must-have, weight=1), were likely to occur in the specific mineral (should-have, weight=0.6) or might be present (may-have, weight=0.3). The weights chosen were arbitrary and have no direct physical meaning. The features found in a particular pixel were then compared to the expected features for each spectrum in the library. For example, if a specific mineral was expected to have three absorption features with respective weights of 1.0, 0.6, and 0.3 (must-have, should-have, and may-have) and it only had two of the features (say the 1.0 and the 0.3 features) then the probability of occurrence of that specific mineral could be represented as $(1.0+0.3)/(1.0 + 0.6 + 0.3) = 0.68$.

To help deal with some of the noise in the AVIRIS data, the results of the spectral features analysis were then assigned a weight of 0.67 in the final decision images while the results of binary encoding (Mazer et al., 1988) were assigned a weight of 0.33. The final products of the expert system analysis were a "continuum-removed" cube with 224 bands containing all of the continuum-removed spectra calculated from the reflectance data, a "feature" cube containing the wavelength positions, depths, FWHMs, and asymmetries for each pixel for the ten strongest absorption features, and an "analysis cube" showing the location and probability of occurrence of 30 minerals based on the weighted combination of binary encoding, and feature analysis in the expert system. Given calibrated data, automated analysis using the expert system described above can be used to produce a preliminary mineral map for the 30 endmembers in less than one hour for a standard 614 line by 512 pixel AVIRIS scene (on a 30 MIPS-class computer).

3. DISCUSSION OF RESULTS

The expert system and spectral unmixing were run on the NGM and the GRSFE AVIRIS data. In the one area of overlap (at the northern end of the flightlines) there is good agreement in the mineral identifications between the two flightlines. Minerals identified in this area include calcite, dolomite, goethite, hematite, and sericite. The middle one third of the GRSFE AVIRIS flightline consists primarily of Tertiary volcanic rocks (Wrucke et al.,1984). This area is dominated in the AVIRIS data by the mineral hematite, likely the result of surface weathering of mafic minerals in the volcanic rocks. The expert system also identified occurrences of montmorillonite, and jarosite in this region. One possible explanation for the montmorillonite concentrations, which appear oval in shape, is that they are associated with small intrusions. This still requires field verification. The southern one third of this area is dominated by Paleozoic sediments (Oakes, 1977; Wrucke et al., 1984). Detailed examination of the AVIRIS image spectra combined with the expert system, linear unmixing, and photointerpretation were used to subdivide these rocks into several different classes. The most obvious of these are nearly pure dolomite and pure calcite units. Alluvial fans derived from these units show similar spectral features. Several additional dolomite and calcite and mixed carbonate/iron oxide units were defined based on their spectral signatures in the AVIRIS data. The distribution of all these units is remarkably similar to lithologies mapped using classical techniques for a portion of the range (Oakes, 1977). The AVIRIS mapping, however, extends over a much larger region and resulted in high quality mineral maps with a minimum of field work.

4. CONCLUSIONS

An expert system has been developed that allows automated identification of Earth surface materials based on their spectral characteristics in imaging spectrometer data. Automated techniques were developed for the extraction and characterization of absorption features by analyzing a suite of laboratory spectra of some of the most common minerals. Critical absorption band characteristics for identification were defined and these were used to develop facts and rules defining a generalized knowledge base for analysis of reflectance spectra that allowed the computer to make decisions similar to those that would be made by an experienced analyst. The expert system produced image maps from AVIRIS data showing the predominant surface mineralogy. Analysis of the AVIRIS data using the expert system provides a rapid means of assessing surface mineralogy and the maps produced accurately represent the surficial geology.

5. ACKNOWLEDGMENTS

6. REFERENCES

Evans, D. L., and Arvidson, R. E., 1990, The Geologic Remote Sensing Field Experiment (GRSFE): Overview of initial results: in Proceedings, IGARSS '90, University of Maryland, College Park, Md., The Institute of Electrical and Electronics Engineers, Inc. (IEEE), New York, p. 1347.

Kruse, F. A., 1988, Use of Airborne Imaging Spectrometer data to map minerals associated with hydrothermally altered rocks in the northern Grapevine Mountains, Nevada and California: Remote Sensing of Environment, v. 24, no. 1, pp. 31-51.

Kruse, F. A., 1990, Artificial Intelligence for Analysis of Imaging Spectrometer Data: Proceedings, ISPRS Commission VII, Working Group 2: "Analysis of High Spectral Resolution Imaging Data", Victoria, B. C., Canada, 17-21 September, 1990, p. 59-68.

Kruse, F. A., Lefkoff, A. B., and Dietz, J. B., 1992, Expert-system based mineral mapping in northern Death Valley, California/Nevada using the Airborne Visible/Infrared Imaging Spectrometer (AVIRIS): Remote Sensing of Environment, Special issue on AVIRIS, (in press).

Mazer, A. S.,Martin, M., Lee, M., and Solomon, J. E., 1988, Image processing software for imaging spectrometry data analysis: Remote Sensing of Environment, v. 24, no. 1, pp. 201-210.

Oakes, E. H., 1977, Geology of the northern Grapevine Mountains, northern Death Valley, California: Unpublished M.S. Thesis, University of Wyoming, Laramie.

Wrucke, C. T., Werschkey, R. S., Raines, G. L., Blakely, R. J., Hoover, D. B, and Miller, M. S., 1984, Mineral resources and mineral resource potential of the Little Sand Spring Wilderness Study Area, Inyo County, California: U. S. Geological Survey Open File Report 84-557, 20 p.

THE EARSEC PROGRAMME IN RELATION TO THE 1991 MAC-EUROPE CAMPAIGN

Wim J. Looyen, Jean Verdebout, Benny M. Sorensen, Giancarlo Maracci, Guido Schmuck, Alois J. Sieber

Commission of the European Communities
Joint Research Centre
Institute for Remote Sensing Applications
Advanced Techniques Unit
I-21020 Ispra (Varese)
Italy

1. INTRODUCTION

The Joint Research Centre (JRC) of the European Commission and the European Space Agency (ESA) have initiated airborne remote sensing activities through a multi-year experiment plan. The project is called: EARSEC (European Airborne Remote Sensing Capabilities). The key-element within EARSEC is the establishment of an operational airborne system which includes:

- a fully polarized high spatial resolution C-and L-band SAR system;
- a multi-channel high spectral resolution imaging spectrometer.

The objectives are:

- to test and verify these highly innovative system types with respect to data processing, calibration and data interpretation;
- to test and verify the SAR system and the imaging spectrometer in support of (operational) projects (e.g. monitoring of agricultural production and tropical biomass burning);
- to complement and support ERS-1 pilot projects over European test sites.

2. EARSEC 1991 PROGRAMME

In 1990 JRC sent out a Call for Proposals for:

- the acquisition of remotely sensed data;
- campaign management;
- the improvement in existing airborne imaging spectrometers and airborne imaging radars;
- the improvement in existing imaging spectrometry and imaging radar data processors;
- collaborative contributions.

In 1991 EARSEC undertook the following activities:

- an airborne campaign using the GER II imaging spectrometer, flown by the German Aerospace Research Establishment (DLR), the CAESAR multispectral scanner (Ccd Airborne Experimental Scanner for Applications in Remote Sensing), flown by the Dutch National

Aerospace Laboratory (NLR). The campaign included aerial photography and ground measurements;
- improvement of the GER II imaging spectrometer to a new generation;
- state-of-art sensor called DAIS-7915;
- improvement to full polarization of the single polarized C-band SAR owned by the Technical University of Denmark.

2.1. EARSEC AIRBORNE CAMPAIGN 1991

The EARSEC airborne campaign took place simultaneously with the MAC Europe campaign to make use of the acquired AIRSAR data and AVIRIS and TMS data for intercalibration. Two test sites are of specific interest:

- The Villingen-Schwenningen area, near Freiburg, in the German Black Forest, where major research is conducted with respect to the effects on restabilisation measures and atmospheric deposition on N- and S-cycling of the eco- and hydrosphere;
- The Ardeche area, in France, where basic research is conducted with respect to the identification of basic soil types, estimation of canopy biochemistry of mediterranean woods and detection of relative amounts of vegetation and soils present in a ground resolution cell.

This paper only discusses the Villingen-Scwenningen area.

An extensive ground-truth measurement campaign was set up to accommodate both the airborne measurements acquired within the framework of the MAC-Europe and EARSEC campaigns.

The main objectives for the optical data analysis of the campaign are:

- to assess the data quality and calibration of the different sensors in terms of Signal-to-Noise ratio (SNR) and Noise-Equivalent-Radiance (NER), to gain experience of importance for the improvement of an European imaging spectrometer;
- to assess CAESAR's bidirectional reflectance properties for canopy structure evaluation by studying the sun-target interaction, validating physically based bidirectional reflectance models for homogeneous and inhomogeneous surfaces, and by retrieving biological parameters;
- to assess the capabilities of the imaging spectrometer for the extraction of biochemical components in vegetated areas.

2.2. IMPROVEMENT OF THE GER II IMAGING SPECTROMETER

The new European sensor will be a significant improvement of the GER II imaging spectrometer. It will consist of 79 channels covering the spectral range from 0.4 to 12.3 µm in semicontiguous intervals. The absolute calibration accuracy of the system is guaranteed to be less than 5 percent. Results from the 1991 campaigns will be used to steer the improvement with respect to data quality and data processing.

3. DATA COLLECTION

During July 1991 the following airborne data were acquired:

Date	Sensor
July 5	AVIRIS, TMS, ER-2 aerial photography

July 18	CAESAR
July 22	AVIRIS, TMS, ER-2 aerial photography
July 23	GER II
July 29	AVIRIS, TMS, ER-2 aerial photography
August 21	Aerial photography

Ground-truth measurements were collected from 7 to 22 June and from 7 to 22 July.

4. DATA ANALYSIS

Preliminary results regarding the three research objectives are shown below. As far as the data quality is concerned: the SNR and NER [μ W cm^{-2} sr^{-1} μm-1] were calculated for three sensors, AVIRIS (only July 5), GER II and CAESAR using a high reflectance calibration target, a homogeneous sandy sports field.

sensor	λ [nm]	SNR	NER	resolution [m]
AVIRIS	548.6	68	0.104	20
GER II	549.5	137.	0.028	10
CAESAR	550	38	0.098	1.25
AVIRIS	667.5	30		20
GER II	669	73	0.053	10
CAESAR	670	63	0.086	1.25
AVIRIS	872	70	0.108	20
GER II	860	66	0.064	10
CAESAR	870	73	0.074	1.25
AVIRIS	2030	5	0.136	20
GER II	2030	17.	0.033	10
AVIRIS	2209	7.4	0.088	20
GER II	2212	22	0.033	10
AVIRIS	2406	0.79	0.229	20
GER II	2412	6.5	0.634	10

More detailed results will be presented during the workshop.

5. CONCLUSIONS

The current data set allows only for a study of data quality and calibration aspects. However, for that purpose, we consider this data set to be of importance. Especially with regard to the improvement of the GER imaging spectrometer, useful conclusions can be drawn to further improve the capabilities of the European spectrometer. The SNR's and NER's need to be improved in order to achieve the design goals of SNR's higher than 150 for the VIS/NIR region and higher than 80 for the SWIR/MIR/TIR region.
The data set also allows for a study of bidirectional information. Research in this area contributes to the development of MODIS-T and MISR.
The extraction of biochemical components in vegetated areas can be achieved by using the high spectral resolution of the AVIRIS. Research should be conducted into the area of atmospheric modelling, to fully explore the benefits of the AVIRIS data.
At present, the final results are not yet available. Major research in the area is established by a program exchange with U.S. scientists, this summer. By that time, all the ground truth data will be available.

PRELIMINARY STATISTICAL ANALYSIS OF AVIRIS/TMS DATA ACQUIRED OVER THE MATERA TEST SITE

Stefania Mattei and Sergio Vetrella
CO.RI.S.T.A. Consortium
P.le Tecchio n.80, 80125 Napoli, Italy

1. INTRODUCTION

In the framework of the MAC Europe campaign, conducted in the summer of 1991, the Matera test site, located in southern Italy, has been overflown by the NASA ER-2, equipped with the TMS and AVIRIS sensors, and the NASA DC-8, equipped with AIRSAR and TOPSAR. The Matera test site extends over an area of about 128 km^2 and includes a flat area that is partially bounded in the northern and southern part by a hilly region.

Due to a tacan error, which caused the plane to go slightly off course, and to scene obscuration by 30% cumulus, only a limited number of images are useful for the test site analysis. Consequently, one image taken on June 20 and two images on July 20 have been requested.

This paper is intended to present the preliminary analysis of TMS/AVIRIS data, which is performed in order to integrate these data with those obtained by the SAR system.

2. GROUND TRUTH

During the airborne campaign, a ground-truth campaign has been conducted (CO.RI.S.T.A. 1991) to get the following information:
- Land cover over 50 different test areas (Fig. 1).
- Type, state, and texture of the vegetation.
- Phenology and diseases.
- Soil humidity and rugosity (Table 1 and Fig. 2).
- Photographs to show the main aspects of the test areas (Fig. 3).

Table 2 lists the main species existing over the areas, with the exception of those covered by bare soil, where the active and passive calibrators were deployed. A digital elevation model has been obtained at a scale of 1:25,000, using the digital data produced by the Italian Geographic Military Institute, and has been registered with respect to the ground-truth maps.

3. TMS/AVIRIS DATA ANALYSIS

Several papers have already emphasized the need to integrate morphological and textural land information with remotely sensed multispectral data, in order to improve classification results.

In the first part of our paper, the geographic information system of the area will be summarized and the procedure for geometric correction and co-registration of TMS and AVIRIS data will be described, taking into account the geometry of the observation and the ancillary data of the airplane. The images will then be introduced in the geographic information system as additional layers, in order to proceed in the classification and statistical analysis of the data and to obtain the spectral signature of different covers.

The experience has shown that there are many different techniques for obtaining the training statistics and for integrating spectral with textural data (G. Asrar 1989). In addition to the need for improving the knowledge of the spectral signature of different land covers, there is also the need for identifying the optimal combination of bands for land cover classification. It is well-known that two basic techniques exist for defining training classes (supervised and unsupervised) and they represent extremes both in terms of the method of defining the training sample and in terms of the method of grouping the training sample into unimodal training classes. Due to this contrast, the possibility exists for four intermediate steps between the two extremes in both parts of the training procedure (P.H. Swain).

In this paper, a multicluster blocks approach will be used with multiple clustering of heterogeneous blocks. This requires the division of the training sample into a series of areas, each containing a mixture of several cover types, which are clustered separately. The different cluster classes must then be combined into meaningful training classes, using a bispectral plot with different transformed divergence values, as a measure of the distance between classes in multidimen-

sional space. Following the classification of the test area, a statistical analysis will be conducted of the AVIRIS 224 channels.

REFERENCES

G. Asrar, "Theory and Applications of Optical Remote Sensing," Wiley, 1989.
CO.RI.S.T.A. Internal Document, "Equator Campaign 1991."
P.H. Swain, "Land Use Classification and Mapping by Machine Assisted Analysis of Landsat Multispectral Scanner Data," LARS Inf. Note 111276.

Table 1. Table for Analysis of Soil Profiles

Profile	Digitalized Point Number	Maximum Value	Mean Value	Standard Deviation	Variation Coefficient
6A	673	45.14	26.927	11.278	0.419
6B	660	68.86	26.249	17.403	0.663
10A	986	105.04	45.683	22.771	0.498
10B	1097	82.35	43.511	21.281	0.489
11A	800	39.37	19.01	9.576	0.504
11B	1292	91	33.336	17.163	0.515
21A	1080	87.7	50.333	21.028	0.418
21B	902	96.28	47.375	25.394	0.536
23A	1294	76.8	40.829	17.09	0.419
23B	980	64.3	33.6	12.65	0.376
41A	1329	84.2	33.225	22.534	0.678
41B	1250	94.8	40.368	22.805	0.565

Note: A = parallel profile and B = perpendicular profile.

Table 2. Main Species Existing Over the Areas Where Calibrators Were Deployed

| Refl. #	General Description	Refl. #	General Description
1	Grass meadow of clover	15	Waxy, maturing, hard wheat growing
2	Physiological, maturating, distichous, barley growing	16	Physiological, maturating, distichous, barley growing
3	Physiological, maturating, distichous, barley growing	18	Physiological-waxy, maturating, distichous, barley growing
4	Lacteal-waxy, maturating, hard wheat growing	21	Ploughed soil
5	Waxy, maturating, hard wheat growing	23	N-S climbed olive-grow
6	NNE-SSW furrow soil	25	Physiological, maturating, barley growing
7	Waxy, maturating, scattered seed broadcast, oat growing	26	Physiological, maturating, hard wheat growing
8	Waxy, maturating, hard wheat growing	27	Waxy-physiological, maturating, oat growing
9	Waxy, maturating, hard wheat growing	29	Physiological, maturating, distichous, barley growing
10	Naturally grassed soil	31	Waxy, maturating, hard wheat growing
11	Naturally grassed soil	39	Waxy, maturating, hard wheat growing
12	Lacteal-waxy, maturating, hard wheat growing	40	Waxy, maturating, hard wheat growing
13	Lacteal-waxy, maturating, hard wheat growing	41	E-W ploughed soil
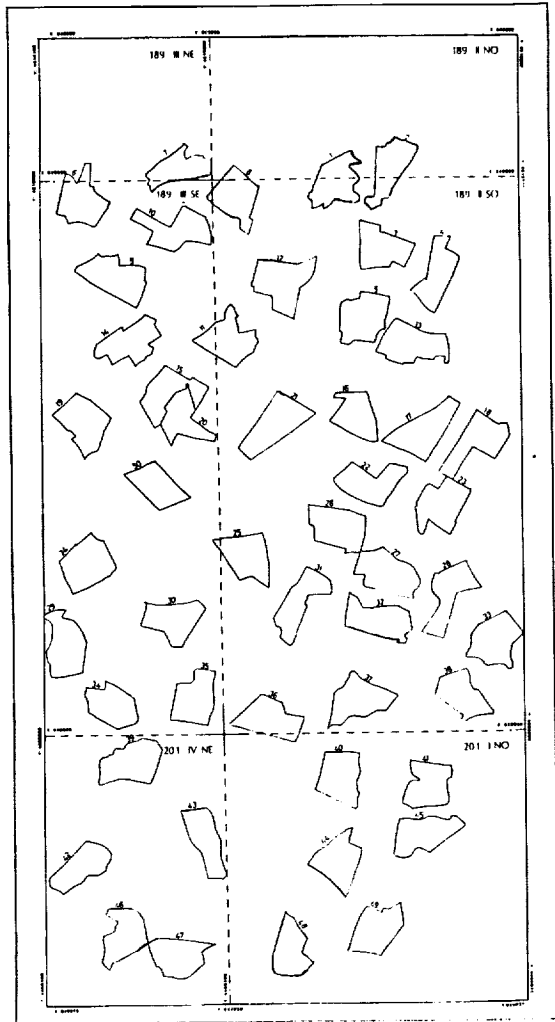
Fig. 1. Locations of test areas.
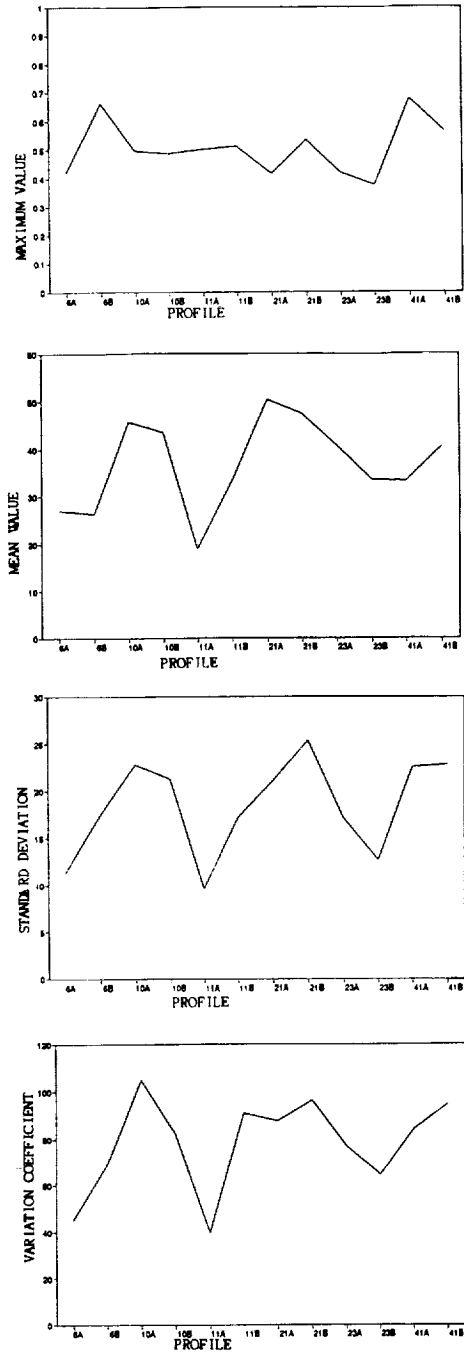
Fig. 2. Variation for each profile of the four parameters: maximum value, mean value, standard deviation, and variation coefficient.

127
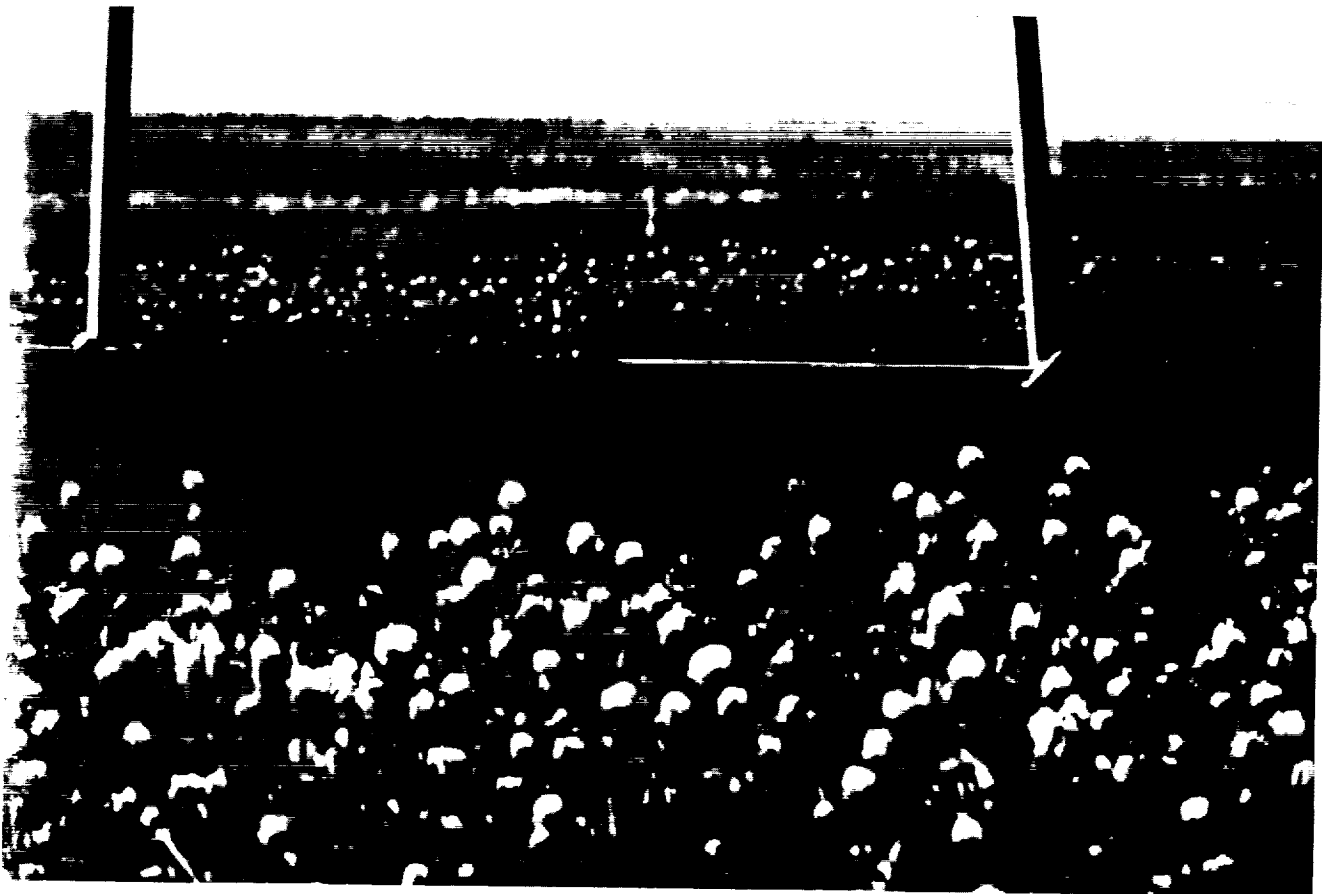
Fig. 3. Photographs of a test area.

AVIRIS DATA AND NEURAL NETWORKS
APPLIED TO AN URBAN ECOSYSTEM

Merrill K. Ridd, University of Utah Research Institute; Niles D. Ritter,
Nevin A. Bryant, and Robert O. Green, Jet Propulsion Laboratory,
Pasadena, California.

1.0   INTRODUCTION

Urbanization is expanding on every continent. Although urban/industrial areas occupy a small percentage of the total landscape of the earth, their influence extends far beyond their borders, affecting terrestrial, aquatic, and atmospheric systems globally. Yet little has been done to characterize urban ecosystems or their linkages to other systems horizontally or vertically. With remote sensing we now have the tools to characterize, monitor, and model urban landscapes world-wide. However, the remote sensing performed on cities so far has concentrated on land-use patterns as distinct from land-cover or composition. The popular Anderson system (Anderson et. al. 1976) is entirely land-use oriented in urban areas.

This paper begins with the premise that characterizing the biophysical composition of urban environments is fundamental to understanding urban/industrial ecosystems, and, in turn, supports the modeling of other systems interfacing with urban systems. Further, it is contended that remote sensing is a tool poised to provide the biophysical composition data to characterize urban landscapes.

2.0   A V-I-S MODEL

A Vegetation-Impervious Surface-Soil (V-I-S) model has been proposed (Ridd, in press) to characterize urban environments. These three components represent a basic distinction of urban biophysical variables, which exhibit highly contrasting influences on energy and moisture flux. They provide a basis for many science and engineering models, such as runoff, transpiration, heat island, etc. Figure 1 shows the V-I-S model. Figure 2 suggests the V-I-S composition for some familiar urban and near-urban environments. If remote sensing can distinguish these compositional variables with accuracy, from the pixel on up to landscape aggregations, urban ecosystem modeling will be advanced substantially.

TM and SPOT data have been inadequate in this effort. Neither system has been shown to distinguish soil and impervious surface adequately. This paper explores the use of AVIRIS data, coupled with a neural network classifier toward a better distinction and mapping of V-I-S composition of urban places.

3.0   AVIRIS and NEURAL NETWORKS

In an effort better to distinguish soil from impervious surfaces both the spectral resolution and the classification procedure are explored. Using

WTJ GenIsis software, characteristic spectral bands were selected from an AVIRIS data set collected over Pasadena on 20 September 1989. By examining the spectral reflectance curves from sample sites, signatures were generated to represent eight categories of cover composition in the urban and nearby environments: Vts (trees and shrubs), Vgg (green grass), Vgd (dry grass), Id (dark impervious), Il (light impervious), Ib (building roofs), S (soil), and W (water). The spectral bands deemed most diagnostic were selected, namely: AVIRIS 12-13 (508-518 nm), AV 29-31 (675-695 nm), AV 50-52 (844-863 nm), AV 99-100 (1263-1273 nm), AV 128-130 (1550-1569 nm), AV 145-147 (1718-1728 nm), AV 180-182 (2020-2040 nm), AV 200-202 (2219-2238 nm). To keep processing time within reason, these were combined and entered into the classifier as follows: channel 1 AV 12-13; channel 2, AV 29-31; channel 3, AV 50-52; channel 4, AV 99-100; channel 5, ratio of AV 145-147/AV 128-130; channel 6, ratio of AV 200-202/AV 180-182.

4.0   RESULTS

Preliminary results are promising. To begin with, merely displaying the Pasadena AVRIS data in a three-channel composite image, using combinations of the above bands, and some others, draws a distinction between soil and impervious surfaces. Clearly the narrow-band sensor is able to distinguish these common urban substances more effectively than broad-band TM and SPOT sensors.

Neural network classification is more than a clustering procedure. It involves a sophisticated internal reiterative process on the basis of spectral signatures per pixel, plus a textural evaluation of pixel groups to derive the final classes. The paper summarizes and displays the results.

5.0   REFERENCES

Anderson, J.R., E. Hardy, J. Roach, R. Whitmer, A land use and land cover classification system for use with remote sensor data, U.S.G.S. Professional Paper 964, 1976.

Ridd, M.K., Exploring a V-I-S (Vegetation-Impervious-Surface-Soil) model for urban ecosystem analysis through remote sensing, International Journal of Remote Sensing, out for peer review.
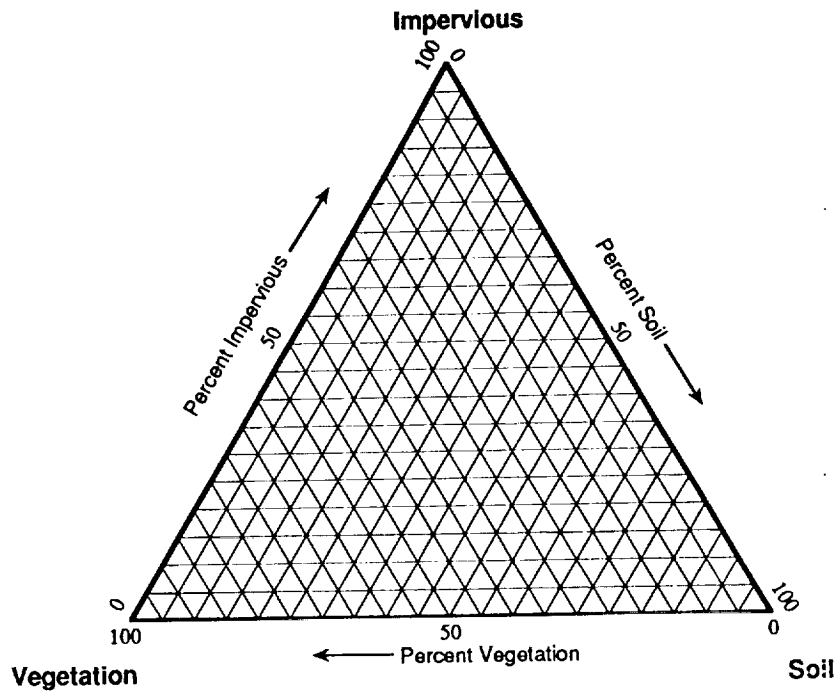
Figure 1. The V-I-S model.
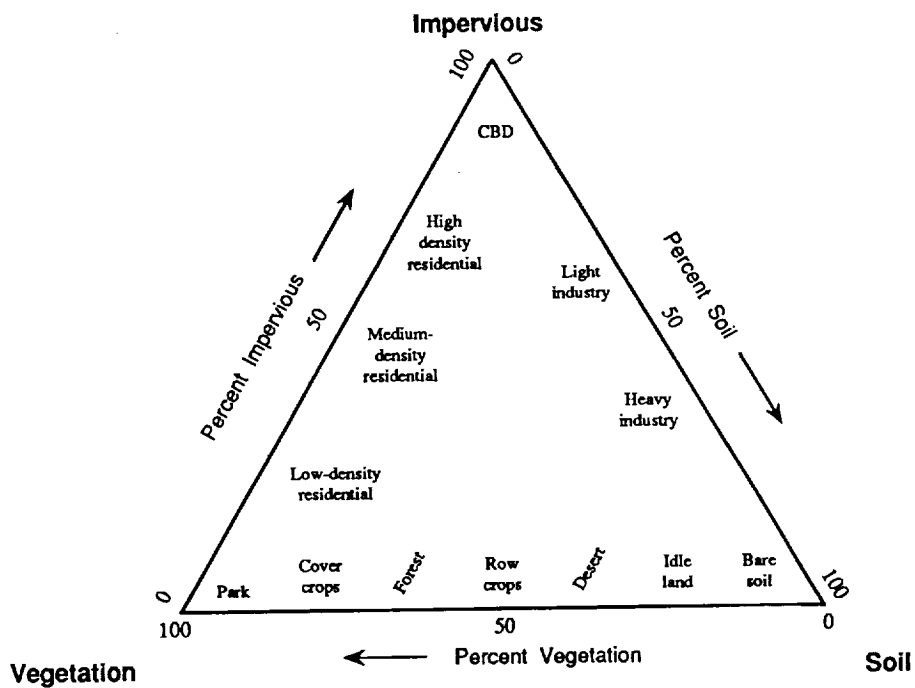
Figure 2. Some familiar urban and near-urban environments placed in
the ternary V-I-S model.

131

Temporal Variation in Spectral Detection Thresholds
of Substrate and Vegetation in AVIRIS Images

Donald E. Sabol Jr., Dar Roberts, Milton Smith, and John Adams

Department of Geological Sciences, AJ-20
University of Washington
Seattle, WA 98195

The ability to map changes over large surface areas over time is one of the advantages in using remote sensing as a monitoring tool. Temporal changes in the surface may be gradual, making them difficult to detect in the short-term, and because they commonly occur at the subpixel scale, they may be difficult to detect in the long-term as well. Also, subtle changes may be real or merely an artifact of image noise. It is, therefore, necessary to understand the factors that limit the detection of surface materials in evaluating temporal data. In this study, we evaluated and compared the spectral detectability of vegetation and soil in the 1990 July and October AVIRIS data of Jasper Ridge, CA.

The spectral detectability of subpixel material in an image depends upon its spectral contrast with background materials, its relative abundance, instrumental noise, and local atmospheric/topographic effects (Sabol et al. 1992). Spectral mixture analysis was used in this study to identify spectral endmembers and determine their spectral fractions for each image pixel. The minimal requirements for potentially physically meaningful fractions are: 1) the fractions are between 0 and 1, and 2) the residuals are low (within the level of system noise) (Smith et al., 1985; Adams et al., 1989). However, Smith et al. [1990] noted that the band residuals decrease as the number of endmembers increases, even when the additional endmembers are not actually present in the image. In this case, the endmember fractions may or may not be realistic, depending on the spectra involved. Additionally, Sabol et al. [1992] noted that the spectral detectability of targets generally decreases as the number of endmembers increases. Therefore, fractions are more physically meaningful , and detectability is enhanced, when the image is modeled using the minimal number of endmembers that result in realistic fractions and low residuals.

In past applications of spectral mixture analysis, only a few endmembers (usually fewer than five) have been used to model a large scene to preclude inclusion of extraneous endmembers. This, however, does not take into account the spectral variability of the surface components that each endmember represents. For example, earlier images of Jasper Ridge have been modeled as mixtures of a soil, green vegetation, senescent vegetation, and shade endmembers (Roberts et al. [1990, 1991], Sabol et al. [1991]). These endmembers, in fact, are "representative" of a type of surface component. In this study, to allow for spectral variability of the components in the scene, a number of spectra representing the range of spectral variation of each component were included in the spectral library and organized as classes. The library (466 spectra) included a green vegetation class, as well as soil, senescent vegetation and shade classes. To find the appropriate endmembers, each pixel was modeled as mixtures of 2 and 3 components, allowing a maximum of one spectrum from each class. The endmembers for each pixel were indicated when the fewest number of endmembers was needed to have realistic fractions and low residuals.

The resultant endmembers were then used to determine the best-case detection threshold of each component (excluding shade). A general outline of the analysis follows:
1) the images were calibrated to reflectance using the methods described by Roberts et al. [1991],

2) the images were modeled as mixtures of endmember groups (described above),
3) the signal-to-noise ratios for each image were determined using the method described by Sabol et al.[1991],
4) the detection thresholds for the different soil and vegetation spectra in the grasslands were determined for each combination of endmembers using the methods described Sabol et al.[1990, 1992].
5) the fractions and detection thresholds from the two data sets were then compared to ascertain actual changes in surface composition and changes due to other effects such as the change in solar illumination angle.

Two general types of shade were found in the image: photometric shade and vegetation shade. Photometric shade, spectrally flat (near zero reflectance) at all but the lower wavelengths, typically occurred in areas where the fraction of green vegetation was minimal (i.e. senescent grasslands, roads, lakes), while vegetation shade , spectrally similar to green vegetation, but with greatly reduced reflectance (maximum reflectance of ~30 %), was a prominent endmember in areas containing significant fractions of green vegetation. Roberts et al. (1991) showed that vegetation-shade is caused by the transmission and scattering of incident radiation through the leaves, and by solving for the shade component, the spectral signature of vegetation-shade for a given area can be determined. To get a more appropriate shade spectrum and to account for the non-linearities in spectral mixing due to green vegetation, we used the methods described by Roberts et al. [1991] to determine the vegetation-shade endmember for the several areas in the image. These spectra were incorporated into the detectability analysis.

A preliminary analysis indicates that for much of the July and October images, 2 image-endmember combinations yielded the most reasonable models. Although the fractions and endmembers are similar between the two images, some subtle differences were observed. For example, a portion of the grasslands at the crest of Jasper Ridge were modeled as a mixture of vegetation shade and senescent vegetation in the July image. This is interpreted as short, shadowed green grass among the taller dry grass. In the October image, the same area was modeled as a mixture of photometric shade and senescent vegetation, indicating that the green grass in the July image had senesced. The spectral signature of the exposed soil in this area was not included as an endmember because it was mimicked by mixtures of the endmembers. Therefore, band residuals were still necessary for detection of materials that were spectrally unique at only a few bands.

By allowing each pixel to be modeled by the most appropriate endmembers in the spectral library, the spectral variability of each surface component throughout an image can be more closely approximated in image analysis. The detectability of any endmember in a pixel, therefore, varied across the image. Soil, for example, which can be represented by a different spectrum in other image pixels, had a different detection threshold from pixel to pixel due to: 1) varying fractions, and 2) varying background endmembers. This data, when combined with spectral mixture analysis in evaluating temporal data, provides a methodology for separating actual changes in surface composition from uncertainties due to system noise and local temporal changes, such as change in the angle of solar illumination.

References

Adams, J.B., Smith, M.O., and Gillespie, A.R., Simple models for complex natural surfaces: A strategy for the hyperspectral era of remote sensing, *Proc. IEEE Intl. Geosci. Remote Sens. Symp. '89, I,* 16-21, 1989.
Roberts, D.A., Smith, M.O., Adams, J.B., Sabol, D.E., Gillespie, A.R., and Willis, S.C., Isolating woody plant material and senescent vegetation from green vegetation in AVIRIS data, *Proc. 2nd Airborne Sci, Workshop:* AVIRIS, Jet Propulsion Laboratory, Pasadena, CA. 4-5 June, 15 pp., 1990.

Roberts, D.A., M.O. Smith, J.B. Adams, and A.R. Gillespie, Leaf spectral types, residuals, and canopy shade in an AVIRIS image, in *Proc. 3rd Airborne Sci. Workshop:* AVIRIS, 20-21 May, *JPL Publ., 91-28*, 43-50, 1991.

Sabol, D.E., J.B. Adams, and M.O. Smith, Predicting the spectral detectability of surface materials using spectral mixture analysis, in *Proceedings of the IEEE International Geoscience Remote Sensing Symposium '90*, 2, 967-970, 1990.

Sabol, D.E., J.B. Adams, and M.O. Smith, Quantitative sub-pixel spectral detection of targets in multispectral images, *J. Geophys. Res., 97*, 2659-2672, 1992.

Sabol, D.E., J.B. Adams, M.O. Smith, and A.R. Gillespie, Target detection thresholds using imaging spectrometer data, in *Proc. 3rd Airborne Sci. Workshop:* AVIRIS, 20-21 May, *JPL Publ., 91-28,*, 99-108, 1991.

Smith , M.O. and Adams, J.B., Strategy for analyzing mixed pixels in remotely sensed imagery, Proc. NASA/JPL Aircraft SAR Workshop, JPL Publ. 85-39, 47-48, 1985.

Smith , M.O., Adams, J.B., and Gillespie, A.R., Reference endmembers for spectral mixture analysis, Proc. 5th Australian Remote Sensing Conf., Perth 1990, 10 pp, 1990.

N94-16707

DISCUSSION OF BAND SELECTION AND METHODOLOGIES FOR THE ESTIMATION OF PRECIPITABLE WATER VAPOUR FROM AVIRIS DATA

Dena Schanzer
Intera Information Technologies Corp.
Ottawa, Ontario, Canada

Karl Staenz
Canada Centre for Remote Sensing
Ottawa, Ontario, Canada

1. INTRODUCTION

An AVIRIS data set acquired over Canal Flats, B.C., on August 14, 1990, was used for the purpose of developing methodologies for surface reflectance retrieval using the 5S atmospheric code (Tanré et al., 1990). A scene of Rogers Dry Lake, California (July 23, 1990), acquired within three weeks of the Canal Flats scene, was used as a potential reference for radiometric calibration purposes and for comparison with other studies using primarily LOWTRAN7 (Green et al., 1991). Previous attempts at surface reflectance retrieval indicated that reflectance values in the gaseous absorption bands had the poorest accuracy (Teillet et al., 1991). Modifications to 5S to use a 1 nm step size, in order to make fuller use of the 20 cm^{-1} resolution of the gaseous absorption data, resulted in some improvement in the accuracy of the retrieved surface reflectance. Estimates of precipitable water vapour using non-linear least squares regression (Gao and Goetz, 1990) and simple ratioing techniques such as the CIBR (Continuum Interpolated Band Ratio) technique (Green et al., 1989) or the narrow/wide technique (Frouin et al., 1990), which relate ratios of combinations of bands to precipitable water vapour through calibration curves, were found to vary widely. The estimates depended on the bands used for the estimation; none provided entirely satisfactory surface reflectance curves.

2. METHODOLOGY

The original intent was to use the Rogers Dry Lake scene and a corresponding PIDAS (Portable Instant Display and Analysis Spectrometer) reflectance curve to provide calibration coefficients for the Canal Flats scene. Radiometric calibration factors were derived by assuming that all of the discrepancy between the 5S predicted radiance and the AVIRIS radiance data could be attributed to calibration uncertainties, as a multiplicative gain factor. Application of these derived calibration coefficients to the AVIRIS data resulted in very smooth reflectance curve retrievals throughout the Rogers Dry Lake scene. However, the effects of even small variations in water vapour within that scene were detectable. Though the reflectance curves retrieved from the Canal Flats scene were smoother using the Rogers Dry Lake calibration coefficients, irregularities were introduced. While some of the irregularities were again in the water vapour absorption regions, others were attributable to image to image differences in calibration.

The nature of these calibration irregularities would indicate that, as a first approximation, calibration uncertainties could be assumed to be constant over the wavelength interval used to estimate water vapour amount. Should such an assumption be reasonable, it would facilitate reliable estimation of water vapour despite these uncertainties. This assumption, along with the assumption that the surface reflectance curve varies linearly over the interval, and with the intrinsic atmospheric reflectance varying linearly as well, results in a combined linear curve. The slope and intercept are unknown and require estimation, together with the estimation of water vapour. Since the

individual effects are not distinguishable, the parameters can not necessarily be interpreted as true surface reflectance unless optical depth and calibration are known. Since the 5S code treats scattering and absorption separately, uncertainties in optical depth have not significantly altered the estimate of water vapour amount. Combining the intrinsic atmospheric reflectance curve with the linear surface reflectance curve, for estimation purposes only, produces a slightly better fit for dark targets, such as water, and is in better agreement with the corresponding CIBR type calculation. This can be explained by the treatment of calibration uncertainties.

Least squares regression achieves optimal parameter estimates when the underlying error distribution is Gaussian. However, the method becomes unreliable with even one outlier present. Since outliers and non-Gaussian noise are common occurrences, robust regression methods with a maximum breakdown point as low as 50% have been developed (Rousseeuw and Leroy, 1987), and applied to image analysis (Meer et al., 1991). These methods are suitable if the researcher has confidence that at least 50% of the data points are "good". "Good" data points are those for which the above assumptions hold, and for which the explanatory model (i.e., the 5S atmospheric code and the gaseous model in particular) is valid. Since gaseous transmittance is poorly modelled in the wings of the water vapour absorption region (Frouin et al., 1990), only a limited number of "good" bands are likely; i.e., the 940 nm, 1130 nm, and bands on the shoulder where gaseous absorption is negligible. Assuming that this small set of bands is "good", robust methods were used to identify other potential bands. This resulting set of consistent bands is dependent on the 5S gaseous model, as well as the AVIRIS calibration at the time of the overflight, and on any deviations from a linear reflectance curve assumption for the targets under investigation.

3.   RESULTS

First, a strong shift in calibration was found between the 1131 and 1141 nm bands in both scenes, making it impossible to bridge the 1130 continuum. Next, other bands within the 940 continuum were excluded due to poor fit (outliers), leaving the following candidates (used for subsequent comparisons): 872, 882, 939, 1035, 1045, and 1055 nm. When considering signatures where liquid water absorption is minimal, one finds that the set of consistent bands is larger, and for the opposite extreme of irrigated fields, the 1035 and possibly the 1045 nm bands should be removed. Since the 939 nm band is the only band from the above set influenced by water vapour absorption, it is not possible to test it as an outlier. Hence, the water vapour estimates based on the consistent set were compared to the estimate with the 1131 nm band included, and found to be within 3% of the original estimate for all sample signatures tested (minimum of 10x10 spatial pixels in each case). That the estimates were consistently lower when the 1131 nm band was included indicates that calibration or the gaseous absorption model is a more serious shortcoming than that of atmospheric scattering and absorption being calculated separately by 5S. For the Canal Flats scene, the 930 nm band could be added to the consistent set, though not for the Rogers Dry Lake scene. This variation in consistent bands is attributed to calibration differences, rather than to the gaseous model.

With both the 920 and 949 nm bands identified as extremely significant outliers, whose effects do not cancel, the narrow/wide technique (911 - 959 nm) would not be expected to perform well. Comparing the estimates based on the narrow/wide bands to the above estimates, we found that they were within the 20% accuracy between the narrow/wide estimate and radiosonde data reported by Frouin et al. (1990). The CIBR uses the 997 nm band, which was found to be unsuitable for the forested targets studied, due to liquid water absorption. Water vapour estimates based on the CIBR bands differed by only 1% for the Rogers Dry Lake scene, but larger differences of up to 4% in forested

sections of Canal Flats and 8% for an irrigated field were observed. Once the bands are selected, estimated values for water vapour were comparable for the different methodologies: simple ratioing (1 equation and 1 unknown); linear reflectance assumption (3 equations and 3 unknowns, but ignores calibration uncertainties); combined linear assumption (3 equations and 3 unknowns); non-linear estimation using more bands than unknowns.

4. CONCLUSIONS

Due to irregularities in calibration, the appropriate bands for water vapour estimation may differ from scene to scene. The linearity of the surface reflectance curves for targets within the scene, and the choice of atmospheric code, may also influence the selection. The quality of the water vapour estimate is limited by the accuracy of the gaseous transmittance model used. While the identification of a set of "good" bands and robust estimation techniques provide the tools for band selection, a three-band calculation would be satisfactory for the purpose of studying spatial variation in water vapour. For surface reflectance retrieval, improvements in the gaseous transmittance model and methods to address the calibration problem in the AVIRIS data are required.

5. ACKNOWLEDGMENTS

6. REFERENCES

R. Frouin, P.-Y. Deschamps and P. Lecomte, *Determination from Space of Atmospheric Total Water Vapour Amounts by Differential Absorption near 940nm: Theory and Airborne Verification*, **Journal of Applied Meteorology**, 29: 1990, pp. 448-460.

B.-C. Gao and A. F. H. Goetz, *Column Atmospheric Water Vapor and Vegetation Liquid Water Retrievals From Airborne Imaging Spectrometer Data*, **Journal of Geophysical Research**, 95-D4: 1990, pp. 3549-3564.

R. O. Green, V. Carrere and J. E. Conel, *Measurement of Atmospheric Water Vapor Using The Airborne Visible/Infrared Imaging Spectrometer*, **Proc. Image Processing '89 Conference**, Sparks, Nevada, 1989, pp. 31-44.

R. O. Green, S. A. Larson and H. I. Novack, *Calibration of AVIRIS Digitized Data*, **Proc. Third Airborne Visible/Infrared Imaging Spectrometer (AVIRIS) Workshop**, Pasadena, California, 1991, pp. 109-118.

P. Meer, D. Mintz, A. Rosenfeld and D. Y. Kim, *Robust Regression Methods for Computer Vision: A Review*, **International Journal of Computer Vision**, 6-1: 1991, pp. 59-70.

P. J. Rousseeuw and A. M. Leroy, *Robust Regression and Outlier Detection*, John Wiley & Sons, New York, 1987.

D. Tanré, C. Deroo, P. Duhaut, M. Herman, J. J. Morcrette, J. Perbos and P. Y. Deschamps, *Description of a computer code to Simulate the Satellite Signal in the Solar Spectrum: the 5S code*, **International Journal of Remote Sensing**, 11-4: 1990, pp. 659-668.

P. M. Teillet, K. Staenz and G. Fedosejevs, *A Prototype Atmospheric Correction Scheme for Airborne Imaging Spectrometer Data*, **Proc. 14th Canadian Symposium on Remote Sensing**, Calgary, Canada, 1991, pp. 394-399.

Abundance Recovery Error Analysis using Simulated AVIRIS Data

William W. Stoner, Joseph C. Harsanyi, William H. Farrand and Jennifer A. Wong

Science Applications International Corporation
803 West Broad Street
Falls Church VA,22046

1.0 Introduction

Measurement noise and imperfect atmospheric correction translate directly into errors in the determination of the surficial abundance of materials from imaging spectrometer data. The effects of errors on abundance recovery have been investigated previously using Monte Carlo simulation methods by Sabol et. al. [1]. The drawback of the Monte Carlo approach is that thousands of trials are needed to develop good statistics on the probable error in abundance recovery. This computational burden invariably limits the number of scenarios of interest that can practically be investigated.

A more efficient approach is based on covariance analysis. The covariance analysis approach expresses errors in abundance as a function of noise in the spectral measurements and provides a closed form result eliminating the need for multiple trials. In this paper, Monte Carlo simulation and covariance analysis are used to predict confidence limits for abundance recovery for a scenario which is modeled as being derived from AVIRIS.

2.0 Abundance Recovery Error Derivation

The visible and near infrared reflectance vector of a surface, $\underline{R}$, is the product of an n x m matrix M of endmember spectra and an m x 1 abundance vector $\underline{A}$

$$\underline{R} = M\underline{A}$$

For simplicity, we assume Lambertian properties for the modeled pixel surface, and we also assume that the surface is level. With these assumptions, we use the n x n diagonal matrices L and T to represent the surface irradiance and atmospheric transmission between the surface and the sensor respectively. The ground reflected radiance at the sensor is represented by the n x 1 vector $LT\underline{R} = LTM\underline{A}$.

In addition to the multiplicative effects on the reflectance vector, upwelling light from thermal radiation and atmospheric scattering is represented by an additive term given by the n x 1 vector $\underline{U}$. The total upward radiance (represented by the n x 1 vector $\underline{D}$) is now given as

$$\underline{D} = TLM\underline{A} + \underline{U} + \underline{N}$$

where $\underline{N}$ is an n x 1 zero mean additive white Gaussian noise vector with covariance $\Sigma_N = \sigma^2 I$ where I is the n x n identity matrix and σ^2 is the noise variance.

The first step in the recovery process is estimation of the atmospheric contributions, denoted by $\hat{T}\hat{L}$ and $\hat{\underline{U}}$. Errors in estimation of these quantities will tend to bias abundance recovery results as well as increase the size of the resultant error distribution.

From a theoretical standpoint, it is useful to consider the case where the atmospheric contributions are perfectly estimated, and the only error is due to random effects such as sensor noise. The equation with the atmospheric effects removed becomes

$$(TL)^{-1}(\underline{D} - \underline{U}) = M\underline{A} + (TL)^{-1}\underline{N}$$

The least squares estimate $\hat{\underline{A}}$ is given by the well known result [2]

$$\hat{\underline{A}} = (M^T M)^{-1} M^T \left((TL)^{-1}(\underline{D} - \underline{U})\right) = \underline{A} + (M^T M)^{-1} M^T (TL)^{-1} \underline{N}$$

The variance-covariance matrix of $\hat{\underline{A}}$ is given by

$$Var(\hat{\underline{A}}) = (M^T M)^{-1} M^T (TL)^{-1} \Sigma_N ((M^T M)^{-1} M^T (TL)^{-1})^T$$

The square roots of the eigenvalues of this matrix are the semi-axes of a hyperdimensional ellipsoid which describes the error distribution of the recovered abundances. The eigenvectors determine the orientation of the ellipsoid. This representation of the abundance estimation error provides a closed form solution for assessing the confidence that the true abundance vector lies within particular limits.

3.0 Simulation Results

Laboratory spectra of a red soil, creosote leaves and dry grass were used to simulate a mixed pixel. The resulting mixed pixel reflectance spectrum was convolved with gains and offsets previously calculated by a simulated empirical line method calibration [3] of the same pixel. The earlier simulation convolved the mixed pixel with the multiplicative and additive effects of a mid-latitude summer atmosphere illuminated with a solar zenith angle of $30°$ as calculated by the LOWTRAN 7 radiative transfer code. The instrumental response of AVIRIS was simulated for the input radiance vector with the output vector consisting of 224 digital numbers corresponding to AVIRIS channels. Additive noise with standard deviation of 5 DN (representing AVIRIS performance circa 1987-1988) was added to the simulated raw AVIRIS data, and the same gains and offsets were used to convert the data back to reflectance providing a perfect atmospheric correction. Finally, the abundances were solved for using singular value decomposition based least squares techniques [4].

Figure 1a shows the projection of the simulation derived error distribution onto 2D planes relating errors in pairs of abundance measurements. Figure 1b shows the theoretical 95% confidence ellipsoid projected onto 2D planes for the same scenario. In order to obtain results comparable to the theoretical error distributions, approximately 10000 trials were needed to obtain the required statistics. The run-time for 10000 trials is approximately two orders of magnitude greater than the theoretical calculation (e.g. 1000 sec vs. 10 sec on a 486 PC).

4.0 Conclusion

The example shown here demonstrates that the orientation and size of an abundance recovery error ellipsoid can be determined accurately with covariance analysis. This approach eliminates the need to generate statistics from which to calculate the error covariance matrix reducing the calculation to a small fraction of the computational burden of the Monte Carlo simulation approach. In further investigations that simulated the current, higher SNR configuration of AVIRIS, the abundance recovery error is

significantly reduced. Thus, given a higher SNR sensor system, greater confidence can be invested in spectral mixture studies.

Acknowledgments

References

[1] Sabol D.E., J.B. Adams and M.O. Smith (1990) Predicting the Spectral Detectability of Surface Materials using Spectral Mixture Analysis: *Proc. of IGARSS '90 Symposium*, 2, 967-970.

[2] Menke, W. (1989) *Geophysical Data Analysis: Discrete Inverse Theory*, Academic Press Inc., San Diego.

[3] Conel, J.E. and R.E. Alley (1985) Lisbon Valley, Utah uranium test site report. *The Joint NASA/Geosat Test Case Project*. H.N. Paley (ed.)

[4] Press, W.H., B.P. Flannery, S.A. Teukolsky and W.T. Vetterling (1986) *Numerical Recipes*, Cambridge University Press, New York.
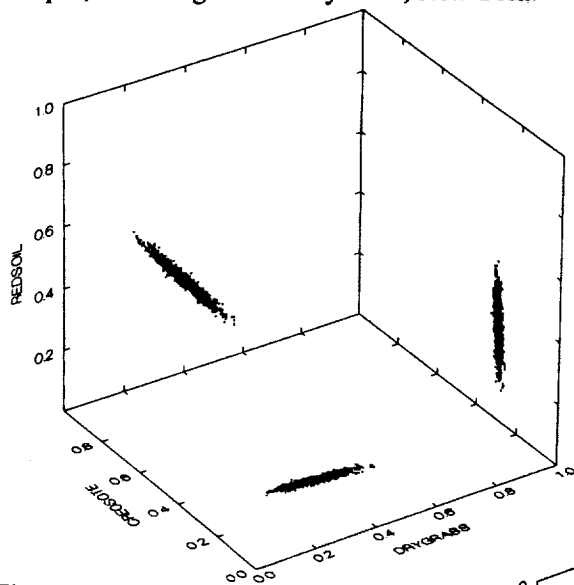
Figure 1a: Projection of 3D Scatter Plot of Abundance Estimates onto 2D planes for case with Red Soil (30%), Creosote Leaves (30%) and Dry Grass (40%).
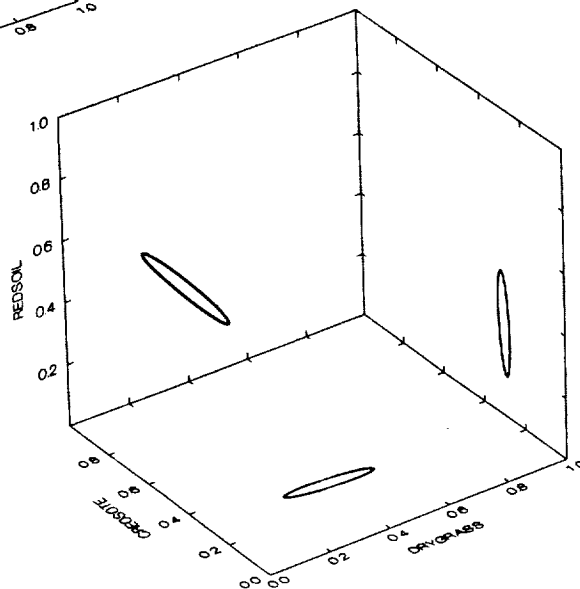

Figure 1b: Theoretical Abundance Recovery Error Ellipsoid for above case projected onto 2D planes. 95% confidence level is represented.

MULTITEMPORAL DIURNAL AVIRIS IMAGES OF A FORESTED ECOSYSTEM

BY

SUSAN L. USTIN
DEPARTMENT OF LAND, AIR, AND WATER RESOURCES
UNIVERSITY OF CALIFORNIA, DAVIS, CA 95616

AND

MILTON O. SMITH, AND JOHN B. ADAMS
DEPARTMENT OF GEOLOGICAL SCIENCES
UNIVERSITY OF WASHINGTON, SEATTLE, WA 98195

INTRODUCTION

Both physiological and ecosystem structural information may be derived from diurnal images. Structural information may be inferred from changes in canopy shadows between images and from changes in spectral composition due to changes in proportions of subpixel mixing resulting from the differences in sun/view angles. Physiological processes having diurnal scales also may be measurable if a stable basis for spectral comparison can be established. Six diurnal images of an area east of Mt. Shasta, CA were acquired on September 22, 1989. This unique diurnal data set provided an opportunity to test the consistency of endmember fractions and residuals. We expected that shade endmember abundances would show the greatest change as lighting geometry changed and less change in the normalized fractional proportion of other endmembers. Diurnal changes in spectral features related to physiological characteristics may be identifiable as changes in wavelength specific residuals.

METHODS

Multitemporal images of AVIRIS data were acquired at 9.97, 10.36, 10.96, 12.97, 13.36, and 13.96 hr local solar time. This resulted in three pairs of images (flight 17; runs 2, 3, 5, 11, 23, 14; segment 1) roughly matched in time before and after local solar noon (Δ 4.2min, Δ16.8 min, and Δ4.2min). The flight schedule was chosen to maximize the diurnal separation between the first and last flightlines (3.99hr) but to minimize the changes in canopy shading due to the diurnal trajectory of the solar zenith angle. The study area included discontinuous ponderosa pine forests, recent clear cuts, Great Basin sagebrush communities, meadows, and narrow riparian zones along drainages. The terrain is relatively flat over most of the area. Sky conditions measured with a Regan Radiometer were clear with optical depth at the theoretical maximum (389km), with low aersols (876.7mbar, 255.8matm O_3). Overflights were acquired at the end of the dry Mediterranean summer about one week after a

relatively heavy precipitation event. Leaf area index was determined from three sites within the flightline from fisheye photographs. Tree height, DBH, and stand density was measured in several stands and biomass estimated from allometric relationships.

Spectral mixture analysis was performed on each of the six AVIRIS images. The iterative mixture analysis resulted in the selection of the same set of library endmembers for each image and converged upon similar gains and offsets for each calibration.

RESULTS

We found that most of the region could be modeled by four endmembers, a green vegetation type characteristic of ponderosa pine foliage in the library, shade, and two nonphotosynthetic endmembers: one having the characteristics of "stems," i.e., resembling bark or having a redish-brown cast, and the other having spectral characteristics consistent with weathered litter. In all cases, dry plant material rather than soils or mineral samples was selected from the spectral library as the best fit to the image endmembers. This is the first example that we are aware of in which more than one nonphotosynthetic canopy component has been identified in AVIRIS images. The nonphotosynthetic fractions are generally negatively correlated, although different community types (dry meadows to mature forests) characteristically fall within restricted regions of the data volume. The two nonphotosynthetic fractions exhibit independent relationships with the green vegetation fraction. Thus, the fraction patterns of these endmembers are independent and appear to be community specific. This suggests that endmember fractions can provide a good method for differentiating communties.

As expected, the shade endmember showed the largest magnitude of diurnal change, although patterns were not symmetric about solar noon and appeared to relate more consistently to community types and structure differences. Normalized green and nonpyhotosynthetic vegetation fractions (rescaled without the shade fraction) exhibited a smaller range of diurnal variation. Figure 1 shows the diurnal pattern in the green vegetation endmember abundances we observed for ten community types. The magnitudes of diurnal patterns were community specific and consistent for given types. They did not exhibit diurnal symmetry expected from sun angle changes. Least evidence of diurnal changes was found in dry meadows and greatest in mature forests. Forests exhibited a trend for decreasing green vegetation fraction during the four hour period. The magnitude of the fraction change appears to be greater than can be explained by calibration errors, although the basis is not understood. These patterns may possibly result from different canopy components being illuminated as sun angles change.
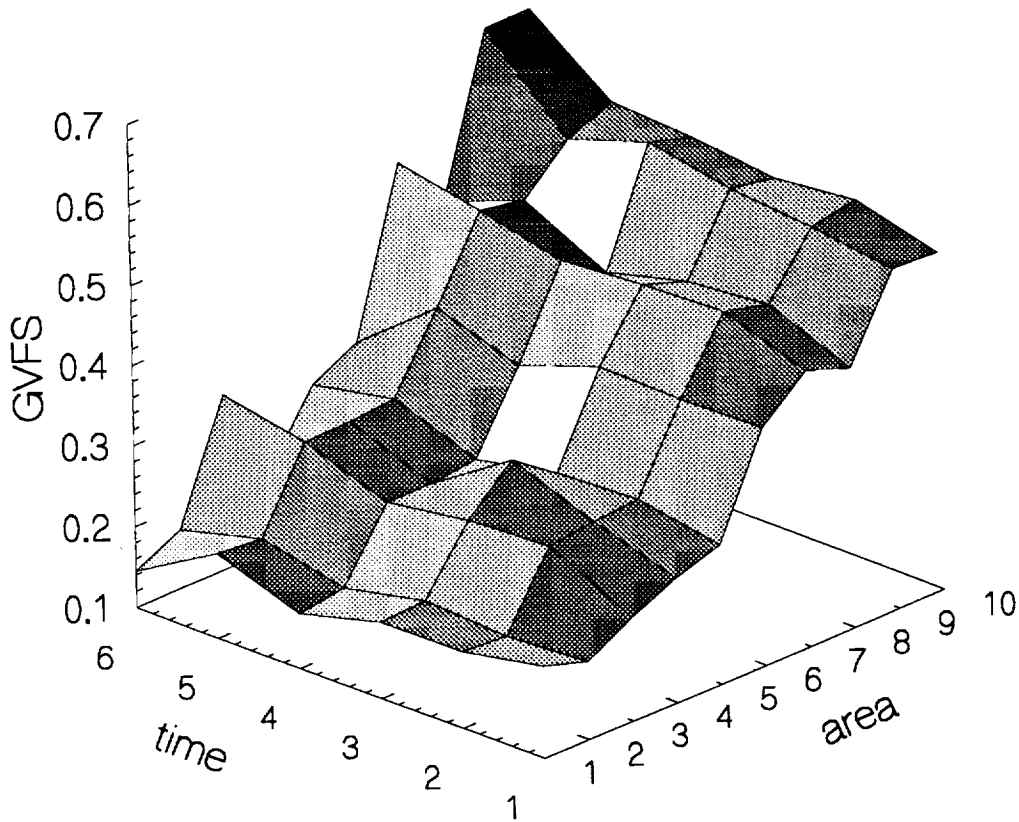
Figure 1. Changes in GVFS in six AVIRIS images of ten areas near Shasta, California. The numbered times correspond to 1) 9.97, 2) 10.36, 3) 10.96, 4) 12.97, 5)13.36, and 6) 13.96 local solar time. The numbered areas correspond to 1) 1st recent clear cut 2) 2nd recent clear cut, 3) 1st older clear cut, 4) 2nd older clear cut, 5) 1st mature second growth ponderosa pine forest, 6) 2nd mature ponderosa pine forest, 7) ponderosa pine plantation, 8) 1st young ponderosa pine forest, 9) 2nd young ponderosa pine forest, and 10) meadow.

A COMPARISON OF LOWTRAN-7 CORRECTED AIRBORNE VISIBLE/INFRARED IMAGING SPECTROMETER (AVIRIS) DATA WITH GROUND SPECTRAL MEASUREMENTS

Pengyang Xu and Ronald Greeley

Department of Geology
Arizona State University
Tempe, Arizona 85287-1404

1. Introduction

Atmospheric correction of imaging spectroscopy data is required for quantitative analysis. Different models have been proposed for atmospheric correction of these data, refer to (*Bosch et al.1990 and Conel et al. 1987*) for discussion of LOWTRAN atmospheric correction model and other models. LOWTRAN-7 is a low-resolution model and computer code for predicting atmospheric transmittance and background radiance from 0 to 50,00 cm^{-1} which was developed by the Air Force Geophysics Laboratory. The AVIRIS data (*Portor et al. 1987*) used here are radiometrically calibrated and include the 09/28/1989 Providence Fan flight line segment 07, California. It includes a dark gravel surface defined as a calibration site by the Geologic Remote Sensing Field Experiment (GRSFE) (*Arvidson et al. 1989*). Several ground measurements of portable spectrometer DAEDALUS AA440 Spectrafax were taken during the GRSFE July, 1989 field campaign. Comparisons of the LOWTRAN-7 corrected AVIRIS data with the ground spectrometer measurement were made in this study.

2. LOWTRAN-7 atmospheric correction of AVIRIS data

Eight pixels of the dark target were chosen from the AVIRIS image. "Noisy" data from AVIRIS bands (1-5, 32-33, 108-117, 153-174, 216-224) were removed. The median value of eight pixel DNs of each band was calculated to represent the data at that band. Medians were used because the median is a more robust estimator of central value than means. The input parameters for the LOWTRAN-7 were mid-latitude summer profile, radiance mode, multiple scattering, surface albedo 0.1, desert aerosols, ground altitude 0.863 km which was read from a topographic map, and local climatological data at the time of the AVIRIS flight (Table 1).

Table 1. Local Weather Data
(Data from Metromonitoring Services F.C.W.O.S. Daggett, CA)

Air Temp. (°C)	Relative Humidity (%)	Wind Speed (m/sec)	Visibility (km)
34.4	16	9.26	56.3

The equation used to calculate the reflectance is

$$\rho = \frac{0.1}{L_g}(L_o - L_{ps})$$

where L_o = observed radiance, i.e. AVIRIS radiance data

Lps = observed radiance due to path scattering
Lg =observed radiance due to ground-reflected radiation
ρ = ground reflectance

assuming horizontally homogeneous atmosphere and flat surface (*Bosch et al.1990*).

3. Calibrating DAEDALUS data

The DAEDALUS instrument measures radiances in 280 channels between 0.45 and 2.4 micrometers. The spectral resolution of the channels varies from 0.01 micrometers in the visible to ~ 0.04 micrometers in the infrared. The raw DAEDALUS data of the dark target is from the GRSFE CD-ROM. Reflectance values are derived by ratioing the measurement of a sample to that of a pressed and bonded halon standard viewed at the same angle. The median values of several measurements were used to estimate the reflectances of the dark surface. The "noisy" data were removed before interpolating the data to AVIRIS wavelength center using the cubic spline technique.

4. Results and conclusion

The LOWTRAN-7 corrected AVIRIS spectral data and calibrated DAEDALUS spectral data were plotted against wavelength (Fig.1). In general, the differences between two spectra are larger after 1.3 μm wavelength than before that. The histogram of the differences between DAEDALUS data and LOWTRAN-7 corrected data (AVIRIS_LT) is shown in Fig.2. From the histogram, most bands of the two data sets agree within 6.0% reflectance. At some bands the data deviated more than 6.0% reflectance. In most bands, DAEDALUS reflectances are higher than LOWTRAN-7 corrected AVIRIS reflectances. Table 2 shows the statistics of the differences between two spectra. The differences between the data sets may be due partly to different seasons of data acquisition.

Table 2.Statistics of the Differences

Minimum	-6.1971402
Maximum	9.0017633
Points	152
Mean	2.3132297
Median	2.2561876
Std Deviation	2.54485100

5. Acknowledgement

The authors would like to thank Dr. Tom Farr for identifying the pixels of the dark target on the AVIRIS image. *Metromonitoring Services* is acknowledged for providing the weather data.

6. References

R.E. Arvidson and D.L. Evans, Geologic Remote Sensing Field Experiment, *Geol. Soc. Amer, Abstracts with Programs*, 21, 1989, A121.

J.M. van den Bosch and R.E. Alley, Application of lowtran 7 as an atmospheric correction to airborne visible/infrared imaging spectrometer (AVIRIS) data, *Proceedings, IGARSS '90*, 1990, 175-177.

J.E. Conel, R.O. Green, G. Vane, C.J. Bruegge, R.E. Alley and B.J. Curtis, Radiometric spectral characteristics and comparison of ways to compensate for the atmosphere, *Imaging Spectroscopy II,Proceedings of SPIE*, 834, 1987, 140-157.

W.M. Portor and H.T. Enmark, A system overview of the Airborne Visible/Infrared Imaging Spectrometer (AVIRIS), *Imaging Spectroscopy II, Proceedings of SPIE*, 834, 1987, 22-31.
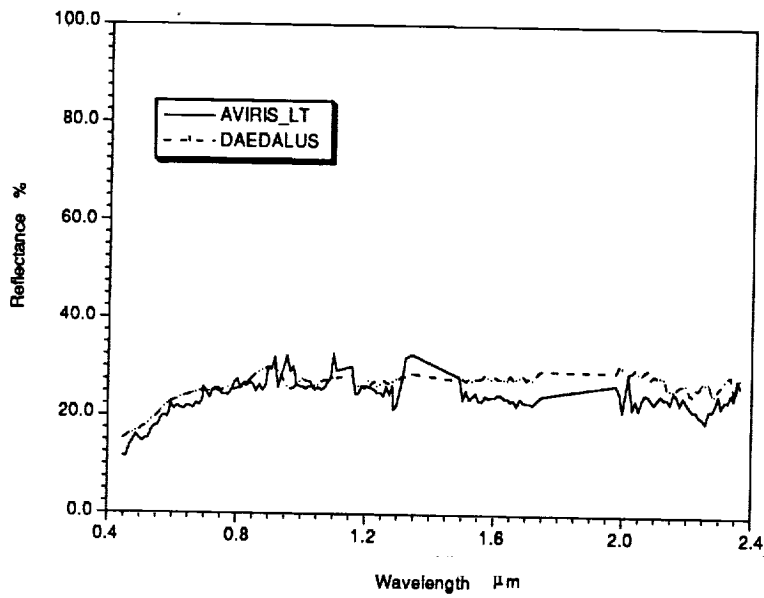
Fig.1. Lowtran-7 corrected AVIRIS data (solid line) vs. ground Daedalus measurement (dashed line) at the GRSFE dark target (Pumping Station near Kelso, CA)
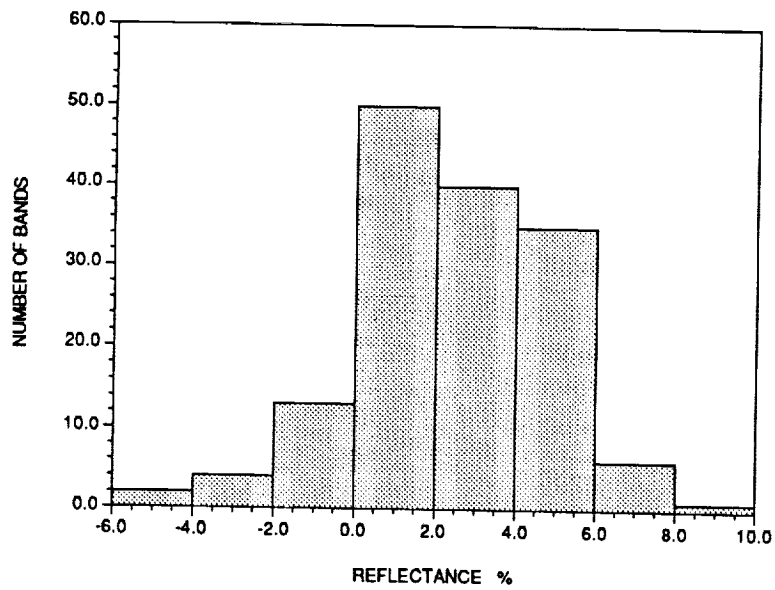
FIG. 2. The histogram of differences between DAEDALUS and AVIRIS_LT data

DISCRIMINATION AMONG SEMI-ARID LANDSCAPE ENDMEMBERS USING THE SPECTRAL ANGLE MAPPER (SAM) ALGORITHM

Roberta H. Yuhas [1], Alexander F.H. Goetz [1], and Joe W. Boardman [2]

[1] Center for the Study of Earth from Space (CSES)
Cooperative Institute for Research in Environmental Sciences (CIRES) and
Department of Geological Sciences
University of Colorado, Boulder, Colorado 80309-0449

[2] CSIRO, North Ryde, NSW 2113, Australia

1. INTRODUCTION

Airborne Visible/Infrared Imaging Spectrometer (AVIRIS) data were acquired during three consecutive seasons of the year (26 September 1989, 22 March 1990, and 7 August 1990) over an area of the High Plains east of Greeley, Colorado. This region contains extensive eolian deposits in the form of stabilized dune complexes (small scale parabolic dunes superimposed on large scale longitudinal and parabolic dunes). Due to the dunes' large scale (2-10 km) and low relief (1-5 m), the scaling relationships that contribute to the evolution of this landscape are nearly impossible to understand without the use of remote sensing. Additionally, climate models indicate that the High Plains could be one of the first areas to experience changes in climate caused by either global warming or cooling (Hansen *et al.*, 1988). During the past 10,000 years there were at least three periods of extensive sand activity, followed by periods of landscape stability, as shown in the stratigraphic record of this area (Forman, *et al.*, 1992). Therefore, if the past is an indication to the future, the monitoring of this landscape and its sensitive ecosystem is important for early detection of regional and global climate change.

2. STUDY AREA CHARACTERISTICS

The dune complexes found along the South Platte River are currently stabilized by a thin cover of shortgrass prairie vegetation species. These include blue grama, sand bluestem, and sandreed bunchgrasses, along with other graminoids and perennial forbs (yucca, sage, cacti). Because there is very little, if any, topsoil over the sands, the land is used primarily for grazing. There are sites along the terraces and floodplain of the South Platte River where the soils are thicker and where either dryland or irrigated farming is conducted. Therefore, a wide range of percent vegetation cover occurs in each image (from 0% in overgrazed or blowout areas to 100% in irrigated fields). In order to fully describe each scene, image endmembers in three categories (vegetation, soil, and water) were chosen. Up to ten total image endmembers were used (see figure 1).

3. SPECTRAL ANGLE MAPPER ALGORITHM

AVIRIS radiance values were converted to reflectance using the scaled surface reflectance method of Gao (Gao, *et al.*, 1991, 1992). This method derives atmospheric water vapor radiance values for each pixel of a scene using the water vapor features found at 0.94 and 1.14 μm. The atmospheric water vapor values are then subtracted from the radiance value of each pixel, resulting in an atmospherically corrected image across the entire 0.4-2.5 μm region.

Atmospherically corrected images were then imported into the Spectral Image Processing System (SIPS) developed at CSES (Kruse, *et al.*, 1992). This package allows one to extract spectra from individual or groups of pixels and compute statistics for regions of similar composition (i.e., the image endmembers). The mean spectra of up to ten endmembers can then be processed using the Spectral Angle Mapper (SAM) algorithm.

This technique, developed by J.W. Boardman, determines the spectral similarity between given reference spectra, *r*, (i.e., the image endmember in this case) and the spectra found at each pixel, *t* (Kruse, *et al.*, 1992). The result of the comparison is reported as the angular difference (in radians) between the two spectra according to the equation:

$$\cos^{-1}\left(\frac{\vec{t} \cdot \vec{r}}{\| \vec{t} \| \cdot \| \vec{r} \|} \right)$$

which can also be written as,

$$\cos^{-1}\left(\frac{\sum_{i=1}^{nb} t_i \, r_i}{\sqrt{\sum_{i=1}^{nb} t_i^2} \sqrt{\sum_{i=1}^{nb} r_i^2}} \right)$$

Here *nb* is the number of bands in the image. Each pair of spectra is treated as a vector in *nb*-space, allowing the similarity of the spectra to be determined without regard to their relative brightness values. The result of the SAM calculation is an image for each reference spectrum, with high values (displayed in brighter values) corresponding to a better match between reference and test spectra.

4. RESULTS

When the ten image endmembers shown in figure 1 were processed via the SAM algorithm, excellent discrimination between the different endmembers was found. Figures 2 and 3 show the SAM results for image endmembers located on the sparsely vegetated dune limbs and the more densely vegetated dune depressions, respectively. We believe these results show the sensitivity of the method since the difference in percent vegetation cover between the two areas indicated above is no greater than 20%. Traditional Normalized Difference Vegetation Index (NDVI) methods show no such discrimination, and only minor discrimination occurs using linear unmixing techniques. Because vegetation cover density is critical to the stability of the landscape, and any climate change would cause this to also change, the SAM algorithm may provide the sensitivity needed to discriminate between minor changes of vegetation cover that could lead to major changes in the landscape, and thus, allow early detection of global climate change.

5. ACKNOWLEDGEMENTS

6. REFERENCES

Forman, S.L., A.F.H. Goetz, and R.H. Yuhas, 1991. Large-scale stabilized dunes on the High Plains of Colorado: Understanding the landscape response to Holocene climates with the aid of images from space: *Geology* **20**, pp. 145-148.

Gao, B.-C., A.F.H. Goetz, and J.A. Zamudio, 1991. Retrievals of surface reflectances from AVIRIS data: in Proceedings, IGARSS '91, University of Maryland, College Park, MD, The Institute of Electrical and Electronics Engineers, Inc., New York, **2**, pp. 669-672.

Gao, B.-C., K.H. Heidebrecht, and A.F.H. Goetz. Derivation of scaled surface reflectances from AVIRIS data: *Remote Sensing of Environment* (submitted), February 1992.

Hansen, J., I. Fung, A. Lacis, D.S. Rind, R. Ruedy, and G. Russell, 1989. Global climate changes as forecast by Goddard Institute for Space Studies three-dimensional model: *Journal of Geophysical Research* **93**, pp. 9341-9364.

Kruse, F.A., A.B. Lefkoff, J.B. Boardman, K.B. Heidebrecht, A.T. Shapiro, P.J. Barloon, and A.F.H. Goetz, 1992. The Spectral Image Processing System (SIPS)--Interactive visualization and analysis of imaging spectrometer data: *Remote Sensing of Environment* (in press, for release July 1992).
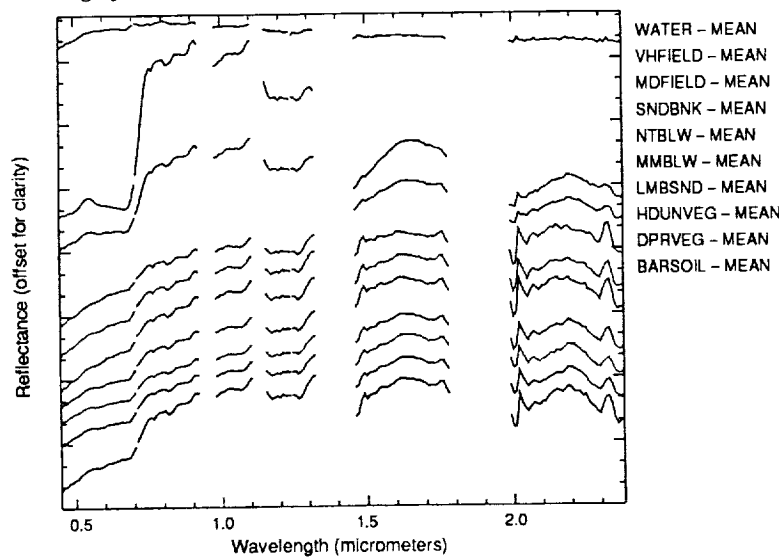
Figure 1. Spectra of the ten image endmembers used as input to SAM.
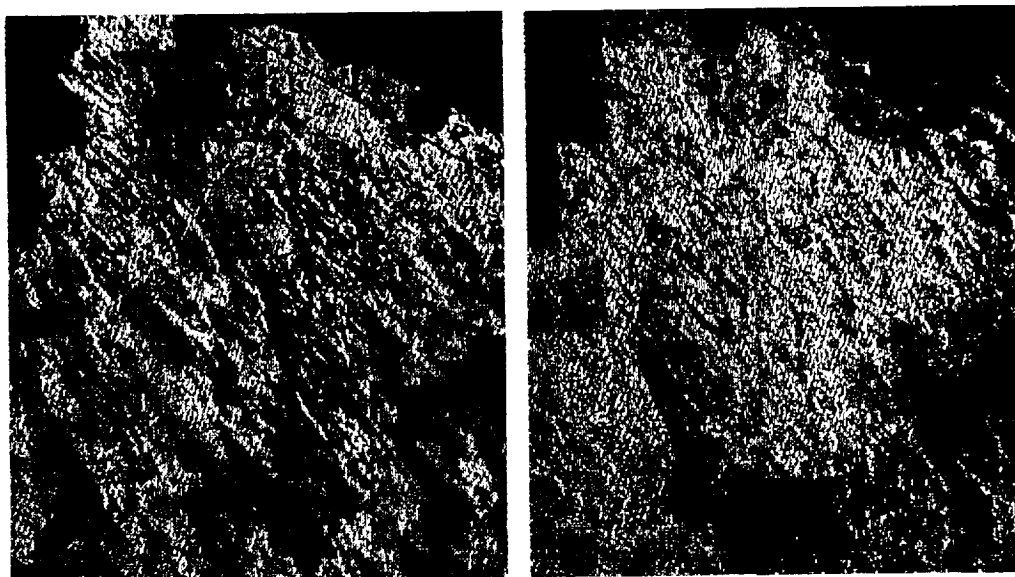
Fig. 2 and 3. SAM images for dune limb (left) and dune depression endmembers (right).

149

546-43
189092

EMPIRICAL RELATIONSHIPS AMONG ATMOSPHERIC VARIABLES FROM RAWINSONDE AND FIELD DATA AS SURROGATES FOR AVIRIS MEASUREMENTS: ESTIMATION OF REGIONAL LAND SURFACE EVAPOTRANSPIRATION

James E. Conel, Gordon Hoover, Anne Nolin,
Ron Alley and Jack Margolis

Jet Propulsion Laboratory
California Institute of Technology
Pasadena, California

Empirical relationships between variables are ways of securing estimates of quantities difficult to measure by remote sensing methods. We explore the use of empirical functions between: (1) atmospheric column moisture abundance W (gm H_2O/cm^2) and surface absolute water vapor density $\rho\bar{q}$ (gm H_2O/cm^3), with ρ density of moist air (gm/cm^3), $\bar{q}$ specific humidity (gm H_2O/gm moist air) and (2) column abundance and surface moisture flux E (gm $H_2O/(cm^2 sec)$) to infer regional evapotranspiration from AVIRIS water vapor mapping data. AVIRIS provides, via analysis of atmospheric water absorption features, estimates of column moisture abundance at very high mapping rate ($\approx$ 100 km^2/40 sec) over large areas at 20 m ground resolution.

To generate surrogates in place of direct AVIRIS observations that represent climatological regimes more diverse than have been available with existing AVIRIS data sets, we examined large collections of rawinsonde soundings - nearly 8500 flights, 1985-1991 - from San Nicholas Island (marine), Pt. Mugu (marine/coastal) and Edwards Air Force Base (arid interior), California, and more than 400 radiosonde soundings taken as part of FIFE (Konza tall grass prairie) in eastern Kansas (Brutsaert and Sugita, 1990). From each of these data sets, empirical relationships were derived between total column water abundance and surface absolute humidity, with correlation coefficients between these variables of ~ 0.90 and standard errors of 20%. In addition, for the very important Kansas data sets, Brutsaert and Sugita (1990) and Sugita and Brutsaert (1990) assembled more than 120 observations of surface latent heat flux (moisture flux) derived from the FIFE network of eddy correlation and Bowen ratio measurement stations that are correlative in time with their radiosonde flights. We calculated the total column moisture from the FIFE radiosonde data and sought further empirical relationships between these column abundances and the observed latent heat (LE) and sensible (H) heat fluxes, as well as friction velocity u∗, and the Obukhov length L, both of which had been calculated from the corresponding radiosonde profiles and surface fluxes by Sugita and Brutsaert (1990) and Brutsaert and Sugita (1990). We expected a good correlation between what we term the net column abundance (difference between the column abundance derived from the surface specific humidity integrated over the column and the observed column abundance) and the surface flux, to emerge if net moisture in the column was derived from local fetchs. This view was reinforced by good to excellent correlations found by Brutsaert and Sugita (1990) and Sugita and Brutsaert (1990) between surface fluxes derived from individual profiles and the observed surface fluxes. In practice, we got poor correlations between W and LE suggesting that the bulk of atmospheric water present over Konza Prairie during these observations represented advected moisture, and

was therefore not of "local" origin. The anticipated simple strategy of using column moisture abundances to estimate surface flux was not applicable to this data set.

Some approximate atmospheric diffusion calculations of column abundance vs fetch, based on atmospheric moisture distributions above surfaces with concentration and with flux boundary conditions and power law vertical dependences of horizontal wind speed and vertical eddy diffusivity, will also be illustrated.

References:

Brutsaert, W., and M. Sugita, 1990, The extent of the unstable Monin-Obukhov layer for temperature and humidity above complex hilly terrain, *Boundary-Layer Meteorology*, **51**, 383-400.

Sugita, M., and W. Brutsaert, 1990, Regional surface fluxes from remotely sensed skin temperature and lower boundary layer measurements, *Water Resour. Res.*, **26(12)**, 2937-2944.

The JPL Spectral Library 0.4 to 2.5 Micrometers

Simon J. Hook, Cindy I. Grove and Earnest D. Paylor II

Jet Propulsion Laboratory / California Institute of Technology
4800 Oak Grove Drive, Pasadena, California
91109

During the 1980's the Geology Group at the Jet Propulsion Laboratory (JPL) gradually acquired a large collection of mineral specimens. The hemispherical reflectance of these specimens in the 0.4 to 2.5 micrometer wavelength region was measured with a Beckman UV5240 Spectrophotometer. In addition, the purity of each specimen was evaluated by X-ray diffraction (XRD) and the chemical composition of certain samples known to deviate strongly from idealized end-member compositions was determined by electron microprobe analysis. The results from 160 of the purest minerals, as determined by XRD, were presented in Grove et al. 1992.

The spectral data for 135 of the minerals in Grove *et al.* 1992 were presented at three different grain sizes to demonstrate the effect of particle size. These were 125-500μm, 45-125μm and <45μm. Ancillary information, which included the mineral name, mineralogy, supplier and sampling locality, was provided with each mineral spectrum. The compositional information obtained by microprobe analysis and accessory minerals identified by XRD were noted with the ancillary information.

In addition, the spectrum acquired from the coarsest grain size available for each sample was processed with a feature-finding algorithm to quantify the characteristics of the spectral absorption features.

All the reflectance spectra presented in Grove *et al.* 1992 were provided in digital form on IBM-compatible 3.5" diskettes included with the publication together with a program for displaying the spectral data and searching for spectral features. The program runs on an IBM-compatible PC with standard VGA graphics.

This presentation summarizes the results presented in Grove *et al.* 1992 and discusses, in detail, the software for displaying and analyzing the spectral data.

Copies of Grove *et al.* 1992 are available free of charge from:

JPL PLDS User Support Office
Geology and Planetology Section
Mail Stop 183-501
JET PROPULSION LABORATORY
4800 Oak Grove Drive
Pasadena, California, 91109

Phone: (818) 354-6363
Facsimile: (818) 354-0966

References

C. I. Grove, S. J. Hook, and E. D. Paylor II. Laboratory Reflectance Spectra of 160 Minerals, 0.4 to 2.5 Micrometers. JPL Publication 92-2, 1992, 405 p.

LOSSLESS COMPRESSION OF AVIRIS DATA: COMPARISON OF METHODS AND INSTRUMENT CONSTRAINTS

R.E. Roger, J.F. Arnold, M.C. Cavenor, and J.A. Richards.

Department of Electrical Engineering, University College,
Australian Defence Force Academy, CANBERRA ACT 2600, Australia.

1. INTRODUCTION

A family of lossless compression methods, allowing exact image reconstruction, are evaluated for compressing AVIRIS image data. The methods are based on Differential Pulse Code Modulation (DPCM). The compressed data have an entropy of order 6 bits/pixel. A theoretical model indicates that significantly better lossless compression is unlikely to be achieved because of limits caused by the noise in the AVIRIS channels.

AVIRIS data differ from data produced by other visible/near-infrared sensors, such as Landsat-TM or SPOT, in several ways. Firstly, the data are recorded at a greater resolution (12 bits, though packed into 16-bit words). Secondly, the spectral channels are relatively narrow and provide continuous coverage of the spectrum, so that the data in adjacent channels are generally highly correlated. Thirdly, the noise characteristics of the AVIRIS are defined by the channels' Noise Equivalent Radiances (NERs), and these NERs show that, at some wavelengths, the least significant 5 or 6 bits of data are essentially noise.

2. COMPRESSION SCHEME

The overall scheme adopted for lossless compression comprises three main elements:

(1)   prediction of the current pixel's value from prior pixels' values;
(2)   differencing to form a residual;
(3)   encoding the residual using a variable or fixed rate code.

The residuals are represented using NBIT bits. Any residual outside the range $-(2^{NBIT-1}-1)$ to $+(2^{NBIT-1}-1)$ is an exceedance. For variable rate coding, the residuals falling within this range are Huffman-encoded. The resulting codebook is optimal for each data set. An exceedance is indicated by the value -2^{NBIT-1}, and its value is transmitted in full (16 bits).

For the methods using optimised predictors, there is an overhead caused by the need to transmit prediction coefficients, and this is set at 32 bits per coefficient. This overhead is significant.

3. PREDICTION SCHEMES

14 prediction schemes have been evaluated. Let $x_{i,j,\lambda}$ represents the value of the pixel in row (line) i, column j, channel (band) λ, and $\hat{x}_{i,j,\lambda}$ be its predicted value. Residuals are formed according to the expression:

$$\text{residual} = x_{i,j,\lambda} - \text{nearest integer to}(\hat{x}_{i,j,\lambda}).$$

For schemes using optimised coefficients, the coefficients (variously a, b, c, or d) are

calculated by the least-squares minimisation of $\Sigma(\hat{x}_{i,j,\lambda} - x_{i,j,\lambda})^2$, where the summation is taken along a line (j varies, i and λ fixed).

Spatial Methods. Fixed Coefficients

Row: $\hat{x}_{i,j,\lambda} = x_{i,j-1,\lambda}.$

Column: $\hat{x}_{i,j,\lambda} = x_{i-1,j,\lambda}.$

Two-point Row-Column: $\hat{x}_{i,j,\lambda} = (x_{i-1,j,\lambda} + x_{i,j-1,\lambda})/2.$

Three-point Row-Column: $\hat{x}_{i,j,\lambda} = (3x_{i-1,j,\lambda} + 3x_{i,j-1,\lambda} - 2x_{i-1,j-1,\lambda})/4.$

Spatial Methods. Optimised Coefficients

Optimised Row: $\hat{x}_{i,j,\lambda} = a + bx_{i,j-1,\lambda}.$

Optimised Column: $\hat{x}_{i,j,\lambda} = a + bx_{i-1,j,\lambda}.$

Optimised Two-point Row: $\hat{x}_{i,j,\lambda} = a + bx_{i,j-1,\lambda} + cx_{i,j-2,\lambda}.$

Optimised Two-point Row/Column Row:

$\hat{x}_{i,j,\lambda} = a + bx_{i,j-1,\lambda} + cx_{i-1,j,\lambda}.$

Spectral Method. Fixed Coefficients

Channel: $\hat{x}_{i,j,\lambda} = x_{i,j,\lambda-1}.$

Spectral Methods. Optimised Coefficients

Mean-corrected: $\hat{x}_{i,j,\lambda} = a + x_{i,j,\lambda-1}.$

One-point channel: $\hat{x}_{i,j,\lambda} = a + bx_{i,j,\lambda-1}.$

Two-point channel: $\hat{x}_{i,j,\lambda} = a + bx_{i,j,\lambda-1} + cx_{i,j,\lambda-2}.$

Three-point channel: $\hat{x}_{i,j,\lambda} = a + bx_{i,j,\lambda-1} + cx_{i,j,\lambda-2} + dx_{i,j,\lambda-3}.$

Spectral-Spatial Method. Optimised Coefficients

Channel-Row: $\hat{x}_{i,j,\lambda} = a + bx_{i,j,\lambda-1} + cx_{i,j-1,\lambda}.$

4. TEST DATA SETS

The schemes have been evaluated using 3 data sets: the complete radiometrically rectified data set for a Jasper Ridge image (Run 05, 07/23/90), and the first six and the last six lines of a Moffett Field image (Run 013, 07/23/90). All 224 channels were used. Some values of the 16-bit pixels fall outside the nominal 12-bit range. Negative values are thought to be caused by radiometric rectification, and values above 4095, by noise. The entropies of the three data sets are 9.82, 9.20 and 9.85 bits/pixel, respectively. Straight application of a UNIX-like *compress* algorithm to the two Moffett Field data sets yields compressed files of 10.73 and 11.53 bits/pixel, respectively.

5. RESULTS

Number of bits per residual: The variation of the compressed image entropy as NBIT (see §2) varies from 13 down to 3 bits has been studied, for both variable and fixed rate coding. As NBIT decreases, the number of exceedances increases, and the compression worsens for variable rate coding. Results below are for 8-bit residuals, which entail losses mostly in the range 0.1-0.25 bit/pixel compared with 13-bit residuals. The pattern of loss is similar for all the methods. Optimal values of NBIT are found for fixed rate coding.

Spatial Methods: Of the 8 methods using spatial prediction, the one named "Two-point Row-Column" provided the best performance (6.88, 6.46, 7.10

155

bits/pixel respectively). To indicate the spread of performance, the worst method for each data set produced 7.42, 6.84 and 7.57 bits/pixel, respectively. The optimised methods produced residuals with lower standard deviations but any reduction in the residuals' entropy was negated by the coefficient overhead.

Spectral Methods: Of the 6 methods using spectral prediction, that called "Two-point Channel" was best (5.90, 5.81, 5.89 bits/pixel). Residuals coded with NBIT=13 improve the compression by no more than 0.10 bit/pixel. The "One-point Channel" method was only marginally worse, by 0.11 bit/pixel for the worst of the three data sets. The compression given by the "Channel-Row" method, which uses both spectral and spatial data, was intermediate between these two methods. Fixed-coefficient Channel DPCM was the worst of all the 15 methods. The "Mean-corrected" method was the second worst method for one Moffett Field data set, but it performed better than all the spatial methods for the other two data sets.

Fixed- vs. Variable-Rate Coding: A similar pattern of results holds for fixed-rate coding. For the best spatial method, "Two-point Row-Column", allocating 8 bits to the residuals provides the best compression overall (8.33, 8.24, 8.45 bits/pixel for the respective data sets). For the spectral methods, 6 bits is the optimum, giving compressed data of, respectively, 7.38, 7.39, 7.47 bits/pixel. Fixed-rate coding is worse than variable-rate coding by about 1.5 bits/pixel.

Dependence of Results on Data: The results for the best spatial method show a spread in compression of 0.64 bit/pixel depending on the data set for variable-rate coding, and of 0.21 bit/pixel for fixed-rate coding. For the best spectral method, the comparative figures are 0.09 and 0.09 bit/pixel. The results for the spectral method are more consistent, varying less across different data sets.

Noise Sensitivity: The variations in the data in Channels 1-4 and Channel 223-224 are dominated by the channel noise (the standard deviation of the data in each of these channels is very close to that channel's NER). If these channels are excluded from the compression evaluation, then the compressions are improved by about 0.2 bit/pixel. There are no exceedances for NBIT=12 and NBIT=13 when these channels are disregarded.

6.   ENTROPY LIMITS DUE TO INSTRUMENT NOISE

The noise in each channel causes a spread in values, and so contributes to the entropy of the data. The noise entropy of a single channel can be calculated by using its NER and assuming a probability distribution. The entropy caused by the noise alone has been modelled numerically, by constructing a univariate probability distribution for all 224 channels. Using the NERs given in the Jasper Ridge and Moffett Field ancillary data sets, this noise entropy is found to be 5.28 bits/pixel for a Gaussian distribution of noise in each channel, and 5.03 bits/pixel for a Laplacian distribution. For the three data sets, the entropies of the residuals produced by the "Three-point channel" spectral method are the lowest. For a value of NBIT=8, the entropies are 5.45, 5.36 and 5.45 bits/pixel respectively.

The similarity of the results for the three data sets, and the closeness of these results to the theoretical values supports the suggestion that lossless compression using spectral information is almost limited by the AVIRIS's channel noise. If the probability distribution of the residuals is similar to that of noise, then a Huffman codebook for variable rate coding might be designed on the basis of instrument parameters, and not have to be derived during the compression process.

SIMULATION OF AVHRR-K BAND RATIOS WITH AVIRIS

Melanie A. Wetzel
Atmospheric Sciences Center, Desert Research Inst.
P.O. Box 60220 Reno, Nevada 89506
Ronald M. Welch
Institute of Atmospheric Science
South Dakota School of Mines and Technology
Rapid City, South Dakota 57701

1.0 INTRODUCTION

The AVHRR-K polar-orbiting imager scheduled for launch by the mid-1990's will include two new near-infrared narrowband detectors, Band 3A, 1.58-1.64 μm, and a modified (narrower) Band 2, 0.84-0.87 μm. The AVIRIS is an ideal testbed for these bands. This paper summarizes the results of a comparison between AVIRIS band ratio values and AVHRR-K radiances simulated from AVIRIS.

Prior analysis of AVIRIS multispectral data has shown that channel ratios can aid in the estimation of scene type and other physical parameters (Gao and Goetz,1990; Berendes et al., 1991). Figure 1 demonstrates the discrimination of surface and cloud types with the ratio of two window-channel radiances corresponding to AVHRR-K. Shown here is the ratio of pixel radiance in a sequence of AVIRIS channels, to the radiance at 0.85 μm (the center of the AVHRR-K Band 2). The largest values are observed for a growing cumulus cloud (A) which undoubtedly contains a large concentration of liquid water. An altostratus cloud area (D) which visually appears glaciated has the lowest ratio value. This is consistent with ice cloud due to the larger absorption coefficient for ice (four times larger than for water at 1.6 μm). The ratio values for two altocumulus scenes (B,C; more likely to contain a mixture of ice and water) fall between A and D. Snow-covered surfaces have the lowest values in Fig. 1, particularly a sun-illuminated sample (H). The ratios are largest in magnitude and show the best separation near the 1.62 μm center of AVHRR-K Band 3A. Thus, the ratio of AVHRR-K Band3A/Band 2 band center wavelengths appears to contain information on cloud properties. However, the AVHRR-K has both a wider bandpass and larger field of view than AVIRIS.

157
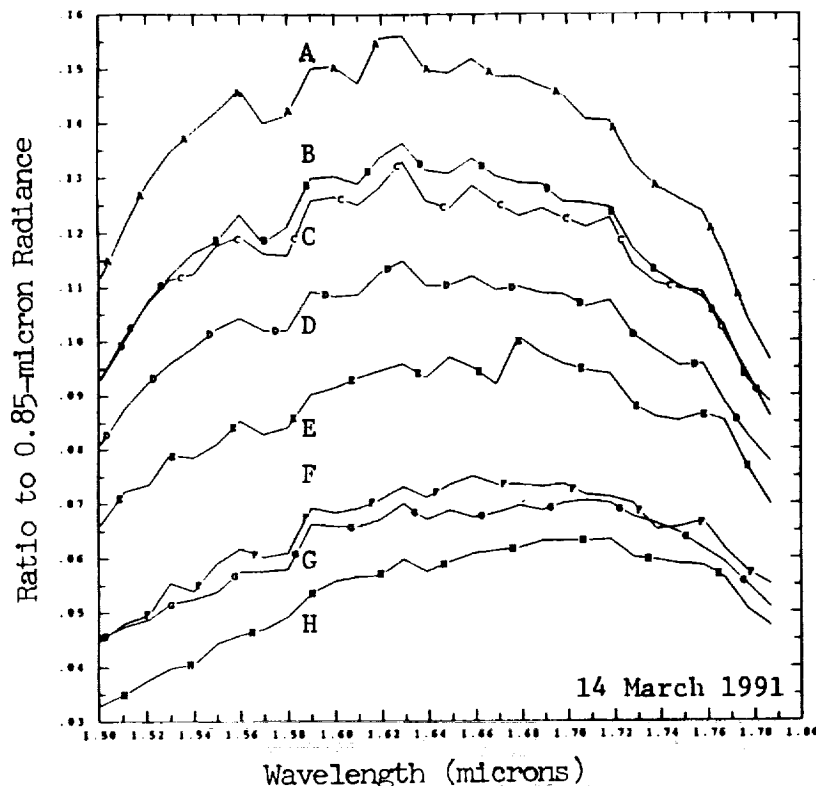
Fig.1. Ratio of AVIRIS radiance at the wavelength
indicated on the abscissa, to that at 0.85 μm, for
isolated growing cumulus (A), altocumulus (B,C),
glaciated altostratus (D), exposed land (E), snow
under shadow (F,G), and sunlit snow (H).

2.0 SIMULATION OF AVHRR-K RADIANCES

The AVHRR-K spectral bandpasses were
simulated with four consecutive AVIRIS channels
for Band 2, and eight consecutive channels for
Band 3A. The channel radiances were numerically
integrated, and a spectral transmittance function
was applied which is similar to the existing AVHRR
shortwave channels. The ratios of these band
radiances are seen as the values in Figure 2, for
a one-pixel field of view. The differences between
these single-pixel values and the 1.62 μm/0.85 μm
AVIRIS radiance ratios at the same points are 1.4%
or less. The effect of the larger field of view
for AVHRR is simulated by successively increasing
the pixel averaging area from 1x1 to 55x55, where
the largest area represents the 1.1 km field of
view of AVHRR. As we note in Figure 2, the
magnitudes and separation of the band ratio values
for the various cloud types are preserved as the
averaging area increases. While the land and snow
surface scenes tend toward a ratio value of 0.08,
the value is distinct from those of the cloud
scenes. This analysis procedure will be carried
out for a large set of image pixels to obtain
statistical results for differing scene types.

158
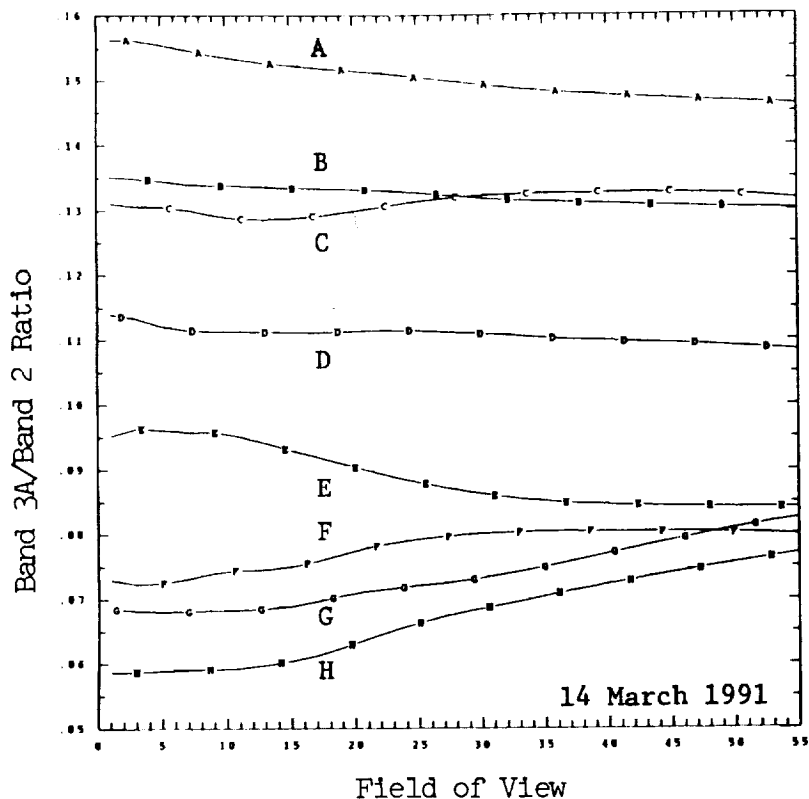
Fig. 2. Ratio of AVHRR-K Band 3A/Band 2 radiances simulated from AVIRIS at a varying field of view (AVIRIS pixels), for the scenes in Fig. 1.

3.0 DISCUSSION

This analysis indicates that predominant particle phase near cloud top may be observable in the AVHRR-K band ratios. Particle size and phase retrievals, using the Adding Model to calculate arrays of cloud spectral reflectance (Wetzel and Vonder Haar, 1991) and LOWTRAN7 to correct AVIRIS reflectance for path radiance and extinction, are being developed and tested against coincident ground-based radar and microwave radiometer observations, and aircraft measurements of in-cloud droplet and crystal size distributions.

4.0 REFERENCES

Berendes, T.A., R.E. Feind, K.-S. Kuo and R.M. Welch, "Cloud base height and optical thickness retrievals using AVIRIS data", Proc., Third AVIRIS Workshop (R. Green, ed.), JPL Publ. 91-28, Jet Propulsion Lab., Pasadena, CA, pp. 232-247, 1991.

Gao, B.-C., and A.F.H. Goetz, "Determination of cloud area from AVIRIS data", Proc., Second AVIRIS Workshop (R. Green, ed.), JPL Publ. 90-54, Jet Propulsion Lab., Pasadena, CA, pp. 157-161, 1990.

Wetzel, M.A., and T.H. Vonder Haar, "Theoretical development and sensitivity tests of a stratus cloud droplet size retrieval method for AVHRR-K/L/M", Rem. Sens. Env., 36, pp.105-119, 1991.